ABSTRACT

THE DESIGN OF ADJUSTABLE SPHERICAL MECHANISMS USING PLANE-TO-SPHERE AND SPHERE-TO-PLANE PROJECTIONS

by
Wen-Tzong Lee

The spherical mechanism is a particular type of spatial mechanism. Due to the orientation of its joint axes and the curvature of its links, the workspaces of spherical mechanisms (whether line segments, closed loops or area regions) are spherical in curvature. This characteristic of spherical mechanisms makes them quite effective and practical in motion path and function generation applications requiring spherical rigid body kinematics.

Although there are design methods available for spherical mechanisms, most of these methods do not consider the design of a single adjustable spherical mechanism. With an adjustable spherical mechanism, the user could for example, relocate the fixed or moving pivots of the spherical mechanism to achieve a greater range of rigid body locations and orientations. Having adjustability would make a single mechanism effective for multiple design applications.

Numerous methods have been published for the design of adjustable planar mechanisms. Unfortunately, the number of design methods for adjustable spherical mechanisms, in comparison, is extremely modest. This research bridges the gap between the need for adjustable spherical mechanism design methods and the design methods available for adjustable planar mechanisms.

This research presents a new method for synthesizing adjustable spherical four and five-bar motion, path and function generators using planar motion, path and function

generation methods respectively. The benefits of this method are twofold. One benefit is that the user can design spherical mechanisms to approximate multiple phases of prescribed rigid-body path points. Another benefit is that the user can design spherical path generators using synthesis methods for planar path generators. By projecting the coordinates of a given spherical mechanism on a plane or the coordinates of a given planar mechanism on a sphere using the method introduced in this work, the user can design both planar and spherical mechanisms respectively. This research introduces sphere-to-plane and plane-to-sphere projection methods with optimization methods to minimize the structural error between the prescribed performance of the adjustable spherical mechanism and the performance achieved by the synthesized adjustable spherical mechanism.

This research considers two-phase moving pivot adjustment problems with constant crank and follower lengths for the spherical mechanism. The spherical mechanisms considered in this research are four-bar motion, path and function generators as well as five-bar motion and path generators. Codified models of the projection and optimization methodologies introduced are also included.

THE DESIGN OF ADJUSTABLE SPHERICAL MECHANISMS USING PLANE-TO-SPHERE AND SPHERE-TO-PLANE PROJECTIONS

by

Wen-Tzong Lee

A Dissertation
Submitted to the Faculty of
New Jersey Institute of Technology
in Partial Fulfillment of the Requirements for the Degree of
Doctor of Philosophy in Mechanical Engineering

Department of Mechanical Engineering

May 2004

APPROVAL PAGE

THE DESIGN OF ADJUSTABLE SPHERICAL MECHANISMS USING PLANE-TO-SPHERE AND SPHERE-TO-PLANE PROJECTIONS

Wen-Tzong Lee

Dr. Rajpal S. Sodhi, Dissertation Advisor — Date
Associate Professor of Mechanical Engineering, NJIT

Dr. Rong-Yaw Chen, Committee Member — Date
Professor of Mechanical Engineering, NJIT

Dr. Sanchoy K. Das, Committee Member — Date
Professor of Industrial and Manufacturing Engineering, NJIT

Dr. Ernest S. Geskin, Committee Member — Date
Professor of Mechanical Engineering, NJIT

Dr. Kevin Russell, Committee Member — Date
Armaments Engineering and Technology Center
US Army Research, Development and Engineering Center
Picatinny Arsenal, New Jersey

BIOGRAPHICAL SKETCH

Author: Wen-Tzong Lee

Degree: Doctor of Philosophy

Date: May 2004

Undergraduate and Graduate Education:

- Doctor of Philosophy in Mechanical Engineering
  New Jersey Institute of Technology, Newark, NJ, USA, 2004

- Master of Science in Mechanical Engineering
  University of Tennessee at Chattanooga, Chattanooga, TN, USA, 1995

- Bachelor of Science in Mechanical Engineering
  Tatung Institute of Technology, Taipei, Taiwan, 1992

Major: Mechanical Engineering

Presentations and Publications:

Wen-Tzong Lee, Kevin Russell, Raj S. Sodhi, "On the Application of Plane-to-Sphere and Sphere-to Plane Projections in Path Generation," Mechanics Based Design of Structures and Machines (submitted) 2004

Wen-Tzong Lee, Kevin Russell, Raj S. Sodhi, "A Computer-Based Model for the Design of Adjustable Spherical Mechanisms," Engineering with Computers (submitted) 2004.

Kevin Russell, Raj S. Sodhi, Wen-Tzong Lee, "On Projection Methods for Multi-Phase Motion Generation of Spherical Mechanisms," ASME Journal Of Mechanical Design (submitted) 2003.

Wen-Tzong Lee, Kevin Russell, Raj S. Sodhi, "On the Design of Function Generators Using Plane-to-Sphere and Sphere-to Plane Projections," JSME International Journal (submitted) 2003.

Wen-Tzong Lee, Kevin Russell, Raj S. Sodhi, "On the Design of Path Generators Using Plane-to-Sphere and Sphere-to Plane Projections," Mechanism and Machine Theory (submitted) 2003.

Wen-Tzong Winston Lee, Rajpal S. Sodhi, "An Object-oriented Framework for Spatial Mechanism Analysis," Proceedings of The 5th Annual International Conference on Industrial Engineering Theory, Applications and Practice, 2000.

Wen-Tzong Lee, "Analysis of Straight Beams By Singularity Functions and Fourier Analysis Employing Maple V," Master's Thesis, University of Tennessee at Chattanooga, 1995.

This dissertation is dedicated to my parents,
my wife, Pei-Hsuan,
and my sons, Kelly and Kevin.

ACKNOWLEDGEMENT

The author obtained much assistance from the faculty of the Department of Mechanical Engineering while pursuing his doctoral studies at New Jersey Institute of Technology. I would like to express my deepest appreciation to my advisor, Dr. Raj Sodhi, who provided his guidance, friendship, and support throughout this research. Special thanks goes to Dr. Rong-Yaw Chen, Dr. Sanchoy K. Das, Dr. Ernest S. Geskin and Dr. Kevin Russell for serving as committee members, reviewing the author's research, and providing the author with many constructive comments and suggestions. Special thanks also goes to the Department of Mechanical Engineering at NJIT for their financial assistance needed to complete this research. Finally, the author would like to thank the vast majority of unnamed supporters, great and small, who helped to make this accomplishment possible.

TABLE OF CONTENTS

TABLE OF CONTENTS
(Continued)

TABLE OF CONTENTS
(Continued)

Chapter **Page**

TABLE OF CONTENTS
(Continued)

Chapter **Page**

LIST OF TABLES

LIST OF TABLES
(Continued)

LIST OF FIGURES

LIST OF FIGURES
(Continued)

LIST OF FIGURES
(Continued)

LIST OF FIGURES
(Continued)

LIST OF FIGURES
(Continued)

LIST OF FIGURES
(Continued)

LIST OF FIGURES
(Continued)

Figure **Page**

CHAPTER 1

INTRODUCTION

1.1 Spherical Four and Five-Bar Mechanisms

The spherical mechanism is a particular type of spatial mechanism. As the name "spherical" implies, some characteristics of this mechanism are like those of a geometric sphere. For example, the joint axes of spherical mechanism all intersect at the same point (the center of the sphere) and the links of a spherical mechanism have constant curvature. Figure 1.1 illustrates a spherical four-bar mechanism. This mechanism is also called the four-revolute spherical or 4R spherical mechanism. The spherical four-bar mechanism has a single degree of freedom. Figure 1.2 illustrates a spherical five-bar mechanism. The spherical five-bar mechanism has two degrees of freedom. Variables $\mathbf{a}_0$ and $\mathbf{b}_0$ in Figures 1.1 and 1.2 denote the fixed pivots. Variables $\mathbf{a}_1$, $\mathbf{b}_1$ and $\mathbf{c}_1$ denote the moving pivots. The **u** variables denote the joint axes of each fixed and moving pivot. Revolute joints connect each link in both the spherical four and five-bar mechanisms.

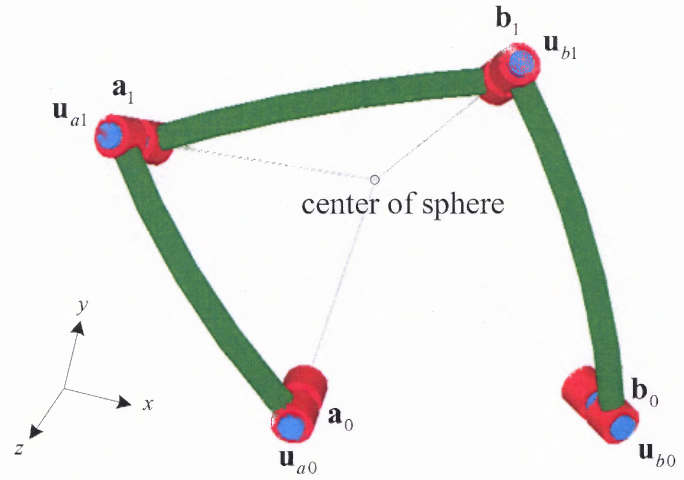

Figure 1.1 The spherical four-bar mechanism.

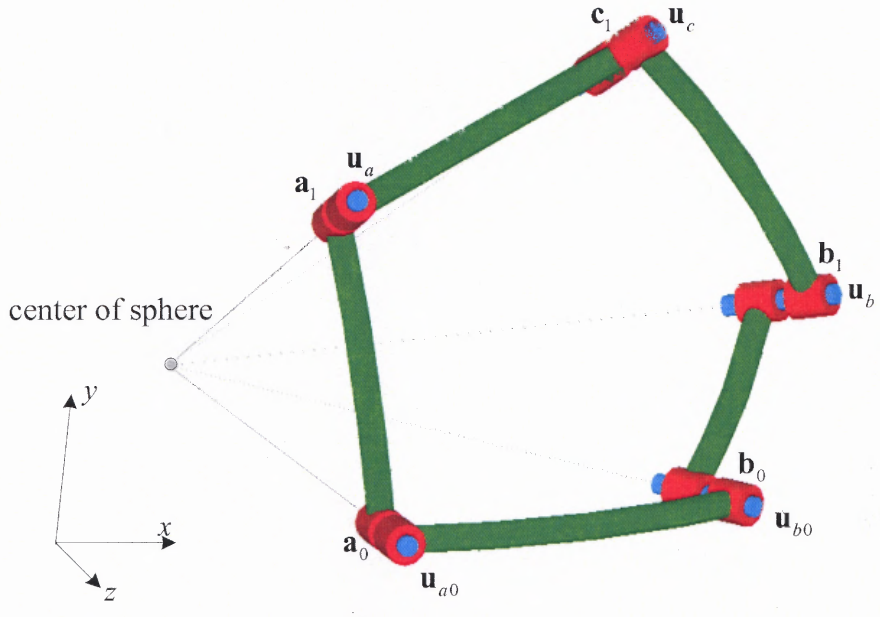

Figure 1.2 The spherical five-bar mechanism.

Due to the orientation of its joint axes and the curvature of its links, the workspaces of spherical mechanisms (whether they are line segments, closed loops or area regions) are spherical in curvature. This characteristic of spherical mechanisms

makes them quite effective and practical in motion path and function generation applications requiring spherical rigid body kinematics.

The capacity for spherical manipulation of rigid bodies in a mechanism has been proven to be very advantageous when the rigid body is a camera (Figure 1.3) or a fan (Figure 1.4). In Figure 1.3 [1], a camera is mounted on a 3-DOF spherical mechanism. This mechanism is called the "Agile Eye" and its responsiveness is comparable to that of the human eye. In Figure 1.4 [2], a fan is mounted to a 1-DOF spherical mechanism. This mechanism is called "The Infinity Fan" and is capable of thoroughly circulating air in a room even when facing a corner. If these spherical mechanisms were designed to have adjustable features (for example, adjustable moving pivots) a single "Agile Eye," "Infinity Fan" then the spherical mechanism would be able to achieve additional rigid-body orientations while incorporating essentially the same hardware.

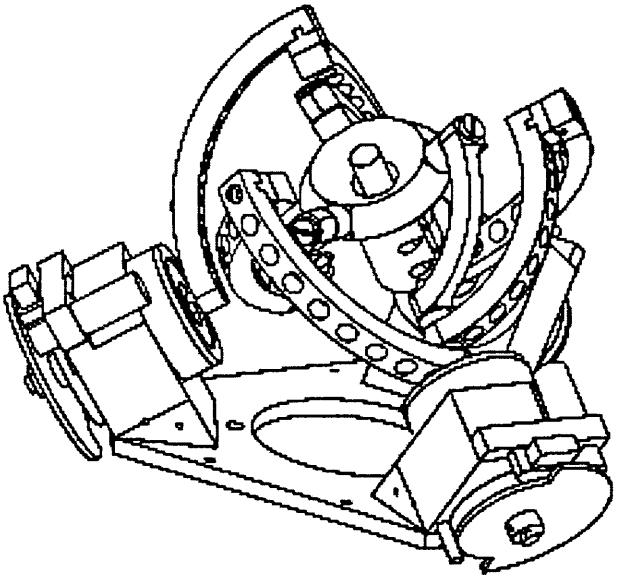

Figure 1.3 A 3-DOF spherical manipulator (the "Agile Eye").

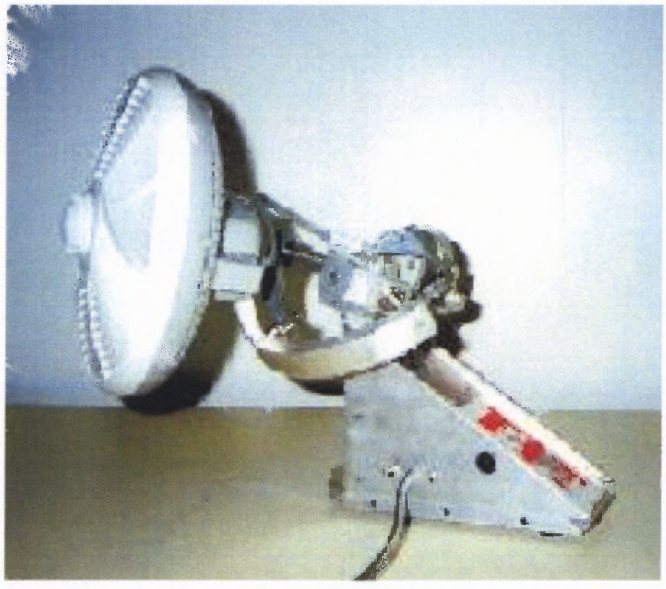

Figure 1.4 A 1-DOF spherical manipulator (the "Infinity Fan").

1.2 Planar Four and Five-Bar Mechanisms

Figure 1.5 illustrates a planar four-bar mechanism. Like the spherical four-bar mechanism, the planar four-bar mechanism has a single degree of freedom. Figure 1.6 illustrates a planar five-bar mechanism. Like the spherical five-bar mechanism, the planar five-bar mechanism has two degrees of freedom. Variables $\mathbf{a}_0$ and $\mathbf{b}_0$ in Figures 1.5 and 1.6 denote the fixed pivots. Variables $\mathbf{a}_1$, $\mathbf{b}_1$ and $\mathbf{c}_1$ denote the moving pivots.

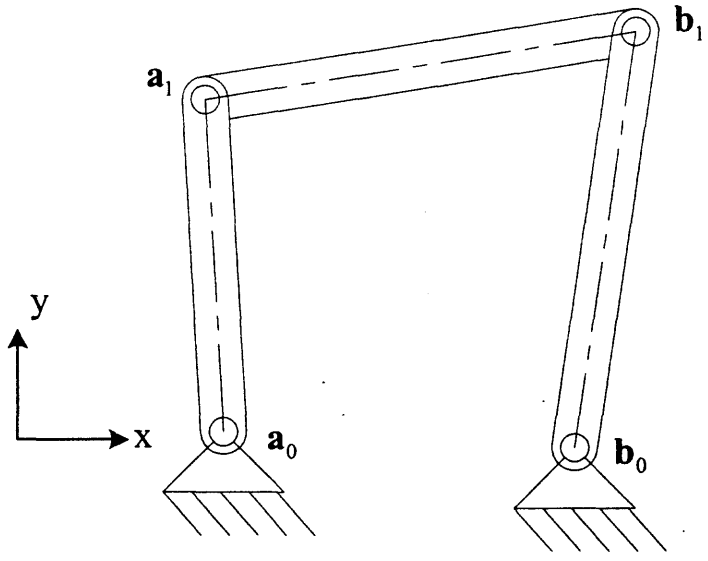

Figure 1.5 The planar four-bar mechanism.

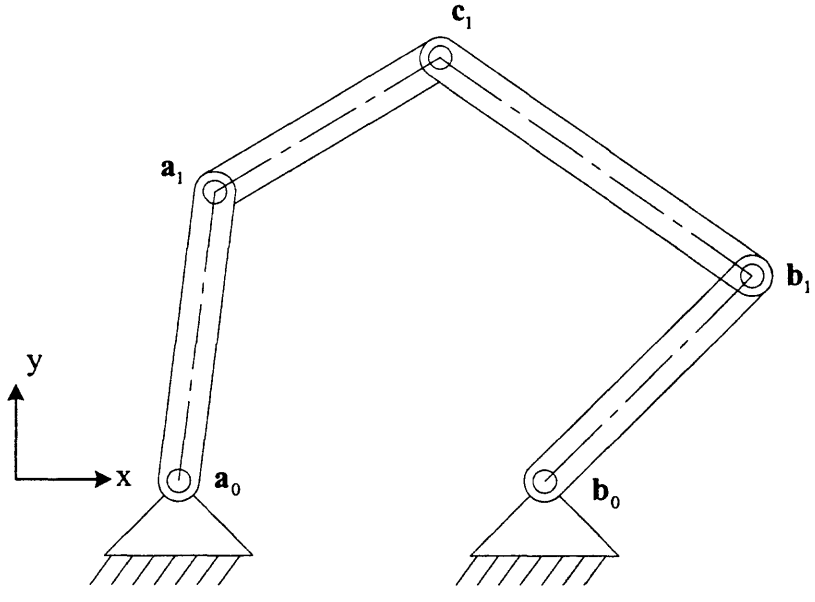

Figure 1.6 The planar five-bar mechanism.

1.3 Path and Multi-Phase Path Generation for Planar Mechanisms

The objective in **path generation** is to synthesize a mechanism to achieve a series of prescribed rigid-body path points. For the five-bar tooling mechanism illustrated in, Figure 1.7, the rigid body is a machining tool and the rigid body points are various locations of the tool tip. The objective in **multi-phase path generation** is to design an adjustable mechanism to achieve multiple series of prescribed rigid-body path points. The advantage of multi-phase path generation is that the user can design a single path generator to achieve multiple series (or phases) of prescribed rigid-body path points using essentially the same hardware. For example, if rigid body path points $\mathbf{p}_1, \mathbf{p}_2$, and $\mathbf{p}_3$ are achieved when the five-bar mechanism illustrated in Figure 1.8 incorporates the moving pivots $\mathbf{a}_1$ and $\mathbf{c}_1$, and rigid body path points $\mathbf{p}_1, \mathbf{p}_4$, and $\mathbf{p}_5$ are achieved when mechanism incorporates moving pivots $\mathbf{a}_{1n}$ and $\mathbf{c}_{1n}$, then the mechanism could be classified as an adjustable path generator.

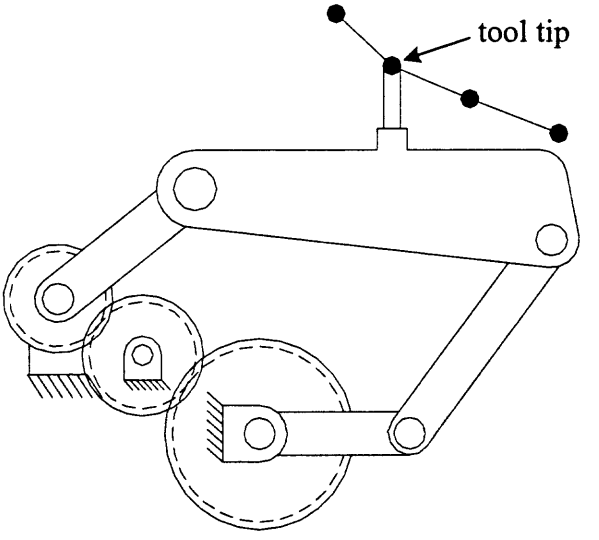

Figure 1.7 Five-bar tooling mechanism.

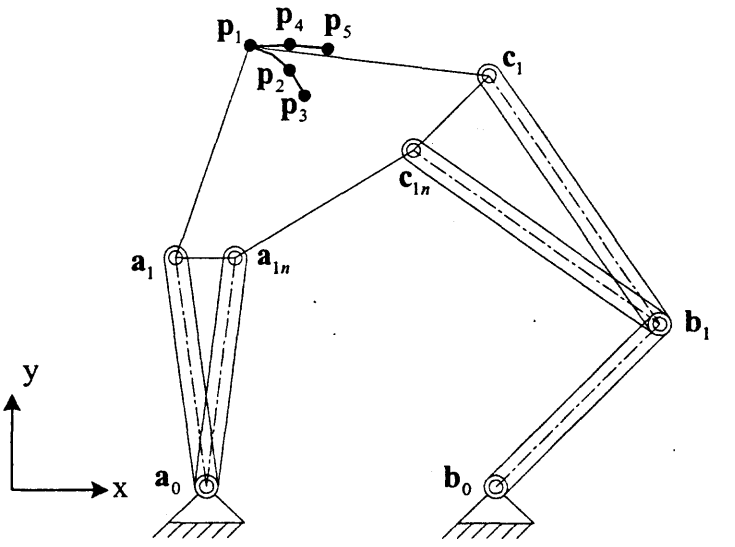

Figure 1.8 Adjustable five-bar path generator and rigid body path points.

Besides moving pivot adjustment, there are some other kinds of adjustable mechanisms, such as crank length adjustment (Figure 1.9), fixed pivot adjustment (Figure 1.10), and fixed pivot and crank length adjustment (Figure 1.11).

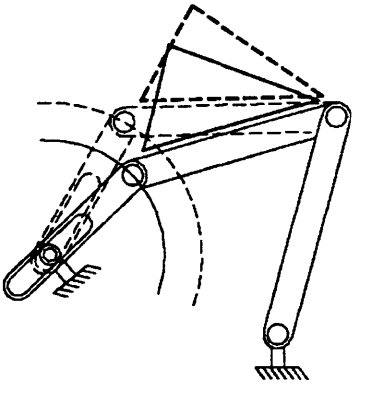

Figure 1.9 Crank length Adjustment.

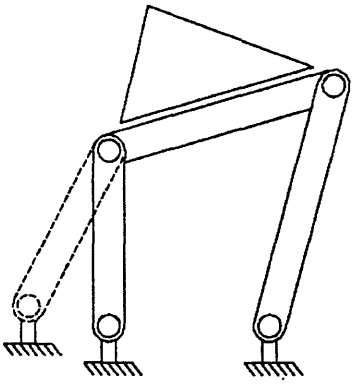

Figure 1.10 Fixed pivot adjustment.

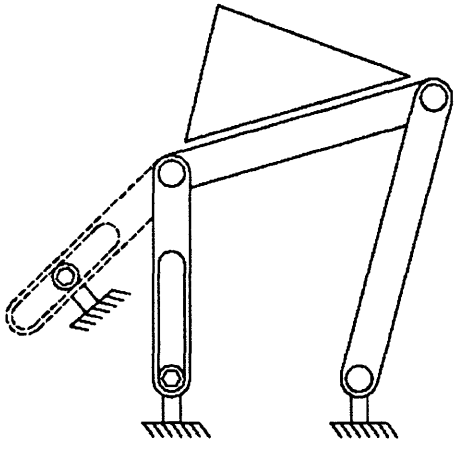

Figure 1.11 Fixed pivot and crank length adjustment.

1.4 Function and Multi-Phase Function Generation for Planar Mechanisms

The objective in **function generation** is to synthesize a mechanism to achieve a series of prescribed input-output link relationships. For the four-bar dial mechanism illustrated in Figure 1.9, reading on one dial and the reading on the other dial are coordinated by a relationship between the input and output links. The objective in **multi-phase function**

generation is to design an adjustable mechanism to achieve multiple series of prescribed input-output link relationships. The advantage of multi-phase function generation is that the user can design a single function generator to achieve multiple series (or phases) of prescribed input-output link relationships using essentially the same hardware. For example, if angles ϕ_1, ϕ_2, and ϕ_3 are achieved when the four-bar mechanism illustrated in Figure 1.10 incorporates the moving pivot $\mathbf{b}_1$, and angles ϕ_1, ϕ_4, and ϕ_5 are achieved when mechanism incorporates moving pivots $\mathbf{b}_{1n}$, then the mechanism could be classified as an adjustable function generator.

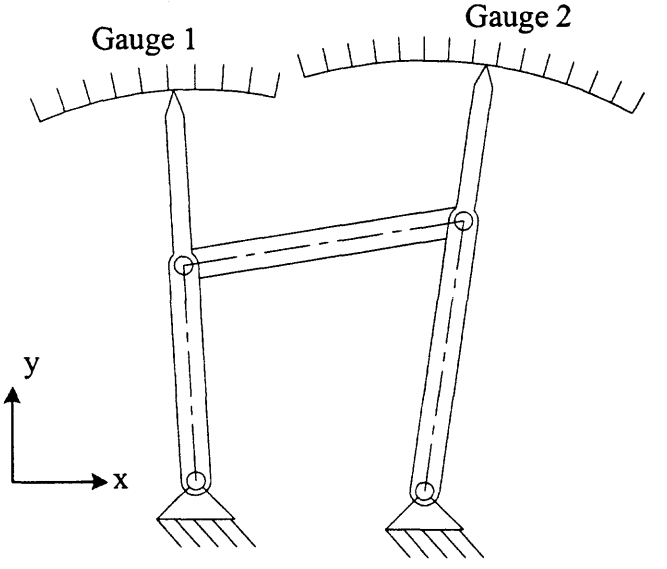

Figure 1.12 Four-bar dial mechanism.

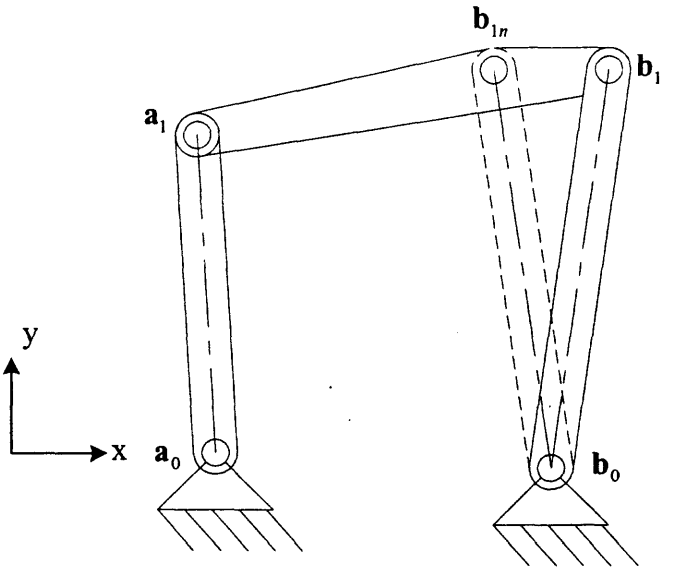

Figure 1.13 Adjustable four-bar function generator.

1.5 Motion and Multi-Phase Motion Generation for Planar Mechanisms

The objective in **motion generation** is to design a mechanism to achieve a series of prescribed rigid-body positions. For the planar five-bar loading mechanism illustrated in, Figure 1.11, the rigid body is the carrying block and the position of the rigid body is represented by various locations on the carrying block (points **p**, **q** and **r**). The objective in **multi-phase motion generation** is to design an adjustable mechanism to achieve multiple series of prescribed rigid-body positions. One advantage of multi-phase motion generation is that the user can design a single motion generator to approximate multiple series (or phases) of prescribed rigid-body positions using essentially the same hardware. For example, if rigid-body position 1, 2 and 3 are achieved when the five-bar mechanism (in Figure 1.12) incorporates the moving pivots $\mathbf{a}_1$ and $\mathbf{c}_1$, and positions 1, 4 and 5 are achieved when $\mathbf{a}_{1n}$ and $\mathbf{c}_{1n}$ are incorporated, this mechanism could be classified as an

adjustable motion generator. As illustrated in Figure 1.12, the mechanism with moving pivots $\mathbf{a}_1$ and $\mathbf{c}_1$ and the mechanism with moving pivots $\mathbf{a}_{1n}$ and $\mathbf{c}_{1n}$ use the same components (or hardware). The only difference between the two mechanisms are the locations of the moving pivots **a** and **c**.

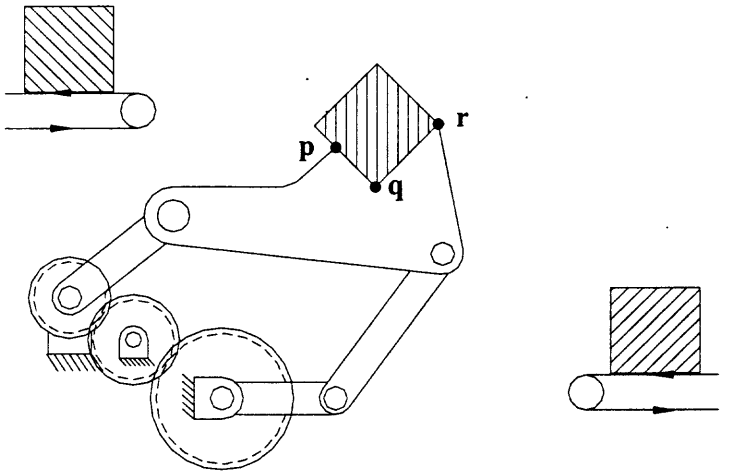

Figure 1.14 Five-bar loading mechanism.

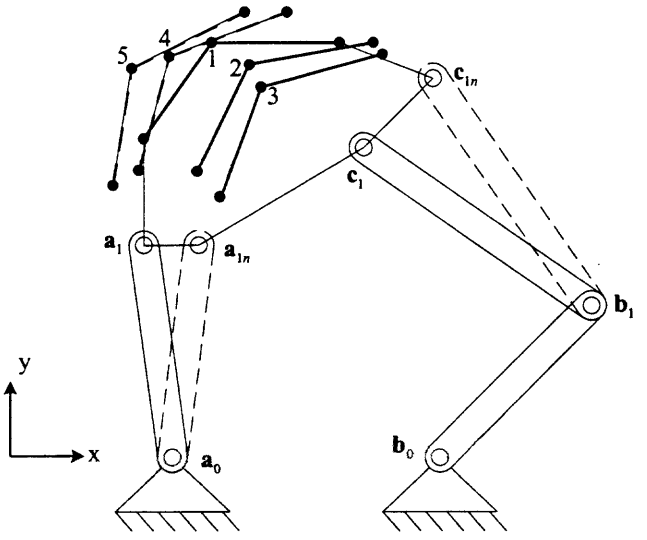

Figure 1.15 Adjustable five-bar motion generator and rigid-body positions.

1.6 Literature Review

Previous work in spherical path generation [3-7] includes the work of Tong and Chiang [3] who developed compatible equations to synthesize spherical path generators based on the relationship between the coupler pole and the mechanisms joints. Chang, Lu and Hwang [4] developed equations for spherical four-bar linkages to trace a coupler curve with two prescribed cusps by using a special case of spherical Burmester curves. Angeles and Liu [5] developed a method to optimize the spherical path generator by formulating the problem as two loops and minimizing the structural error between the two loops. Lin [6] used a continuation method to synthesize spherical four-bar path generators. Funabshi, Iwatsuki and Yoshiaki [7] considered path generation using spherical four-bar mechanisms with adjustable crank lengths.

Previous work in the area of planar path generation [3,7-21] includes the work of Tao and Krishnamoorthy [8] who presented a graphical method to synthesize a four-bar path generator to produce different coupler curves by adjusting the length of the crank link. Kay and Haws [9] developed generalized design equations for a path generating cam-link mechanism. Zhou and Cheung [10] developed a generic algorithm to obtain the global solution for continuous path generation by measuring the link length structural error instead of the structural error between the prescribed curve and generated curve. Ullah and Kota [11] introduced a new method to optimize the structural in path generation by using the Fourier function to describe the coupler curve. Tong and Chang [3] developed compatible equations to synthesize planar path generators based on the relation shop between the coupler pole and the mechanism joints. Sandor, Kaufman, Erdman, Foster, Sadler, Smith and Kerashaw [12] introduced a geared linkage for path

generation. Bali and Chand [13] presented a synthesis method for planer five-bar path generation with prescribed timing and variable topology for motion between extreme positions using the complex number method. Starns and Fulgrad [14] presented a synthesis method for a geared five-bar path generating mechanism using continuation methods. Connor, Douglas and Gilmartin [15] presented a methodology for the synthesis of hybrid, five-bar path generating mechanisms. Freudenstein and Roth [16] developed a numerical method-based synthesis approach for path generators. McGovern and Sandor [17] presented a method to synthesize adjustable function generators using complex variables. Funabshi, Iwatsuki and Yoshiaki [7] considered path generation using planar four-bar mechanisms with adjustable crank lengths. Chang [18] proposed synthesis methods to design mechanisms that are adjustable to tracing variable circular arcs with prescribed velocities. Beaudrot [19] introduced a synthesis method by which planar four-bar mechanisms can be adjusted to achieve multiple linear paths. In the work of Shimojima, Ogawa, Fujiwara and Sato [20], adjusting methods and the types of outputs are classified and planar four-bar and multi-link mechanisms are synthesized by considering pressure angles and the rations of link lengths. Tao and Yan [21] considered the design of adjustable planar linkages to achieve variable circular arcs.

Previous work in spherical function generation [5, 7, 22-25] includes the work of Liu and Angeles [5] who developed an optimization method for four-bar function generators. In this method, the design error is formulated as an equality-constrained minimization problem. The authors also introduced an optimization method for four-bar spherical function generators under mobility constraints [22]. Lin and Chiang [23] introduced a synthesis method for five-bar spherical function generators using the pole

method. Sodhi and Wilhelm [24] presented an expanded set of computer input-output angle solutions curves for use in designing four-revolute spherical function generators. Chen and Chiang [25] developed a fourth-order synthesis method for spherical four-bar function generators using relative pole equations. Funabshi, Iwatsuki and Yoshiaki [7] considered function generation using spherical four-bar mechanisms with adjustable crank lengths.

Previous work in the area of planar function generation [7, 12, 22, 23, 26-35] includes the work of Raot [26] who introduced a four-bar, epicyclical gear train mechanism that can develop a function of two independent variables. Watanable [27] developed an analytical method for the synthesis of a planar four-bar mechanism to generate an approximate function over a finite interval. Chuang and Chiang [28] presented an optimum solution for a planar four-bar function generator concerning both structural error and transmission angle. Chiang, Pennestri and Chung [29] introduced computer-based methods for higher order synthesis of four-bar function generators. Beale and Simionescu [30] presented an optimum synthesis method for the planar four-bar function generator using the Akermann steering linkage as an example. Todorov [31] presented a dimensional synthesis method for planar function generators. Yin and Wu [32] introduced an optimal model of a function generator that considers the effects of radial clearances in joints and structural error. Liu and Angeles [22] introduced an optimization scheme for four-bar planar function generators under mobility constraints. Lin and Chiang [23] introduced a synthesis method for five-bar planar function generators using the pole method. McGovern and Sandor [33] presented a method to synthesize adjustable function generators using complex variables. Naik and Amarnath

[34] presented a method to synthesize an adjustable four-bar function generator using five-bar linkage theory. Sandor, Kaufman, Erdman, Foster, Sadler, Smith and Kerashaw [12] introduced a geared linkage for function generation. Basu and Farhang [35] presented a mamthematical formulation for the analysis and design of two-input, small crank, five-bar mechanisms for function generation. Funabshi, Iwatsuki and Yoshiaki [7] considered function generation using planar four-bar mechanisms with adjustable crank lengths.

Previous work in spherical mechanism design, analysis and motion generation [36-42] includes the work of Furlong and Vance [36] who presented a new approach using a virtual reality environment to design spherical mechanisms. Sodhi and Shoup [37, 38] presented relationship between the axodes and the geometric configuration of the spherical four-revolute mechanism and a general analytical method for synthesizing the four-revolute spherical mechanism based on the fixed axode. Gilmartin and Duffy [39] examined type and mobility analysis of the spherical four-link mechanism. McCarthy and Bodduluri [40, 41] considered the generalization of planar rectification theory to spherical 4R mechanisms as well as an approach to the finite position synthesis of spherical four-bar linkages that unites traditional precision theory with recent results in approximate position synthesis. Ruth and McCarthy [42] described a computer-aided design software system for spherical four-bar linkages that is based on Burmester's planar theory. Lin [6] used a continuation method to synthesize spherical four-bar motion generators.

Previous work in planar mechanism design, analysis and motion generation [12, 43-47] includes the work of Wang and Sodhi [43] who developed a method for the

synthesizing an adjustable moving pivot four-bar mechanism for multi-phase motion generation. Ahmad [44] produced a summary of synthesis methods for four-bar linkages with adjustable crank pivots for different motion generation problems. Sandor, Kaufman, Erdman, Foster, Sadler, Smith and Kerashaw [12] introduced a geared linkage for motion generation. Dhingra and Mani [45] developed a computer-based approach for synthesizing six different link and geared mechanisms to achieve finite and multiply-separated positions. Wilhelm [46] introduced multi-phase motion generation methods for planar four-bar mechanisms. Chuenchom and Kota [47] presented generalized analytical methods for designing adjustable mechanisms based of the synthesis of adjustable dyads.

1.7 Research Objectives

Although there are methods available for the design of spherical mechanisms (as described in the literature review included in Section 1.6), most of these methods do not consider the design of a single adjustable spherical mechanism. With an adjustable spherical mechanism, the user could relocate the mixed or moving pivots of the mechanism to achieve a new mechanism configuration, and subsequently, additional motion, path or function generation applications.

The primary objective of this research is to develop new methods for the design of four and five-bar spherical mechanisms for multi-phase motion, path and motion generation. With such methods, the user could design four and five-bar spherical mechanisms to achieve multiple phase of prescribed rigid-body positions, path points or crank and follower displacement angles using essentially the same hardware.

In accordance to the synthesis of adjustable spherical four and five-bar mechanisms, another objective of the research is to develop an optimization method to minimize the structural error of the synthesized adjustable spherical mechanisms. Using such a method in accordance with multi-phase motion, path and function generation methods, the user could design adjustable spherical motion, path and function generators with optimum parameters for minimum structural errors in rigid-body positions, path points or crank and follower displacement angles respectively.

To achieve the primary objective, methods for the design of adjustable planar four and five-bar mechanisms for-multi-phase motion, path and function generation are also developed in this research. With such methods, the user could design four and five-bar planar mechanisms to achieve multiple phase of prescribed rigid-body positions, path points or crank and follower displacement angles using essentially the same hardware.

1.8 Research Methodology

Using the theories of planar rigid-body guidance, planar rigid-body point guidance and planar four-bar crank and follower displacement angle relationships, design equations were developed under constant-length constraints. For planar mechanism synthesis, these equations govern the fixed-pivot locations, moving-pivot locations and link lengths in accordance with the prescribed rigid-body points, rigid-body path points and crank and follower displacement angles. The design equations were developed to include multi-phase motion path and function generation for planar four and five-bar mechanisms.

Using the geometric relationships between spheres, planes, line-sphere intersections and line-plane intersections, projection methods were developed. With the

developed plane-to-sphere and sphere-to-plane projection methods, the user could project the joint coordinates of a planar mechanism (essentially, points on a plane) to the surface of a specified sphere (resulting in a spherical mechanism).

Optimization methods were developed to minimize the structural errors in the rigid-body positions, path points and crank and follower displacement angles of adjustable spherical motion, path and function generators (respectively) synthesized using plane-to-sphere projection. The optimization approach capitalizes on the relationship between structural error and the projection length in plane-to-sphere projections.

Codified models of the developed multi-phase motion, path and function generation equations, the plane-to-sphere and sphere-to-plane projection methods and the optimization method were built using the mathematical analysis software MATHEMATICA. With these codified models, the user can design adjustable spherical four and five-bar motion, path and function generators with minimum structural error on a computer.

CHAPTER 2

ADJUSTABLE PLANAR MECHANISMS AND DESIGN EQUATIONS

The design equations for the synthesis for adjustable planar mechanisms are introduced in this chapter. Unlike non-adjustable planar mechanisms, adjustable planar mechanisms can be designed to achieve multiple mechanism configurations (and subsequently multiple phases of prescribed motion, path or function generation parameters) using essentially the same hardware. Specifically, this chapter includes the design equations for adjustable four-bar motion, path and function generators and adjustable five-bar motion and path generators.

2.1 Adjustable Planar Four-Bar Path Generator

Figure 2.1 illustrates the planar four-bar path generator. Link $\mathbf{a}_0$-$\mathbf{a}_1$ is the designated crank link and link $\mathbf{b}_0$-$\mathbf{b}_1$ is the designated follower link. Links $\mathbf{a}_0$-$\mathbf{a}_1$ and $\mathbf{b}_0$-$\mathbf{b}_1$ of the mechanism must satisfy the constant length condition only. Given a fixed pivot $\mathbf{b}_0$ and a moving pivot $\mathbf{b}_1$, the constant length condition in Equation 2.1 [48,49] must be satisfied when synthesizing the crank and follower links of the planar four-bar mechanism.

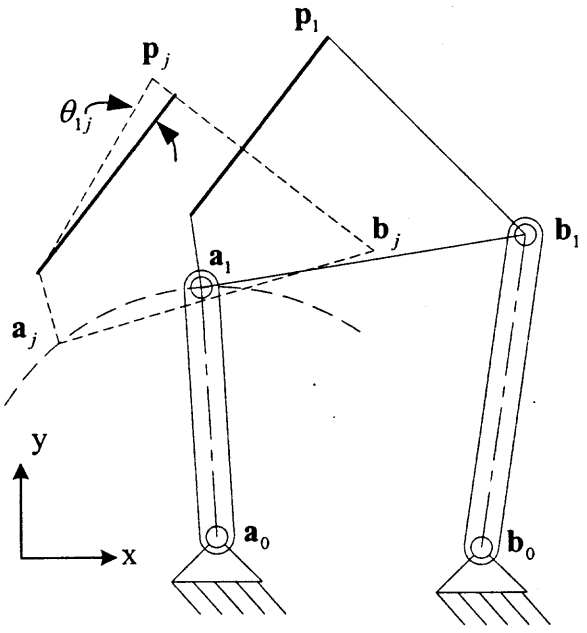

Figure 2.1 The planar four-bar path generator with rigid body point **p** and orientation angle θ.

$$(\mathbf{b}_j - \mathbf{b}_0)^T(\mathbf{b}_j - \mathbf{b}_0) = (\mathbf{b}_1 - \mathbf{b}_0)^T(\mathbf{b}_1 - \mathbf{b}_0) \quad j = 2, 3, \ldots . n \tag{2.1}$$

where

$$\mathbf{b}_0 = (b_{0x}, b_{0y}, 1), \mathbf{b}_1 = (b_{1x}, b_{1y}, 1), \mathbf{b}_j = [D_{ij}]\mathbf{b}_1,$$

and

$$[D_{1j}] = \begin{bmatrix} \cos\theta_{1j} & -\sin\theta_{1j} & p_{jx} - p_{1x}\cos\theta_{1j} + p_{1y}\sin\theta_{1j} \\ \sin\theta_{1j} & \cos\theta_{1j} & p_{jy} - p_{1x}\sin\theta_{1j} - p_{1y}\cos\theta_{1j} \\ 0 & 0 & 1 \end{bmatrix}. \tag{2.2}$$

Equation 2.1 is rewritten as Equation 2.3. In Equation 2.3, the variable R represents the length of the follower link.

$$(\mathbf{b}_j - \mathbf{b}_0)^T(\mathbf{b}_j - \mathbf{b}_0) = R^2 \quad j = 2, 3, \ldots . n \tag{2.3}$$

Variable **p** in Equation 2.2 represents the coordinates of the rigid body curve points. Variable θ represents the angular displacement between position "1" and "j" of the rigid

body. Since there are four variables (b_{0x}, b_{0y}, b_{1x} and b_{1y}), a maximum of five rigid body curve points can be prescribed, with no arbitrary choice of parameter for a single phase (see Table 2.1).

In Table 2.1, the **maximum** numbers of prescribed rigid body curve points for the planar four-bar path generator for several phases are given. The number of fixed and moving pivot coordinates for the crank and follower links determines the maximum number of rigid body curve points that the user can prescribe. The example problem in Section 6.1 demonstrates the design of a planar and spherical four-bar path generator to achieve a two-phase moving pivot adjustment application.

Table 2.1 Prescribed Rigid Body Curve Point and Phase Variations for the Adjustable Planar Four-Bar Path Generator

		Crank or Follower Links	
Number of phases	Max. number of rigid body curve points	Number of unknowns	Number of free choices
1	5	4	0
2	8	6	0
3	11	8	0
n	5 + 3(n – 1)	2 + 2n	0

In the two-phase, adjustable moving pivot example problem in Section 6.1, the required unknowns are $\mathbf{a}_0$, $\mathbf{a}_1$, $\mathbf{a}_{1n}$, $\mathbf{b}_0$, $\mathbf{b}_1$ and $\mathbf{b}_{1n}$. The unknowns, $\mathbf{a}_0$ and $\mathbf{b}_0$, represent the fixed pivots of the planar four-bar mechanism. The unknowns, $\mathbf{a}_1$, $\mathbf{a}_{1n}$, $\mathbf{b}_1$ and $\mathbf{b}_{1n}$, represent the moving pivots in phase 1 and phase 2 of the planar four-bar mechanism. Since each of these unknowns has two components, there are a total of 12 variables to determine.

$\mathbf{a}_0 = (a_{0x}, a_{0y})$, $\mathbf{a}_1 = (a_{1x}, a_{1y})$, $\mathbf{a}_{1n} = (a_{1nx}, a_{1ny})$,

$\mathbf{b}_0 = (b_{0x}, b_{0y})$, $\mathbf{b}_1 = (b_{1x}, b_{1y})$, $\mathbf{b}_{1n} = (b_{1nx}, b_{1ny})$.

Equations 2.4 through 2.8 were used to calculate five of the six unknowns in $\mathbf{a}_0$, $\mathbf{a}_1$ and $\mathbf{a}_{1n}$. The variable a_{0x} and the link length R_1 are specified.

$$([D_{12}]\mathbf{a}_1 - \mathbf{a}_0)^T([D_{12}]\mathbf{a}_1 - \mathbf{a}_0) - R_1^2 = 0 \tag{2.4}$$

$$([D_{13}]\mathbf{a}_1 - \mathbf{a}_0)^T([D_{13}]\mathbf{a}_1 - \mathbf{a}_0) - R_1^2 = 0 \tag{2.5}$$

$$([D_{14}]\mathbf{a}_1 - \mathbf{a}_0)^T([D_{14}]\mathbf{a}_1 - \mathbf{a}_0) - R_1^2 = 0 \tag{2.6}$$

$$([D_{56}]\mathbf{a}_{1n} - \mathbf{a}_0)^T([D_{56}]\mathbf{a}_{1n} - \mathbf{a}_0) - R_1^2 = 0 \tag{2.7}$$

$$([D_{57}]\mathbf{a}_{1n} - \mathbf{a}_0)^T([D_{57}]\mathbf{a}_{1n} - \mathbf{a}_0) - R_1^2 = 0 \tag{2.8}$$

Equations 2.9 through 2.13 were used to calculate five of the six unknowns in $\mathbf{b}_0$, $\mathbf{b}_1$ and $\mathbf{b}_{1n}$. The variable b_{0x} and the link length R_2 are specified.

$$([D_{12}]\mathbf{b}_1 - \mathbf{b}_0)^T([D_{12}]\mathbf{b}_1 - \mathbf{b}_0) - R_2^2 = 0 \tag{2.9}$$

$$([D_{13}]\mathbf{b}_1 - \mathbf{b}_0)^T([D_{13}]\mathbf{b}_1 - \mathbf{b}_0) - R_2^2 = 0 \tag{2.10}$$

$$([D_{14}]\mathbf{b}_1 - \mathbf{b}_0)^T([D_{14}]\mathbf{b}_1 - \mathbf{b}_0) - R_2^2 = 0 \tag{2.11}$$

$$([D_{56}]\mathbf{b}_{1n} - \mathbf{b}_0)^T([D_{56}]\mathbf{b}_{1n} - \mathbf{b}_0) - R_2^2 = 0 \tag{2.12}$$

$$([D_{57}]\mathbf{b}_{1n} - \mathbf{b}_0)^T([D_{57}]\mathbf{b}_{1n} - \mathbf{b}_0) - R_2^2 = 0 \tag{2.13}$$

2.2 Adjustable Planar Four-Bar Function Generator

The planar four-bar function generator is illustrated in Figure 2.2. In this work, link $\mathbf{a}_0$-$\mathbf{a}_1$ is the designated crank link and link $\mathbf{b}_0$-$\mathbf{b}_1$ is the designated follower link. Link $\mathbf{a}_1$-$\mathbf{b}_1$ of the planar four-bar mechanism must satisfy the constant length condition only. Given a fixed pivots $\mathbf{a}_0$=(0,0) and $\mathbf{b}_0$=(1,0), the constant length condition in Equation 2.14 [48,49]

must be satisfied when synthesizing the crank and follower links of the planar function generator.

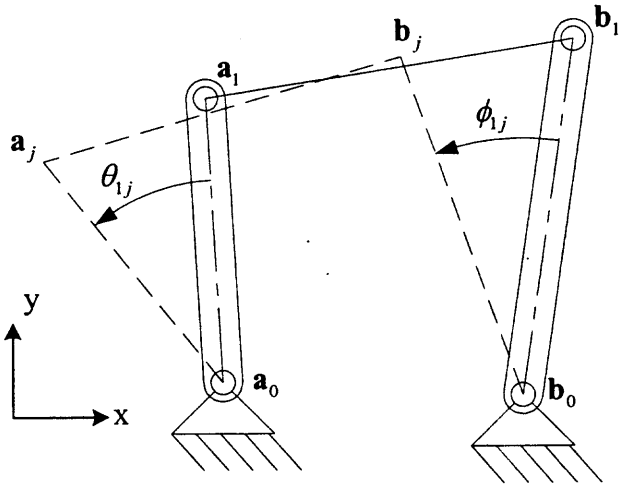

Figure 2.2 The planar four-bar function generator with displacement angles θ_{1j} and ϕ_{1j}.

$$(\mathbf{a}_j - \mathbf{b}_1)^T (\mathbf{a}_j - \mathbf{b}_1) = (\mathbf{a}_1 - \mathbf{b}_1)^T (\mathbf{a}_1 - \mathbf{b}_1) \quad j = 2, 3, \ldots . n \tag{2.14}$$

where

$$\mathbf{a}_1 = (a_{1x}, a_{1y}, 1),\ \mathbf{b}_1 = (b_{1x}, b_{1y}, 1),\ \mathbf{a}_j = [D_{1j}]\mathbf{a}_1,$$

and

$$[D_{1j}] = \begin{bmatrix} \cos(\theta_{1j} - \phi_{1j}) & -\sin(\theta_{1j} - \phi_{1j}) & 1 - \cos\phi_{1j} \\ \sin(\theta_{1j} - \phi_{1j}) & \cos(\theta_{1j} - \phi_{1j}) & \sin\phi_{1j} \\ 0 & 0 & 1 \end{bmatrix}. \tag{2.15}$$

Equation 2.14 can be rewritten as Equation 2.16. In Equation 2.16, the variable L_2 represents the length of the coupler (sometimes called rigid body) link. Although the moving pivots of both the crank and follower link of the planar four-bar mechanism are adjustable, only the length of the follower link will be adjusted (not the crank link) in this work.

$$(\mathbf{a}_j - \mathbf{b}_1)^T (\mathbf{a}_j - \mathbf{b}_1) = L_2 \quad j = 2, 3, \ldots . n \tag{2.16}$$

Variables θ_{1j} and ϕ_{1j} in Equation 2.15 represent the angular displacements of the crank and follower links. Since there are four variables (a_{1x}, a_{1y}, b_{1x} and b_{1y}), a maximum of four crank and follower displacement angles can be prescribed, with no arbitrary choice of parameter for a single phase (see Table 2.2).

In Table 2.2, the maximum numbers of prescribed crank and follower displacement angles for the adjustable planar four-bar function generator for several phases are given. The number of moving pivot coordinates for the crank and follower links determines the maximum number of crank and follower displacement angles. The example problem in Section 6.2 demonstrates the design of a planar and spherical four-bar function generator to achieve a two-phase moving pivot adjustment application.

Table 2.2 Prescribed Displacement Angle and Phase Variations for the Adjustable Planar Four-Bar Function Generator

		Crank or Follower Links	
Number of phases	Max. number of displacement angles	Number of unknowns	Number of free choices
1	4	4	0
2	8	8	0
3	12	12	0
n	4+4n	4+4n	0

In the two-phase, adjustable moving pivot example problem in Section 6.2, the required unknowns are $\mathbf{a}_1$, $\mathbf{b}_1$ and $\mathbf{b}_{1n}$. These unknowns represent the moving pivots in phase 1 and phase 2 of the planar four-bar mechanism. Since each of these unknowns has two components, there are a total of 6 variables to determine.

$\mathbf{a}_1 = (a_{1x}, a_{1y})$, $\mathbf{b}_1 = (b_{1x}, b_{1y})$, $\mathbf{b}_{1n} = (b_{1nx}, b_{1ny})$.

Equations 2.17 through 2.21 were used to calculate five of the six unknowns in $\mathbf{a}_1$, $\mathbf{b}_1$ and $\mathbf{b}_{1n}$. The variable a_{1x} and the link length L_2 are specified.

$$([D_{12}]\mathbf{a}_1 - \mathbf{b}_1)^T ([D_{12}]\mathbf{a}_1 - \mathbf{b}_1) - L_2 = 0 \tag{2.17}$$

$$([D_{13}]\mathbf{a}_1 - \mathbf{b}_1)^T ([D_{13}]\mathbf{a}_1 - \mathbf{b}_1) - L_2 = 0 \tag{2.18}$$

$$([D_{14}]\mathbf{a}_1 - \mathbf{b}_1)^T ([D_{14}]\mathbf{a}_1 - \mathbf{b}_1) - L_2 = 0 \tag{2.19}$$

$$([D_{15}]\mathbf{a}_1 - \mathbf{b}_{1n})^T ([D_{15}]\mathbf{a}_1 - \mathbf{b}_{1n}) - L_2 = 0 \tag{2.20}$$

$$([D_{16}]\mathbf{a}_1 - \mathbf{b}_{1n})^T ([D_{16}]\mathbf{a}_1 - \mathbf{b}_{1n}) - L_2 = 0 \tag{2.21}$$

2.3 Adjustable Planar Four-Bar Motion Generator

The planar four-bar motion generator is illustrated in Figure 2.3. In this work, link $\mathbf{a}_0$-$\mathbf{a}_1$ is the designated crank link and link $\mathbf{b}_0$-$\mathbf{b}_1$ is the designated follower link. Links $\mathbf{a}_0$-$\mathbf{a}_1$ and $\mathbf{b}_0$-$\mathbf{b}_1$ of the planar four-bar mechanism must satisfy the constant length condition only since its fixed and moving pivot joint axes remain parallel. Given a fixed pivot $\mathbf{b}_o$ and a moving pivot $\mathbf{b}_1$, the constant length condition in Equation 2.22 [48,49] must be satisfied when synthesizing the crank and follower links of the planar four-bar mechanism.

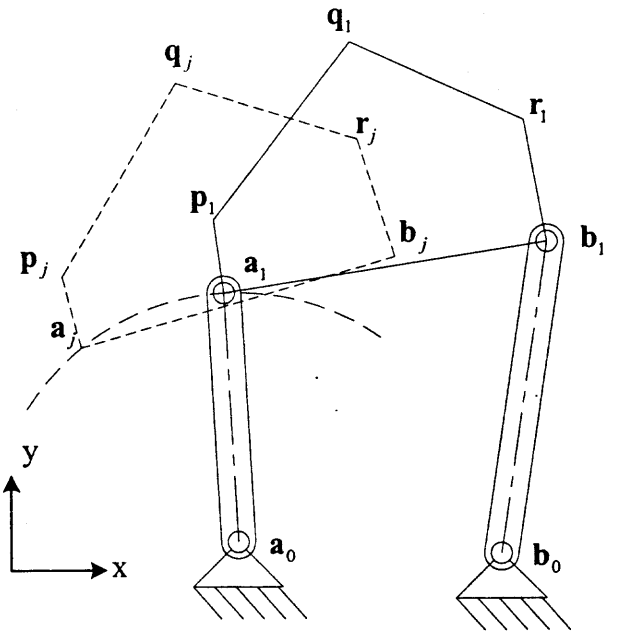

Figure 2.3 The planar four-bar motion generator with rigid body points **p**, **q** and **r**.

$$(\mathbf{b}_j - \mathbf{b}_0)^T(\mathbf{b}_j - \mathbf{b}_0) = (\mathbf{b}_1 - \mathbf{b}_0)^T(\mathbf{b}_1 - \mathbf{b}_0) \quad j = 2, 3, \ldots . n \tag{2.22}$$

where

$$\mathbf{b}_0 = (b_{0x}, b_{0y}, 1), \mathbf{b}_1 = (b_{1x}, b_{1y}, 1), \mathbf{b}_j = [D_{1j}]\mathbf{b}_1,$$

and

$$\left[D_{1j}\right] = \begin{bmatrix} p_{jx} & q_{jx} & r_{jx} \\ p_{jy} & q_{jy} & r_{jy} \\ 1 & 1 & 1 \end{bmatrix} \begin{bmatrix} p_{1x} & q_{1x} & r_{1x} \\ p_{1y} & q_{1y} & r_{1y} \\ 1 & 1 & 1 \end{bmatrix}^{-1}. \tag{2.23}$$

Equation 2.22 can be rewritten as Equation 2.24. In Equation 2.24, the variable R represents the length of the crank or follower link.

$$(\mathbf{b}_j - \mathbf{b}_0)^T(\mathbf{b}_j - \mathbf{b}_0) = R^2 \quad j = 2, 3, \ldots . n \tag{2.24}$$

Equation 2.23 is a rigid body displacement matrix. It is a derivative of the spatial rigid body displacement matrix [48,49]. Given the coordinates for a rigid body in position "i"

and the subsequent "j," matrix $[D_{ij}]$ is the transformation matrix required to transform coordinates from position "i" to position "j." Variables **p**, **q** and **r** in Equation 2.23 represent the position of the rigid body in two-dimensional space. Although the position of a rigid body in two-dimensional space is commonly described by a single point and a displacement angle (**p** and θ for example), the author chose to describe the rigid body using three points for computational purposes. If the user prefers to describe the rigid body using conventional notation, the displacement matrix in Equation 2.23 will be replaced with the conventional plane rigid body displacement matrix [48,49]. Since there are four variables (b_{0x}, b_{0y}, b_{1x} and b_{1y}), a maximum of five rigid body positions can be prescribed, with no arbitrary choice of parameter for a single phase (see Table 2.3).

Points **p, q** and **r** should not all lie on the same line in each rigid body position. Taking this precaution prevents the rows in the rigid body displacement matrix (Equation 2.23) from becoming proportional. With proportional rows, this matrix could not be inverted.

In Table 2.3, the **maximum** numbers of prescribed rigid body positions for the adjustable planar four-bar motion generator for several phases are given. The number of fixed and moving pivot coordinates for the crank and follower links determines the maximum number of rigid body positions. The example problem in Section 6.3 demonstrates the design of a planar and spherical four-bar motion generator to achieve a two-phase moving pivot adjustment application.

Table 2.3 Prescribed Rigid Body Position and Phase Variations for the Adjustable Planar Four-Bar Mechanism

		Crank or Follower Links	
Number of phases	Max. number of rigid body positions	Number of unknowns	Number of free choices
1	5	4	0
2	8	6	0
3	11	8	0
n	5 + 3(n – 1)	2 + 2n	0

In the two-phase, adjustable moving pivot example problem in Section 6.3, the required unknowns are $\mathbf{a}_0$, $\mathbf{a}_1$, $\mathbf{a}_{1n}$, $\mathbf{b}_0$, $\mathbf{b}_1$ and $\mathbf{b}_{1n}$. The unknowns $\mathbf{a}_0$ and $\mathbf{b}_0$ represent the fixed pivots of the planar four-bar mechanism. The unknowns $\mathbf{a}_1$, $\mathbf{a}_{1n}$, $\mathbf{b}_1$ and $\mathbf{b}_{1n}$ represent the moving pivots in phase 1 and phase 2 of the planar four-bar mechanism. Since each of these unknowns has two components, there are a total of 12 variables to determine.

$\mathbf{a}_0 = (a_{0x}, a_{0y})$, $\mathbf{a}_1 = (a_{1x}, a_{1y})$, $\mathbf{a}_{1n} = (a_{1nx}, a_{1ny})$,

$\mathbf{b}_0 = (b_{0x}, b_{0y})$, $\mathbf{b}_1 = (b_{1x}, b_{1y})$, $\mathbf{b}_{1n} = (b_{1nx}, b_{1ny})$.

Equations 2.25 through 2.29 were used to calculate five of the six unknowns in $\mathbf{a}_0$, $\mathbf{a}_1$ and $\mathbf{a}_{1n}$. The variable a_{0x} and the link length R_1 are specified. Variable R_1 represents the link $\mathbf{a}_1 - \mathbf{a}_0$.

$$([D_{12}]\mathbf{a}_1 - \mathbf{a}_0)^T([D_{12}]\mathbf{a}_1 - \mathbf{a}_0) - R_1^2 = 0 \tag{2.25}$$

$$([D_{13}]\mathbf{a}_1 - \mathbf{a}_0)^T([D_{13}]\mathbf{a}_1 - \mathbf{a}_0) - R_1^2 = 0 \tag{2.26}$$

$$([D_{14}]\mathbf{a}_1 - \mathbf{a}_0)^T([D_{14}]\mathbf{a}_1 - \mathbf{a}_0) - R_1^2 = 0 \tag{2.27}$$

$$([D_{56}]\mathbf{a}_{1n} - \mathbf{a}_0)^T([D_{56}]\mathbf{a}_{1n} - \mathbf{a}_0) - R_1^2 = 0 \tag{2.28}$$

$$([D_{57}]\mathbf{a}_{1n} - \mathbf{a}_0)^T([D_{57}]\mathbf{a}_{1n} - \mathbf{a}_0) - R_1^2 = 0 \tag{2.29}$$

Equations 2.30 through 2.34 were used to calculate five of the six unknowns in $\mathbf{b}_0$, $\mathbf{b}_1$ and $\mathbf{b}_{1n}$. The variable b_{0x} and the link lengths R_2 are specified. Variable R_2 represents the link $\mathbf{b}_1 - \mathbf{b}_0$.

$$([D_{12}]\mathbf{b}_1 - \mathbf{b}_0)^T([D_{12}]\mathbf{b}_1 - \mathbf{b}_0) - R_2^2 = 0 \tag{2.30}$$

$$([D_{13}]\mathbf{b}_1 - \mathbf{b}_0)^T([D_{13}]\mathbf{b}_1 - \mathbf{b}_0) - R_2^2 = 0 \tag{2.31}$$

$$([D_{14}]\mathbf{b}_1 - \mathbf{b}_0)^T([D_{14}]\mathbf{b}_1 - \mathbf{b}_0) - R_2^2 = 0 \tag{2.32}$$

$$([D_{56}]\mathbf{b}_{1n} - \mathbf{b}_0)^T([D_{56}]\mathbf{b}_{1n} - \mathbf{b}_0) - R_2^2 = 0 \tag{2.33}$$

$$([D_{57}]\mathbf{b}_{1n} - \mathbf{b}_0)^T([D_{57}]\mathbf{b}_{1n} - \mathbf{b}_0) - R_2^2 = 0 \tag{2.34}$$

2.4 Adjustable Planar Five-Bar Path Generator

The planar five-bar path generator is illustrated in Figure 2.4. In this work, links $\mathbf{a}_0$-$\mathbf{a}_1$ and $\mathbf{b}_0$-$\mathbf{b}_1$ are the driving links (denoted by driving link angles θ and ϕ). Links $\mathbf{a}_0$-$\mathbf{a}_1$ and $\mathbf{b}_1$-$\mathbf{c}_1$ of the planar five-bar mechanism are synthesized using the constant length condition only. The constant length constraint Equations 2.35 and 2.36 [48,49] are satisfied when synthesizing links $\mathbf{a}_0$-$\mathbf{a}_1$ and $\mathbf{b}_1$-$\mathbf{c}_1$ of the planar five-bar mechanism.

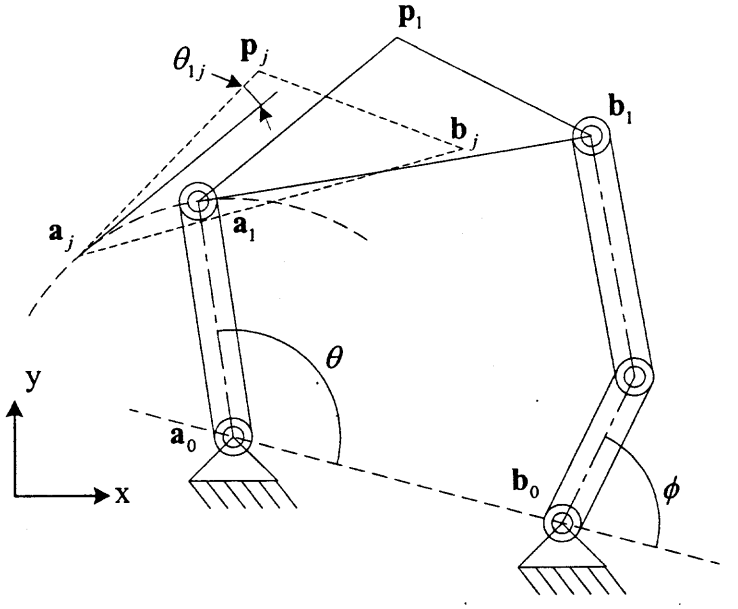

Figure 2.4 Planar five-bar path generator with driving link angles θ, ϕ, and rigid body path point **p**.

$$(\mathbf{a}_j - \mathbf{a}_0)^T(\mathbf{a}_j - \mathbf{a}_0) = (\mathbf{a}_1 - \mathbf{a}_0)^T(\mathbf{a}_1 - \mathbf{a}_0) \quad j = 2, 3, \ldots . n \tag{2.35}$$

$$(\mathbf{c}_j - \mathbf{b}_j)^T(\mathbf{c}_j - \mathbf{b}_j) = (\mathbf{c}_1 - \mathbf{b}_1)^T(\mathbf{c}_1 - \mathbf{b}_1) \quad j = 2, 3, \ldots . n \tag{2.36}$$

where

$\mathbf{a}_0 = (a_{0x}, a_{0y}, 1)$, $\mathbf{a}_1 = (a_{1x}, a_{1y}, 1)$, $\mathbf{a}_j = [D_{1j}]\mathbf{a}_1$,

$\mathbf{b}_1 = (b_{0x} + R_4\cos(\phi_1), b_{0y} + R_4\sin(\phi_1), 1)$, $\mathbf{b}_j = [T_j]\mathbf{b}_1$,

$\mathbf{c}_1 = (c_{1x}, c_{1y}, 1)$, $\mathbf{c}_j = [D_{1j}]\mathbf{c}_1$,

and

$$[D_{1j}] = \begin{bmatrix} \cos\theta_{1j} & -\sin\theta_{1j} & p_{jx} - p_{1x}\cos\theta_{1j} + p_{1y}\sin\theta_{1j} \\ \sin\theta_{1j} & \cos\theta_{1j} & p_{jy} - p_{1x}\sin\theta_{1j} - p_{1y}\cos\theta_{1j} \\ 0 & 0 & 1 \end{bmatrix}, \tag{2.37}$$

$$[T_j] = \begin{bmatrix} \cos(\delta\phi_j) & -\sin(\delta\phi_j) & -b_{0x}\cos(\delta\phi_j) + b_{0y}\sin(\delta\phi_j) + b_{0x} \\ \sin(\delta\phi_j) & \cos(\delta\phi_j) & -b_{0x}\sin(\delta\phi_j) - b_{0y}\cos(\delta\phi_j) + b_{0y} \\ 0 & 0 & 1 \end{bmatrix}. \tag{2.38}$$

Equations 2.35 and 2.36 can be rewritten as Equations 2.39 and 2.40. In Equation 2.39, the variable R_1 represents the length of link $\mathbf{a}_0$-$\mathbf{a}_1$ and the variable R_3 represents the length of link $\mathbf{b}_1$-$\mathbf{c}_1$ in Equation 2.40. The variable R_4 represents the length of link $\mathbf{b}_0$-$\mathbf{b}_1$

$$(\mathbf{a}_j - \mathbf{a}_0)^T(\mathbf{a}_j - \mathbf{a}_0) = R_1^2 \quad j = 2, 3, \ldots . n \tag{2.39}$$

$$(\mathbf{c}_j - \mathbf{b}_j)^T(\mathbf{c}_j - \mathbf{b}_j) = R_3^2 \quad j = 2, 3, \ldots . n \tag{2.40}$$

Since there are four variables in each equation (a_{0x}, a_{0y}, a_{jx}, a_{jy} and b_{jx}, b_{jy}, c_{jx} and c_{jy}), a maximum of five rigid body path points can be prescribed, with no arbitrary choice of parameter for a single phase (see Table 2.4).

In Table 2.4, the **maximum** numbers of prescribed rigid body path points for the adjustable planar five-bar path generator for several phases are given. The number of fixed and moving pivot coordinates for the links to be synthesized (links $\mathbf{a}_0$-$\mathbf{a}_1$ and $\mathbf{b}_1$-$\mathbf{c}_1$) determines the maximum number of rigid body path points. The example problem in Section 6.4 demonstrates the design of a planar and spherical five-bar path generator to achieve a two-phase moving pivot adjustment application.

Table 2.4 Prescribed Rigid Body Position and Phase Variations for the Adjustable Planar Five-Bar Mechanism

		Link $\mathbf{a}_0$-$\mathbf{a}_1$		**Link $\mathbf{b}_1$-$\mathbf{c}_1$**	
Number of phases	Max. # of rigid body	Number of unknowns	Number of free choices	Number of unknowns	Number of free choices
1	5	4	0	6	2
2	8	6	0	8	2
3	11	8	0	10	2
n	5 + 3(n – 1)	2 + 2n	0	6+2(n – 1)	2

In the two-phase, adjustable moving pivot example problem in Section 6.4, the required unknowns are $\mathbf{a}_0$, $\mathbf{a}_1$, $\mathbf{a}_{1n}$, $\mathbf{b}_1$, $\mathbf{c}_1$ and $\mathbf{c}_{1n}$. The unknown variables $\mathbf{a}_0$, $\mathbf{a}_1$, $\mathbf{b}_1$, and $\mathbf{c}_1$ represent the fixed and moving pivots required for the planar five-bar mechanism to achieve the prescribed rigid body path points in phase 1. The unknown variables $\mathbf{a}_{1n}$ and $\mathbf{c}_{1n}$ represent the moving pivot adjustments required to achieve the prescribed rigid body path points in phase 2. Since each of these variables except $\mathbf{b}_1$ has two unknown components, and $\mathbf{b}_1$ has four unknowns (b_{0x}, b_{0y}, R_4 and ϕ), there are a total of 14 variables to determine.

$$\mathbf{a}_0 = (a_{0x}, a_{0y}),\ \mathbf{a}_1 = (a_{1x}, a_{1y}),\ \mathbf{a}_{1n} = (a_{1nx}, a_{1ny}),$$

$$\mathbf{b}_1 = (b_{0x} + R_4\cos(\phi_1),\ b_{0y} + R_4\sin(\phi_1),\ 1),\ \mathbf{c}_1 = (c_{1x}, c_{1y}),\ \mathbf{c}_{1n} = (c_{1nx}, c_{1ny}).$$

Equations 2.41 through 2.45 were used to calculate five of the six unknowns in $\mathbf{a}_0$, $\mathbf{a}_1$ and $\mathbf{a}_{1n}$. The variable a_{0x} and the link length R_1 were specified.

$$([D_{12}]\mathbf{a}_1 - \mathbf{a}_0)^T([D_{12}]\mathbf{a}_1 - \mathbf{a}_0) - R_1^2 = 0 \tag{2.41}$$

$$([D_{13}]\mathbf{a}_1 - \mathbf{a}_0)^T([D_{13}]\mathbf{a}_1 - \mathbf{a}_0) - R_1^2 = 0 \tag{2.42}$$

$$([D_{14}]\mathbf{a}_1 - \mathbf{a}_0)^T([D_{14}]\mathbf{a}_1 - \mathbf{a}_0) - R_1^2 = 0 \tag{2.43}$$

$$([D_{56}]\mathbf{a}_{1n} - \mathbf{a}_0)^T([D_{56}]\mathbf{a}_{1n} - \mathbf{a}_0) - R_1^2 = 0 \tag{2.44}$$

$$([D_{57}]\mathbf{a}_{1n} - \mathbf{a}_0)^T([D_{57}]\mathbf{a}_{1n} - \mathbf{a}_0) - R_1^2 = 0 \tag{2.45}$$

In gear-driven, chain-driven and belt-driven five-bar mechanisms, the driving link angles have a functional relationship (e.g. $\delta\phi = f(\delta\theta) = k*\delta\theta$ in Figure 2.4). This relationship depends on the ratios of the gears, sprockets or pulleys connecting both driving links in the mechanism. To accommodate such drive types for the planar five-bar mechanism, the driving link angle θ must be determined first. After calculating $\mathbf{a}_0$, $\mathbf{a}_1$ and $\mathbf{a}_{1n}$, the driving link angle θ could be determined by the Cosine Law (Equation

2.46). After calculating this angle for every $[D_{1j}]$ position of link $\mathbf{a}_0$-$\mathbf{a}_1$, the user can then establish a $\delta\phi = f(\delta\theta) = k*\delta\theta$ relationship and calculate the other driving link angle ϕ. The angle $\delta\phi$ in Equation 2.38 is the difference between angles ϕ and ϕ_1 in Equation 2.36.

$$\theta_i = \cos^{-1}\left[\frac{\mathbf{u}.\mathbf{v}}{|\mathbf{u}|.|\mathbf{v}|}\right] \quad , \text{ where } \mathbf{u} = \overline{\mathbf{a}_0\mathbf{a}} \text{ , } \mathbf{v} = \overline{\mathbf{b}_0\mathbf{a}_0} \tag{2.46}$$

Equations 2.47 through 2.51 were used to calculate five of the eight unknowns in $\mathbf{b}_1$, $\mathbf{c}_1$ and $\mathbf{c}_{1n}$. The variables b_{0x}, b_{0y}, ϕ (in variable $\mathbf{b}_1$) and the link length R_3 were specified.

$$([D_{12}]\mathbf{c}_1 - [T_1]\mathbf{b}_1)^T([D_{12}]\mathbf{c}_1 - [T_1]\mathbf{b}_1) - R_3^2 = 0 \tag{2.47}$$

$$([D_{13}]\mathbf{c}_1 - [T_2]\mathbf{b}_1)^T([D_{13}]\mathbf{c}_1 - [T_2]\mathbf{b}_1) - R_3^2 = 0 \tag{2.48}$$

$$([D_{14}]\mathbf{c}_1 - [T_3]\mathbf{b}_1)^T([D_{14}]\mathbf{c}_1 - [T_3]\mathbf{b}_1) - R_3^2 = 0 \tag{2.49}$$

$$([D_{56}]\mathbf{c}_{1n} - [T_6]\mathbf{b}_1)^T([D_{56}]\mathbf{c}_{1n} - [T_6]\mathbf{b}_1) - R_3^2 = 0 \tag{2.50}$$

$$([D_{57}]\mathbf{c}_{1n} - [T_7]\mathbf{b}_1)^T([D_{57}]\mathbf{c}_{1n} - [T_7]\mathbf{b}_1) - R_3^2 = 0 \tag{2.51}$$

2.5 Adjustable Planar Five-Bar Motion Generator

The planar five-bar motion generator is illustrated in Figure 2.5. In this work, links $\mathbf{a}_0$-$\mathbf{a}_1$ and $\mathbf{b}_0$-$\mathbf{b}_1$ are the driving links (denoted by driving link angles θ and ϕ). Links $\mathbf{a}_0$-$\mathbf{a}_1$ and $\mathbf{b}_1$-$\mathbf{c}_1$ of the planar five-bar mechanism are synthesized using the constant length condition only. The constant length constraint Equations 2.52 and 2.53 [48,49] are satisfied when synthesizing links $\mathbf{a}_0$-$\mathbf{a}_1$ and $\mathbf{b}_1$-$\mathbf{c}_1$ of the planar five-bar mechanism. The variable R_4 represents the length of link $\mathbf{b}_0$-$\mathbf{b}_1$.

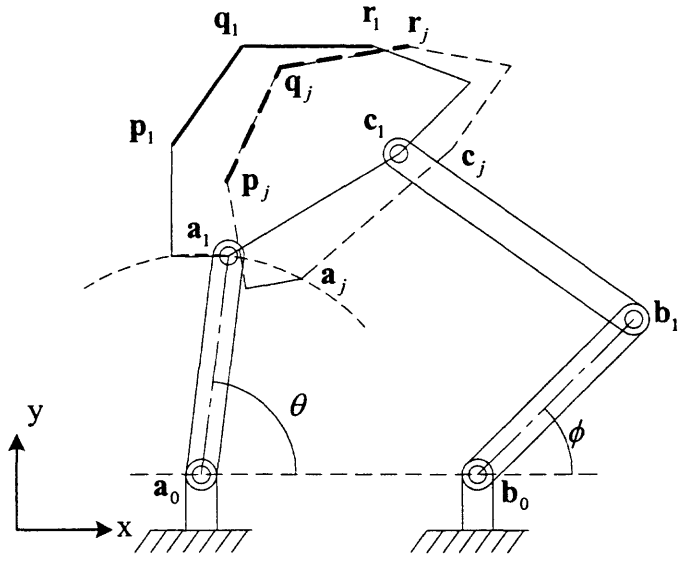

Figure 2.5 Planar five-bar motion generator with driving link angles θ, ϕ and rigid body position points p, q and r.

$$(\mathbf{a}_j - \mathbf{a}_0)^T(\mathbf{a}_j - \mathbf{a}_0) = (\mathbf{a}_1 - \mathbf{a}_0)^T(\mathbf{a}_1 - \mathbf{a}_0) \quad j = 2, 3, \ldots . n \tag{2.52}$$

$$(\mathbf{c}_j - \mathbf{b}_j)^T(\mathbf{c}_j - \mathbf{b}_j) = (\mathbf{c}_1 - \mathbf{b}_1)^T(\mathbf{c}_1 - \mathbf{b}_1) \quad j = 2, 3, \ldots . n \tag{2.53}$$

where

$\mathbf{a}_0 = (a_{0x}, a_{0y}, 1)$, $\mathbf{a}_1 = (a_{1x}, a_{1y}, 1)$, $\mathbf{a}_j = [D_{1j}]\mathbf{a}_1$,

$\mathbf{b}_1 = (b_{0x} + R_4\cos(\phi_1), b_{0y} + R_4\sin(\phi_1), 1)$, $\mathbf{b}_j = [T_j]\mathbf{b}_1$,

$\mathbf{c}_1 = (c_{1x}, c_{1y}, 1)$, $\mathbf{c}_j = [D_{1j}]\mathbf{c}_1$,

and

$$[D_{1j}] = \begin{bmatrix} p_{jx} & q_{jx} & r_{jx} \\ p_{jy} & q_{jy} & r_{jy} \\ 1 & 1 & 1 \end{bmatrix} \begin{bmatrix} p_{1x} & q_{1x} & r_{1x} \\ p_{1y} & q_{1y} & r_{1y} \\ 1 & 1 & 1 \end{bmatrix}^{-1}, \tag{2.54}$$

$$[T_j] = \begin{bmatrix} \cos(\delta\phi_j) & -\sin(\delta\phi_j) & -b_{0x}\cos(\delta\phi_j) + b_{0y}\sin(\delta\phi_j) + b_{0x} \\ \sin(\delta\phi_j) & \cos(\delta\phi_j) & -b_{0x}\sin(\delta\phi_j) - b_{0y}\cos(\delta\phi_j) + b_{0y} \\ 0 & 0 & 1 \end{bmatrix}. \tag{2.55}$$

Equations 2.52 and 2.53 can be rewritten as Equations 2.56 and 2.57. In Equation 2.56, the variable R_1 represents the length of link $\mathbf{a}_0$-$\mathbf{a}_1$ and the variable R_3 represents the length of link $\mathbf{b}_1$-$\mathbf{c}_1$ in Equation 2.57.

$$(\mathbf{a}_j - \mathbf{a}_0)^T(\mathbf{a}_j - \mathbf{a}_0) = R_1^2 \quad j = 2, 3, \ldots . n \tag{2.56}$$

$$(\mathbf{c}_j - \mathbf{b}_j)^T(\mathbf{c}_j - \mathbf{b}_j) = R_3^2 \quad j = 2, 3, \ldots . n \tag{2.57}$$

Equation 2.54 is a rigid body displacement matrix. It is a derivative of the spatial rigid body displacement matrix [48,49]. Given the coordinates for a rigid body in position "i" and the subsequent "j," matrix $[D_{ij}]$ is the transformation matrix required to transform coordinates from position "i" to position "j."Variables **p**, **q** and **r** in Equation 2.54 represent the position of the rigid-body in two-dimensional space. Although the position of a rigid body in two-dimensional space is commonly described by a single point and a displacement angle (**p** and θ for example), the authors chose to describe the rigid body using three points for computational purposes. If the user prefers to describe the rigid body using conventional notation, the displacement matrix in Equation 2.54 can

be replaced with the conventional plane rigid body displacement matrix. Since there are four variables in each equation (a_{0x}, a_{0y}, a_{1x}, a_{0y} and b_{1x}, b_{1y}, c_{1x} and c_{1y}), a maximum of five rigid body positions can be achieved with no arbitrary choice of parameter for a single phase (see Table 2.5).

Points **p, q** and **r** should not all lie on the same line in each rigid body position. Taking this precaution prevents the rows in the rigid body displacement matrix (Equation 2.54) from becoming proportional. With proportional rows, this matrix could not be inverted.

In Table 2.5, the **maximum** numbers of prescribed rigid body positions for the adjustable planar five-bar motion generator for several phases are given. The number of fixed and moving pivot coordinates for the links to be synthesized (links $\mathbf{a}_0$-$\mathbf{a}_1$ and $\mathbf{b}_1$-$\mathbf{c}_1$) determines the maximum number of rigid body positions. The example problem in Section 6.5 demonstrates the design of a planar and spherical five-bar mechanism motion generator to achieve a two-phase moving pivot adjustment application.

Table 2.5 Prescribed Rigid Body Position and Phase Variations for the Adjustable Planar Five-Bar Mechanism

		Link $\mathbf{a}_0$-$\mathbf{a}_1$		**Link $\mathbf{b}_1$-$\mathbf{c}_1$**	
Number of phases	Max. number of rigid body	Number of unknowns	Number of free choices	Number of unknowns	Number of free choices
1	5	4	0	6	2
2	8	6	0	8	2
3	11	8	0	10	2
n	5 + 3(n – 1)	2 + 2n	0	6+2(n – 1)	2

In the two-phase, adjustable moving pivot example problem in Section 6.5, the required unknowns are $\mathbf{a}_0$, $\mathbf{a}_1$, $\mathbf{a}_{1n}$, $\mathbf{b}_1$, $\mathbf{c}_1$ and $\mathbf{c}_{1n}$. The unknown variables $\mathbf{a}_0$, $\mathbf{a}_1$, $\mathbf{b}_1$, and $\mathbf{c}_1$ represent the fixed and moving pivots required for the planar five-bar mechanism to

achieve the prescribed rigid body path points in phase 1. The unknown variables $\mathbf{a}_{1n}$ and $\mathbf{c}_{1n}$ represent the moving pivot adjustments required to achieve the prescribed rigid body path points in phase 2. Since each of these variables except $\mathbf{b}_1$ has two unknown components, and $\mathbf{b}_1$ has four unknowns (b_{0x}, b_{0y}, R_4 and ϕ), there are a total of 14 variables to determine.

$\mathbf{a}_0 = (a_{0x}, a_{0y})$, $\mathbf{a}_1 = (a_{1x}, a_{1y})$, $\mathbf{a}_{1n} = (a_{1nx}, a_{1ny})$,

$\mathbf{b}_1 = (b_{0x} + R_4\cos(\phi_1), b_{0y} + R_4\sin(\phi_1), 1)$, $\mathbf{c}_1 = (c_{1x}, c_{1y})$,

$\mathbf{c}_{1n} = (c_{1nx}, c_{1ny})$.

Equations 2.58 through 2.62 were used to calculate five of the six unknowns in $\mathbf{a}_0$, $\mathbf{a}_1$ and $\mathbf{a}_{1n}$. The variable a_{0x} and the link length R_1 were specified.

$$([D_{12}]\mathbf{a}_1 - \mathbf{a}_0)^T([D_{12}]\mathbf{a}_1 - \mathbf{a}_0) - R_1^2 = 0 \tag{2.58}$$

$$([D_{13}]\mathbf{a}_1 - \mathbf{a}_0)^T([D_{13}]\mathbf{a}_1 - \mathbf{a}_0) - R_1^2 = 0 \tag{2.59}$$

$$([D_{14}]\mathbf{a}_1 - \mathbf{a}_0)^T([D_{14}]\mathbf{a}_1 - \mathbf{a}_0) - R_1^2 = 0 \tag{2.60}$$

$$([D_{56}]\mathbf{a}_{1n} - \mathbf{a}_0)^T([D_{56}]\mathbf{a}_{1n} - \mathbf{a}_0) - R_1^2 = 0 \tag{2.61}$$

$$([D_{57}]\mathbf{a}_{1n} - \mathbf{a}_0)^T([D_{57}]\mathbf{a}_{1n} - \mathbf{a}_0) - R_1^2 = 0 \tag{2.62}$$

In gear-driven, chain-driven and belt-driven five-bar mechanisms, the driving link angles have a functional relationship (e.g. $\delta\phi = f(\delta\theta) = k \cdot \delta\theta$ in Figure 2.5). This relationship depends on the ratios of the gears, sprockets or pulleys connecting both driving links in the mechanism. To accommodate such drive types for the planar five-bar mechanism, the driving link angle θ must be determined first. After calculating $\mathbf{a}_0$, $\mathbf{a}_1$ and $\mathbf{a}_{1n}$, the driving link angle θ could be determined by the Cosine Law (Equation 2.63). After calculating this angle for every $[D_{1j}]$ position of link $\mathbf{a}_0$-$\mathbf{a}_1$, the user can then

establish a $\delta\phi = f(\delta\theta) = k \cdot \delta\theta$ relationship and calculate the other driving link angle ϕ. The angle $\delta\phi$ in Equation 2.55 is the difference between angles ϕ and ϕ_1 in Equation 2.53.

$$\theta_1 = \cos^{-1}\left[\frac{\mathbf{u}.\mathbf{v}}{|\mathbf{u}|.|\mathbf{v}|}\right] \text{ , where } \mathbf{u} = \overline{\mathbf{a}_0\mathbf{a}} \text{ , } \mathbf{v} = \overline{\mathbf{b}_0\mathbf{a}_0} \tag{2.63}$$

Equations 2.64 through 2.68 were used to calculate five of the eight unknowns in $\mathbf{b}_1$, $\mathbf{c}_1$ and $\mathbf{c}_{1n}$. The variables b_{0x}, b_{0y}, ϕ (in variable $\mathbf{b}_1$) and the link length R_3 were specified.

$$([D_{12}]\mathbf{c}_1 - [T_1]\mathbf{b}_1)^T([D_{12}]\mathbf{c}_1 - [T_1]\mathbf{b}_1) - R_3^2 = 0 \tag{2.64}$$

$$([D_{13}]\mathbf{c}_1 - [T_2]\mathbf{b}_1)^T([D_{13}]\mathbf{c}_1 - [T_2]\mathbf{b}_1) - R_3^2 = 0 \tag{2.65}$$

$$([D_{14}]\mathbf{c}_1 - [T_3]\mathbf{b}_1)^T([D_{14}]\mathbf{c}_1 - [T_3]\mathbf{b}_1) - R_3^2 = 0 \tag{2.66}$$

$$([D_{56}]\mathbf{c}_{1n} - [T_6]\mathbf{b}_1)^T([D_{56}]\mathbf{c}_{1n} - [T_6]\mathbf{b}_1) - R_3^2 = 0 \tag{2.67}$$

$$([D_{57}]\mathbf{c}_{1n} - [T_7]\mathbf{b}_1)^T([D_{57}]\mathbf{c}_{1n} - [T_7]\mathbf{b}_1) - R_3^2 = 0 \tag{2.68}$$

CHAPTER 3

ADJUSTABLE SPHERICAL MECHANISMS

This chapter introduces several classifications of adjustable spherical mechanisms. Like adjustable planar mechanisms, adjustable spherical mechanisms can be designed to achieve multiple mechanism configurations (and subsequently multiple phases of prescribed motion, path or function generation parameters) using essentially the same hardware. The particular adjustable spherical mechanisms introduced in this chapter are four-bar motion, path and function generators and adjustable five-bar motion and path generators. This chapter also introduces the displacement equations for spherical four and five-bar mechanisms.

3.1 Adjustable Spherical Four-Bar Path Generator

Figure 3.1 illustrates an adjustable spherical four-bar path generator. Point **p** represents the rigid body point. To achieve the prescribed rigid body curve points in phase I, the moving pivots incorporated are $\mathbf{a}_1$ and $\mathbf{b}_1$. To achieve the prescribed rigid body curve points in phase II, the moving pivots incorporated are $\mathbf{a}_{1n}$ and $\mathbf{b}_{1n}$. Links $\mathbf{a}_0$-$\mathbf{a}_1$ and $\mathbf{a}_0$-$\mathbf{a}_{1n}$ are the designated crank links and links $\mathbf{b}_0$-$\mathbf{b}_1$ and $\mathbf{b}_0$-$\mathbf{b}_{1n}$ are the designated follower links.

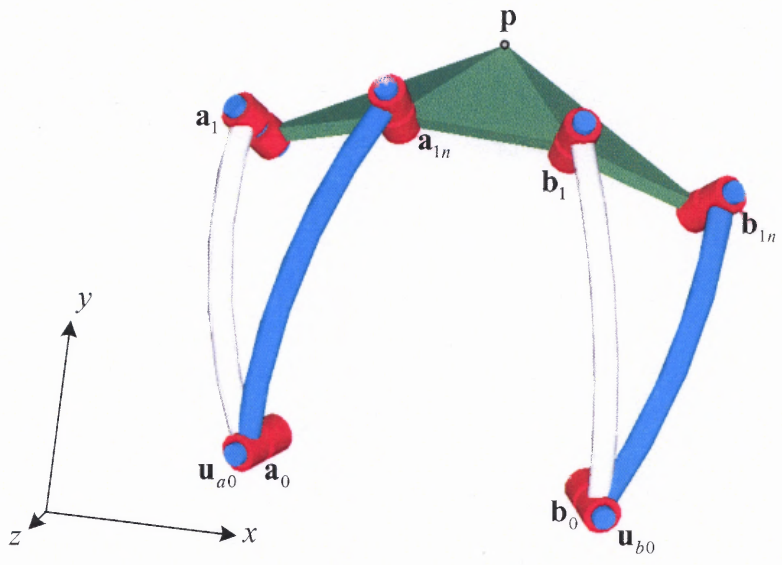

Figure 3.1 The adjustable spherical four-bar path generator.

3.2 Adjustable Spherical Four-Bar Function Generator

Figure 3.2 illustrates an adjustable spherical four-bar function generator. Angles θ and ϕ represent the angular displacements of the crank and follower links. To achieve the prescribed angular displacements in phase I, the moving pivots incorporated are $\mathbf{a}_1$ and $\mathbf{b}_1$. To achieve the prescribed angular displacements in phase II, the moving pivots incorporated are $\mathbf{a}_1$ and $\mathbf{b}_{1n}$. Link $\mathbf{a}_0$-$\mathbf{a}_1$ is the designated crank link and links $\mathbf{b}_0$-$\mathbf{b}_1$ and $\mathbf{b}_0$-$\mathbf{b}_{1n}$ are the designated follower links.

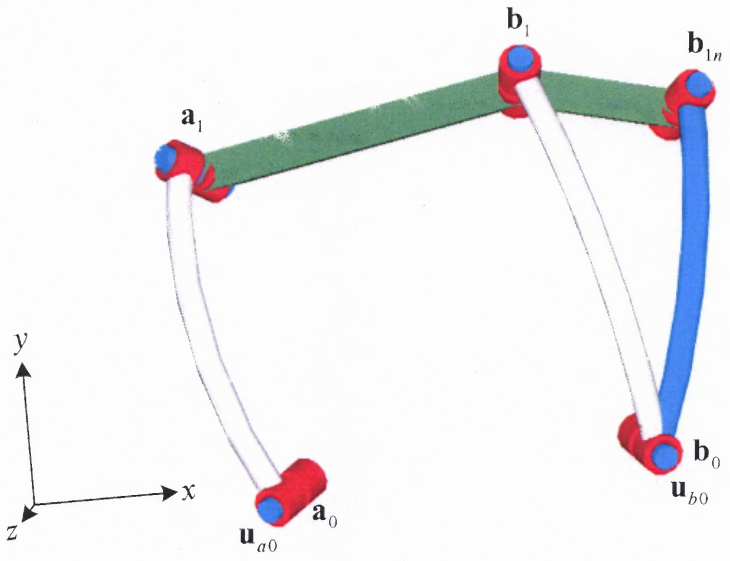

Figure 3.2 The adjustable spherical four-bar function generator.

3.3 Adjustable Spherical Four-Bar Motion Generator

Figure 3.3 illustrates an adjustable spherical four-bar function generator. Points **p**, **q** and **r** represent the position of the rigid body. To achieve the prescribed rigid body position in phase I, the moving pivots incorporated are $\mathbf{a}_1$ and $\mathbf{b}_1$. To achieve the prescribed rigid body positions in phase II, the moving pivots incorporated are $\mathbf{a}_{1n}$ and $\mathbf{b}_{1n}$. Links $\mathbf{a}_0$-$\mathbf{a}_1$ and $\mathbf{a}_0$-$\mathbf{a}_{1n}$ are the designated crank links and links $\mathbf{b}_0$-$\mathbf{b}_1$ and $\mathbf{b}_0$-$\mathbf{b}_{1n}$ are the designated follower links.

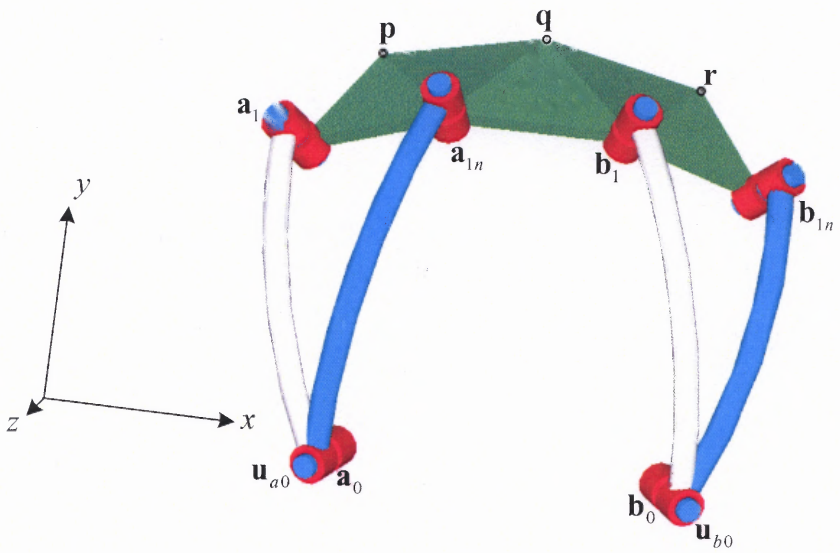

Figure 3.3 The adjustable spherical four-bar motion generator.

3.4 Spherical Four-Bar Mechanism and Rigid Body Displacement Equations

The displacement equations described in this section are associated with the spherical four-bar path, function and motion generators introduced in Sections 3.1, 3.2 and 3.3. The point **p** shown in Figure 3.3 represents a rigid body point on a spherical R-R dyad. The position of point **p** is calculated by Equation 3.1.

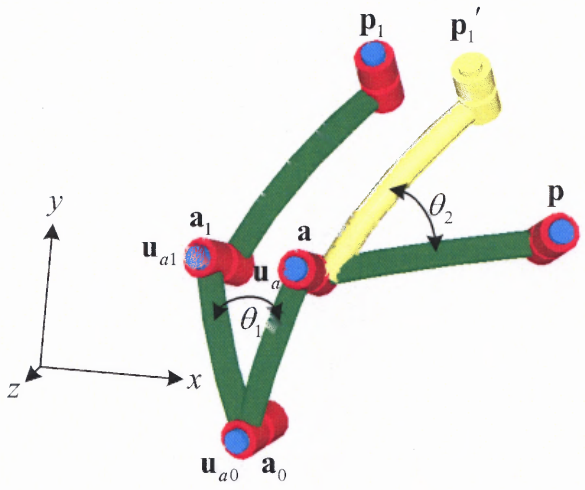

Figure 3.4 Spherical four-bar mechanism R-R dyad.

$$\mathbf{p} = [R_{\theta 2,\, ua}](\mathbf{p}_1' - \mathbf{a}) + \mathbf{a} \tag{3.1}$$

where

$$\mathbf{p}_1' = [R_{\theta 1,\, ua0}](\mathbf{p}_1 - \mathbf{a}_0) + \mathbf{a}_0 \tag{3.2}$$

$$\mathbf{a} = [R_{\theta 1,\, ua0}](\mathbf{a}_1 - \mathbf{a}_0) + \mathbf{a}_0 \tag{3.3}$$

$$\mathbf{u}_a = [R_{\theta 1,\, ua0}]\mathbf{u}_{a1} \tag{3.4}$$

and

$$[R_{\theta,u}] = \begin{bmatrix} u_x^2(1-\cos\theta)+\cos\theta & u_x u_y(1-\cos\theta)-u_z\sin\theta & u_x u_z(1-\cos\theta)+u_y\sin\theta \\ u_x u_y(1-\cos\theta)+u_z\sin\theta & u_y^2(1-\cos\theta)+\cos\theta & u_y u_z(1-\cos\theta)-u_x\sin\theta \\ u_x u_z(1-\cos\theta)-u_y\sin\theta & u_y u_z(1-\cos\theta)+u_x\sin\theta & u_z^2(1-\cos\theta)+\cos\theta \end{bmatrix} \tag{3.5}$$

In this research, dual-number method [50] was used to build the displacement equations for the spherical four-bar mechanism illustrated in Figure 3.5. These displacement equations are given in Equations 3.9 through 3.17. Equations 3.9 through 3.17 are used to calculate angles θ_2 through θ_4 in Figure 3.5. Variable $\theta 1$ is prescribed. When solving for angles $\theta 2$, $\theta 3$, and $\theta 4$, six variables ($\cos(\theta 2)$, $\sin(\theta 2)$, $\cos(\theta 3)$, $\sin(\theta 3)$,

cos(θ4), sin(θ4)) are unknown. Equations 3.9 through 3.14 are used to calculate the six unknown variables in angles θ2, θ3, and θ4.

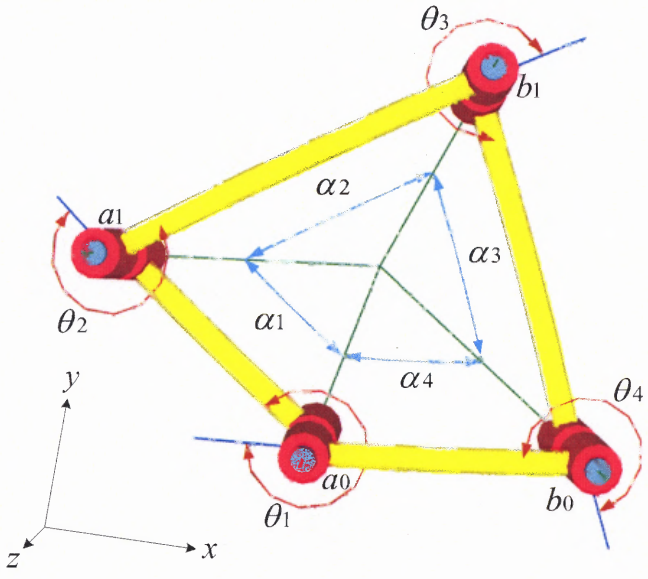

Figure 3.5 Spherical four-bar mechanism with relative joint rotation angles (θ) and joint axis angles (α).

Given

$$ {}^{2}_{3}\hat{M} \cdot {}^{3}_{4}\hat{M} - {}^{1}_{2}\hat{M}^{T} \cdot {}^{4}_{1}\hat{M}^{T} = 0 \tag{3.6} $$

therefore

$$ \begin{bmatrix} z11 & z12 & z13 \\ z21 & z22 & z23 \\ z31 & z32 & z33 \end{bmatrix} = \begin{bmatrix} 0 & 0 & 0 \\ 0 & 0 & 0 \\ 0 & 0 & 0 \end{bmatrix} \tag{3.7} $$

where

$$ {}^{n}_{n+1}\hat{M} = \begin{bmatrix} \cos\theta_n & -\cos\alpha_n \sin\theta_n & \sin\alpha_n \sin\theta_n \\ \sin\theta_n & \cos\alpha_n \cos\theta_n & -\sin\alpha_n \cos\theta_n \\ 0 & \sin\alpha_n & \cos\alpha_n \end{bmatrix} \tag{3.8} $$

$$ z11 = c\theta_2 \cdot c\theta_3 - c\theta_1 \cdot c\theta_4 - c\alpha_2 \cdot s\theta_2 \cdot s\theta_3 + c\alpha_4 \cdot s\theta_1 \cdot s\theta_4 \tag{3.9} $$

$$z12 = -c\alpha_4 \cdot c\theta_4 \cdot s\theta_1 - c\alpha_2 \cdot c\alpha_3 \cdot c\theta_3 \cdot s\theta_2 + s\alpha_2 \cdot s\alpha_3 \cdot s\theta_2 - c\alpha_3 \cdot c\theta_2 \cdot s\theta_3 - c\theta_1 \cdot s\theta_4 \tag{3.10}$$

$$z13 = -s\alpha_4 \cdot s\theta_1 + c\alpha_3 \cdot s\alpha_2 \cdot s\theta_2 + c\alpha_2 \cdot c\theta_3 \cdot s\alpha_3 \cdot s\theta_2 + c\theta_2 \cdot s\alpha_3 \cdot s\theta_3 \tag{3.11}$$

$$z21 = c\alpha_1 \cdot c\theta_4 \cdot s\theta_1 + c\theta_3 \cdot s\theta_2 + c\alpha_2 \cdot c\theta_2 \cdot s\theta_3 + c\alpha_1 \cdot c\alpha_4 \cdot c\theta_1 \cdot s\theta_4 - s\alpha_1 \cdot s\alpha_4 \cdot s\theta_4 \tag{3.12}$$

$$z22 = c\alpha_2 \cdot c\alpha_3 \cdot c\theta_2 \cdot c\theta_3 - c\alpha_1 \cdot c\alpha_4 \cdot c\theta_1 \cdot c\theta_4 - c\theta_2 \cdot s\alpha_2 \cdot s\alpha_3 + c\theta_4 \cdot s\alpha_1 \cdot s\alpha_4 - c\alpha_3 \cdot s\theta_2 \cdot s\theta_3 + c\alpha_1 \cdot s\theta_1 \cdot s\theta_4 \tag{3.13}$$

$$z23 = -c\alpha_4 \cdot s\alpha_1 - c\alpha_3 \cdot c\theta_2 \cdot s\alpha_2 - c\alpha_2 \cdot c\theta_2 \cdot c\theta_3 \cdot s\alpha_3 - c\alpha_1 \cdot c\theta_1 \cdot s\alpha_4 + s\alpha_3 \cdot s\theta_2 \cdot s\theta_3 \tag{3.14}$$

$$z31 = -c\theta_4 \cdot s\alpha_1 \cdot s\theta_1 + s\alpha_2 \cdot s\theta_3 - c\alpha_4 \cdot c\theta_1 \cdot s\alpha_1 \cdot s\theta_4 - c\alpha_1 \cdot s\alpha_4 \cdot s\theta_4 \tag{3.15}$$

$$z32 = c\alpha_4 \cdot c\theta_1 \cdot c\theta_4 \cdot s\alpha_1 + c\alpha_3 \cdot c\theta_3 \cdot s\alpha_2 + c\alpha_2 \cdot s\alpha_3 + c\alpha_1 \cdot c\theta_4 \cdot s\alpha_4 - s\alpha_1 \cdot s\theta_1 \cdot s\theta_4 \tag{3.16}$$

$$z33 = c\alpha_2 \cdot c\alpha_3 - c\alpha_1 \cdot c\alpha_4 - c\theta_3 \cdot s\alpha_2 \cdot s\alpha_3 + c\theta_1 \cdot s\alpha_1 \cdot s\alpha_4 \tag{3.17}$$

In Equations 3.9 through 3.17, variables "cθ" and "sθ" represent cos(θ) and sin(θ) respectively and variables "cα" and "sα" represent cos(α) and sin(α), respectively.

3.5 Adjustable Spherical Five-Bar Path Generator

Figure 3.6 illustrates an adjustable spherical five-bar path generator. Point **p** represents the rigid body point. To achieve the prescribed rigid body curve points in phase I, the moving pivots incorporated are $\mathbf{a}_1$ and $\mathbf{c}_1$. To achieve the prescribed rigid body curve points in phase II, the moving pivots incorporated are $\mathbf{a}_{1n}$ and $\mathbf{c}_{1n}$. Links $\mathbf{a}_0$-$\mathbf{a}_1$, $\mathbf{a}_0$-$\mathbf{a}_{1n}$ and $\mathbf{b}_0$-$\mathbf{b}_1$ are the designated crank links.

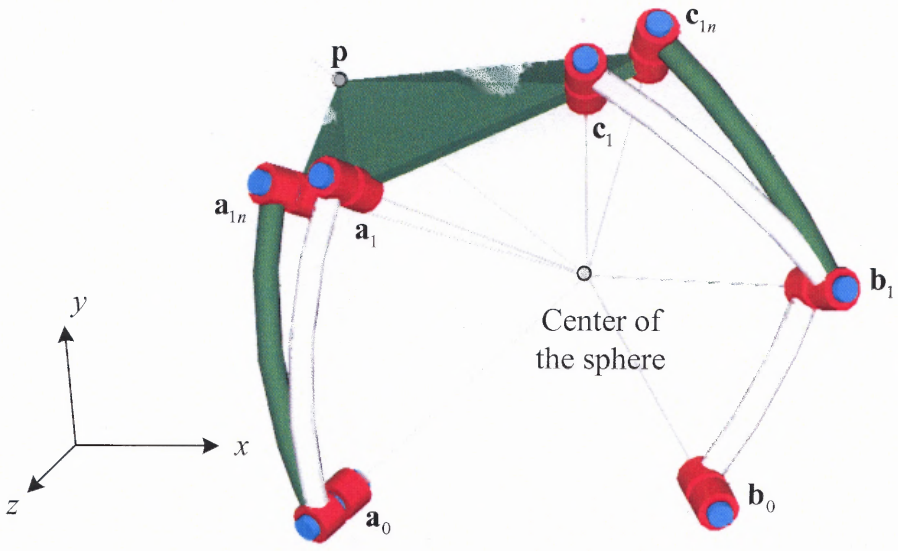

Figure 3.6 The adjustable spherical five-bar path generator.

3.6 Adjustable Spherical Five-Bar Motion Generator

Figure 3.7 illustrates an adjustable spherical five-bar path generator. Points **p**, **q** and **r** represent the position of the rigid body. To achieve the prescribed rigid body curve points in phase I, the moving pivots incorporated are $\mathbf{a}_1$ and $\mathbf{c}_1$. To achieve the prescribed rigid body curve points in phase II, the moving pivots incorporated are $\mathbf{a}_{1n}$ and $\mathbf{c}_{1n}$. Links $\mathbf{a}_0$-$\mathbf{a}_1$, $\mathbf{a}_0$-$\mathbf{a}_{1n}$, and $\mathbf{b}_b$-$\mathbf{b}_1$ are the designated crank links.

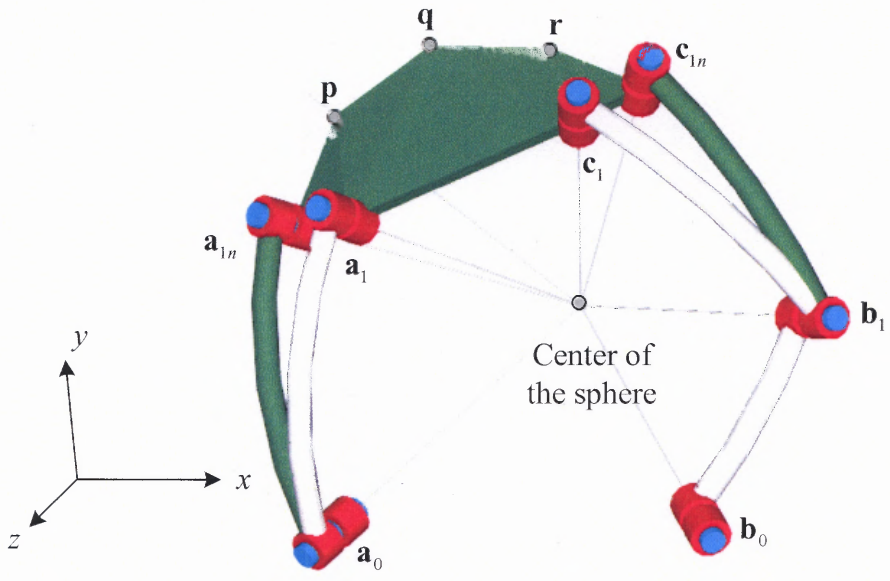

Figure 3.7 The five-bar motion generator.

3.7 Spherical Five-Bar Mechanism and Rigid Body Displacement Equations

The displacement equations described in this section are associated with the spherical five-bar path and motion generators introduced in Sections 3.6 and 3.7. The point **p** shown in Figure 3.8 represents a rigid body point on a spherical R-R dyad. The position of point **p** is calculated by Equation 3.18.

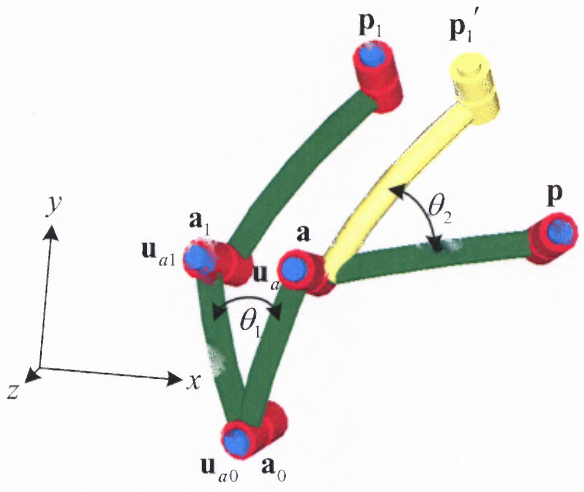

Figure 3.8 Spherical five-bar mechanism R-R dyad.

$$\mathbf{p} = [R_{\theta 2,\, ua}](\mathbf{p}_1' - \mathbf{a}) + \mathbf{a} \tag{3.18}$$

where

$$\mathbf{p}_1' = [R_{\theta 1,\, ua0}](\mathbf{p}_1 - \mathbf{a}_0) + \mathbf{a}_0 \tag{3.19}$$

$$\mathbf{a} = [R_{\theta 1,\, ua0}](\mathbf{a}_1 - \mathbf{a}_0) + \mathbf{a}_0 \tag{3.20}$$

$$\mathbf{u}_a = [R_{\theta 1,\, ua0}]\mathbf{u}_{a1} \tag{3.21}$$

and

$$[R_{\theta,u}] = \begin{bmatrix} u_x^2(1-\cos\theta)+\cos\theta & u_x u_y(1-\cos\theta)-u_z\sin\theta & u_x u_z(1-\cos\theta)+u_y\sin\theta \\ u_x u_y(1-\cos\theta)+u_z\sin\theta & u_y^2(1-\cos\theta)+\cos\theta & u_y u_z(1-\cos\theta)-u_x\sin\theta \\ u_x u_z(1-\cos\theta)-u_y\sin\theta & u_y u_z(1-\cos\theta)+u_x\sin\theta & u_z^2(1-\cos\theta)+\cos\theta \end{bmatrix} \tag{3.22}$$

In this research, dual-number method [50] was used to build the displacement equations for the spherical four-bar mechanism illustrated in Figure 3.9. These displacement equations are given in Equations 3.26 through 3.34. Equations 3.26 through 3.33 are used to calculate angles θ_2 through θ_5 in Figure 3.5. Variable $\theta 1$ is prescribed. When solving for angles $\theta 2$, $\theta 3$, and $\theta 4$, eight variables ($\cos(\theta 2)$, $\sin(\theta 2)$,

cos(θ3), sin(θ3), cos(θ4), sin(θ4), cos(θ5), sin(θ5)) are unknown. Equations 3.26 through 3.33 are used to calculate the six unknown variables in angles θ2, θ3, θ4, and θ5.

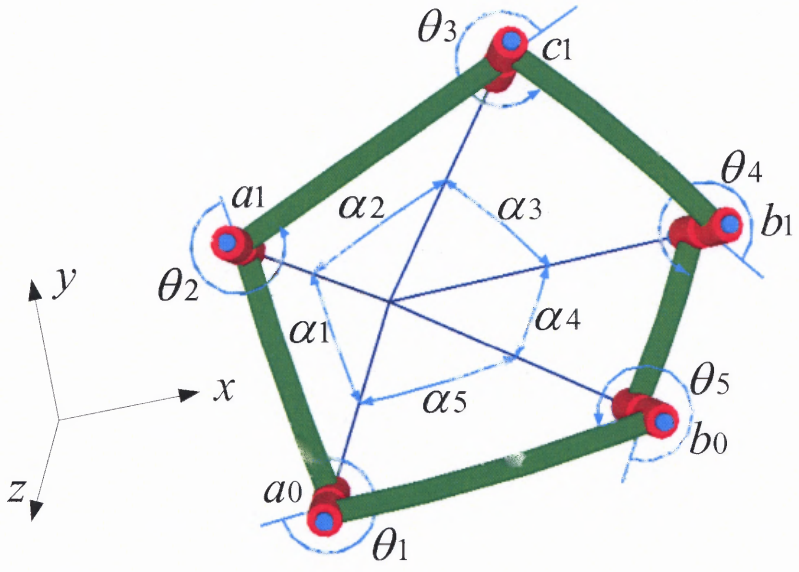

Figure 3.9 Spherical five-bar mechanism with relative joint rotation angles (θ) and joint axis angles (α).

Given

$$ {}^{2}_{3}\hat{M} \cdot {}^{3}_{4}\hat{M} - {}^{1}_{2}\hat{M}^{T} \cdot {}^{5}_{1}\hat{M}^{T} \cdot {}^{4}_{5}\hat{M}^{T} = 0 \tag{3.23} $$

therefore

$$ \begin{bmatrix} z11 & z12 & z13 \\ z21 & z22 & z23 \\ z31 & z32 & z33 \end{bmatrix} = \begin{bmatrix} 0 & 0 & 0 \\ 0 & 0 & 0 \\ 0 & 0 & 0 \end{bmatrix} \tag{3.24} $$

where

$$ {}^{n}_{n+1}\hat{M} = \begin{bmatrix} \cos\theta_n & -\cos\alpha_n \sin\theta_n & \sin\alpha_n \sin\theta_n \\ \sin\theta_n & \cos\alpha_n \cos\theta_n & -\sin\alpha_n \cos\theta_n \\ 0 & \sin\alpha_n & \cos\alpha_n \end{bmatrix} \tag{3.25} $$

$$z11 = c\theta_2\ c\theta_3 - c\alpha_2\ s\theta_2\ s\theta_3 - s\alpha_4\ s\alpha_5\ s\theta_1\ s\theta_4 + c\alpha_4\ s\theta_4(c\alpha_5\ c\theta_5\ s\theta_1 + c\theta_1\ s\theta_5)$$

$$-c\theta_4(c\theta_1\ c\theta_5 - c\alpha_5\ s\theta_1\ s\theta_5) \tag{3.26}$$

$$z12 = c\theta_4\ s\alpha_4\ s\alpha_5\ s\theta_1 - c\alpha_2\ c\alpha_3\ c\theta_3\ s\theta_2 + s\alpha_2\ s\alpha_3\ s\theta_2 - c\alpha_3\ c\theta_2\ s\theta_3 -$$

$$c\alpha_4\ c\theta_4(c\alpha_5\ c\theta_5\ s\theta_1 + c\theta_1\ s\theta_5) - s\theta_4(c\theta_1\ c\theta_5 - c\alpha_5\ s\theta_1\ s\theta_5) \tag{3.27}$$

$$z13 = -c\alpha_4\ s\alpha_5\ s\theta_1 + c\alpha_3\ s\alpha_2\ s\theta_2 + c\alpha_2\ c\theta_3\ s\alpha_3\ s\theta_2 +$$

$$c\theta_2\ s\alpha_3\ s\theta_3 - s\alpha_4(c\alpha_5\ c\theta_5\ s\theta_1 + c\theta_1\ s\theta_5) \tag{3.28}$$

$$z21 = c\theta_3\ s\theta_2 + c\alpha_2\ c\theta_2\ s\theta_3 - s\alpha_4(c\alpha_5\ s\alpha_1 + c\alpha_1\ c\theta_1\ s\alpha_5)s\theta_4 -$$

$$c\theta_4(-c\alpha_1\ c\theta_5\ s\theta_1 - c\alpha_1\ c\alpha_5\ c\theta_1\ s\theta_5 + s\alpha_1\ s\alpha_5\ s\theta_5) +$$
$$c\alpha_4\ s\theta_4(c\alpha_1\ c\alpha_5\ c\theta_1\ c\theta_5 - c\theta_5\ s\alpha_1\ s\alpha_5 - c\alpha_1\ s\theta_1\ s\theta_5) \tag{3.29}$$

$$z22 = c\alpha_2\ c\alpha_3\ c\theta_2\ c\theta_3 - c\theta_2\ s\alpha_2\ s\alpha_3 + c\theta_4\ s\alpha_4(c\alpha_5\ s\alpha_1 + c\alpha_1\ c\theta_1\ s\alpha_5) -$$

$$c\alpha_3\ s\theta_2\ s\theta_3 - s\theta_4(-c\alpha_1\ c\theta_5\ s\theta_1 - c\alpha_1\ c\alpha_5\ c\theta_1\ s\theta_5 + s\alpha_1\ s\alpha_5\ s\theta_5) -$$
$$c\alpha_4\ c\theta_4(c\alpha_1\ c\alpha_5\ c\theta_1\ c\theta_5 - c\theta_5\ s\alpha_1\ s\alpha_5 - c\alpha_1\ s\theta_1\ s\theta_5) \tag{3.30}$$

$$z23 = -c\alpha_3\ c\theta_2\ s\alpha_2 - c\alpha_2\ c\theta_2\ c\theta_3\ s\alpha_3 - c\alpha_4(c\alpha_5\ s\alpha_1 + c\alpha_1\ c\theta_1\ s\alpha_5) +$$

$$s\alpha_3\ s\theta_2\ s\theta_3 - s\alpha_4(c\alpha_1\ c\alpha_5\ c\theta_1\ c\theta_5 - c\theta_5\ s\alpha_1\ s\alpha_5 - c\alpha_1\ s\theta_1\ s\theta_5) \tag{3.31}$$

$$z31 = s\alpha_2\ s\theta_3 - s\alpha_4(c\alpha_1\ c\alpha_5 - c\theta_1\ s\alpha_1\ s\alpha_5)s\theta_4 -$$

$$c\theta_4(c\theta_5\ s\alpha_1\ s\theta_1 + c\alpha_5\ c\theta_1\ s\alpha_1\ s\theta_5 + c\alpha_1\ s\alpha_5\ s\theta_5) +$$
$$c\alpha_4\ s\theta_4(-c\alpha_5\ c\theta_1\ c\theta_5\ s\alpha_1 - c\alpha_1\ c\theta_5\ s\alpha_5 + s\alpha_1\ s\theta_1\ s\theta_5) \tag{3.32}$$

$$z32 = c\alpha_3\ c\theta_3\ s\alpha_2 + c\alpha_2\ s\alpha_3 + c\theta_4\ s\alpha_4(c\alpha_1\ c\alpha_5 - c\theta_1\ s\alpha_1\ s\alpha_5) -$$

$$s\theta_4(c\theta_5\ s\alpha_1\ s\theta_1 + c\alpha_5\ c\theta_1\ s\alpha_1\ s\theta_5 + c\alpha_1\ s\alpha_5\ s\theta_5) -$$
$$c\alpha_4\ c\theta_4(-c\alpha_5\ c\theta_1\ c\theta_5\ s\alpha_1 - c\alpha_1\ c\theta_5\ s\alpha_5 + s\alpha_1\ s\theta_1\ s\theta_5) \tag{3.33}$$

$$z33 = c\alpha_2\ c\alpha_3 - c\theta_3\ s\alpha_2\ s\alpha_3 - c\alpha_4(c\alpha_1\ c\alpha_5 - c\theta_1\ s\alpha_1\ s\alpha_5) -$$

$$s\alpha_4(-c\alpha_5\ c\theta_1\ c\theta_5\ s\alpha_1 - c\alpha_1\ c\theta_5\ s\alpha_5 + s\alpha_1\ s\theta_1\ s\theta_5) \tag{3.34}$$

In Equations 3.26 through 3.34, variables "$c\theta$" and "$s\theta$" represent $\cos(\theta)$ and $\sin(\theta)$ respectively and variables "$c\alpha$" and "$s\alpha$" represent $\cos(\alpha)$ and $\sin(\alpha)$, respectively.

CHAPTER 4

PLANE-TO-SPHERE AND SPHERE-TO-PLANE PROJECTION METHODS

This chapter introduces the plane-to-sphere and sphere-to-plane projection used to design spherical mechanisms (given planar mechanisms) and planar mechanisms (given spherical mechanisms) respectively. In plane-to-sphere projection, each joint coordinate of a planar mechanism is projected on the surface of a specified sphere. In sphere-to-plane projection, each joint coordinate of a spherical mechanism is projected on a specified plane. The chapter also includes an optimization method to minimize the structural error in plane-to-sphere projections.

4.1 Plane-to-Sphere and Sphere-to-Plane Projection Methods

The joints and rigid body points of a planar mechanism could be projected on the surface of a sphere. Figures 4.1 and 4.2 illustrate the projection of a point on a plane (x_p,y_p,z_p) to a point on the surface of a sphere (x_s,y_s,z_s). The projection line passes through the center of the sphere (the global origin). As Figures 4.1 and 4.2 illustrate, the plane that the point lies on (and ultimately the planar mechanism) is parallel to the x-y plane of the global coordinate system and is offset from the x-y plane by a distance "d" along the z-axis.

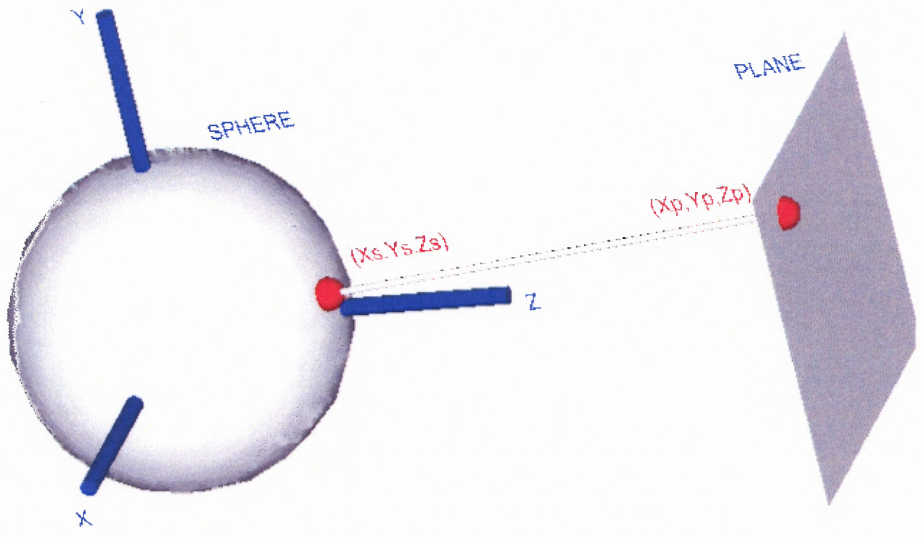

Figure 4.1 Plane-to-Sphere projection.

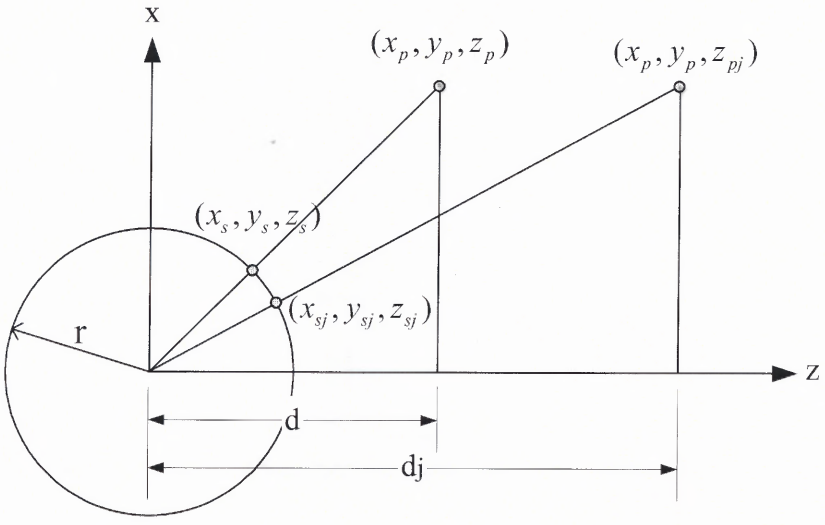

Figure 4.2 Plane-to-Sphere projection in X-Z plane.

The equation for the plane is given in Equation 4.1. The projection length "d" is the distance between the center of the sphere and the plane. The center of the sphere is coincident with global origin and the surface of the sphere is represented by the Equation

4.2 where variable "r" is the radius of the sphere. The projection line from the point on the plane (x_p,y_p,z_p) to center of the sphere is represented by Equation 4.3. The point of intersection between the projection line and the surface of the sphere (x_s,y_s,z_s) is expressed in Equation 4.4.

$$z = d \tag{4.1}$$

$$x^2 + y^2 + z^2 = r^2,\ r \le d \tag{4.2}$$

$$\begin{cases} x = x_p \cdot t \\ y = y_p \cdot t \\ z = z_p \cdot t = d \cdot t \end{cases},\ t \in R \tag{4.3}$$

$$\begin{cases} x_s = x_p \cdot t \\ y_s = y_p \cdot t \\ z_s = d \cdot t \end{cases},\ \text{where } t = \frac{\sigma \cdot r}{\sqrt{d^2 + x_p^{\,2} + y_p^{\,2}}},\ \text{and } \sigma = \pm 1 \text{ is a sign variable} \tag{4.4}$$

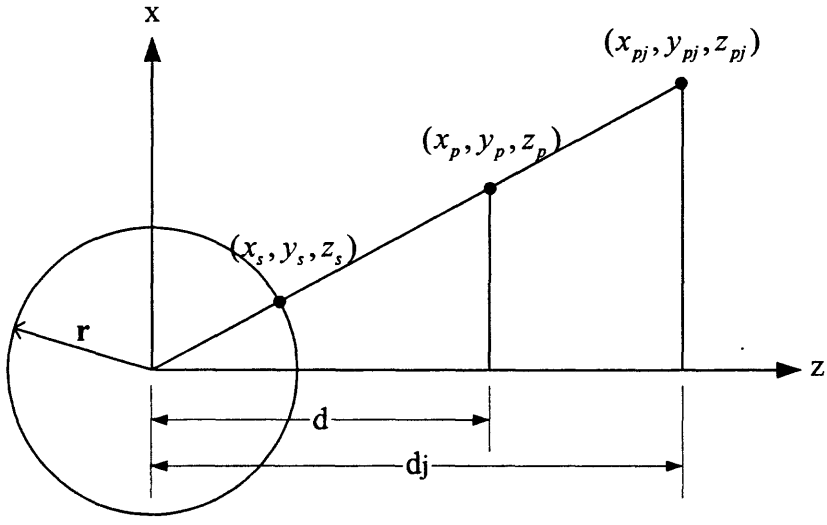

Figure 4.3 Sphere-to-Plane projection in X-Z plane.

The joints and rigid body points of a spherical mechanism could be projected on a plane. Figure 4.3 illustrates the projection of a point on a sphere (x_s,y_s,z_s) to a point on a plane (x_p,y_p,z_p). Again, the projection line passes through the center of the sphere (the global origin). As Figure 4.3 illustrates, the origin of the sphere that the point lies on (and ultimately the spherical mechanism) is coincident with the origin of the global coordinate system and the projection plane is offset from the x-y plane by a distance "d" along the z-axis.

The projection line from the center of the sphere to the point on the sphere (x_s,y_s,z_s) and the point of intersection between the projection line and the plane (x_p,y_p,z_p) is expressed in Equation 4.5.

$$\begin{cases} x_p = k \cdot x_s \\ y_p = k \cdot y_s \\ z_p = k \cdot z_s = d, \ then \ \ k = d / z_s \end{cases} \tag{4.5}$$

4.2 Structural Error Calculation

4.2.1 Structural Error Calculation for Path Generation

In this work, the structural error in path generation is the difference between the prescribed rigid body path points and the points achieved by the synthesized path generator. In Figure 4.4, the structural error S_{err} (Equation 4.6) is the magnitude of the difference between the prescribed points (p_p) and those achieved by the synthesized mechanism (p_g).

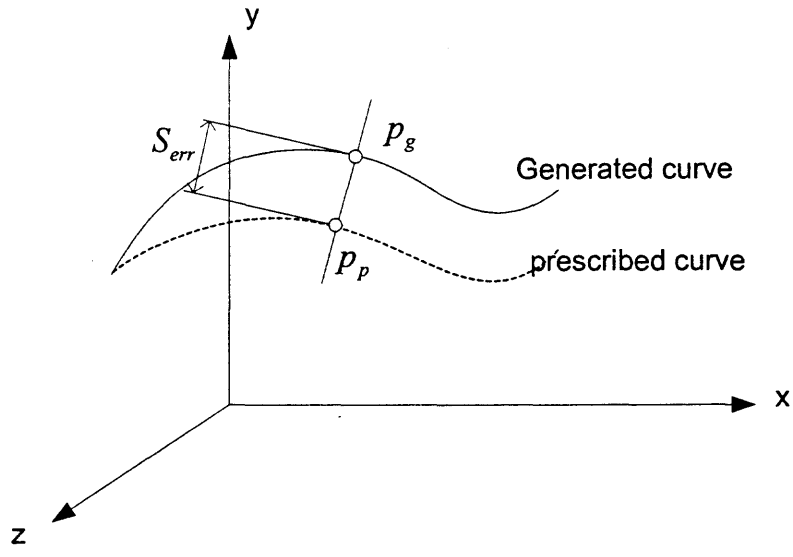

Figure 4.4 Structural error in path generation.

$$S_{err} = \sqrt{(p_{px} - p_{gx})^2 + (p_{py} - p_{gy})^2 + (p_{pz} - p_{gz})^2} \tag{4.6}$$

The magnitude of the projection offset distance "d" and the radius of the sphere determines the overall scale of the synthesized. For example, as "d" gets larger (for a fixed sphere radius "r") the overall scale of the projected spherical mechanism decreases as well. The structural error is multiplied by the projection length in sphere-to-plane projection to enable the user to compare structural errors for spherical mechanisms at different projection-offset distances. The structural error is divided by the projection length in plane-to-sphere projection to enable the user to compare structural errors for spherical mechanisms at different projection offset distances.

4.2.2 Structural Error Calculation for Motion Generation

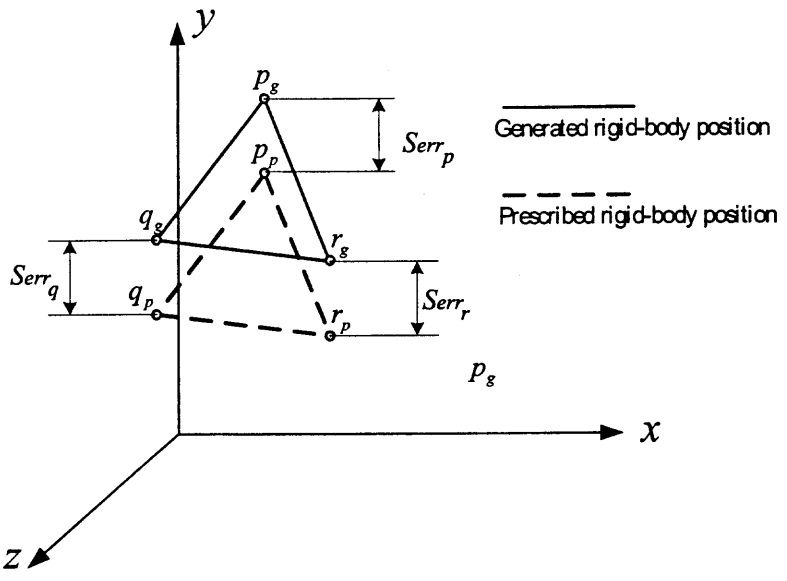

Figure 4.5 Structural error in motion generation.

In this work, the structural error in motion generation is the difference between the prescribed rigid body positions and those points achieved by the synthesized motion generator. In Figure 4.5, the structural error S_{err} (Equation 4.7) is the magnitude of the average difference between the prescribed positions ($\mathbf{p}_p$, $\mathbf{q}_p$, $\mathbf{r}_p$) and those achieved by the synthesized mechanism ($\mathbf{p}_g$, $\mathbf{q}_g$, $\mathbf{r}_g$).

$$S_{err} = (Serr_p + Serr_q + Serr_r)/3 = (\sqrt{(p_{px} - p_{gx})^2 + (p_{py} - p_{gy})^2 + (p_{pz} - p_{gz})^2} +$$

$$\sqrt{(q_{px} - q_{gx})^2 + (q_{py} - q_{gy})^2 + (q_{pz} - q_{gz})^2} +$$

$$\sqrt{(r_{px} - r_{gx})^2 + (r_{py} - r_{gy})^2 + (r_{pz} - r_{gz})^2})/3 \qquad (4.7)$$

The magnitude of the projection offset distance "d" and the radius of the sphere determines the overall scale of the synthesized. For example, as "d" gets larger (for a fixed sphere radius "r") the overall scale of the projected spherical mechanism decreases

as well. The structural error is multiplied by the projection length in sphere-to-plane projection to enable the user to compare structural errors for spherical mechanisms at different projection-offset distances. The structural error is divided by the projection length in plane-to-sphere projection to enable the user to compare structural errors for spherical mechanisms at different projection offset distances.

CHAPTER 5

COMPUTER MODEL FOR OPTIMIZATION METHOD

This chapter introduces the algorithms and codified models of plane-to-sphere projection and optimization methods. The mathematical analysis software MATHEMATICA was used to build and implement the models. Using the codified models, the user can project the joint coordinates of a given planar mechanism onto a sphere and determine the optimum projection length to minimize the structural error of the resulting spherical mechanism.

5.1 Optimization Method for Plane-to-Sphere Projection Method

The author used the mathematical analysis software MATHEMATICA to codify the plane-to-sphere projection and optimization method. Figure 5.1 illustrates the flowchart of the computer models. This research also includes the MATHEMATICA models used in this work to design adjustable spherical motion, path and function generators (see Appendix B). The adjustable path generation MATHEMATICA model (for spherical four-bar mechanisms) is used as an example in this section.

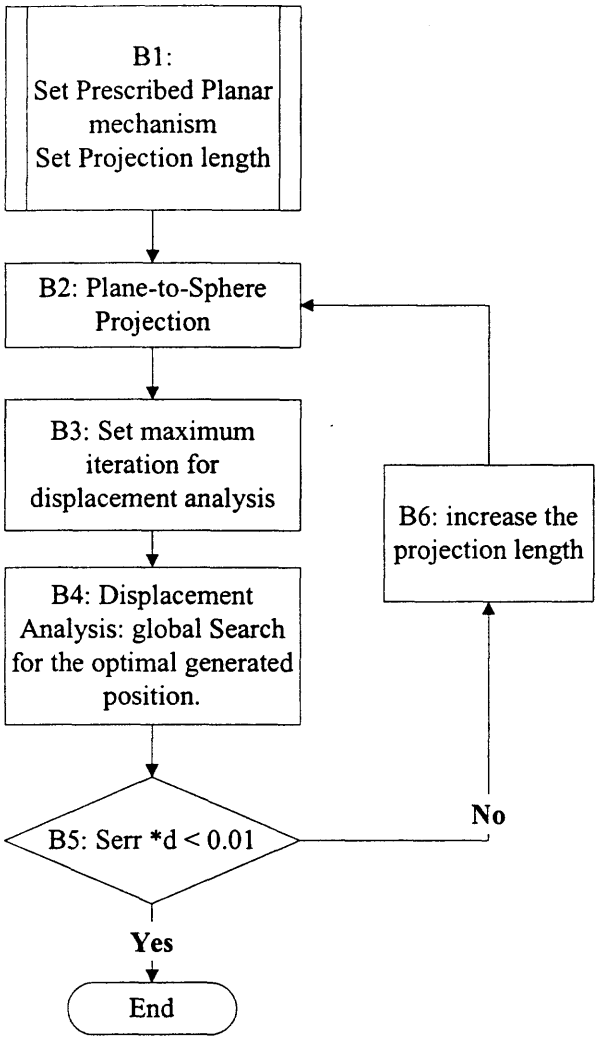

Figure 5.1 Flowchart for MATHEMATICA models.

In block 1 of the flowchart (part 1 of Section 5.2), the user provides the prescribed planar rigid body points and the fixed and moving pivots of the synthesized planar four-bar path generator. Because it would be most likely that only the prescribed **spherical** rigid body points would be available in spherical path generation applications, the spherical points must be projected onto a plane using the sphere-to-plane projection method. The MATHEMATICA model of the plane-to-sphere projection method is provided in Section 5.2. Performing the projection would convert the spherical points

into planar points-making them compatible with planar path generation methods. When the prescribed planar rigid body points are calculated, the user can synthesize a planar path generator using the synthesis method provided in Section 2.1 or any other adjustable path generation method available.

In block 2 of the flowchart (part 2 of Section 5.2), the planar rigid body points and the fixed and moving pivots of the synthesized planar path generator are projected onto a sphere. The radius of the sphere, projection length and the number of solution iterations are user-defined.

Blocks 3, 4 and 5 (parts 3 through 6 in Section 5.2) represent an iterative procedure in which the structural error between the rigid body points achieved by the adjustable spherical path generator and the prescribed rigid body points of this mechanism is calculated. The user must determine whether the structural error calculated is sufficient by comparing it to an acceptable error value. If the calculated error is not acceptable, the user increases the projection length and recalculates the structural error. As demonstrated in the example problems throughout Chapter 6, structural error decreases with respect to an increasing projection length (in motion, path and function generation). If the error is acceptable, the end result would be an adjustable spherical path generator that approximates the prescribed rigid body points within the desired structural error.

Figure 5.2 illustrates parts 3 through 6 in Section 5.2. This figure is a detailed flowchart of blocks 3 and 4 in Figure 5.1. The kinematic parameters of the spherical path generator are calculated in blocks 1 through 3 of Figure 5.2. These parameters include the input and output crank angles and the orientation angles of the intermediate links of

the spherical mechanism. The kinematic parameters are used as initial positions of the mechanism for displacement analysis. In part 4 of Section 5.2, lines 39 through 54 are the codified Dual Number [50] displacement equations for the spherical four-bar mechanism.

Blocks 4 and 5 in Figure 5.2 represent lines 57 through 70 in Section 5.2. The spherical mechanism is displaced a full crank rotation incrementally using the codified Dual Number equations. Block 5 in Figure 5.2 represents lines 61 through 70 in Section 5.2. All of the crank displacement angles and intermediate link displacement angles are tabulated. Block 6 in Figure 5.2 represents the part 5 of Section 5.2, where the displacement equations are defined. Using the tabulated displacement angles of the spherical path generator, the calculated link lengths and initial position angles, the location of the moving pivot (**a**) and the rigid body points are calculated for each increment of the displacement cycle of the spherical mechanism in part 5 of Section 5.2.

Block 7 in Figure 5.2 represents part 6 in Section 5.2, where lines 82 through 85 search for the optimal position of the rigid body points for the last position of a phase. Minimizing the last position of a phase is necessary since it carries the greatest structural error. The result of part 6 are rigid body points for each increment of the displacement cycle of the spherical path generator. In lines 86 and 87 of Section 5.2, the structural error between each of the tabulated rigid body point and each prescribed rigid body point and the minimum error is displayed. If the calculated structural error is greater than desired, the user can increase the projection length in line 3 of Section 5.2 and recalculate a new structural error. By increasing the projection length gradually over a range and

calculating the structural error for each projection length, the structural error plots in the example problems throughout Chapter 6 were generated.

As written, the model in Section 5.2 will calculate the structural error for rigid body point 4 (the rigid body point variables for position 4 or "p4" are used in line 81 in Section 5.2). To calculate the structural error of another position, the **p** variable in line 81 of the model in Section 5.2 must be replaced with those of the desired position (for example, for position "n" the variable must be "pn").

To achieve the rigid body points in phase 1 for the spherical four-bar path generator, the moving pivots $\mathbf{a}_1$ and $\mathbf{b}_1$ are used and the moving pivots $\mathbf{a}_{1n}$ and $\mathbf{b}_{1n}$ are used to achieve the positions in phase 2. As written, the model in Section 5.2 incorporates the phase 1 moving pivots in lines 28 through 35. To incorporate the phase 2 moving pivots ($\mathbf{a}_{1n}$ and $\mathbf{b}_{1n}$), the user must replace variable "a1" and "b1" with "a1n" and "b1n" in lines 28 through 35.

In this section, the MATHEMATICA model for adjustable spherical four-bar path generation in Appendix B.1 is used as an example. The MATHEMATICA models for adjustable spherical four-bar function and motion generation are given in Appendix B.2 and B.3, respectively. The MATHEMATICA models for adjustable spherical five-bar path and motion generation are given in Appendix B.4 and B.5, respectively.

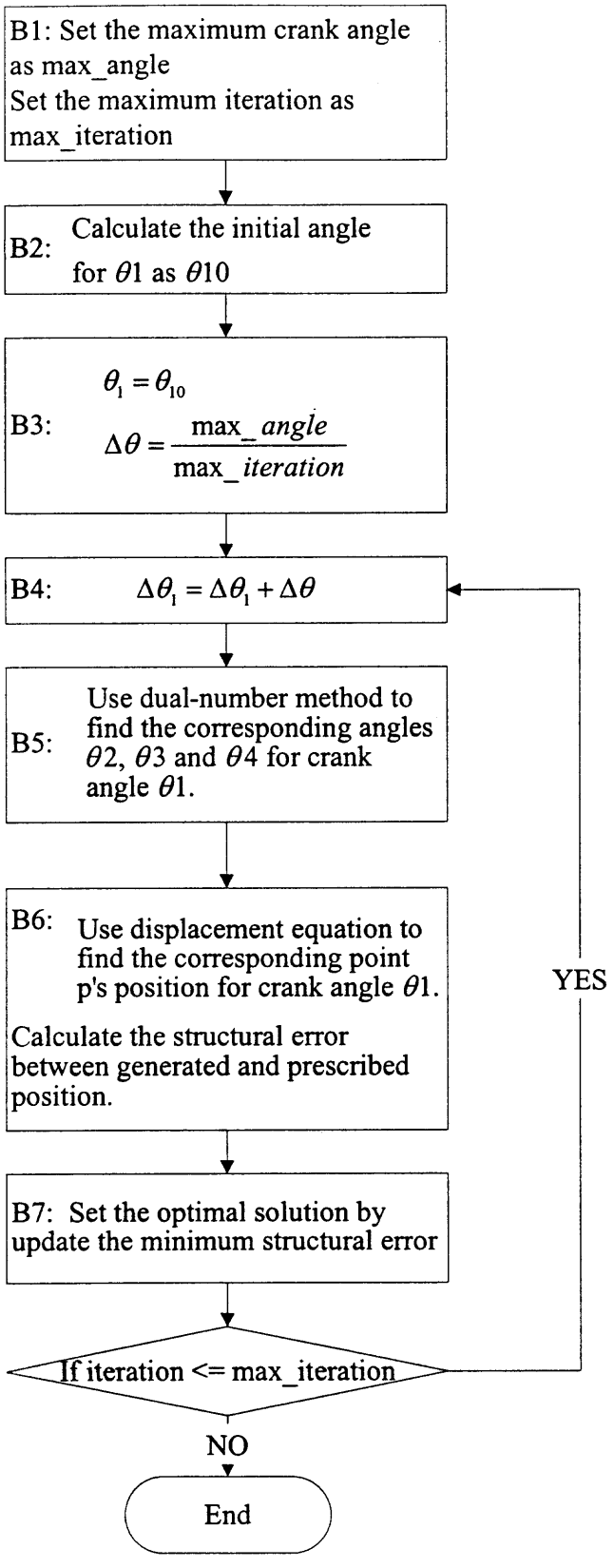

Figure 5.2 Detailed flow chart of blocks 3 and 4 in Figure 5.1.

5.2 MATHEMATICA Model of Plane-to-Sphere Projection and Optimization for Adjustable Spherical Four-Bar Path Generator

The following MATHEMATICA model illustrates the plane-to-sphere projection method for four-bar path generator. The model was divided into six parts and that could make the model more readable.

Part 1: User-defined problem input

```
1.    TheMaxIterations=500;
2.    ProjLength=7
3.    RadofSphere=1;
4.    Plane2Sphere[{x_,y_},r_,d_]:={r*x/Sqrt[d^2+x^2+y^2],r*y/Sqrt[d^2+
      x^2+y^2],r*d/Sqrt[d^2+x^2+y^2]}
5.    p1p={-0.6953,1.2291};p2p={-0.6019,1.3026};
6.    p3p={-0.5020,1.3675};p4p={-0.3964,1.4233};
7.    p5p={-0.6953,1.2291};p6p={-0.5883,1.2796};
8.    p7p={-0.4774,1.3193};
9.    a0p={0.0000,-0.0092378};
10.   a1p={-0.76744,0.63171};
11.   a1np={-0.45554,0.88092};
12.   b0p={1.0000,-0.016575};
13.   b1p={0.58693,1.4253};
14.   b1np={1.0472,1.4827};
```

Part 2: Plane-to-sphere projection

```
15.   p1=Plane2Sphere[p1p,RadofSphere,ProjLength]
16.   p2=Plane2Sphere[p2p,RadofSphere,ProjLength]
17.   p3=Plane2Sphere[p3p,RadofSphere,ProjLength]
18.   p4=Plane2Sphere[p4p,RadofSphere,ProjLength]
19.   p5=Plane2Sphere[p5p,RadofSphere,ProjLength]
20.   p6=Plane2Sphere[p6p,RadofSphere,ProjLength]
21.   p7=Plane2Sphere[p7p,RadofSphere,ProjLength]
22.   a0=Plane2Sphere[a0p,RadofSphere,ProjLength];
23.   a1=Plane2Sphere[a1p,RadofSphere,ProjLength];
24.   a1n=Plane2Sphere[a1np,RadofSphere,ProjLength];
25.   b0=Plane2Sphere[b0p,RadofSphere,ProjLength];
26.   b1=Plane2Sphere[b1p,RadofSphere,ProjLength];
27.   b1n=Plane2Sphere[b1np,RadofSphere,ProjLength];
```

Part 3: Calculate initial position variables of the spherical mechanism

```
28.   α1=ArcCos[a0.a1/Sqrt[a0.a0]/Sqrt[a1.a1]];
29.   α2=ArcCos[a1.b1/Sqrt[b1.b1]/Sqrt[a1.a1]];
30.   α3=ArcCos[b1.b0/Sqrt[b1.b1]/Sqrt[b0.b0]];
31.   α4=ArcCos[a0.b0/Sqrt[a0.a0]/Sqrt[b0.b0]];
32.   cα1=Cos[α1];sα1=Sin[α1];cα2=Cos[α2];sα2=Sin[α2];
33.   cα3=Cos[α3];sα3=Sin[α3];cα4=Cos[α4];sα4=Sin[α4];
34.   AngleBTAxes[{ax_,ay_,az_},{bx_,by_,bz_}]:={-(az by-ay bz)/(-ay
      bx+ax by),-(az bx-ax bz)/(ay bx-ax by),1}
```

```
35.   alpha1v=AngleBTAxes[a0,a1];
36.   alpha4v=AngleBTAxes[a0,b0];
37.   ϕ10=ArcCos[alpha1v.alpha4v/Sqrt[alpha1v.alpha1v]/Sqrt[alpha4v.alp
      ha4v]];
38.   ϕ10=Pi-ϕ10+Pi;
```

Part 4: Spherical mechanism Dual-Number displacement equations.

```
39.   ClearAll[cθ1,sθ1,cθ2,sθ2,cθ3,sθ3,cθ4,sθ4];
40.   M[cθ_,sθ_,cα_,sα_]:={{cθ,-cα sθ,sα sθ},{sθ,cα cθ,-sα cθ},{0,sα,
          cα}}
41.   M2=M[cθ2,sθ2,cα2,sα2];
42.   M3=M[cθ3,sθ3,cα3,sα3];
43.   M4=M[cθ4,sθ4,cα4,sα4];
44.   M1=M[cθ1,sθ1,cα1,sα1];
45.   Z=M2.M3- Transpose[M1].Transpose[M4];
46.   z11=Z[[1,1]];
47.   z12=Z[[1,2]];
48.   z13=Z[[1,3]];
49.   z21=Z[[2,1]];
50.   z22=Z[[2,2]];
51.   z23=Z[[2,3]];
52.   z31=Z[[3,1]];
53.   z32=Z[[3,2]];
54.   z33=Z[[3,3]];
55.   cθ2g=-0.3;sθ2g=-0.9;cθ3g=-0.17;sθ3g=-0.9;
56.   cθ4g=-0.17;sθ4g=-0.9;
57.   For[ϕ1=ϕ10;k=1,
58.      k≤TheMaxIterations,
59.      ϕ1=ϕ1-20/TheMaxIterations*Pi/180.;k=k+1,
60.      cθ1=Cos[ϕ1];sθ1=Sin[ϕ1];
61.      Angles=FindRoot[{z11==0,z12==0,z13==0,z21==0,z22==0,
             z23==0},{cθ2,cθ2g},{sθ2,sθ2g},{cθ3,cθ3g},
             {sθ3,sθ3g},{cθ4,cθ4g},{sθ4,sθ4g}];
62.      cθ2g=Angles[[1,2]];sθ2g=Angles[[2,2]];
63.      cθ3g=Angles[[3,2]];sθ3g=Angles[[4,2]];
64.      cθ4g=Angles[[5,2]];sθ4g=Angles[[6,2]];
65.      anscθ2=Angles[[1,2]];anssθ2=Angles[[2,2]];
66.      θ2=Which[anscθ2≥0 && anssθ2≥0,ArcCos[anscθ2],
             anscθ2<0 && anssθ2>0,ArcCos[anscθ2],
             anscθ2≤0 && anssθ2≤0,2*Pi-ArcCos[anscθ2],
             anscθ2>0 && anssθ2<0,-ArcCos[anscθ2]];
67.      If[k==1,θ2begin=θ2,];
68.      deltaθ2[k]=θ2-θ2begin;
69.      deltaθ1[k]=ϕ1-ϕ10;
70.   ]
```

Part 5: Displacement analysis for spherical four-bar path generator

```
71.   Ru[α_,u_]:={{u[[1,1]]^2*(1-Cos[α])+Cos[α],
      u[[1,1]] u[[2,1]] (1-Cos[α])-u[[3,1]] Sin[α],
      u[[1,1]] u[[3,1]] (1-Cos[α])+u[[2,1]] Sin[α]},
      {u[[1,1]] u[[2,1]] (1-Cos[α])+u[[3,1]] Sin[α],
      u[[2,1]]^2 (1-Cos[α])+Cos[α],
      u[[2,1]] u[[3,1]] (1-Cos[α])-u[[1,1]] Sin[α]},
      {u[[1,1]] u[[3,1]] (1-Cos[α])-u[[2,1]] Sin[α],
```

```
      u[[2,1]] u[[3,1]] (1-Cos[α])+u[[1,1]] Sin[α],
      u[[3,1]]^2 (1-Cos[α])+Cos[α]}};
72.   uak={{uax},{uay},{uaz}};
73.   a0axis={{a0[[1]]},{a0[[2]]},{a0[[3]]}};
74.   b0axis={{b0[[1]]},{b0[[2]]},{b0[[3]]}};
75.   For[k=1,k≤TheMaxIterations,k++,
76.      NewA1[k]=Ru[delta01[k],a0axis].(a1-a0)+a0;
77.      a1axis={{NewA1[k][[1]]},{NewA1[k][[2]]},
            {NewA1[k][[3]]}};
78.      p1temp[k]=Ru[delta01[k],a0axis].(p1-a0)+a0;
79.      NewP1[k]=Ru[delta02[k],a1axis].(p1temp[k]-NewA1[k])+NewA1[k];
80.   ]
```

Part 6: Search for the optimum mechanism solution for the rigid body point

```
81.   P11=p4;
82.   For[k=1;minsqrt=9999;myk,k≤TheMaxIterations,k++,
83.      toleranceErr[k]=Sqrt[(NewP1[k][[1]]-P11[[1]])^2+
            (NewP1[k][[2]]-P11[[2]])^2+(NewP1[k][[3]]-P11[[3]])^2];
84.      If[minsqrt>toleranceErr[k],
            minsqrt=toleranceErr[k];myk=k,];
85.   ]
86.   myanswer2[ProjLength]={myk,delta01[myk]*180/Pi,
         NewP1[myk],
87.   ProjLength,minsqrt*ProjLength}
```

CHAPTER 6

SPHERICAL MECHANISM SYNTHESIS EXAMPLES

This chapter includes an array of example problems in which all of the theory, methods and models introduced in this work are demonstrated. Applications such as the design of adjustable planar and spherical four-bar motion, path and function generators and the design of adjustable planar and spherical five-bar motion and path generators are included in this chapter. Methods such as the plane-to-sphere and sphere-to-plane projections and the plane-to-sphere optimization method are included as well as the application of the codified MATHEMATICA models introduced in Chapter 5 are demonstrated in the example problems.

6.1 Synthesis of Adjustable Four-Bar Spherical and Planar Path Generators

6.1.1 Plane-to-Sphere Projection

This particular problem depicts a situation where the user wants to calculate the spherical equivalent of an adjustable planar four-bar path generator. In this situation, the user would already have prescribed planar rigid body points. The end objective in this example is to calculate the parameters of an adjustable spherical four-bar path generator that would achieve the prescribed planar rigid body points (when projected onto a sphere). The x and y-coordinates of seven prescribed planar rigid-body points and orientation angles are listed in Table 6.1.

Table 6.1 Prescribed Rigid-Body Points and Orientation Angles for the Adjustable Planar Four-Bar Path Generator

	p	θ_{1j} [Deg.]
Pos. 1	-0.69530, 1.22910	
Pos. 2	-0.60190, 1.30260	2.15730
Pos. 3	-0.50200, 1.36750	4.21840
Pos. 4	-0.39640, 1.42330	6.19050
Pos. 5	-0.69530, 1.22910	
Pos. 6	-0.58830, 1.27960	1.91820
Pos. 7	-0.47740, 1.31930	3.77960

Using Equations 6.1 through 6.10, the prescribed rigid-body parameters in Table 6.1 and the following initial guesses ($a_{0x} = 0$, $b_{0x} = 1$, $R_1 = 1$, $R_2 = 1.5$):

$a_{0y} = 0.1$, $\mathbf{a}_1 = (-0.7, 0.6)$, $\mathbf{a}_{1n} = (-0.5, 0.7)$,

$b_{0y} = 0.1$, $\mathbf{b}_1 = (0.6, 1.5)$, $\mathbf{b}_{1n} = (1.0, 1.4)$,

the adjustable planar four-bar path generator solutions converge to

$a_{0y} = -0.0092378$, $\mathbf{a}_1 = (-0.76744, 0.63171)$, $\mathbf{a}_{1n} = (-0.45554, 0.88092)$,

$b_{0y} = -0.016575$, $\mathbf{b}_1 = (0.58693, 1.4253)$, $\mathbf{b}_{1n} = (1.0472, 1.4827)$.

The positions achieved by the synthesized adjustable planar four-bar path generator (see Figure 6.1) are given in Table 6.2. Equations 6.1 through 6.10 are identical to Equations 2.4 through 2.13.

$$([D_{12}]\mathbf{a}_1 - \mathbf{a}_0)^T([D_{12}]\mathbf{a}_1 - \mathbf{a}_0) - R_1^2 = 0 \tag{6.1}$$

$$([D_{13}]\mathbf{a}_1 - \mathbf{a}_0)^T([D_{13}]\mathbf{a}_1 - \mathbf{a}_0) - R_1^2 = 0 \tag{6.2}$$

$$([D_{14}]\ \mathbf{a}_1 - \mathbf{a}_0)^T([D_{14}]\ \mathbf{a}_1 - \mathbf{a}_0) - R_1^2 = 0 \tag{6.3}$$

$$([D_{56}]\mathbf{a}_{1n} - \mathbf{a}_0)^T([D_{56}]\mathbf{a}_{1n} - \mathbf{a}_0) - R_1^2 = 0 \tag{6.4}$$

$$([D_{57}]\mathbf{a}_{1n} - \mathbf{a}_0)^T([D_{57}]\mathbf{a}_{1n} - \mathbf{a}_0) - R_1^2 = 0 \tag{6.5}$$

$$([D_{12}]\mathbf{b}_1 - \mathbf{b}_0)^T([D_{12}]\mathbf{b}_1 - \mathbf{b}_0) - R_2^2 = 0 \tag{6.6}$$

$$([D_{13}]\mathbf{b}_1 - \mathbf{b}_0)^T([D_{13}]\mathbf{b}_1 - \mathbf{b}_0) - R_2^2 = 0 \tag{6.7}$$

$$([D_{14}]\mathbf{b}_1 - \mathbf{b}_0)^T([D_{14}]\mathbf{b}_1 - \mathbf{b}_0) - R_2^2 = 0 \tag{6.8}$$

$$([D_{56}]\mathbf{b}_{1n} - \mathbf{b}_0)^T([D_{56}]\mathbf{b}_{1n} - \mathbf{b}_0) - R_2^2 = 0 \tag{6.9}$$

$$([D_{57}]\mathbf{b}_{1n} - \mathbf{b}_0)^T([D_{57}]\mathbf{b}_{1n} - \mathbf{b}_0) - R_2^2 = 0 \tag{6.10}$$

Table 6.2 Planar Rigid-Body Points Generated by the Synthesized Adjustable Four-Bar Path Generator

Pos.	p
Pos. 1	-0.69530, 1.22910
Pos. 2	-0.60184, 1.30248
Pos. 3	-0.50191, 1.36740
Pos. 4	-0.39632, 1.42320
Pos. 5	-0.69530, 1.22910
Pos. 6	-0.58830, 1.27954
Pos. 7	-0.47739, 1.31925

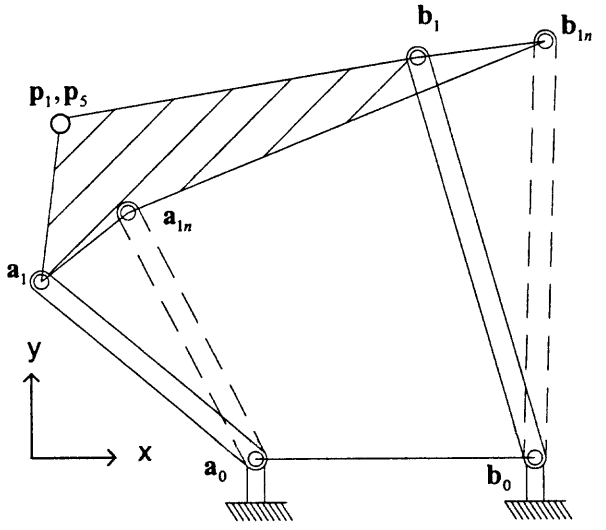

Figure 6.1 Synthesized adjustable planar four-bar path generator.

As previously mentioned, the end objective in this example is to calculate the parameters of an adjustable spherical four-bar path generator that would achieve the prescribed planar rigid body positions in Table 6.1 when projected onto a sphere. Using the plane-to-sphere projection method described in Section 4.1, each joint coordinate of the synthesized adjustable planar four-bar path generator is projected onto a specified sphere. This origin of this sphere is coincident with the origin of the coordinate system and the synthesized planar mechanism lies on plane parallel to the x-y plane and offset from the origin by a distance "d" along the z-axis (see Figure 4.2).

The magnitude of the offset distance "d" is inversely proportional to the structural error between the prescribed "projected" rigid body points and the points achieved by the projected adjustable spherical four-bar path generator. Plots of the structural errors between the prescribed and generated rigid body points of the adjustable spherical four-bar path generator are illustrated in Figures 6.2 through 6.6 (for each rigid body point). As these figures illustrate, as the magnitude of the projection length "d" increases, the structural error decreases.

In this example a projection length of 11, and subsequently a structural error (S_{err}*d) less than 0.001 in Figures 6.2 through 6.6, was selected. The sphere onto which the planar rigid body points were projected has a radius of 1. The prescribed rigid body points (from Table 6.1) projected onto a sphere or radius 1 and offset distance 11 are given in Table 6.3. The projected fixed and moving pivots of the synthesized adjustable spherical four-bar path generator are given in Table 6.4. The plane-to-sphere projections were performed using the MATHEMATICA model in Appendix B.1. In Table 6.4, the joint axes for the projected fixed and moving pivots of the adjustable spherical four-bar

path generator are the unit vectors from the center of the sphere (the origin of the coordinate system) to each fixed and moving pivot. The adjustable spherical four-bar path generator is illustrated in Figure 6.7.

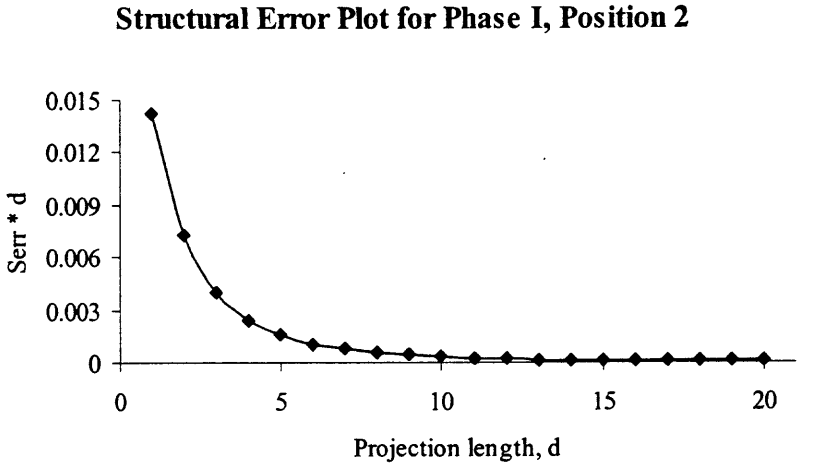

Figure 6.2 Structural error plot for phase I, position 2.

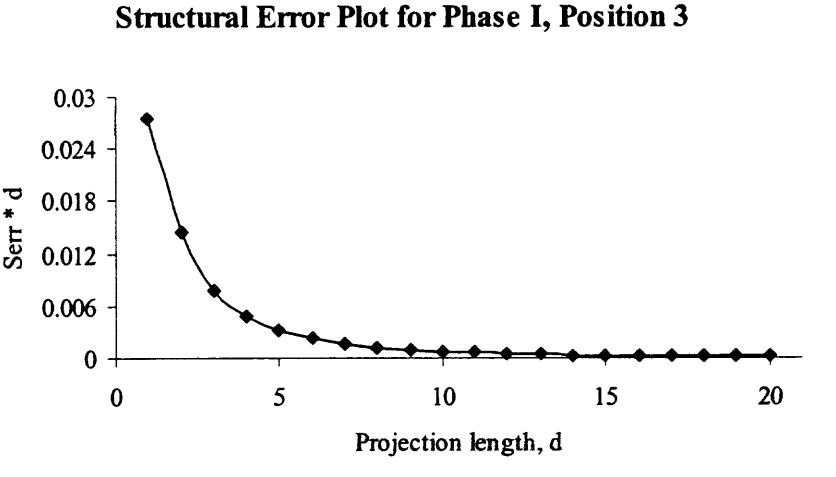

Figure 6.3 Structural error plot for phase I, position 3.

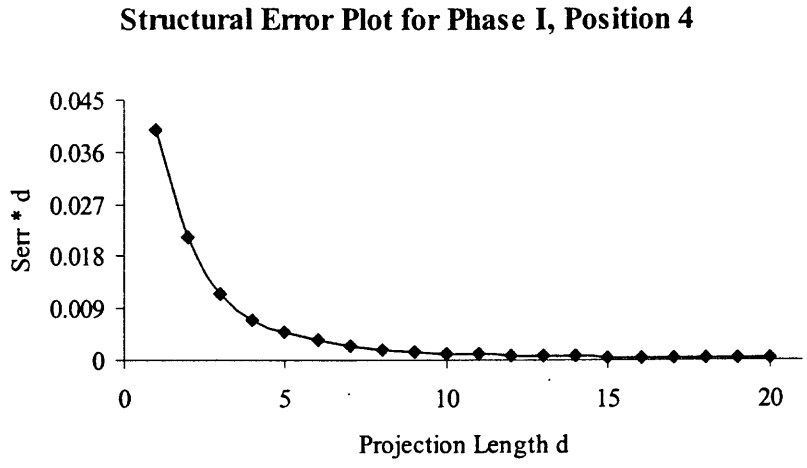

Figure 6.4 Structural error plot for phase I, position 4.

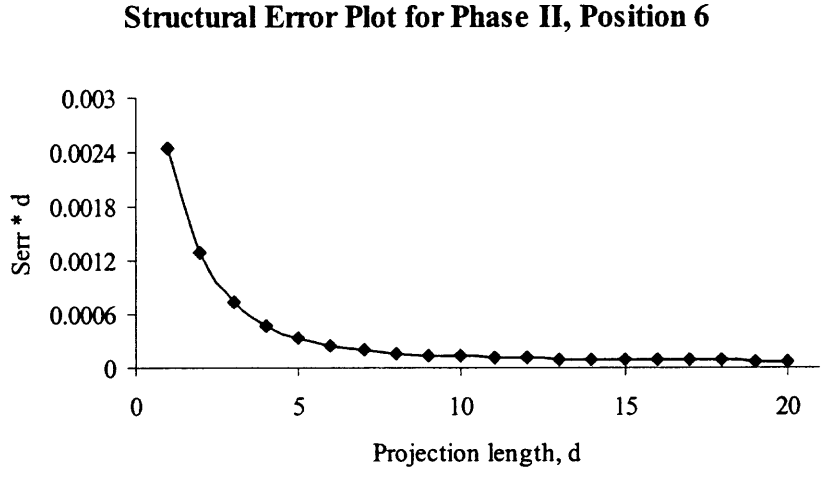

Figure 6.5 Structural error plot for phase II, position 6.

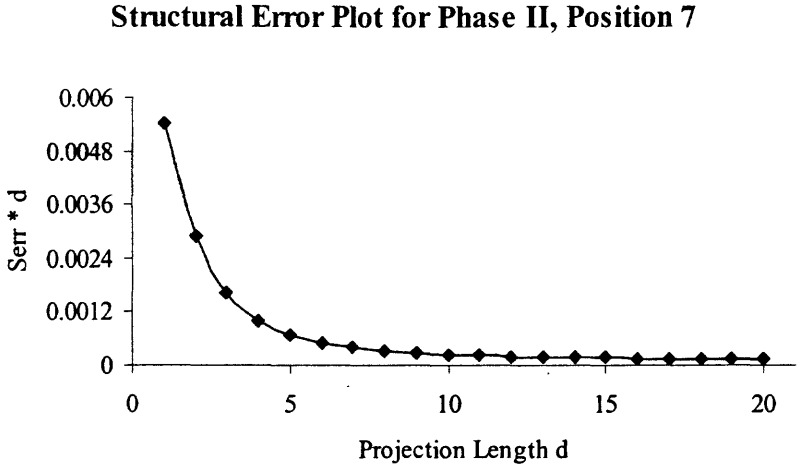

Figure 6.6 Structural error plot for phase II, position 7.

Table 6.3 Prescribed Projected Rigid-Body Points for the Adjustable Spherical Four-Bar Path Generator

Pos.	p
Pos. 1	-0.06270, 0.11083, 0.99186
Pos. 2	-0.05426, 0.11742, 0.99160
Pos. 3	-0.04524, 0.12324, 0.99135
Pos. 4	-0.03572, 0.12824, 0.99110
Pos. 5	-0.06270, 0.11083, 0.99186
Pos. 6	-0.05305, 0.11539, 0.99190
Pos. 7	-0.04305, 0.11897, 0.99196

Table 6.4 Projected Fixed and Moving Pivots of the Adjustable Spherical Four-Bar Path Generator

$\mathbf{a}_0$	0.00000, -0.00084, 1.00000
$\mathbf{a}_1$	-0.06948, 0.05720, 0.99594
$\mathbf{a}_{1n}$	-0.04125, 0.07976, 0.99596
$\mathbf{b}_0$	0.09054, -0.00150, 0.99589
$\mathbf{b}_1$	0.05284, 0.12832, 0.99032
$\mathbf{b}_{1n}$	0.09393, 0.13299, 0.98666

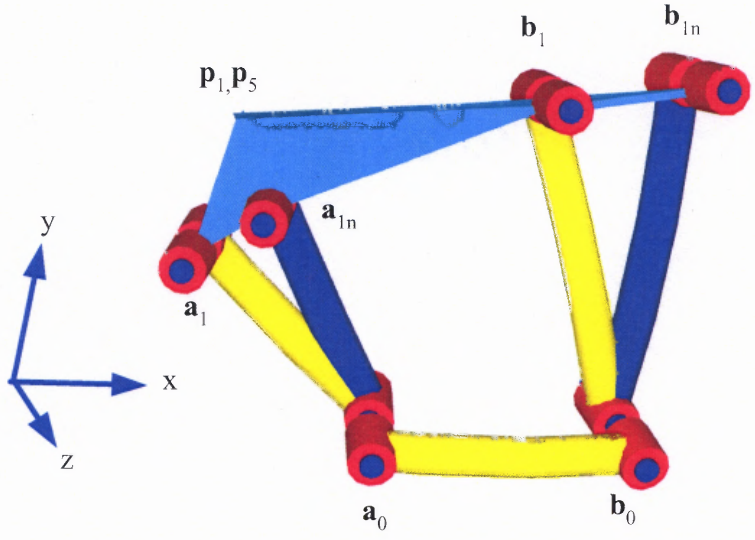

Figure 6.7 The adjustable spherical four-bar path generator calculated by plane-to-sphere projection.

Using the MATHEMATICA model located in Appendix B.1, the rigid-body points achieved by the adjustable spherical four-bar path generator were calculated along with the measured structural error. The rigid body points achieved by the adjustable spherical four-bar path generator and the measured structural error are given in Table 6.5.

Table 6.5 Rigid-Body Points Achieved by the Adjustable Spherical Four-Bar Path Generator

Pos.	p	d^*S_{err} [10^{-4}]
Pos. 1	-0.06270, 0.11083, 0.99186	
Pos. 2	-0.05427, 0.11744, 0.99160	2.23607
Pos. 3	-0.04527, 0.12329, 0.99134	5.91608
Pos. 4	-0.03575, 0.12832, 0.99109	8.60233
Pos. 5	-0.06270, 0.11083, 0.99186	
Pos. 6	-0.05305, 0.11538, 0.99191	1.41421
Pos. 7	-0.04304, 0.11896, 0.99197	1.73205

6.1.2 Sphere-to-Plane Projection

Given the synthesized adjustable spherical four-bar path generator in the previous sub-section, the parameters of a kinematically-equivalent adjustable planar four-bar path generator will be calculated to demonstrate the structural error difference between plane-to-sphere and sphere-to-plane projections. Using the sphere-to-plane projection method described in Section 4.1, each joint coordinate of the synthesized adjustable spherical four-bar path generator is projected onto a specified plane as described in Section 4.1. The origin of this sphere is coincident with the origin of the coordinate system and the synthesized planar path generator lies on plane parallel to the X-Y plane and offset from the origin by a distance "d" along the z-axis.

As indicated in to Figures 6.8 through 6.12, the magnitude of the offset distance "d" has no effect on the structural error between the prescribed projected rigid body points and the rigid body points achieved by the projected adjustable planar four-bar path generator. This is due to the joint axes varying with the projection length in plane-to-sphere projections but remaining constant with varying projection lengths in sphere-to-plane projection.

No matter what projection length is specified, the prescribed rigid body points of the adjustable planar four-bar path generator illustrated in Figure 6.1 are achieved precisely when projecting the synthesized adjustable spherical four-bar path generator onto a plane. Figures 6.8 through 6.12 illustrate the structural error between the prescribed projected rigid body points and the points achieved by the projected adjustable planar four-bar path generator (for each rigid body point).

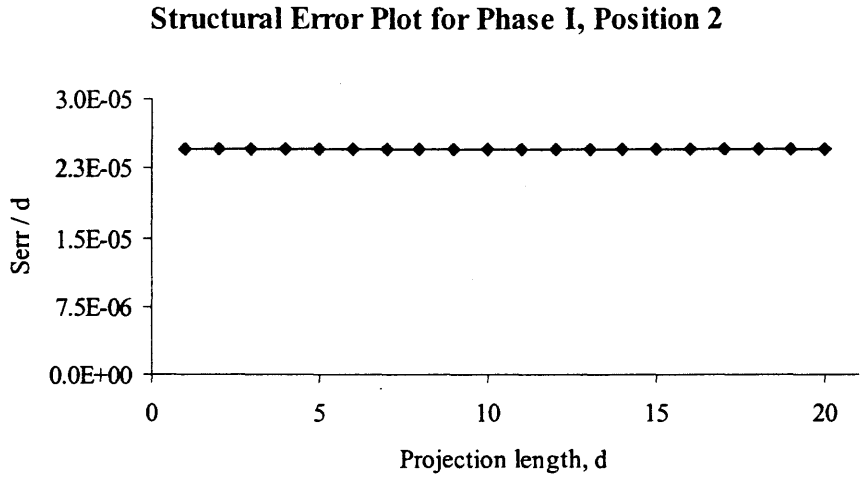

Figure 6.8 Structural error plot for phase I, position 2.

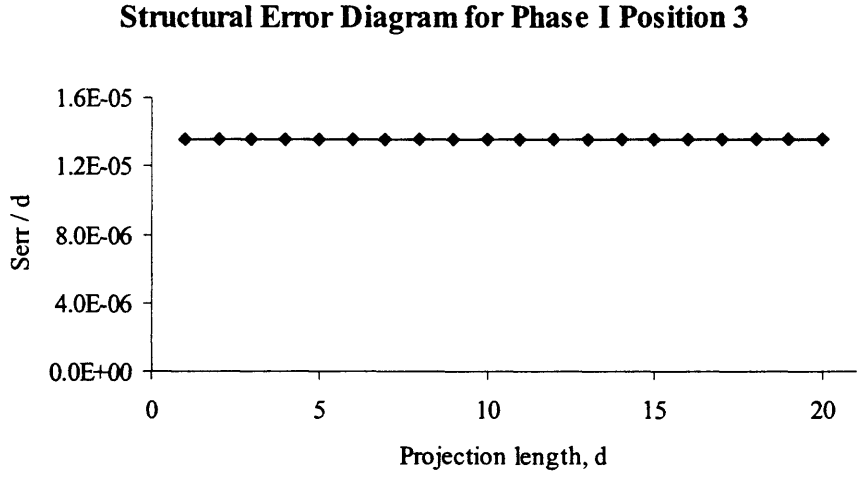

Figure 6.9 Structural error plot for phase I, position 3.

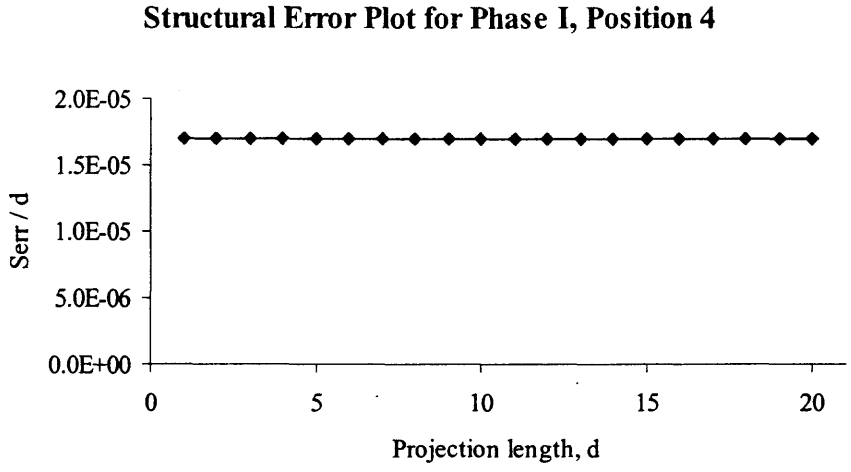

Figure 6.10 Structural error plot for phase I, position 4.

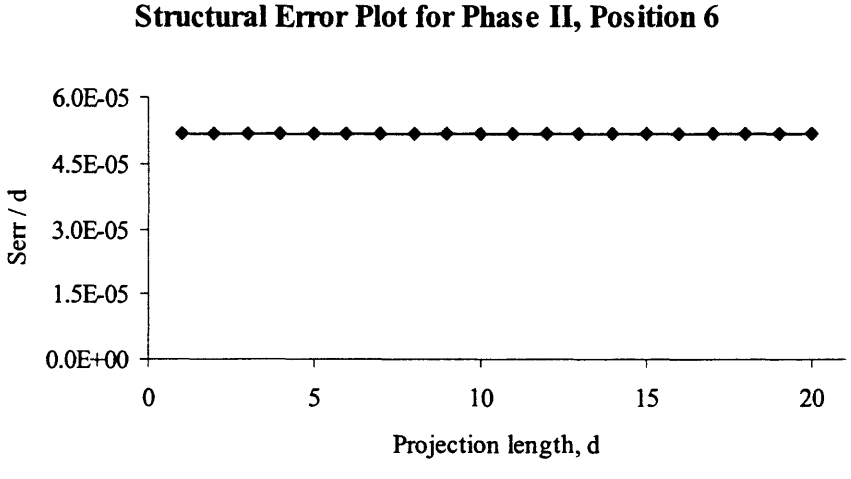

Figure 6.11 Structural error plot for phase II, position 6.

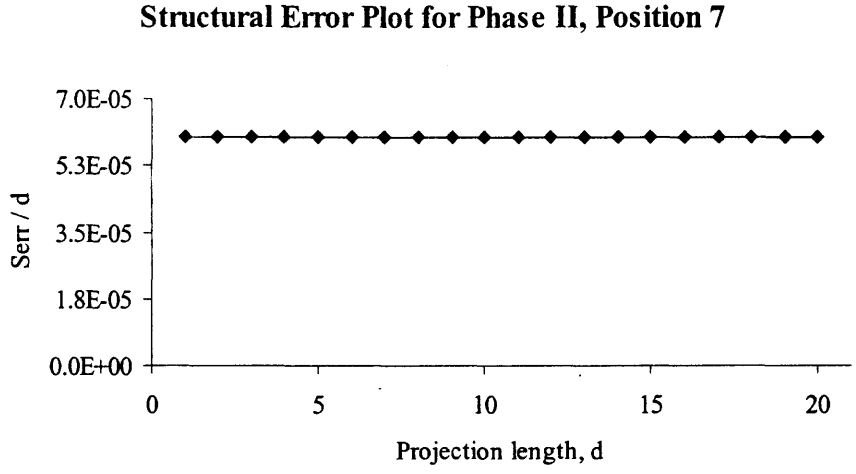

Figure 6.12 Structural error plot for phase II, position 7.

6.2 Synthesis of Adjustable Four-Bar Spherical and Planar Function Generators

6.2.1 Plane-to-Sphere Projection

This particular problem depicts a situation where the user wants to calculate the spherical equivalent of an adjustable planar four-bar function generator. In this situation, the user would already have prescribed planar crank and follower displacement angles. The end objective in this example is to calculate the parameters of an adjustable spherical four-bar function generator that would achieve the prescribed planar crank and follower displacement angles. Seven prescribed crank and follower displacement angles are listed in Table 6.1.

Table 6.6 Prescribed Crank and Follower Link Angular Displacements for the Adjustable Planar Four-Bar Function Generator

	θ_{1j} [Deg.]	ϕ_{1j} [Deg.]
Pos. 1-2	10.0	7.5043
Pos. 1-3	20.0	14.9632
Pos. 1-4	30.0	22.2630
Pos. 1-5	15.0	9.7349
Pos. 1-6	30.0	18.9815

Equations 6.11 through 6.15 were used to calculate five of the six unknowns in $\mathbf{a}_1$, $\mathbf{b}_1$ and $\mathbf{b}_{1n}$. The variable a_{1x} and the coupler length L_2 were specified (a_{1x} = -0.2 and L_2 = 1). Using the following initial guesses:

a_{1y}= 0.7, $\mathbf{b}_1$= (0.6, 1.3), $\mathbf{b}_{1n}$= (0.7, 1.2),

the planar four-bar function generator converges to

a_{1y}= 0.6838, $\mathbf{b}_1$= (0.7713, 0.9218), $\mathbf{b}_{1n}$= (0.7267, 1.0590).

The displacement angles achieved by the synthesized adjustable planar four-bar function generator (see Figure 6.13) are given in Table 6.7. Equations 6.11 through 6.15 are identical to Equations 2.17 through 2.21.

$$([D_{12}]\mathbf{a}_1 - \mathbf{b}_1)^T ([D_{12}]\mathbf{a}_1 - \mathbf{b}_1) - L_2^2 = 0 \tag{6.11}$$

$$([D_{13}]\mathbf{a}_1 - \mathbf{b}_1)^T ([D_{13}]\mathbf{a}_1 - \mathbf{b}_1) - L_2^2 = 0 \tag{6.12}$$

$$([D_{14}]\mathbf{a}_1 - \mathbf{b}_1)^T ([D_{14}]\mathbf{a}_1 - \mathbf{b}_1) - L_2^2 = 0 \tag{6.13}$$

$$([D_{15}]\mathbf{a}_1 - \mathbf{b}_{1n})^T ([D_{15}]\mathbf{a}_1 - \mathbf{b}_{1n}) - L_2^2 = 0 \tag{6.14}$$

$$([D_{16}]\mathbf{a}_1 - \mathbf{b}_{1n})^T ([D_{16}]\mathbf{a}_1 - \mathbf{b}_{1n}) - L_2^2 = 0 \tag{6.15}$$

Table 6.7 Crank and Follower Link Displacement Angles Achieved by the Adjustable Planar Four-Bar Function Generator

Pos.	θ_{1j} [Deg.]	ϕ_{1j} [Deg.]
Pos. 1-2	10.0	7.5045
Pos. 1-3	20.0	14.9634
Pos. 1-4	30.0	22.2632
Pos. 1-5	15.0	9.7240
Pos. 1-6	30.0	18.9697

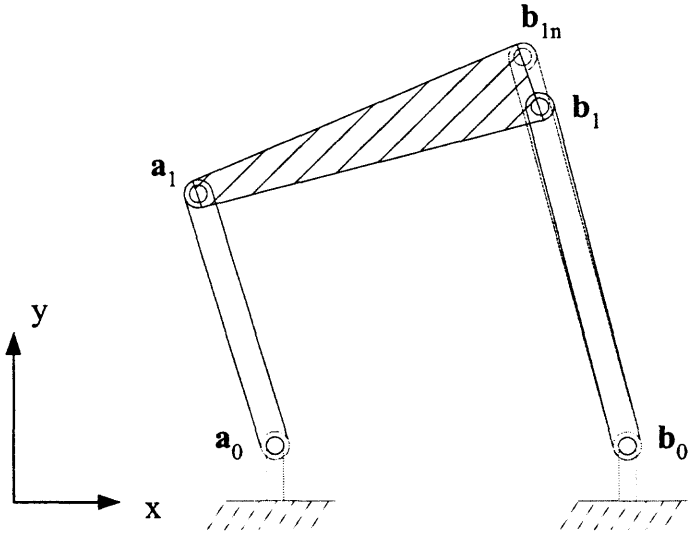

Figure 6.13 Synthesized adjustable planar four-bar function generator.

As previously mentioned, the end objective in this example is to calculate the parameters of an adjustable spherical four-bar function generator that would achieve the prescribed planar crank and follower displacement angles in Table 6.6. Using the plane-to-sphere projection method described in Section 4.1, each joint coordinate of the synthesized adjustable planar four-bar function generator is projected onto a specified sphere. This origin of this sphere is coincident with the origin of the coordinate system

and the synthesized planar mechanism lies on plane parallel to the x-y plane and offset from the origin by a distance "d" along the z-axis (see Figure 4.2).

The magnitude of the offset distance "d" is inversely proportional to the structural error between the prescribed displacement angles and the angles achieved by the projected adjustable spherical four-bar function generator. In this work, structural error in function generation is defined as the error $|\phi_p - \phi_g|/\phi_p$ (Equation 6.16), where ϕ_p is the prescribed displacement angle and ϕ_g is the displacement angle achieved by the synthesized adjustable spherical four-bar function generator. Plots of the structural error s between the projected and generated displacement angles of the adjustable spherical four-bar function generator are illustrated in Figures 6.14 through 6.18 (for each displacement angle). As these figures illustrate, the magnitude of the projection length "d" increases as the structural error decreases.

$$error = \frac{|\phi_p - \phi_g|}{\phi_p} \tag{6.16}$$

In this example, a projection length of 10 and subsequently an error (Serr*d) less than 0.005 in Figures 6.14 through 6.18 was selected. In addition, the sphere onto which the planar function generator parameters are projected has a radius of 1. The prescribed crank and follower displacement angles for the spherical function generator are given in Table 6.6. The projected fixed and moving pivots of the synthesized adjustable planar four-bar function generator are given in Table 6.8. These plane-to-sphere projections were performed using the MATHEMATICA model in Appendix B.2. In Table 6.8, the joint axes for the projected fixed and moving pivots of the adjustable spherical four-bar function generator are the unit vectors from the center of the sphere (the origin of the

coordinate system) to each fixed and moving pivot. The adjustable spherical four-bar function generator is illustrated in Figure 6.19.

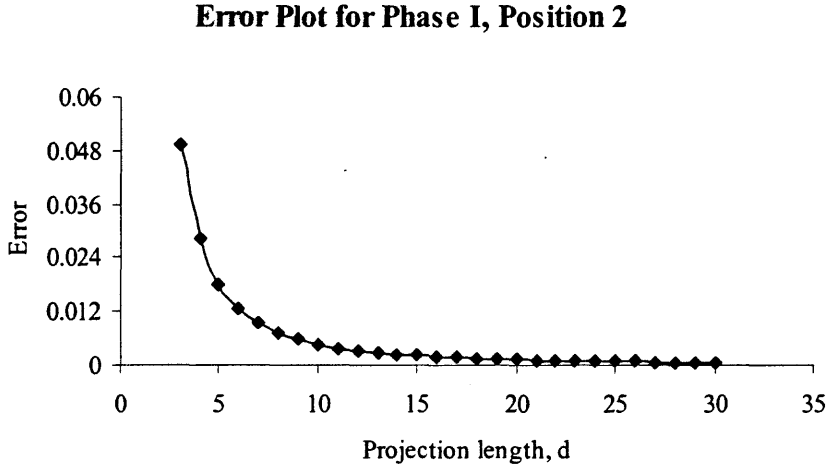

Figure 6.14 Error plot for phase I, position 2.

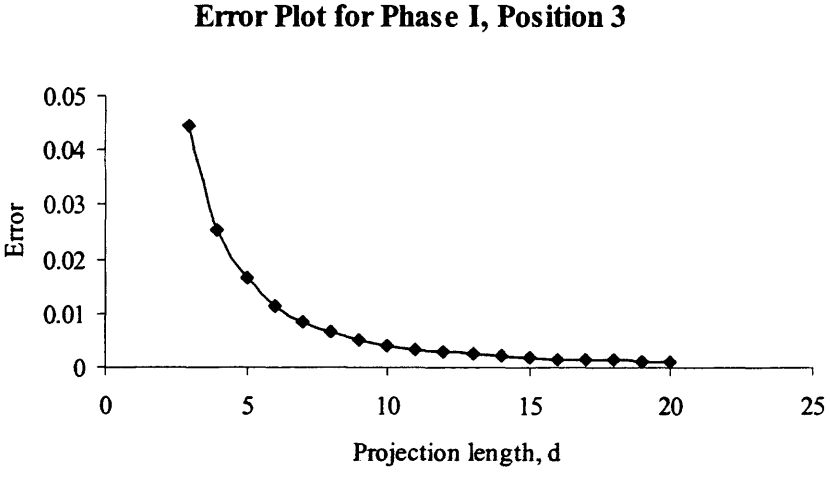

Figure 6.15 Error plot for phase I, position 3.

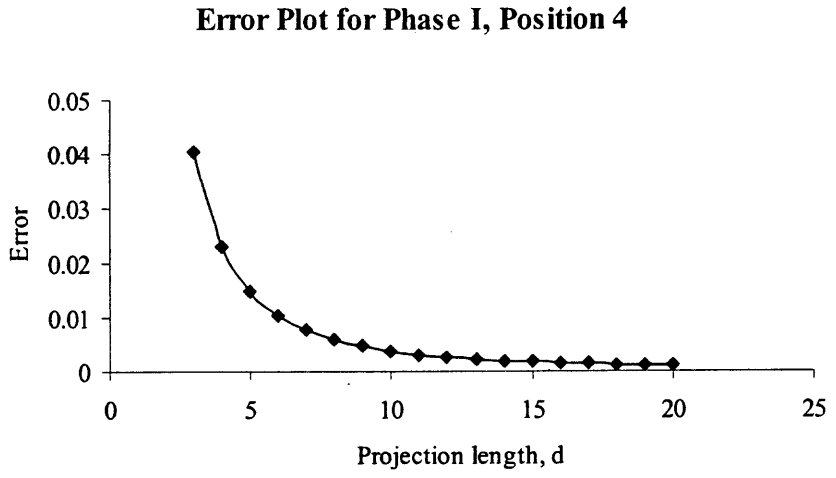

Figure 6.16 Error plot for phase I, position 4.

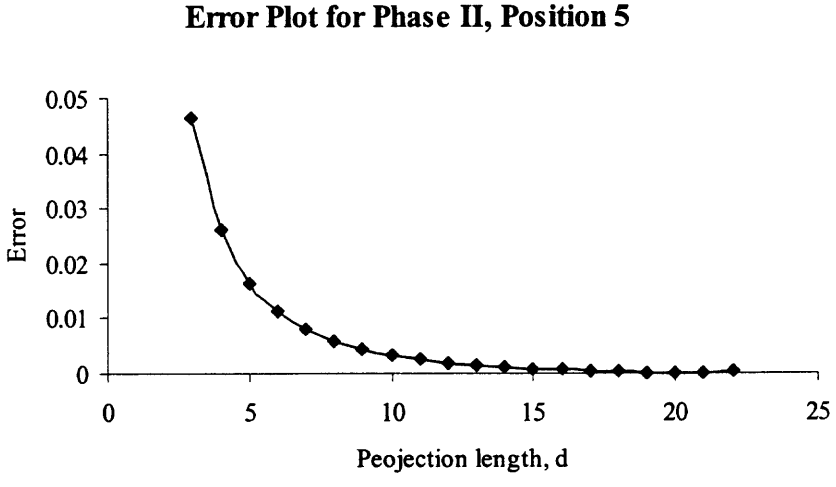

Figure 6.17 Error plot for phase II, position 5.

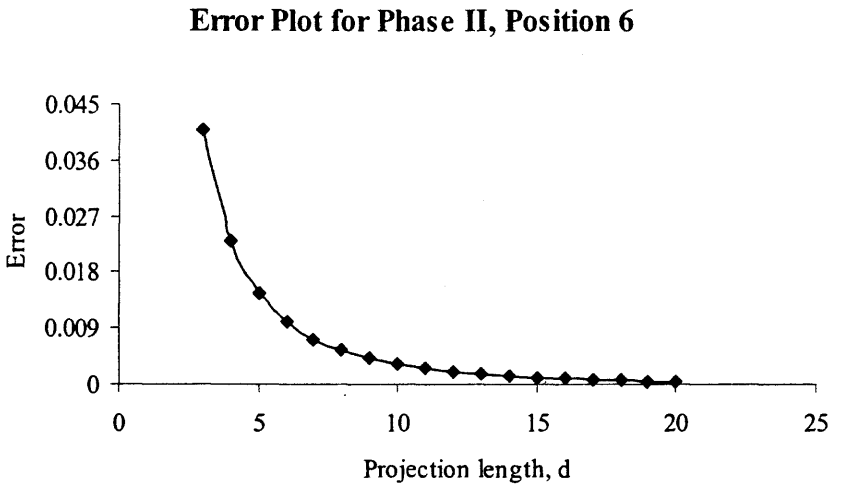

Figure 6.18 Error plot for phase II, position 6.

Table 6.8 Projected Fixed and Moving Pivots of the Adjustable Spherical Four-Bar Function Generator

$\mathbf{a}_0$	0.0, 0.0, 1.0
$\mathbf{a}_1$	-0.00667, 0.02279, 0.99970
$\mathbf{b}_0$	0.03331, 0.0, 0.99940
$\mathbf{b}_1$	0.02569, 0.03070, 0.9992
$\mathbf{b}_{1n}$	0.02420, 0.03527, 0.99910

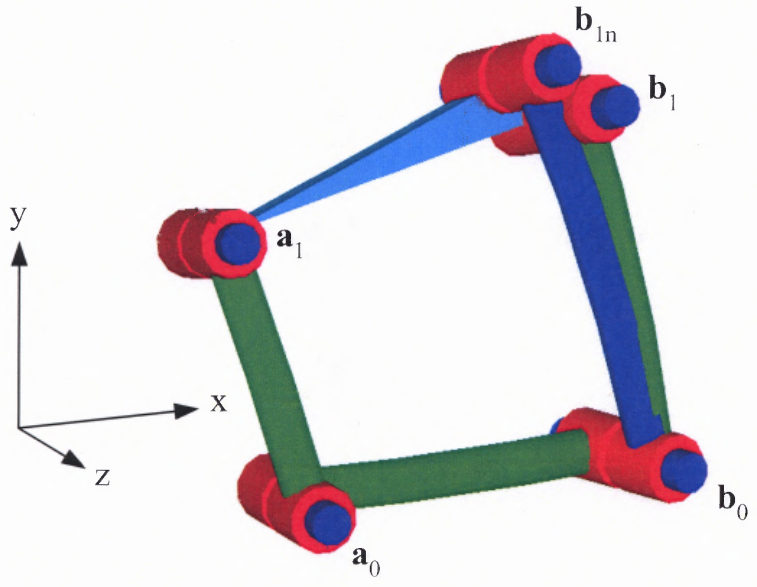

Figure 6.19 The adjustable spherical four-bar path generator calculated by plane-to-sphere projection.

Using the MATHEMATICA model located in Appendix B.2, the crank and follower link displacement angles achieved by the adjustable spherical four-bar function generator were calculated along with measured displacement angle error. The displacement crank and follower angles achieved by the adjustable spherical four-bar function generator and the measured displacement angle error are given in Table 6.9.

Table 6.9 Displacement Angles Achieved by the Adjustable Spherical Four-Bar Function Generator.

Pos.	θ_{1j} [Deg.]	ϕ_{1j} [Deg.]	Error
Pos. 1-2	10.0	7.5387	0.0046
Pos. 1-3	20.0	15.0255	0.0042
Pos. 1-4	30.0	22.3474	0.0038
Pos. 1-5	15.0	9.7669	0.0033
Pos. 1-6	30.0	19.0433	0.0032

6.2.2 Sphere-to-Plane Projection

Given the synthesized adjustable spherical four-bar function generator in the previous sub-section, the parameters of a kinematically-equivalent adjustable planar four-bar function generator will be calculated to demonstrate the structural error difference between plane-to-sphere and sphere-to-plane projections. Using the sphere-to-plane projection method described in Section 4.1, each joint coordinate of the synthesized adjustable spherical four-bar function generator was projected onto a specified plane as described in Section 4.1. This origin of this sphere is coincident with the origin of the coordinate system and the synthesized planar function generator lies on plane parallel to the X-Y plane and offset from the origin by a distance "d" along the z-axis.

As indicated in Figures 6.20 through 6.24, the magnitude of the offset distance "d" has no effect on the structural error between the crank and follower displacement angles and the displacement angles achieved by the adjustable planar four-bar function generator. This is due to the joint axes varying with the projection length in plane-to-sphere projections but remaining constant with varying projection lengths in sphere-to-plane projection.

No matter what projection length is specified, the adjustable planar four-bar function generator illustrated in Figure 6.13 is achieved precisely when projecting the synthesized adjustable spherical four-bar function generator onto a plane. Figures 6.20 through 6.24 illustrate the structural error between the prescribed crank and follower displacement angles and the angles achieved by the projected adjustable planar four-bar function generator (for each displacement angle).

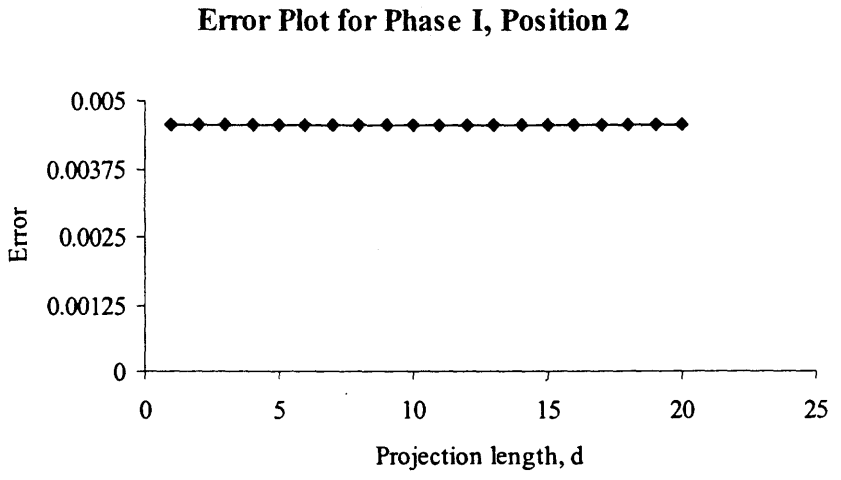

Figure 6.20 Error plot for phase I, position 2.

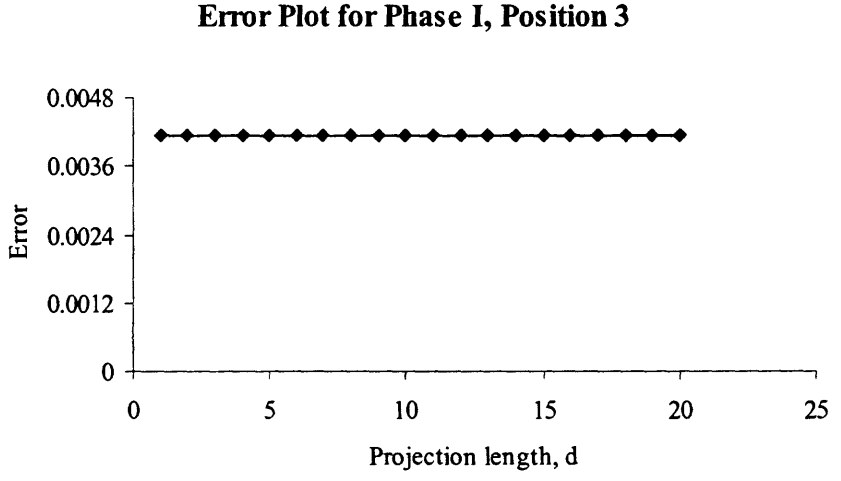

Figure 6.21 Error plot for phase I, position 3.

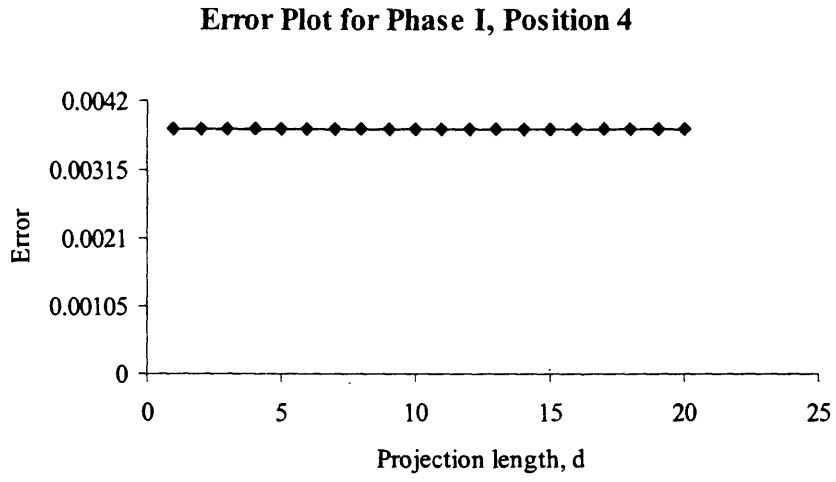

Figure 6.22 Error plot for phase I, position 3.

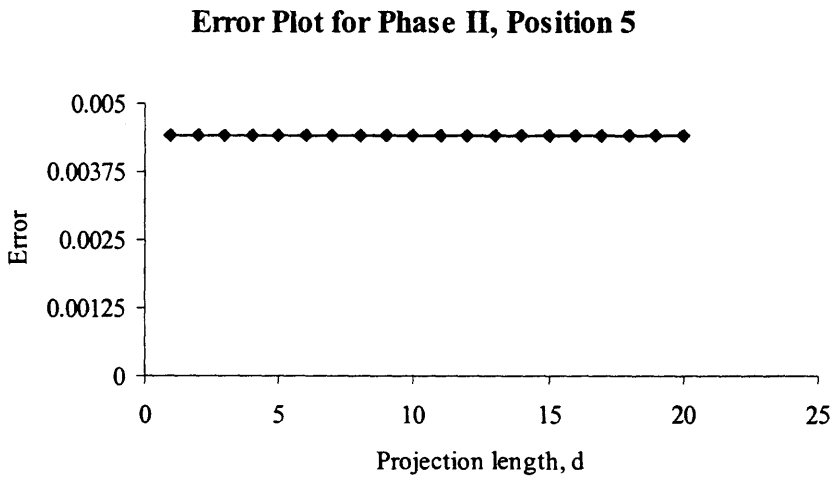

Figure 6.23 Error plot for phase II, position 5.

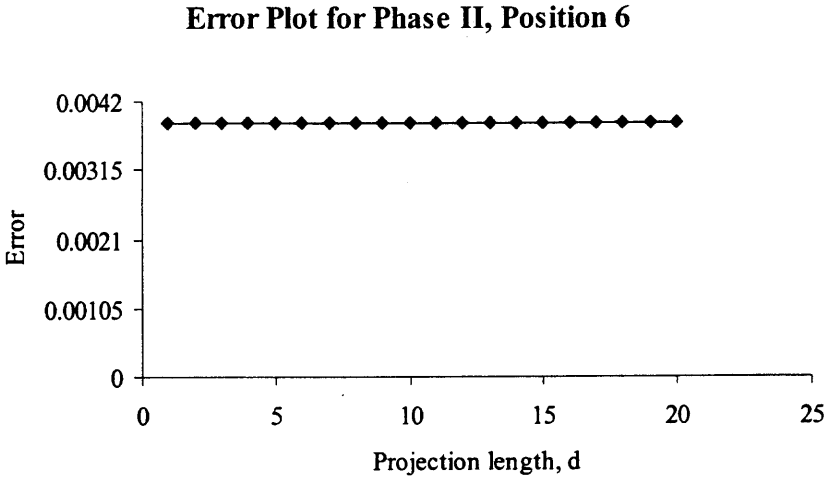

Figure 6.24 Error plot for phase II, position 6.

6.3 Synthesis of Adjustable Four-Bar Spherical and Planar Motion Generators

6.3.1 Plane-to-Sphere Projection

This particular problem depicts a situation where the user wants to calculate an adjustable spherical four-bar motion generator given prescribed spherical rigid body positions. The end objective in this example is to calculate the parameters of an adjustable spherical four-bar motion generator that would achieve the prescribed spherical rigid body positions.

The x, y and z-coordinates of seven prescribed spherical rigid-body positions are listed in Table 6.10. The positions in Table 6.10 lie on a sphere with a radius of 1 unit. It is the design intent that one mechanism adjustment achieves position 1 through 4 and another mechanism adjustment achieves position 5 through 6.

Using the sphere-to-plane projection method described in Section 4.1, the planar rigid-body positions in Table 6.11 are calculated. The positions in Table 6.11 are the spherical rigid-body positions in Table 6.10 projected onto a plane at an offset distance on 7 units (d_j = 7) along the z-axis from the origin of the coordinate system. As illustrated in Figures 4.1, the origin of the coordinate system is coincident with the origin of the sphere containing the prescribed rigid body positions.

Table 6.10 Prescribed Rigid Body Points for the Adjustable Spherical Four-Bar Motion Generator

Pos.	p	q	r
Pos. 1	-0.02733, 0.19212, 0.98099	0.00551, 0.27613, 0.96111	0.12076, 0.25322, 0.95984
Pos. 2	-0.01571, 0.19792, 0.98009	0.01877, 0.28080, 0.95958	0.13321, 0.25522, 0.95766
Pos. 3	-0.00362, 0.20285, 0.97920	0.03238, 0.28464, 0.95809	0.14595, 0.25648, 0.95547
Pos. 4	0.00886, 0.20687, 0.97833	0.04627, 0.28758, 0.95664	0.15894, 0.25696, 0.95326
Pos. 5	-0.02733, 0.19212, 0.98099	0.00551, 0.27613, 0.96111	0.12076, 0.25322, 0.95984
Pos. 6	-0.01628, 0.19486, 0.98070	0.01492, 0.27909, 0.96015	0.13018, 0.25762, 0.95744
Pos. 7	-0.00518, 0.19657, 0.98048	0.02418, 0.28111, 0.95937	0.13945, 0.26131, 0.95513

Table 6.11 Prescribed Projected Rigid-body Positions for the Adjustable Planar Four-Bar Motion Generator

Pos.	p	q	r
Pos. 1	-0.19502, 1.3709	0.04013, 2.01112	0.88069, 1.84670
Pos. 2	-0.11220, 1.41358	0.13692, 2.04840	0.97370, 1.86553
Pos. 3	-0.02588, 1.45011	0.23658, 2.07964	1.06926, 1.87903
Pos. 4	0.06339, 1.48017	0.33857, 2.10430	1.16713, 1.88691
Pos. 5	-0.19502, 1.37090	0.04013, 2.01112	0.88069, 1.84670
Pos. 6	-0.116203, 1.39086	0.10878, 2.03471	0.95177, 1.88350
Pos. 7	-0.03698, 1.40338	0.17643, 2.05111	1.02201, 1.91510

Now that the spherical rigid-body positions have been projected onto a plane, they are planar rigid-body positions and an adjustable planar motion generator can be designed to approximate these positions. Equations 6.17 through 6.21 are used to calculate five of the six unknowns in $\mathbf{a}_0$, $\mathbf{a}_1$ and $\mathbf{a}_{1n}$. Equations 6.22 through 6.26 are used to calculate five of the six unknowns in $\mathbf{b}_0$, $\mathbf{b}_1$ and $\mathbf{b}_{1n}$. These equations are identical to Equations 2.25 through 2.34. The variable a_{0x} and the link length R_1 are specified ($a_{0x} = 0$ and $R_1 = 1$). The variable b_{0x} and the link length R_2 are specified ($b_{0x} = 1.5$ and $R_2 = 1.5$). Using the following initial guesses:

$a_{0y} = 0.1$, $\mathbf{a}_1 = (-0.6, 0.7)$, $\mathbf{a}_{1n} = (-0.2, 0.9)$,

$b_{0y} = 0.1$, $\mathbf{b}_1 = (1.2, 1.3)$, $\mathbf{b}_{1n} = (0.8, 1.2)$,

the planar four-bar motion generator solutions converges to

$a_{0y} = -0.0296205$, $\mathbf{a}_1 = (-0.63841, 0.739811)$, $\mathbf{a}_{1n} = (-0.260941, 0.935936)$,

$b_{0y} = -0.0947279$, $\mathbf{b}_1 = (1.28369, 1.38921)$, $\mathbf{b}_{1n} = (0.839684, 1.25246)$.

The synthesized adjustable planar four-bar motion generator is illustrated in Figure 6.25.

$$([D_{12}]\mathbf{a}_1 - \mathbf{a}_0)^T([D_{12}]\mathbf{a}_1 - \mathbf{a}_0) - R_1^2 = 0 \tag{6.17}$$

$$([D_{13}]\mathbf{a}_1 - \mathbf{a}_0)^T([D_{13}]\mathbf{a}_1 - \mathbf{a}_0) - R_1^2 = 0 \tag{6.18}$$

$$([D_{14}]\mathbf{a}_1 - \mathbf{a}_0)^T([D_{14}]\mathbf{a}_1 - \mathbf{a}_0) - R_1^2 = 0 \tag{6.19}$$

$$([D_{56}]\mathbf{a}_{1n} - \mathbf{a}_0)^T([D_{56}]\mathbf{a}_{1n} - \mathbf{a}_0) - R_1^2 = 0 \tag{6.20}$$

$$([D_{57}]\mathbf{a}_{1n} - \mathbf{a}_0)^T([D_{57}]\mathbf{a}_{1n} - \mathbf{a}_0) - R_1^2 = 0 \tag{6.21}$$

$$([D_{12}]\mathbf{b}_1 - \mathbf{b}_0)^T([D_{12}]\mathbf{b}_1 - \mathbf{b}_0) - R_2^2 = 0 \tag{6.22}$$

$$([D_{13}]\mathbf{b}_1 - \mathbf{b}_0)^T([D_{13}]\mathbf{b}_1 - \mathbf{b}_0) - R_2^2 = 0 \tag{6.23}$$

$$([D_{14}]\mathbf{b}_1 - \mathbf{b}_0)^T([D_{14}]\mathbf{b}_1 - \mathbf{b}_0) - R_2^2 = 0 \tag{6.24}$$

$$([D_{56}]\mathbf{b}_{1n} - \mathbf{b}_0)^T([D_{56}]\mathbf{b}_{1n} - \mathbf{b}_0) - R_2^2 = 0 \tag{6.25}$$

$$([D_{57}]\mathbf{b}_{1n} - \mathbf{b}_0)^T([D_{57}]\mathbf{b}_{1n} - \mathbf{b}_0) - R_2^2 = 0 \tag{6.26}$$

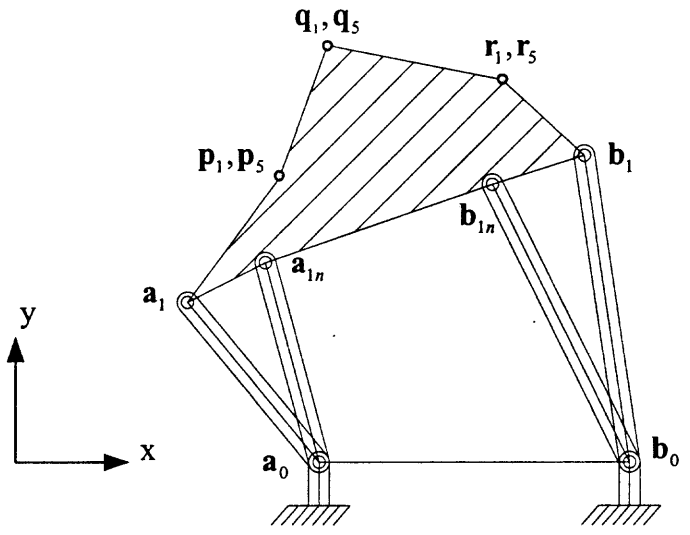

Figure 6.25 Synthesized adjustable planar four-bar motion generator.

Now that a mechanism solution has been calculated for the projected planar rigid-body positions, the joints of the adjustable planar four-bar motion generator are projected back onto a sphere with a radius of 1 unit to determine the joints of the adjustable spherical motion generator required to achieve the prescribed rigid-body positions in Table 6.10.

Using the MATHEMATICA model in Appendix B.3, the error plots in Figures 6.26 through 6.30 were generated for each rigid body position of the adjustable spherical four-bar motion generator. These figures illustrate that the structural error between the prescribed and achieved rigid-body positions of the adjustable spherical four-bar motion generator decreases as the projection length increases.

For this example, the maximum allowable error (Serr * d) for each rigid body position is 0.01 units. Since the sphere-to-plane projection length is 7 units, the plane-to-sphere projection length is also 7 units to maintain the scale of the prescribed rigid-body

positions. With a plane-to-sphere projection length of 7 units, the maximum structural error obtained is approximately 0.008 units for rigid body position 4 and 0.005 for position 7.

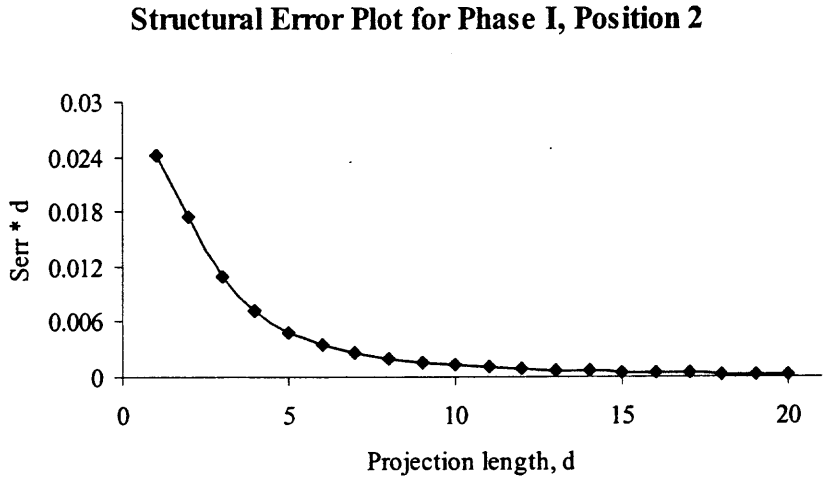

Figure 6.26 Structural error plot for phase I, position 2.

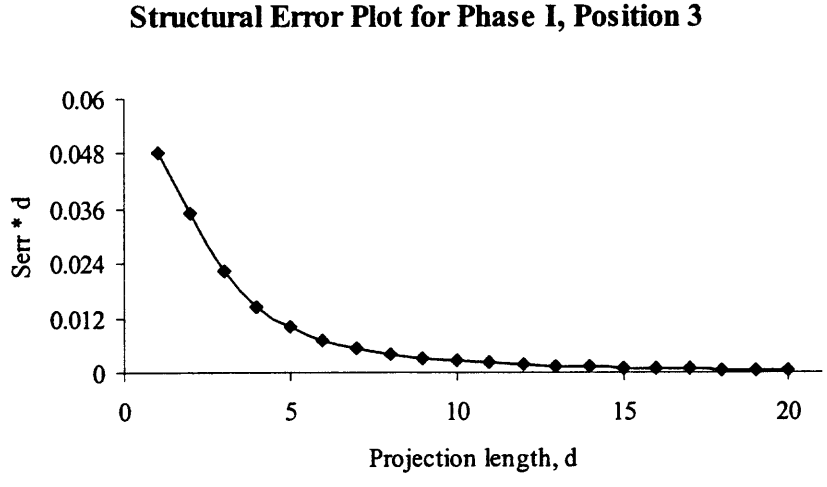

Figure 6.27 Structural error plot for phase I, position 3.

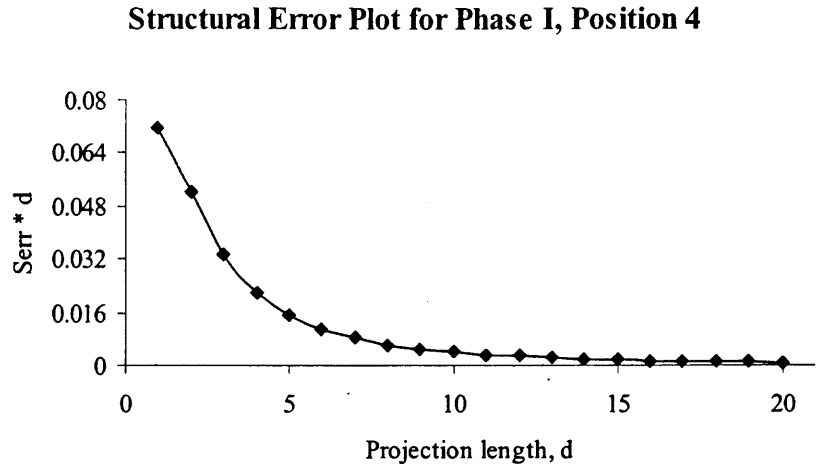

Figure 6.28 Structural error plot for phase I, position 4.

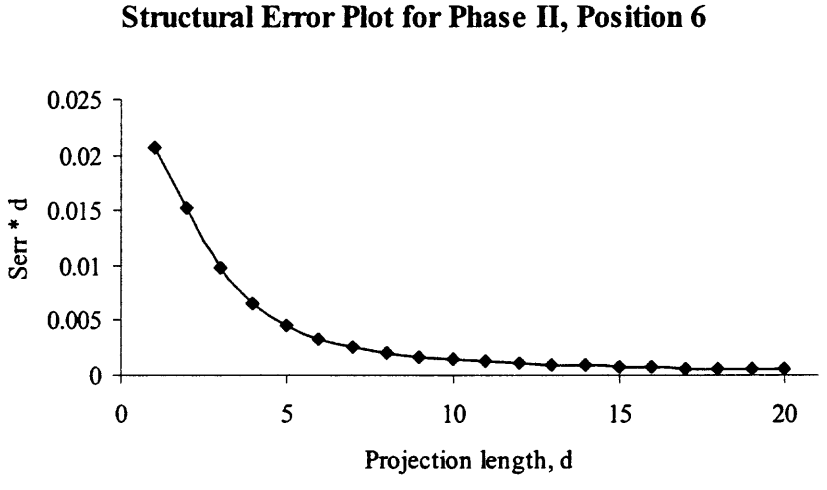

Figure 6.29 Structural error plot for phase II, position 6.

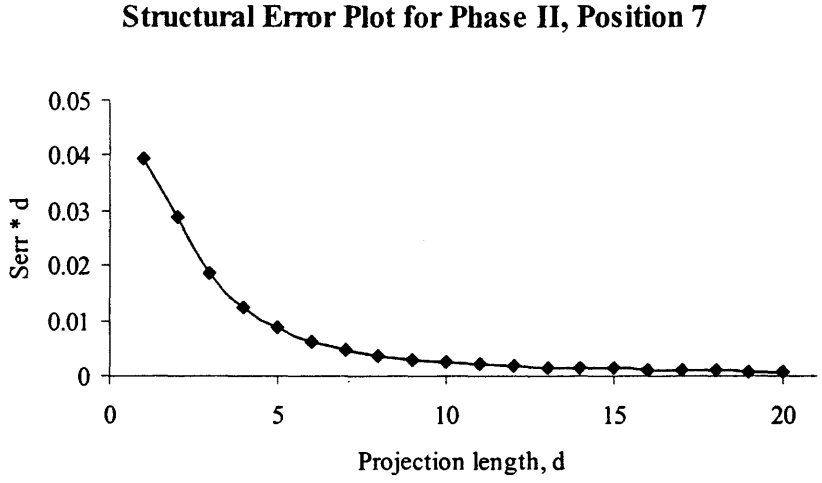

Figure 6.30 Structural error plot for phase II, position 7.

Using a projection length of 7 units in plane-to-sphere projection results in the adjustable spherical four-bar motion generator fixed and moving pivots given in Table 6.12. Figure 6.31 illustrates a graphical representation of the synthesized adjustable spherical four-bar motion generator. Table 6.13 includes the rigid-body positions achieved by the adjustable spherical four-bar motion generator along with the calculated structural error.

Table 6.12 Projected Fixed and Moving Pivots for the Adjustable Spherical Four-Bar Motion Generator

$\mathbf{a}_0$	0, -0.00423, 0.99999
$\mathbf{a}_1$	-0.09033, 0.10467, 0.99040
$\mathbf{a}_{1n}$	-0.03692, 0.13244, 0.99050
$\mathbf{b}_0$	0.20951, -0.01323, 0.97772
$\mathbf{b}_1$	0.17704, 0.19159, 0.96538
$\mathbf{b}_{1n}$	0.11727, 0.17491, 0.97758

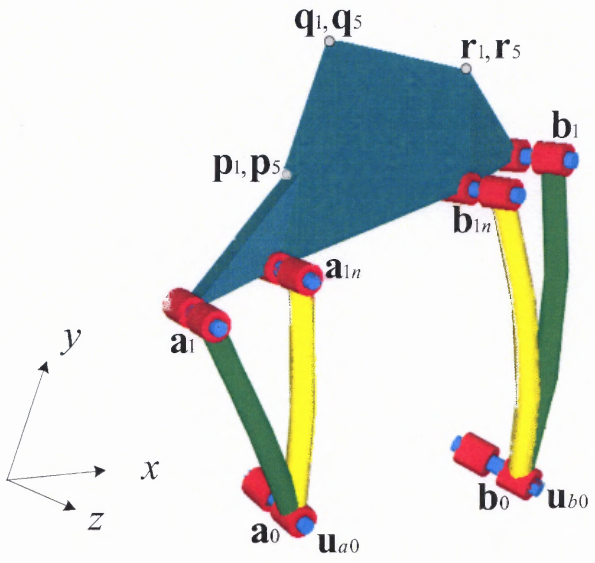

Figure 6.31 The adjustable spherical four-bar motion generator calculated by plane-to-sphere projection.

Table 6.13 Rigid-Body Positions Achieved by the Adjustable Spherical Four-Bar Motion Generator

Pos.	p	q	r	S_{err}*d [10^{-3}]
1	-0.02733, 0.19212, 0.98099	0.00551, 0.27613, 0.96111	0.12076, 0.25322, 0.95984	
2	-0.01586, 0.19800, 0.98007	0.01867, 0.28116, 0.95948	0.13338, 0.25572, 0.95751	2.575
3	-0.00388, 0.20305, 0.97916	0.03221, 0.28537, 0.95788	0.14634, 0.25751, 0.95513	5.296
4	0.00847, 0.20722, 0.97826	0.04603, 0.28870, 0.95631	0.15955, 0.25854, 0.95273	8.148
5	-0.02733, 0.19212, 0.98099	0.00551, 0.27613, 0.96111	0.12076, 0.25322, 0.95984	
6	-0.01640, 0.19492, 0.98068	0.01484, 0.27936, 0.96007	0.13041, 0.25825, 0.95724	2.622
7	-0.00533, 0.19668, 0.98045	0.02411, 0.28162, 0.95922	0.13997, 0.26252, 0.95472	4.915

6.3.2 Sphere-to-Plane Projection

Given the synthesized spherical four-bar motion generator in the previous sub-section, the parameters of a kinematically-equivalent adjustable planar four-bar motion generator will be calculated to demonstrate the structural error difference between plane-to-sphere and sphere-to-plane projections. Using the sphere-to-plane projection method described

in Section 4.1, each joint coordinate of the synthesized adjustable spherical four-bar motion generator is projected on a specified plane as described in Section 4.1. The origin of this sphere is coincident with the origin of the coordinate system and the synthesized planar motion generator lies on plane parallel to the X-Y plane and offset from the origin by a distance "d" along the z-axis.

As indicated in Figures 6.32 through 6.36, the magnitude of the offset distance "d" has no effect on the structural error between the prescribed projected rigid body positions and the positions achieved by the projected adjustable planar four-bar motion generator. This is due to the joint axes varying with the projection length in plane-to-sphere projections but remaining constant with varying projection lengths in sphere-to-plane projections.

No matter what projection length is specified, the adjustable planar four-bar path generator given in Figure 6.25 is achieved precisely when projecting the synthesized adjustable spherical path generator onto a plane. Figures 6.32 through 6.36 illustrate the structural error between the prescribed projected rigid body positions and the positions achieved by the adjustable planar four-bar motion generator (for each rigid body position).

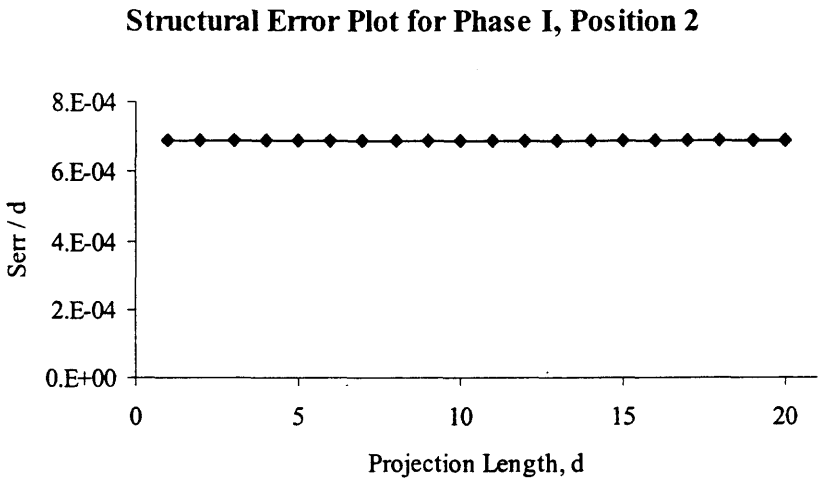

Figure 6.32 Structural error plot for phase I, position 2.

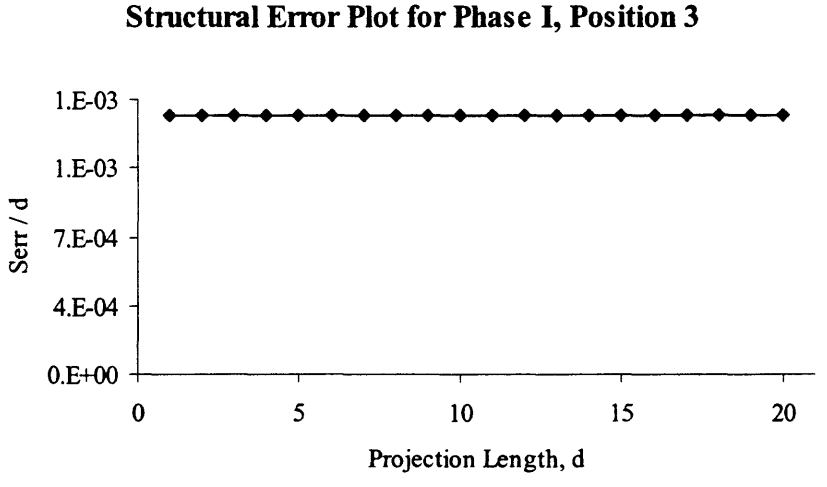

Figure 6.33 Structural error plot for phase I, position 3.

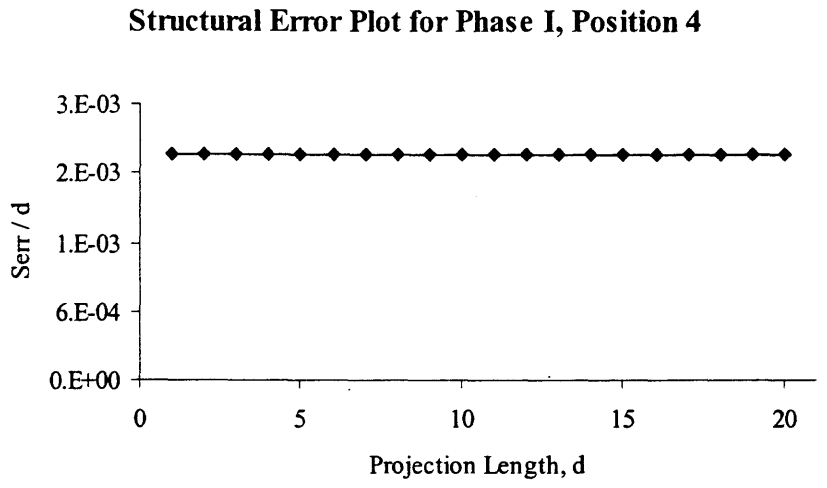

Figure 6.34 Structural error plot for phase I, position 4.

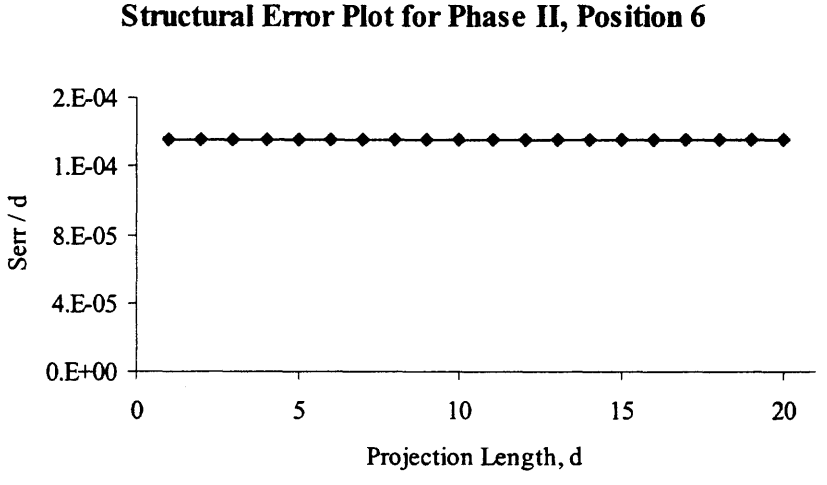

Figure 6.35 Structural error plot for phase II, position 6.

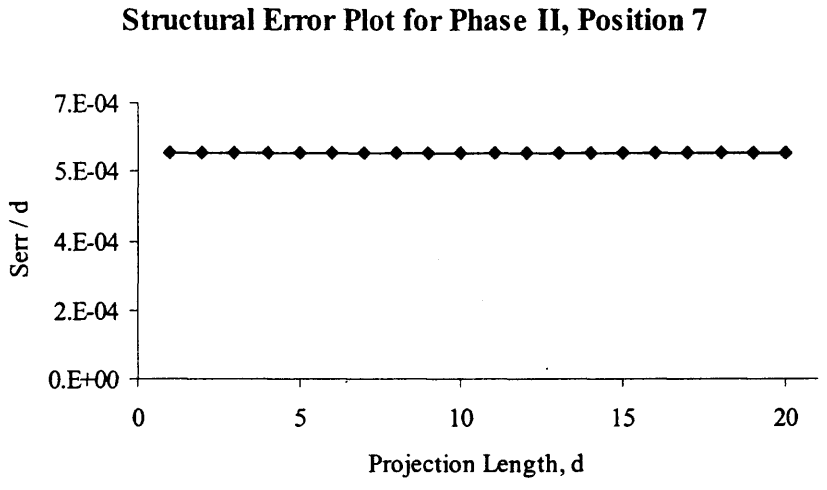

Figure 6.36 Structural error plot for phase II, position 7.

6.4 Synthesis of Adjustable Five-Bar Spherical and Planar Path Generators

6.4.1 Plane-to-Sphere Projection

This particular problem depicts a situation where the user wants to calculate an adjustable spherical five-bar path generator given prescribed spherical rigid body points. The end objective in this example is to calculate the parameters of an adjustable spherical five-bar path generator that would achieve the prescribed spherical rigid body points.

The x, y and z-coordinates of seven prescribed spherical rigid body points are listed in Table 6.14. The positions in Table 6.14 lie on a sphere with a radius of 1 unit. It is the design intent that one mechanism adjustment achieves positions 1 through 4 and another mechanism adjustment achieves positions 5 through 7.

Using the sphere-to-plane projection method described in Section 4.1, the planar rigid-body positions in Table 6.15 were calculated. The positions in Table 6.15 are the

spherical rigid-body positions in Table 6.15 projected onto a plane at an offset distance of 5 units ($d_j = 5$) along the z-axis from the origin of the coordinate system. As illustrated in Figure 5.1, the origin of the coordinate system is coincident with the origin of the sphere containing the prescribed rigid body positions.

Table 6.14 Prescribed Rigid Body Points for the Adjustable Spherical Five-Bar Path Generator

Pos.	p	q
Pos. 1	0.03393, 0.35490, 0.93429	-0.02644, 0.19433, 0.98058
Pos. 2	0.05158, 0.34898, 0.93571	0.00722, 0.18343, 0.98301
Pos. 3	0.06711, 0.33704, 0.93910	0.03969, 0.16656, 0.98523
Pos. 4	0.07946, 0.31904, 0.94441	0.07001, 0.14400, 0.98710
Pos. 5	0.03393, 0.35490, 0.93429	-0.02644, 0.19433, 0.98058
Pos. 6	0.06647, 0.35564, 0.93226	0.00771, 0.19596, 0.98058
Pos. 7	0.09752, 0.35146, 0.93111	0.04162, 0.19165, 0.98058

Table 6.15 Prescribed Projected Rigid-Body Points and Orientation Angles for the Adjustable Planar Five-Bar Path Generator

Pos.	p	θ_{1j} [Deg.]
Pos. 1	0.18158, 1.89930	
Pos. 2	0.27562, 1.86479	4.82323
Pos. 3	0.35731, 1.79448	9.87692
Pos. 4	0.42069, 1.68910	15.26541
Pos. 5	0.18158, 1.89930	
Pos. 6	0.35650, 1.90741	-0.04825
Pos. 7	0.52368, 1.88732	0.31107

Now that the spherical rigid-body positions have been projected onto a plane, they are planar rigid-body positions and an adjustable planar path generator can be designed to approximate these positions. Equations 6.27 through 6.31 are used to calculate five of

the six unknowns in $\mathbf{a}_0$, $\mathbf{a}_1$ and $\mathbf{a}_{1n}$. These equations are identical to Equations 2.41 through 2.45. The variable a_{0x} and the link length R_1 were specified ($a_{0x} = 0$ and $R_1 = 1$). Using the following initial guesses:

$a_{0y} = 0.01$, $\mathbf{a}_1 = (0.1, 0.9)$, $\mathbf{a}_{1n} = (-0.1, 0.9)$,

the adjustable planar five-bar path generator solutions converges to

$a_{0y} = 0.\ 00041$, $\mathbf{a}_1 = (0.12192, 0.99304)$, $\mathbf{a}_{1n} = (-0.13450, 0.99126)$.

$$([D_{12}]\mathbf{a}_1 - \mathbf{a}_0)^T([D_{12}]\mathbf{a}_1 - \mathbf{a}_0) - R_1^2 = 0 \tag{6.27}$$

$$([D_{13}]\mathbf{a}_1 - \mathbf{a}_0)^T([D_{13}]\mathbf{a}_1 - \mathbf{a}_0) - R_1^2 = 0 \tag{6.28}$$

$$([D_{14}]\mathbf{a}_1 - \mathbf{a}_0)^T([D_{14}]\mathbf{a}_1 - \mathbf{a}_0) - R_1^2 = 0 \tag{6.29}$$

$$([D_{56}]\mathbf{a}_{1n} - \mathbf{a}_0)^T([D_{56}]\mathbf{a}_{1n} - \mathbf{a}_0) - R_1^2 = 0 \tag{6.30}$$

$$([D_{57}]\mathbf{a}_{1n} - \mathbf{a}_0)^T([D_{57}]\mathbf{a}_{1n} - \mathbf{a}_0) - R_1^2 = 0 \tag{6.31}$$

Using Equation 6.32, the displacement angles ($\delta\theta$) for this link were calculated. These displacement angles are -10°, -20°, and -30° for phase 1 and -10° and -20° for phase 2. The displacements for angle ϕ were calculated using the relationship of $\delta\phi = f(\delta\theta) = 0.5*\delta\theta$. With this relationship, displacement $\delta\phi$ angles of -5°, -10° and -15° for phase 1 and -5° and -10° for phase 2 were calculated.

$$\theta_1 = \cos^{-1}\left[\frac{\mathbf{u}.\mathbf{v}}{|\mathbf{u}|.|\mathbf{v}|}\right], \text{ where } \mathbf{u} = \overline{\mathbf{a}_0\mathbf{a}}, \mathbf{v} = \overline{\mathbf{b}_0\mathbf{a}_0} \tag{6.32}$$

$$([D_{12}]\mathbf{c}_1 - [T_1]\mathbf{b}_1)^T([D_{12}]\mathbf{c}_1 - [T_1]\mathbf{b}_1) - R_3^2 = 0 \tag{6.33}$$

$$([D_{13}]\mathbf{c}_1 - [T_2]\mathbf{b}_1)^T([D_{13}]\mathbf{c}_1 - [T_2]\mathbf{b}_1) - R_3^2 = 0 \tag{6.34}$$

$$([D_{14}]\mathbf{c}_1 - [T_3]\mathbf{b}_1)^T([D_{14}]\mathbf{c}_1 - [T_3]\mathbf{b}_1) - R_3^2 = 0 \tag{6.35}$$

$$([D_{56}]\mathbf{c}_{1n} - [T_6]\mathbf{b}_1)^T([D_{56}]\mathbf{c}_{1n} - [T_6]\mathbf{b}_1) - R_3^2 = 0 \tag{6.36}$$

$$([D_{57}]\mathbf{c}_{1n} - [T_7]\mathbf{b}_1)^T([D_{57}]\mathbf{c}_{1n} - [T_7]\mathbf{b}_1) - R_3^2 = 0 \tag{6.37}$$

Equations 6.33 through 6.37 were used to calculate five of the eight unknowns in $\mathbf{b}_1$, $\mathbf{c}_1$ and $\mathbf{c}_{1n}$. Equations 6.32 through 6.37 are identical to Equations 2.46 through 2.51. The variable $\mathbf{b}_0$, the link R_4 and the initial value of angle ϕ were specified ($\mathbf{b}_0 = (1.25, 0)$, $R_4 = 1$, $\phi = 45°$).

Using the following initial guesses:

$R_3 = 1.0$, $\mathbf{c}_1 = (0.9, 1.5)$, $\mathbf{c}_{1n} = (1.2, 1.8)$,

the adjustable planar five-bar path generator solutions converges to

$\mathbf{c}_1 = (0.89096, 1.45454)$, $\mathbf{c}_{1n} = (1.21704, 1.77820)$, $R_3 = 1.30204$.

The synthesized adjustable planar five-bar path generator is illustrated in Figure 6.37. A gear train was incorporated in the synthesized adjustable planar five-bar path generator. Since the prescribed relationship between the driving link displacement angles was $\delta\phi = f(\delta\theta) = 0.5*\delta\theta$, a 2:1 gear ratio between both driving links is required. The same ratio is required if pulleys, sprockets or independent motors are incorporates in the driving links.

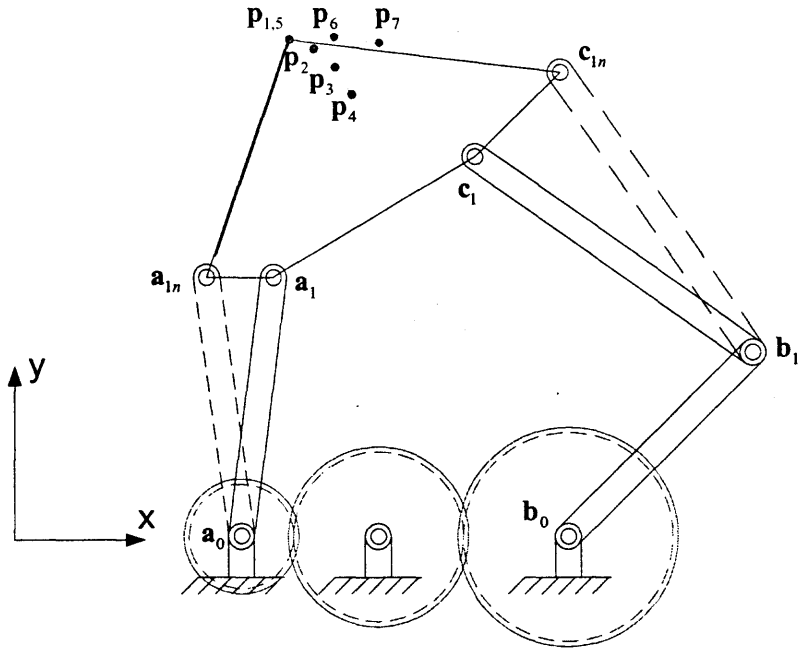

Figure 6.37 The synthesized adjustable planar five-bar path generator.

Although an adjustable planar five-bar path generator has been synthesized, an adjustable spherical five-bar path generator is needed to approximate the prescribed rigid body positions in Table 6.14. Using the MATHEMATICA model in Appendix B.4, each joint coordinate of the synthesized planar five-bar mechanism is projected onto a sphere of unit radius.

The structural error plots for each rigid body position are illustrated in Figures 6.38 through 6.42. As these figures illustrate, the structural error (S_{err} * d) decreases as the magnitude of the projection length "d" increases.

In this example, a projection length of 5 (and subsequently, a structural error less than 0.01 in Figures 6.38 through 6.42) was selected. Table 6.16 includes the fixed and moving pivots of the synthesized adjustable spherical five-bar path generator projected onto a sphere. Figure 6.43 illustrates the synthesized adjustable spherical five-bar path

generator. The rigid body points achieved by the adjustable spherical five-bar path generator are given in Table 6.17 along with the measured structural error. With a plane-to-sphere projection length of 5 units, the maximum structural error (S_{err} * d) calculated is approximately 0.0098 units for rigid body position 4 and 0.0066 for position 7.

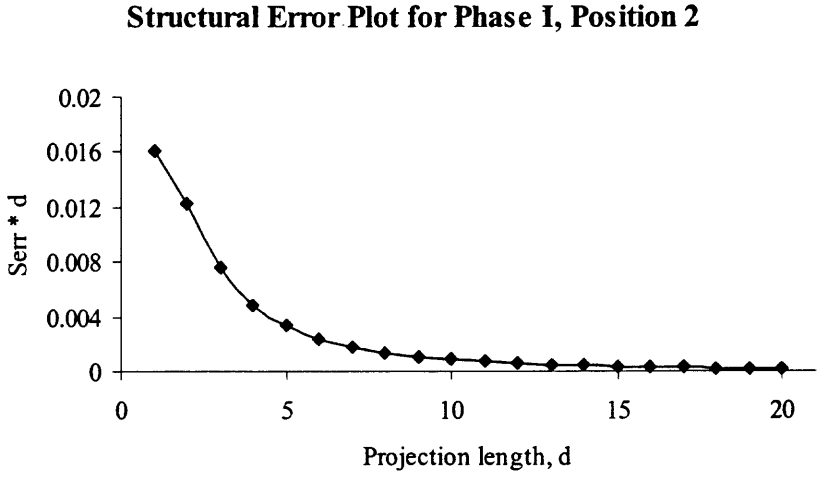

Figure 6.38 Structural error plot for phase I, position 2.

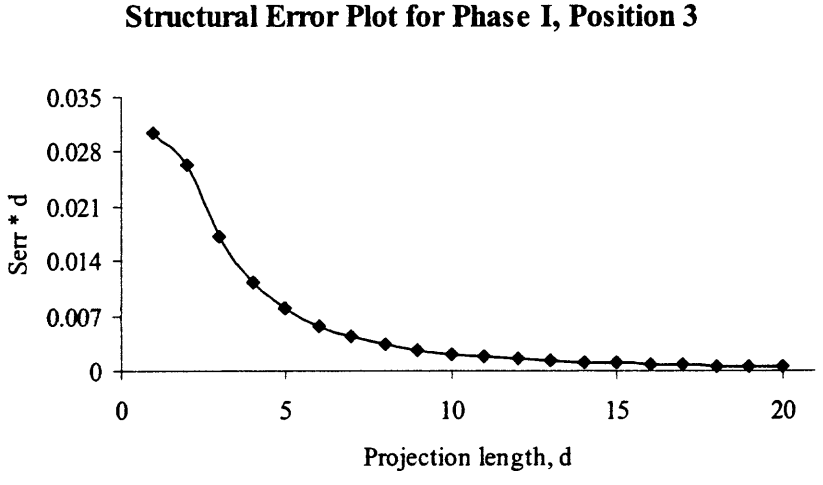

Figure 6.39 Structural error plot for phase I, position 3.

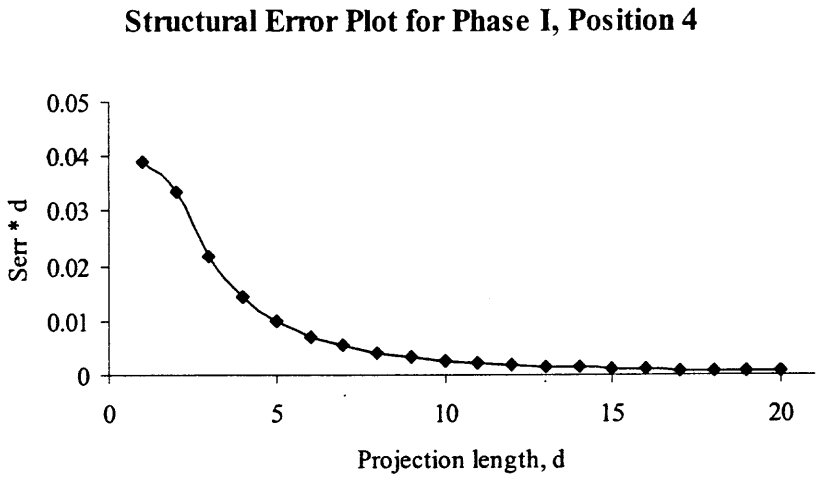

Figure 6.40 Structural error plot for phase I, position 4.

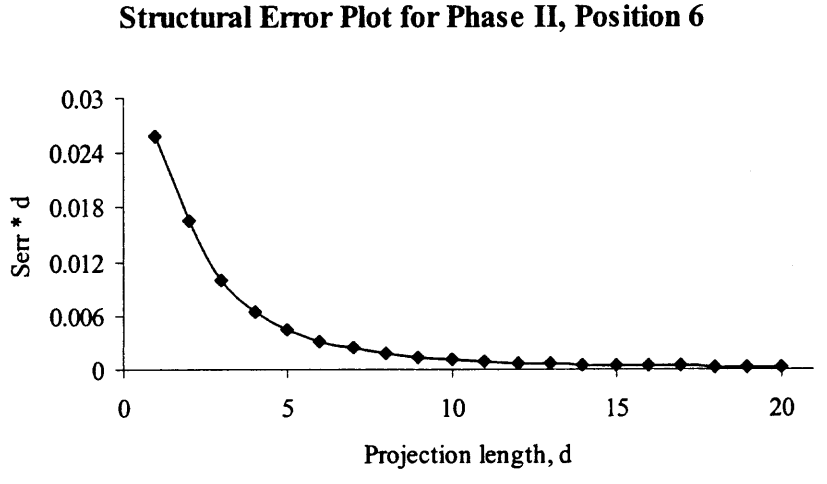

Figure 6.41 Structural error plot for phase II, position 6.

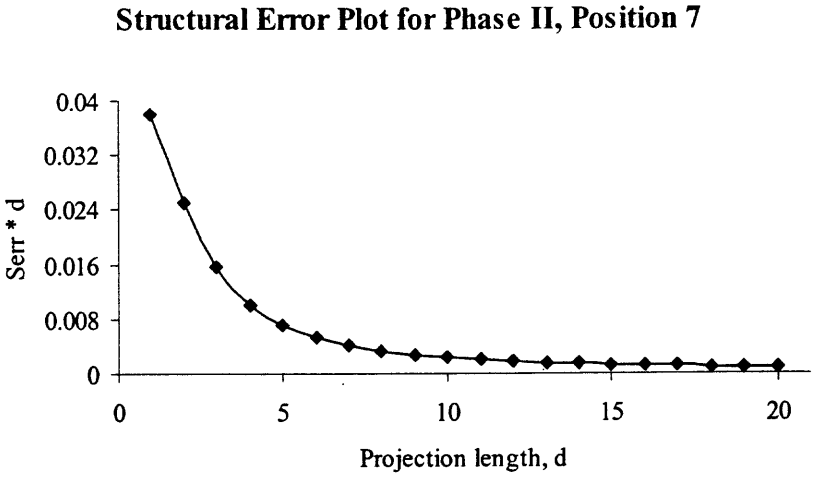

Figure 6.42 Structural error plot for phase II, position 7.

Table 6.16 Projected Fixed and Moving Pivots for the Synthesized Adjustable Spherical Five-Bar Path Generator

$\mathbf{a}_0$	0, 0.00008, 1.
$\mathbf{a}_1$	0.02391, 0.19475, 0.98056
$\mathbf{a}_{1n}$	-0.02638, 0.19440, 0.98057
$\mathbf{b}_0$	0.24254, 0, 0.97014
$\mathbf{b}_1$	0.36137, 0.13057, 0.92323
$\mathbf{c}_1$	0.16865, 0.27533, 0.94644
$\mathbf{c}_{1n}$	0.22353, 0.32660, 0.91835

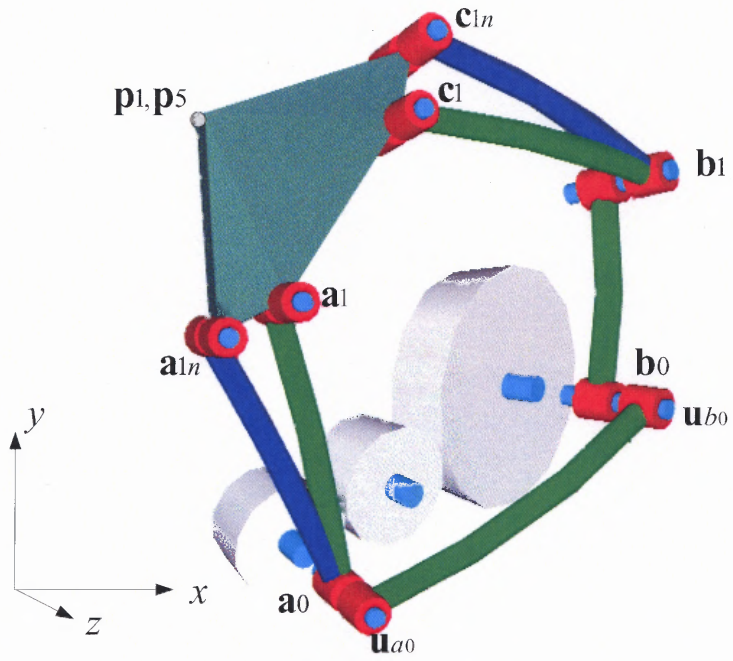

Figure 6.43 The adjustable spherical five-bar path generator calculated by plane-to-sphere projection.

Table 6.17 Rigid-Body Positions Achieved by the Synthesized Adjustable Spherical Five-Bar Path Generator

	p	Serr * d [10^{-3}]
Pos. 1	0.03393, 0.35490, 0.93429	
Pos. 2	0.05124, 0.34845, 0.93593	3.3
Pos. 3	0.06589, 0.33614, 0.93950	7.8
Pos. 4	0.07771, 0.31824, 0.94482	9.8
Pos. 5	0.03393, 0.35490, 0.93429	
Pos. 6	0.06653, 0.35645, 0.93194	4.4
Pos. 7	0.09780, 0.35265, 0.93063	6.6

6.4.2 Sphere-to-Plane Projection

Given the synthesized spherical five-bar path generator in the previous sub-section, the parameters of a kinematically-equivalent adjustable planar five-bar path generator will be calculated to demonstrate the structural error difference between plane-to-sphere and sphere-to-plane projections. Using the sphere-to-plane projection method described in section4.1, each joint coordinate of the synthesized spherical path generator is projected onto a specified plane as described in Section 4.1. The origin of this sphere is coincident with the origin of the coordinate system and the synthesized adjustable planar five-bar path generator lies on plane parallel to the X-Y plane and offset from the origin by a distance "d" along the z-axis.

As indicated in Figures 6.44 through 6.48, the magnitude of the offset distance "d" has no effect on the structural error between the prescribed projected points and the points achieved by the projected adjustable planar five-bar path generator. This is due to the joint axes varying in orientation with the projection length in plane-to-sphere projections but remaining constant with varying projection lengths in sphere-to-plane projections.

No matter the projection length is specified, the adjustable planar five-bar path generator illustrated in Figure 6.37 is achieved precisely when projecting the synthesized adjustable spherical five-bar path generator onto a plane. Figures 6.44 through 6.48 illustrate the structural error between the prescribed projected rigid body points and the points achieved by the adjustable planar five-bar path generator (for each rigid body point).

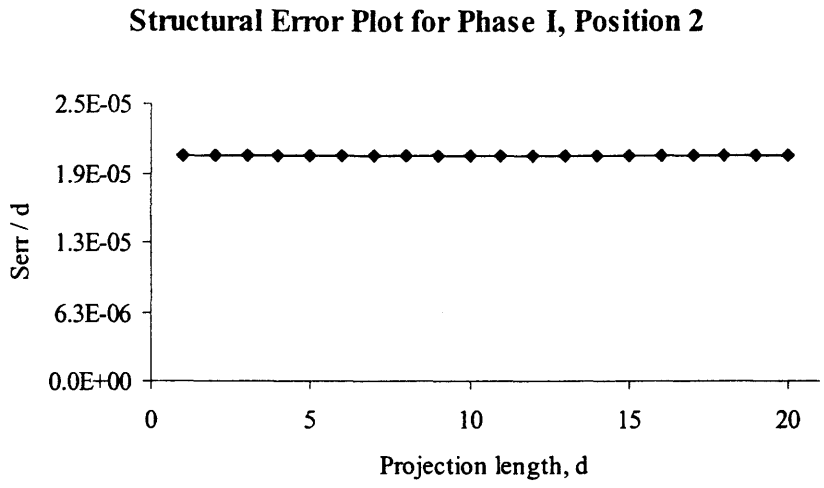

Figure 6.44 Structural error plot for phase I, position 2.

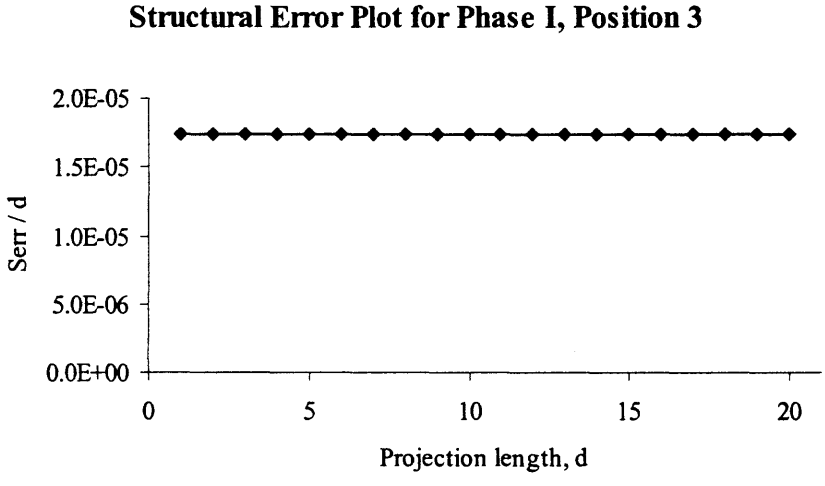

Figure 6.45 Structural error plot for phase I, position 3.

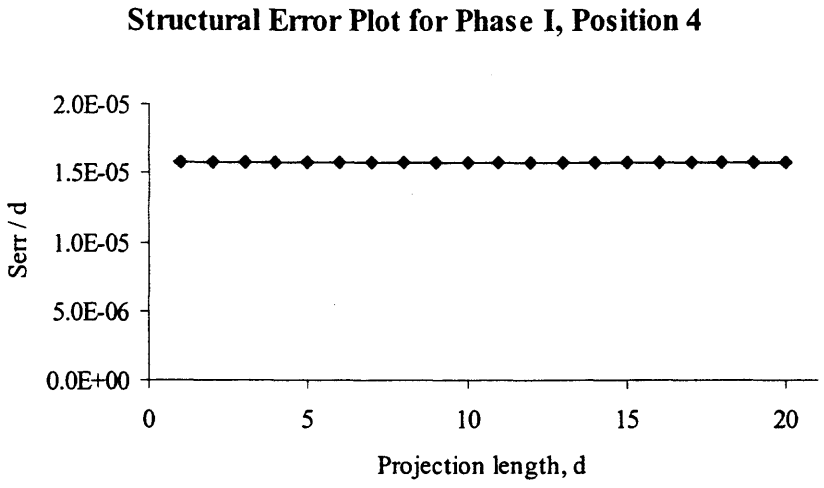

Figure 6.46 Structural error plot for phase I, position 4.

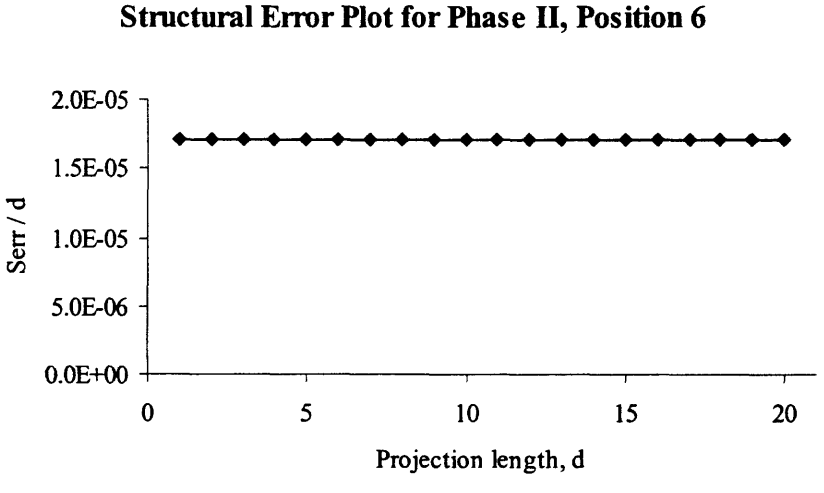

Figure 6.47 Structural error plot for phase II, position 6.

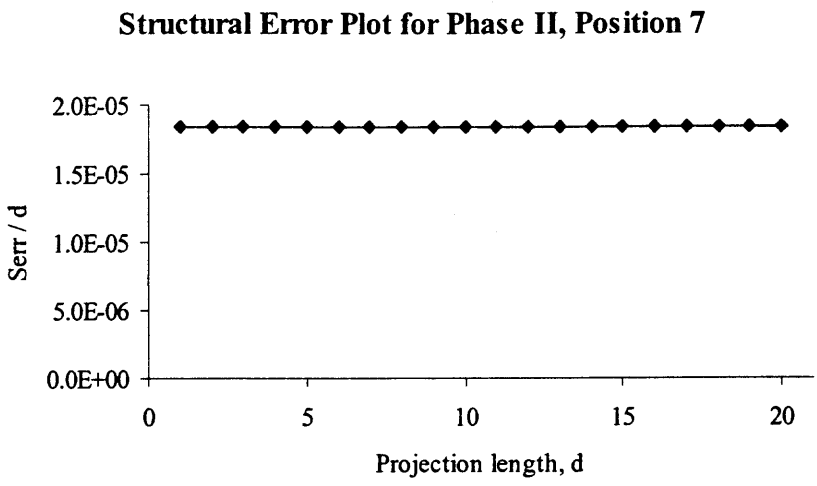

Figure 6.48 Structural error plot for phase II, position 7.

6.5 Synthesis of Adjustable Five Bar Spherical and Planar Motion Generators

6.5.1 Plane-to-Sphere Projection

This particular problem depicts a situation where the user wants to calculate an adjustable spherical five-bar motion generator given prescribed spherical rigid body positions. The end objective in this example is to calculate the parameters of an adjustable spherical five-bar motion generator that would achieve the prescribed spherical rigid body positions.

The x, y and z-coordinates of seven prescribed rigid body positions are listed in Table 6.18. The positions in Table 6.18 lie onto a sphere with a radius of 1 unit. It is the design intent that one mechanism adjustment achieves position 1 through 4 and another mechanism adjustment achieves position 5 through 7.

Using the sphere-to-plane projection method described in Section 4.1, the planar rigid-body positions in Table 6.19 were calculated. The positions in Table 6.19 are the spherical rigid-body positions in Table 6.18 projected onto a plane at an offset distance on 6 units ($d_j = 6$) along the z-axis from the origin of the coordinate system. As illustrated in Figure 4.1, the origin of the coordinate system is coincident with the origin of the sphere containing the prescribed rigid body positions.

Table 6.18 Prescribed Rigid Body Positions for the Adjustable Spherical Five-Bar Motion Generator

Pos.	p	q	r
Pos. 1	-0.02180, 0.24170, 0.97011	0.02937, 0.30795, 0.95095	0.12226, 0.30577, 0.94422
Pos. 2	-0.00092, 0.23265, 0.97256	0.04373, 0.30286, 0.95203	0.13581, 0.30743, 0.94183
Pos. 3	0.01869, 0.21822, 0.97572	0.05623, 0.29246, 0.95462	0.14687, 0.30427, 0.94119
Pos. 4	0.03622, 0.19845, 0.97944	0.06596, 0.27677, 0.95867	0.15448, 0.29655, 0.94244
Pos. 5	-0.02180, 0.24170, 0.97011	0.02937, 0.30795, 0.95095	0.12226, 0.30577, 0.94422
Pos. 6	0.00642, 0.24303, 0.97000	0.05700, 0.30874, 0.94944	0.14917, 0.30571, 0.94037
Pos. 7	0.03388, 0.23955, 0.97029	0.08333, 0.30531, 0.94860	0.17473, 0.30211, 0.93712

Table 6.19 Prescribed Projected Rigid-Body Positions for the Adjustable Planar Five Bar Motion Generator

Pos.	p	q	r
Pos. 1	-0.1348, 1.4949	0.1853, 1.9430	0.7769, 1.9430
Pos. 2	-0.0057, 1.4356	0.2758, 1.9089	0.8653, 1.9584
Pos. 3	0.1150, 1.3422	0.3537, 1.8385	0.9366, 1.9397
Pos. 4	0.2220, 1.2158	0.4130, 1.7323	0.9838, 1.8879
Pos. 5	-0.1348, 1.4949	0.1853, 1.9430	0.7769, 1.9430
Pos. 6	0.0397, 1.5033	0.3602, 1.9511	0.9518, 1.9506
Pos. 7	0.2095, 1.4813	0.5271, 1.9311	1.1187, 1.9343

Now that the spherical rigid-body positions have been projected onto a plane, they are planar rigid-body positions and an adjustable planar motion generator can be designed to approximate these positions. Equations 6.38 through 6.42 were used to calculate five of the six unknowns in $\mathbf{a}_0$, $\mathbf{a}_1$ and $\mathbf{a}_{1n}$. These equations are identical to Equations 2.58 through 2.62. The variable a_{0x} and the link length R_1 were specified ($a_{0x} = 0$ and $R_1 = 1$). Using the following initial guesses:

$$a_{0y} = 0.01,\ \mathbf{a}_1 = (0.01, 0.9),\ \mathbf{a}_{1n} = (-0.20, 0.90),$$

the adjustable planar five-bar motion generator solutions converges to

a_{0y} = -0.0023, $\mathbf{a}_1$ = (0.1212, 0.9903), $\mathbf{a}_{1n}$ = (-0.1350, 0.9885).

$$([D_{12}]\mathbf{a}_1 - \mathbf{a}_0)^T([D_{12}]\mathbf{a}_1 - \mathbf{a}_0) - R_1^2 = 0 \quad (6.38)$$

$$([D_{13}]\mathbf{a}_1 - \mathbf{a}_0)^T([D_{13}]\mathbf{a}_1 - \mathbf{a}_0) - R_1^2 = 0 \quad (6.39)$$

$$([D_{14}]\mathbf{a}_1 - \mathbf{a}_0)^T([D_{14}]\mathbf{a}_1 - \mathbf{a}_0) - R_1^2 = 0 \quad (6.40)$$

$$([D_{56}]\mathbf{a}_{1n} - \mathbf{a}_0)^T([D_{56}]\mathbf{a}_{1n} - \mathbf{a}_0) - R_1^2 = 0 \quad (6.41)$$

$$([D_{57}]\mathbf{a}_{1n} - \mathbf{a}_0)^T([D_{57}]\mathbf{a}_{1n} - \mathbf{a}_0) - R_1^2 = 0 \quad (6.42)$$

Using Equation 6.43, the displacement angles ($\delta\theta$) for this link were calculated. These displacement angles are -10°, -20°, and -30° for phase 1 and -10° and -20° for phase 2. The displacements for angle ϕ were calculated using the relationship $\delta\phi = f(\delta\theta) = 0.5*\delta\theta$. With this relationship, displacement $\delta\phi$ angles of -5°, -10° and -15° for phase 1 and -5° and -10° for phase 2 were calculated.

$$\theta_1 = \cos^{-1}\left[\frac{\mathbf{u}.\mathbf{v}}{|\mathbf{u}|.|\mathbf{v}|}\right] \text{ , where } \mathbf{u} = \overline{\mathbf{a}_0\mathbf{a}} \text{ , } \mathbf{v} = \overline{\mathbf{b}_0\mathbf{a}_0} \quad (6.43)$$

$$([D_{12}]\mathbf{c}_1 - [T_1]\mathbf{b}_1)^T([D_{12}]\mathbf{c}_1 - [T_1]\mathbf{b}_1) - R_3^2 = 0 \quad (6.44)$$

$$([D_{13}]\mathbf{c}_1 - [T_2]\mathbf{b}_1)^T([D_{13}]\mathbf{c}_1 - [T_2]\mathbf{b}_1) - R_3^2 = 0 \quad (6.45)$$

$$([D_{14}]\mathbf{c}_1 - [T_3]\mathbf{b}_1)^T([D_{14}]\mathbf{c}_1 - [T_3]\mathbf{b}_1) - R_3^2 = 0 \quad (6.46)$$

$$([D_{56}]\mathbf{c}_{1n} - [T_6]\mathbf{b}_1)^T([D_{56}]\mathbf{c}_{1n} - [T_6]\mathbf{b}_1) - R_3^2 = 0 \quad (6.47)$$

$$([D_{57}]\mathbf{c}_{1n} - [T_7]\mathbf{b}_1)^T([D_{57}]\mathbf{c}_{1n} - [T_7]\mathbf{b}_1) - R_3^2 = 0 \quad (6.48)$$

Equations 6.44 through 6.48 were used to calculate five of the eight unknowns in $\mathbf{b}_1$, $\mathbf{c}_1$ and $\mathbf{c}_{1n}$. Equations 6.43 through 6.48 are identical to Equations 2.63 through 2.68. The variable $\mathbf{b}_0$, the link R_4 and the initial value of angle ϕ were specified ($\mathbf{b}_0$ = (1.25, 0), R_4 = 1, ϕ = 45°).

Using the following initial guesses:

$R_3 = 1.0$, $\mathbf{c}_1 = (0.7, 1.6)$, $\mathbf{c}_{1n} = (1.0, 1.9)$,

the planar five-bar mechanism solutions converged to

$R_3 = 1.3037$, $\mathbf{c}_1 = (0.8894, 1.4552)$, $\mathbf{c}_{1n} = (1.2153, 1.7792)$.

The synthesized adjustable planar five-bar motion generator is illustrated in Figure 6.49. A gear train was incorporated in the synthesized adjustable planar five-bar motion generator. Since the prescribed relationship between the driving link displacement angles was $\delta\phi = f(\delta\theta) = 0.5*\delta\theta$, a 2:1 gear ratio between both driving links is required. The same ratio is required if pulleys, sprockets or independent motors are incorporates in the driving links.

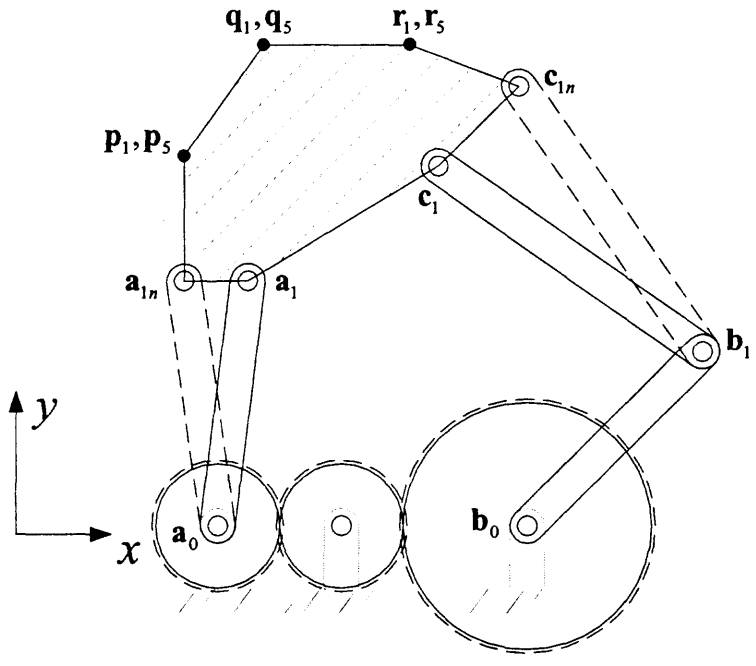

Figure 6.49 The synthesized adjustable planar five-bar motion generator

Although an adjustable planar five-bar motion generator has been synthesized, an adjustable spherical five-bar motion generator is needed to approximate the prescribed rigid body positions in Table 6.18. Using the MATHEMATICA model in Appendix B.5, each joint coordinate of the synthesized planar five-bar motion generator is projected onto a sphere of unit radius.

The structural error plots for reach rigid body position are illustrated in Figures 6.50 through 6.54. As these figures illustrate, the structural error (S_{err} * d) decreases as the magnitude of the projection length "d" increases.

In this example, a projection length of 6 (and subsequently a structural error less than 0.01 in Figures 6.50 and 6.54) was selected. Table 6.20 includes the fixed and moving pivots of the synthesized adjustable spherical five-bar motion generator projected onto a sphere. Figure 6.55 illustrates the synthesized adjustable spherical five-bar motion generator. The rigid body positions achieved by the adjustable spherical five-bar motion generator are given in Table 6.21 along with the measured structural error. With a plane-to-sphere projection length of 6 units, the maximum structural error (S_{err} * d) calculated is approximately 0.008 units for rigid body position 4 and 0.007 for position 7 shown as Table 6.21.

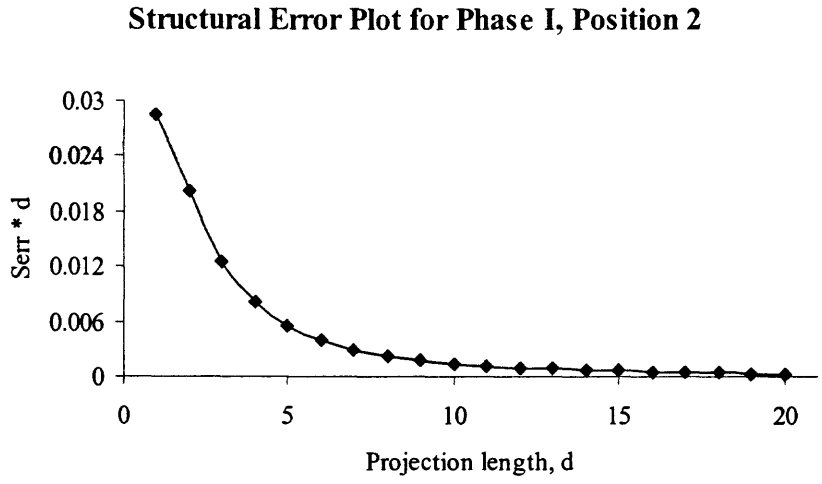

Figure 6.50 Structural error plot for phase I, position 2.

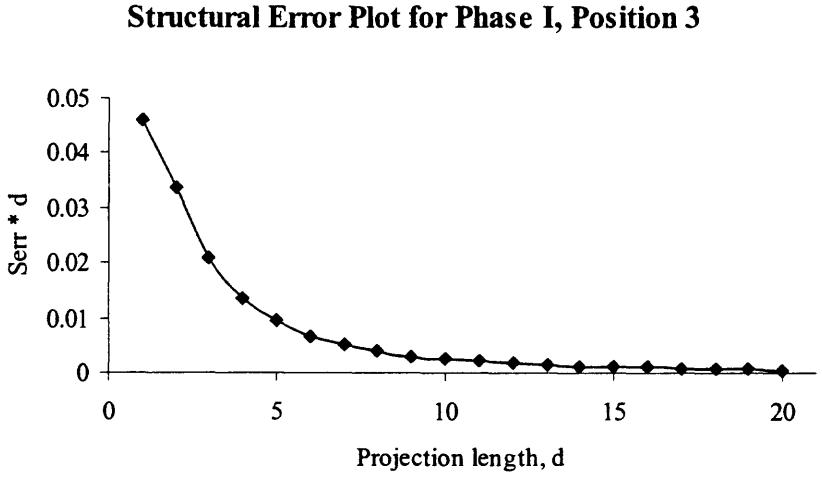

Figure 6.51 Structural error plot for phase I, position 3.

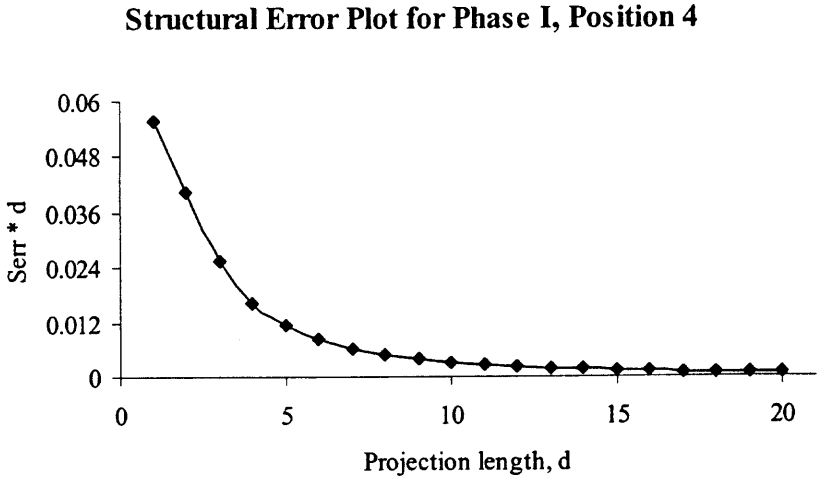

Figure 6.52 Structural error plot for phase I, position 4.

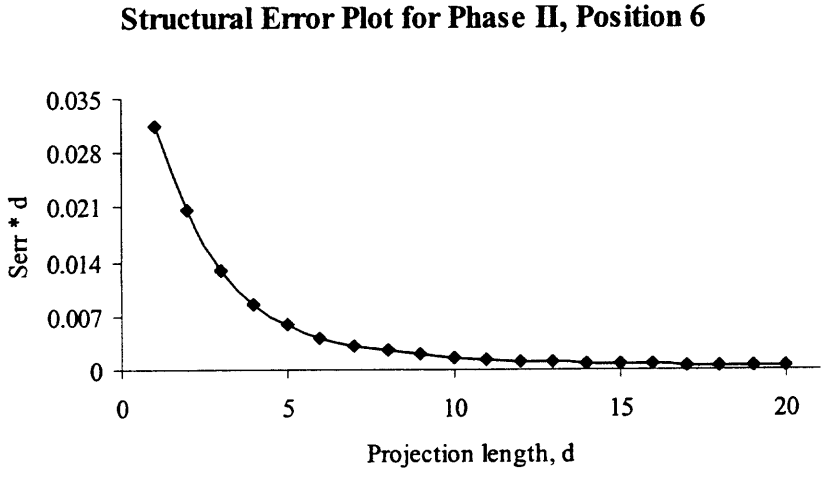

Figure 6.53 Structural error plot for phase II, position 6.

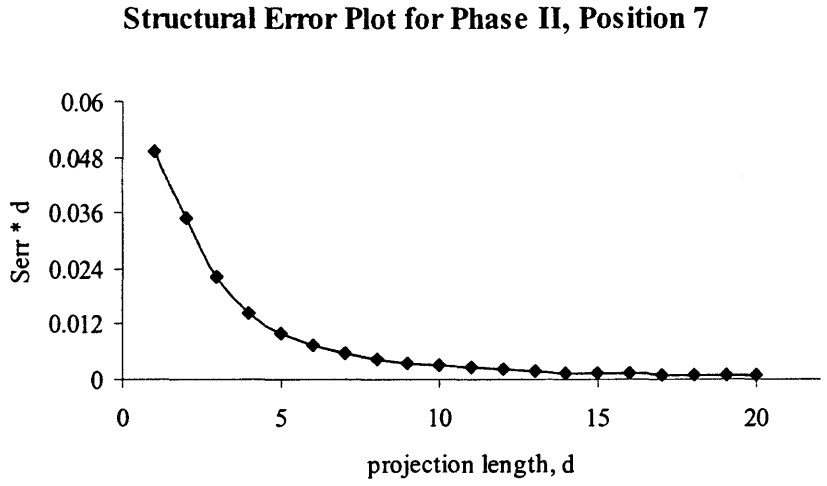

Figure 6.54 Structural error plot for phase II, position 7.

Table 6.20 Projected Fixed and Moving Pivots of the Synthesized Adjustable Spherical Five-Bar Motion Generator

$\mathbf{a}_0$	0, -0.0004, 1
$\mathbf{a}_1$	0.0199, 0.1628, 0.9865
$\mathbf{a}_{1n}$	-0.0222, 0.1625, 0.9865
$\mathbf{b}_0$	0.2040, 0.0, 0.9790
$\mathbf{b}_1$	0.3082, 0.1113, 0.9448
$\mathbf{c}_1$	0.1426, 0.2333, 0.9619
$\mathbf{c}_{1n}$	0.1906, 0.2791, 0.9412

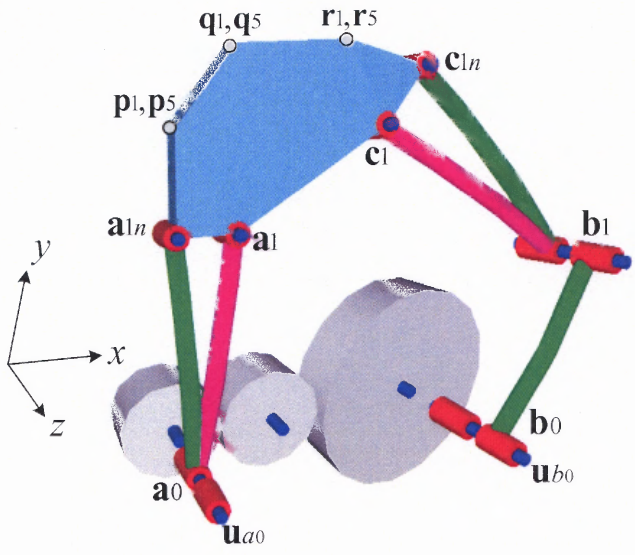

Figure 6.55 The adjustable spherical five-bar motion generator calculated by plane-to-sphere projection.

Table 6.21 Rigid-Body Positions Achieved by the Synthesized Adjustable Spherical Five-Bar Motion Generator

	p	q	r	S_{err} * d
Pos. 1	-0.0218, 0.2417, 0.9701	0.0294, 0.3079, 0.9509	0.1223, 0.3058, 0.9442	
Pos. 2	-0.0011, 0.2321, 0.9727	0.0434, 0.3026, 0.9521	0.1358, 0.3083, 0.9415	0.0039
Pos. 3	0.0181, 0.2175, 0.9759	0.0556, 0.2918, 0.9549	0.1466, 0.3056, 0.9408	0.0067
Pos. 4	0.0353, 0.1978, 0.9796	0.0652, 0.2756, 0.9590	0.1540, 0.2979, 0.9421	0.0081
Pos. 5	-0.0218, 0.2417, 0.9701	0.0294, 0.3079, 0.9509	0.1223, 0.3058, 0.9442	
Pos. 6	0.0064, 0.2431, 0.9700	0.0570, 0.3093, 0.9493	0.1497, 0.3071, 0.9398	0.0042
Pos. 7	0.0339, 0.2395, 0.9703	0.0834, 0.3061, 0.9483	0.1758, 0.3045, 0.9362	0.0074

6.5.2 Sphere-to-Plane Projection

Given the synthesized adjustable spherical five-bar motion generator in the previous sub-section, the parameters of a kinematically equivalent planar motion generator will be calculated to demonstrate the structural error difference between plane-to-sphere and sphere-to-plane projections. Using the sphere-to-plane projection method described in Section 4.1, each joint coordinate of the synthesized spherical motion generator is projected onto a specified plane as described in Section 4.1. The origin of this sphere is coincident with the origin of the coordinate system and the synthesized planar mechanism lies on plane parallel to the X-Y plane and offset from the origin by a distance "d" along the z-axis.

According to Figures 6.56 through 6.60, the magnitude of the offset distance "d" has no effect on the structural error between the prescribed projected rigid body positions and the positions achieved by the projected adjustable planar five-bar motion generator. This is due to the joint axes varying with the projection length in plane-to-sphere projections but remaining constant with varying projection lengths in sphere-to-plane projections.

No matter what projection length is specified, the adjustable planar five-bar motion generator illustrated in Figure 6.49 is achieved precisely when projecting the synthesized adjustable spherical five bar motion generator onto a plane. Figures 6.56 through 6.60 illustrate the structural error between the prescribed projected rigid body positions and the positions achieved by the adjustable planar five-bar motion generator (for each rigid body position).

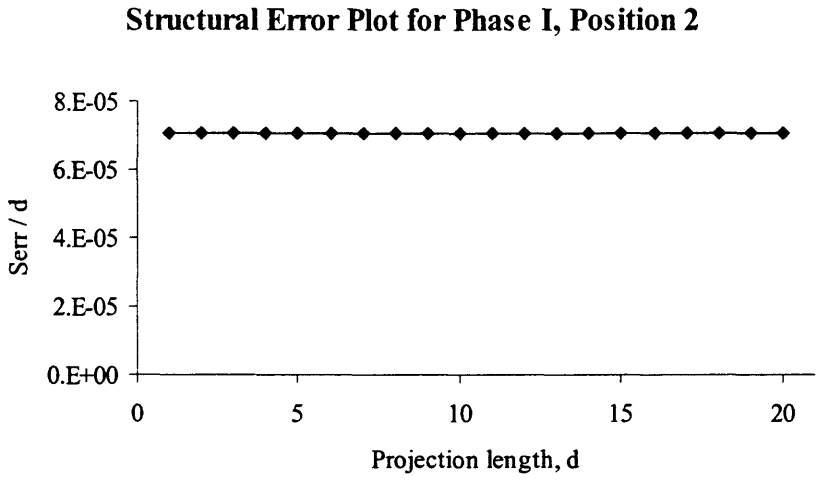

Figure 6.56 Structural error plot for phase I, position 2.

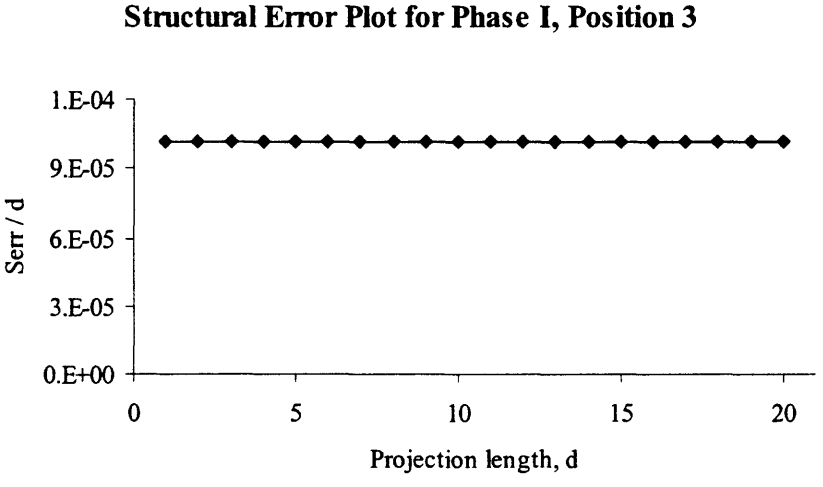

Figure 6.57 Structural error plot for phase I, position 3.

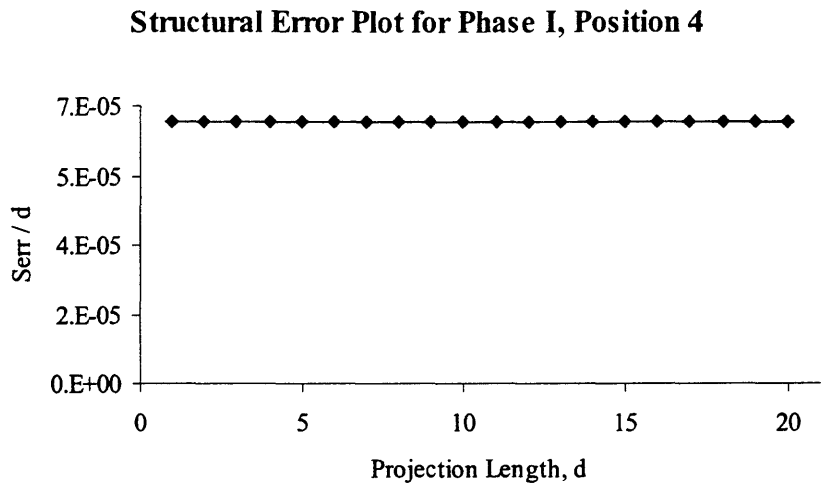

Figure 6.58 Structural error plot for phase I, position 4.

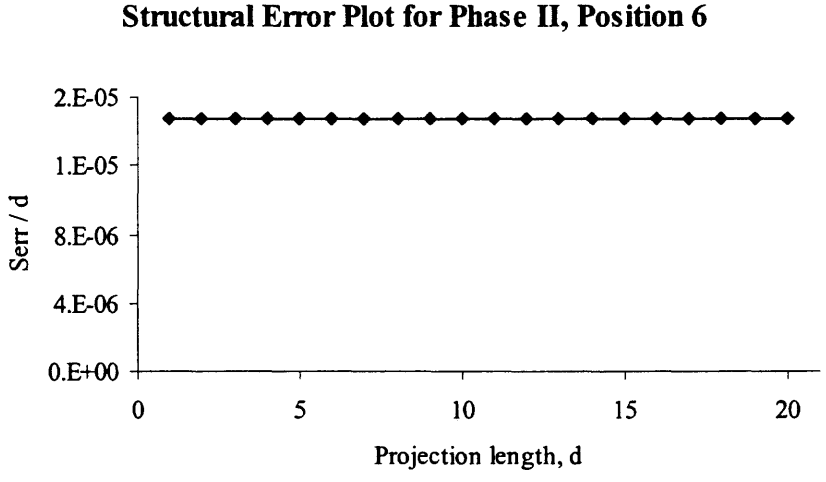

Figure 6.59 Structural error plot for phase II, position 6.

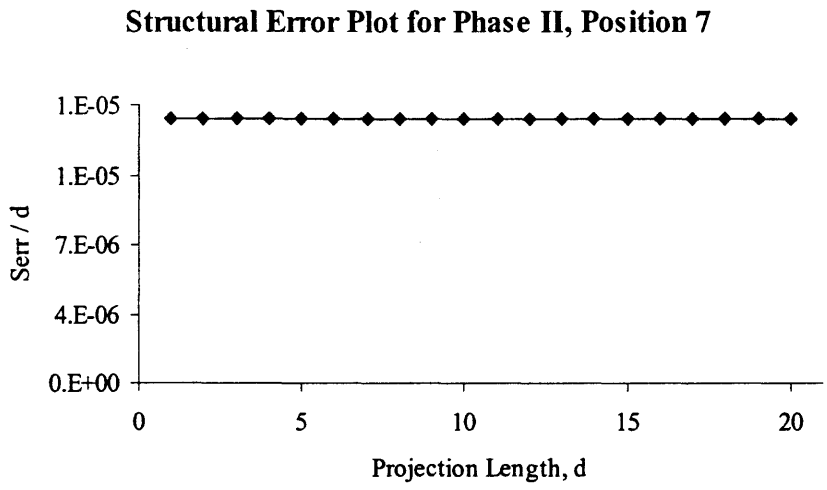

Figure 6.60 Structural error plot for phase II, position 7.

CHAPTER 7

DISCUSSION AND CONCLUSION

In this work, the mathematical analysis software package MATHEMATICA was used to compute the plane-to-sphere and sphere-to-plane projection methods. This package can express a numerical value to well over ten significant figures. Since all of the numerical figures calculated in this work are dimensionless, the dimensionless term "unit" was often used as a suffix to describe them. In the Plane-to-Sphere projection example problems in Chapter 6, the structural errors for positions 4 and 7 (as opposed to the intermediate positions) were used to determine the projection length because the structural error at these positions (the last position of each phase) are the greatest.

In the MATHEMATICA models located in Appendix B, the user must determine whether the calculated structural error is sufficient by comparing it to an acceptable error value. If the calculated error is not acceptable, the user increases the projection length and recalculates another structural error.

The adjustable spherical five-bar path and motion generators synthesized in Chapter 6 can be driven by attaching motors to the input and output links or by employing a train of bevel gears. If the latter option is employed, the designer must select (or design) bevel gears [51] that will fit the overall shaft angle (the angle between joint axes $\mathbf{u}_{a0}$ and $\mathbf{u}_{b0}$) and maintain the prescribed input-output link displacement ratio (the gear ratio).

Throughout the example problems in Chapter 6, the term "kinematically-equivalent" was often used. Given a spherical mechanism, a kinematically-equivalent

planar mechanism is one where the rigid-body displacements (or crank and follower displacement angles in function generation) between the two mechanisms are identical. Rigid body displacement is not to be confused with rigid body position because , for all practical purposes, the rigid body positions between planar and spherical mechanisms could never be identical due to their workspaces.

The theory mathematical modeling and application of a new technique for synthesizing adjustable four and five-bar path, function and motion generators in two ways was presented and demonstrates in this work. First, given an adjustable **planar** four or fiver-bar path, function or motion generator, the user can design a kinematically-equivalent adjustable **spherical** four or five-bar path, function or motion generator respectively. Second, given an adjustable spherical four or five-bar path, function or motion generator, the user can design a kinematically-equivalent adjustable planar path, function of motion generator. The benefits of this method are twofold. One benefit is that adjustable spherical and planar four and five-bar mechanisms can be designed for multi-phase motion, path and function generation applications. Another benefit is that spherical and planar four-and five-bar motion, path and function generators can be designed using synthesis methods for planar and spherical motion, path and function generators respectively. Two-phase moving pivot adjustment problems with constant crank and follower lengths are considered in this work.

APPENDIX A

PLANE AND SPHERICAL MECHANISM DISPLACEMENT EQUATIONS BY DUAL-NUMBER METHOD

A.1 Displacement Equations for Planar Four-Bar Mechanism

Equation A.1 defines the displacement of an arbitrary rigid body point **p** on an R-R dyad of a planar four-bar mechanism (see Figure A.1).

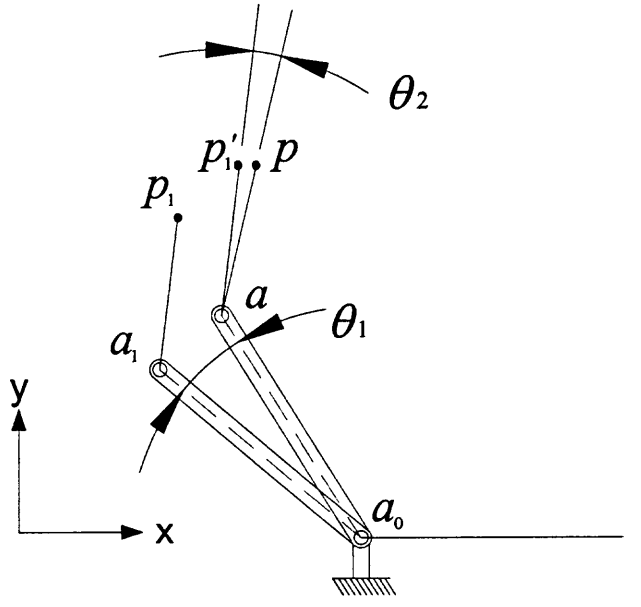

Figure A.1 Displacement of a planar mechanism R-R dyad

$$\mathbf{p} = [R_{\theta 2}](\mathbf{p}_1' - \mathbf{a}) + \mathbf{a} \tag{A.1}$$

where

$$\mathbf{p}_1' = [R_{\theta 1}](\mathbf{p}_1 - \mathbf{a}_0) + \mathbf{a}_0 \tag{A.2}$$

$$\mathbf{a} = [R_{\theta 1}](\mathbf{a}_1 - \mathbf{a}_0) + \mathbf{a}_0 \tag{A.3}$$

and

$$[R_\theta] = \begin{bmatrix} \cos\theta & -\sin\theta & 0 \\ \sin\theta & \cos\theta & 0 \\ 0 & 0 & 1 \end{bmatrix} \tag{A.4}$$

Equations A.8 through A.16 are used to calculate angles θ_1 through θ_4 (see figure A.2). These equations were derived using the dual number formulation [50] in Equations A.5 through A.7.

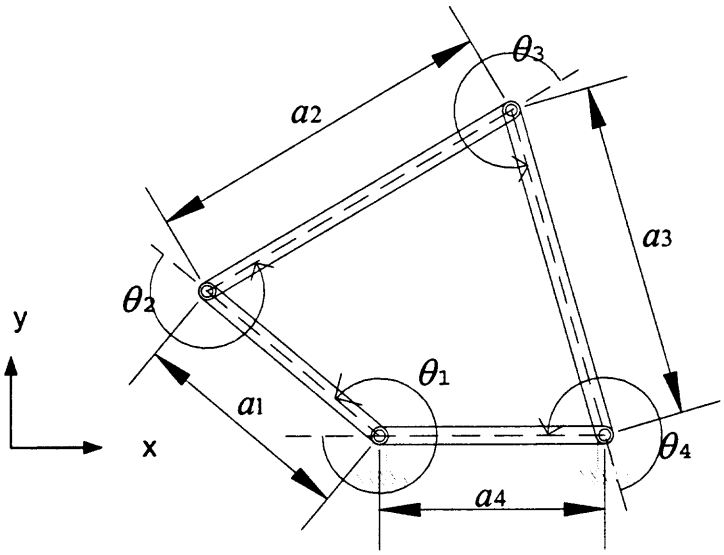

Figure A.2 Planar four bar mechanism with relative joint rotation angles (θ) and linkage lengths (a).

Given

$$\hat{M}_3^2 \cdot \hat{M}_4^3 - \hat{M}_2^{1T} \cdot \hat{M}_1^{4T} = 0 \tag{A.5}$$

therefore

$$\begin{bmatrix} z11 & z12 & z13 \\ z21 & z22 & z23 \\ z31 & z32 & z33 \end{bmatrix} = \begin{bmatrix} 0 & 0 & 0 \\ 0 & 0 & 0 \\ 0 & 0 & 0 \end{bmatrix} \tag{A.6}$$

where

$${}^{n}_{n+1}\hat{M} = \begin{bmatrix} \cos\theta_n & -\sin\theta_n & ea_n \cdot \sin\theta_n \\ \sin\theta_n & \cos\theta_n & -ea_n \cdot \cos\theta_n \\ 0 & ea_n & 1 \end{bmatrix} \tag{A.7}$$

and

$$z11 = (c\theta_2 \cdot c\theta_3 - c\theta_1 \cdot c\theta_4 - s\theta_2 \cdot s\theta_3 + s\theta_1 \cdot s\theta_4)e^0 \tag{A.8}$$

$$z12 = (-c\theta_4 \cdot s\theta_1 - c\theta_3 \cdot s\theta_2 - c\theta_2 \cdot s\theta_3 - c\theta_1 \cdot s\theta_4)e^0 + (a_2 \cdot a_3 \cdot s\theta_2)e^2 \tag{A.9}$$

$$z13 = (-a_4 \cdot s\theta_1 + a_2 \cdot s\theta_2 + a_3 \cdot c\theta_3 \cdot s\theta_2 + a_3 \cdot c\theta_2 \cdot s\theta_3)e^1 \tag{A.10}$$

$$z21 = (c\theta_4 \cdot s\theta_1 + c\theta_3 \cdot s\theta_2 + c\theta_2 \cdot s\theta_3 + c\theta_1 \cdot s\theta_4)e^0 + (-a_1 \cdot a_4 \cdot s\theta_4)e^2 \tag{A.11}$$

$$\begin{aligned} z22 = {} & (c\theta_2 \cdot c\theta_3 - c\theta_1 \cdot c\theta_4 - s\theta_2 \cdot s\theta_3 + s\theta_1 \cdot s\theta_4)e^0 + \\ & (-a_2 \cdot a_3 \cdot c\theta_2 + a_1 \cdot a_4 \cdot c\theta_4)e^2 \end{aligned} \tag{A.12}$$

$$z23 = (-a_1 - a_4 \cdot c\theta_1 - a_2 \cdot c\theta_2 - a_3 \cdot c\theta_2 \cdot c\theta_3 + a_3 \cdot s\theta_2 \cdot s\theta_3)e^1 \tag{A.13}$$

$$z31 = (-a_1 \cdot c\theta_4 \cdot s\theta_1 + a_2 \cdot s\theta_3 - a_4 \cdot s\theta_4 - a_1 \cdot c\theta_1 \cdot s\theta_4)e^1 \tag{A.14}$$

$$z32 = (a_3 + a_2 \cdot c\theta_3 + a_4 \cdot c\theta_4 + a_1 \cdot c\theta_1 \cdot c\theta_4 - a_1 \cdot s\theta_1 \cdot s\theta_4)e^1 \tag{A.15}$$

$$z33 = (a_1 \cdot a_4 \cdot c\theta_1 - a_2 \cdot a_3 \cdot c\theta_3)e^2 \tag{A.16}$$

In Equations A.8 through A.16, the coefficient of e^0 is the real component. The coefficient of e^1 is the dual component. Variables "cθ" and "sθ" represent cos(θ) and sin(θ), respectively.

A.2 Displacement Equations for Spherical Four-Bar Mechanism

Equation A.17 defines the displacement of an arbitrary rigid body point **p** on an R-R dyad of a spherical four-bar mechanism (see figure A.3).

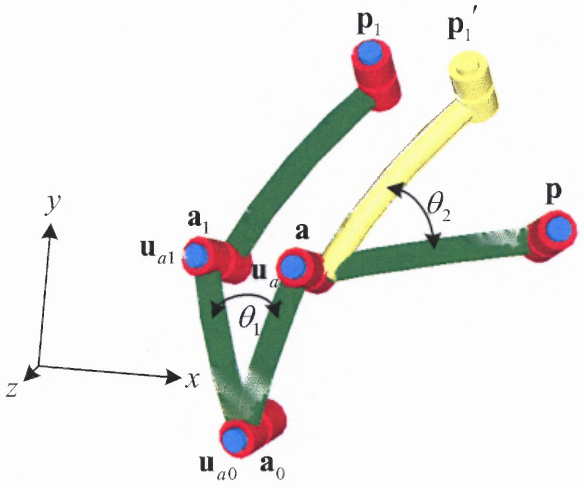

Figure A.3 Displacement of a spherical mechanism R-R dyad.

$$\mathbf{p} = [R_{\theta 2,\, ua}](\mathbf{p}_1' - \mathbf{a}) + \mathbf{a} \tag{A.17}$$

where

$$\mathbf{p}_1' = [R_{\theta 1,\, ua0}](\mathbf{p}_1 - \mathbf{a}_0) + \mathbf{a}_0 \tag{A.18}$$

$$\mathbf{a} = [R_{\theta 1,\, ua0}](\mathbf{a}_1 - \mathbf{a}_0) + \mathbf{a}_0 \tag{A.19}$$

$$\mathbf{u}_a = [R_{\theta 1,\, ua0}]\mathbf{u}_{a1} \tag{A.20}$$

and

$$[R_{\theta,u}] = \begin{bmatrix} u_x^2(1-\cos\theta)+\cos\theta & u_x u_y(1-\cos\theta)-u_z\sin\theta & u_x u_z(1-\cos\theta)+u_y\sin\theta \\ u_x u_y(1-\cos\theta)+u_z\sin\theta & u_y^2(1-\cos\theta)+\cos\theta & u_y u_z(1-\cos\theta)-u_x\sin\theta \\ u_x u_z(1-\cos\theta)-u_y\sin\theta & u_y u_z(1-\cos\theta)+u_x\sin\theta & u_z^2(1-\cos\theta)+\cos\theta \end{bmatrix} \tag{A.21}$$

Equations A.25 through A.33 are used to calculate angles θ_1 through θ_4 (see figure A.4). These equations were derived using the dual number formulation [50] in Equations A.22 through A.24.

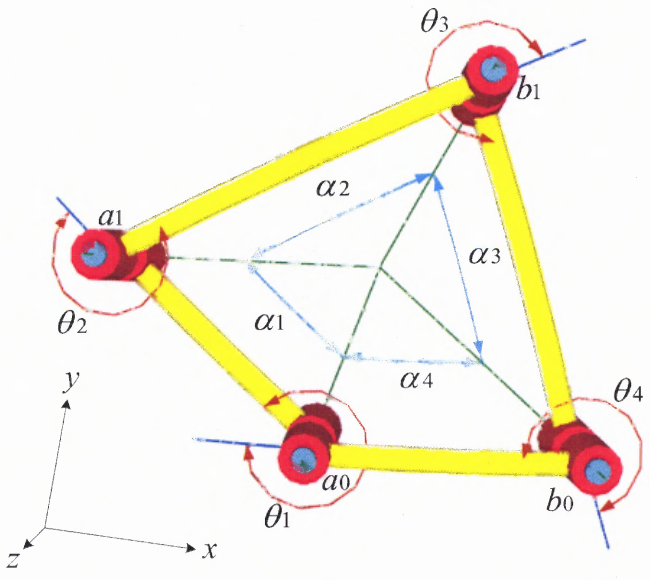

Figure A.4 Spherical four-bar mechanism with relative joint rotation angles (θ) and joint axis angles (α).

Given

$$ {}^{2}_{3}\hat{M} \cdot {}^{3}_{4}\hat{M} - {}^{1}_{2}\hat{M}^{T} \cdot {}^{4}_{1}\hat{M}^{T} = 0 \tag{A.22} $$

therefore

$$ \begin{bmatrix} z11 & z12 & z13 \\ z21 & z22 & z23 \\ z31 & z32 & z33 \end{bmatrix} = \begin{bmatrix} 0 & 0 & 0 \\ 0 & 0 & 0 \\ 0 & 0 & 0 \end{bmatrix} \tag{A.23} $$

where

$$ {}^{n}_{n+1}\hat{M} = \begin{bmatrix} \cos\theta_n & -\cos\alpha_n \sin\theta_n & \sin\alpha_n \sin\theta_n \\ \sin\theta_n & \cos\alpha_n \cos\theta_n & -\sin\alpha_n \cos\theta_n \\ 0 & \sin\alpha_n & \cos\alpha_n \end{bmatrix} \tag{A.24} $$

$$z11 = c\theta_2 \cdot c\theta_3 - c\theta_1 \cdot c\theta_4 - c\alpha_2 \cdot s\theta_2 \cdot s\theta_3 + c\alpha_4 \cdot s\theta_1 \cdot s\theta_4 \tag{A.25}$$

$$z12 = -c\alpha_4 \cdot c\theta_4 \cdot s\theta_1 - c\alpha_2 \cdot c\alpha_3 \cdot c\theta_3 \cdot s\theta_2 + s\alpha_2 \cdot s\alpha_3 \cdot s\theta_2 - c\alpha_3 \cdot c\theta_2 \cdot s\theta_3 - c\theta_1 \cdot s\theta_4 \tag{A.26}$$

$$z13 = -s\alpha_4 \cdot s\theta_1 + c\alpha_3 \cdot s\alpha_2 \cdot s\theta_2 + c\alpha_2 \cdot c\theta_3 \cdot s\alpha_3 \cdot s\theta_2 + c\theta_2 \cdot s\alpha_3 \cdot s\theta_3 \tag{A.27}$$

$$z21 = c\alpha_1 \cdot c\theta_4 \cdot s\theta_1 + c\theta_3 \cdot s\theta_2 + c\alpha_2 \cdot c\theta_2 \cdot s\theta_3 + c\alpha_1 \cdot c\alpha_4 \cdot c\theta_1 \cdot s\theta_4 - s\alpha_1 \cdot s\alpha_4 \cdot s\theta_4 \tag{A.28}$$

$$z22 = c\alpha_2 \cdot c\alpha_3 \cdot c\theta_2 \cdot c\theta_3 - c\alpha_1 \cdot c\alpha_4 \cdot c\theta_1 \cdot c\theta_4 - c\theta_2 \cdot s\alpha_2 \cdot s\alpha_3 + c\theta_4 \cdot s\alpha_1 \cdot s\alpha_4 - c\alpha_3 \cdot s\theta_2 \cdot s\theta_3 + c\alpha_1 \cdot s\theta_1 \cdot s\theta_4 \tag{A.29}$$

$$z23 = -c\alpha_4 \cdot s\alpha_1 - c\alpha_3 \cdot c\theta_2 \cdot s\alpha_2 - c\alpha_2 \cdot c\theta_2 \cdot c\theta_3 \cdot s\alpha_3 - c\alpha_1 \cdot c\theta_1 \cdot s\alpha_4 + s\alpha_3 \cdot s\theta_2 \cdot s\theta_3 \tag{A.30}$$

$$z31 = -c\theta_4 \cdot s\alpha_1 \cdot s\theta_1 + s\alpha_2 \cdot s\theta_3 - c\alpha_4 \cdot c\theta_1 \cdot s\alpha_1 \cdot s\theta_4 - c\alpha_1 \cdot s\alpha_4 \cdot s\theta_4 \tag{A.31}$$

$$z32 = c\alpha_4 \cdot c\theta_1 \cdot c\theta_4 \cdot s\alpha_1 + c\alpha_3 \cdot c\theta_3 \cdot s\alpha_2 + c\alpha_2 \cdot s\alpha_3 + c\alpha_1 \cdot c\theta_4 \cdot s\alpha_4 - s\alpha_1 \cdot s\theta_1 \cdot s\theta_4 \tag{A.32}$$

$$z33 = c\alpha_2 \cdot c\alpha_3 - c\alpha_1 \cdot c\alpha_4 - c\theta_3 \cdot s\alpha_2 \cdot s\alpha_3 + c\theta_1 \cdot s\alpha_1 \cdot s\alpha_4 \tag{A.33}$$

In Equations A.25 through A.33 variables "cθ" and "sθ" represent cos(θ) and sin(θ) respectively and variables "cα" and "sα" represent cos(α) and sin(α), respectively.

A.3 Displacement Equations for Planar Five-Bar Mechanism

Equation A.34 defines the displacement of an arbitrary rigid body point **p** on an R-R dyad of a planar five-bar mechanism (see Figure A.5).

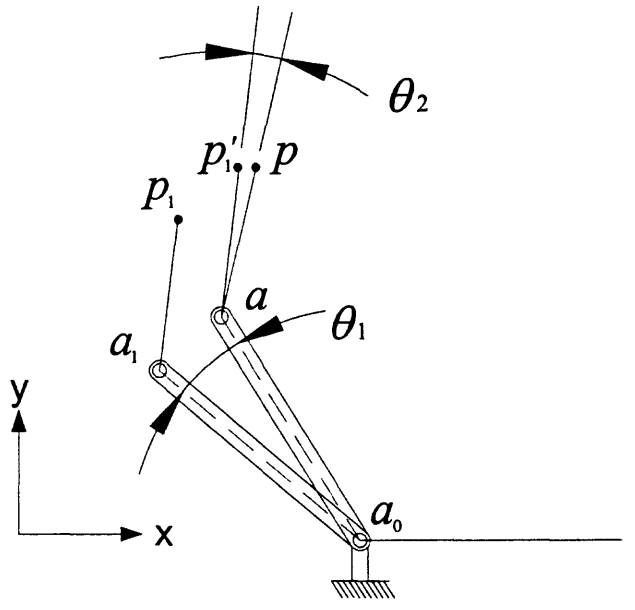

Figure A.5 Displacement of a planar mechanism R-R dyad.

$$\mathbf{p} = [R_{\theta 2}](\mathbf{p}_1' - \mathbf{a}) + \mathbf{a} \tag{A.34}$$

where

$$\mathbf{p}_1' = [R_{\theta 1}](\mathbf{p}_1 - \mathbf{a}_0) + \mathbf{a}_0 \tag{A.35}$$

$$\mathbf{a} = [R_{\theta 1}](\mathbf{a}_1 - \mathbf{a}_0) + \mathbf{a}_0 \tag{A.36}$$

and

$$[R_\theta] = \begin{bmatrix} \cos\theta & -\sin\theta & 0 \\ \sin\theta & \cos\theta & 0 \\ 0 & 0 & 1 \end{bmatrix} \tag{A.37}$$

Equations A.41 through A.49 are used to calculate angles θ_1 through θ_5 (see Figure A.6). These equations were derived using the dual number formulation [50] in Equations A.38 through A.40.

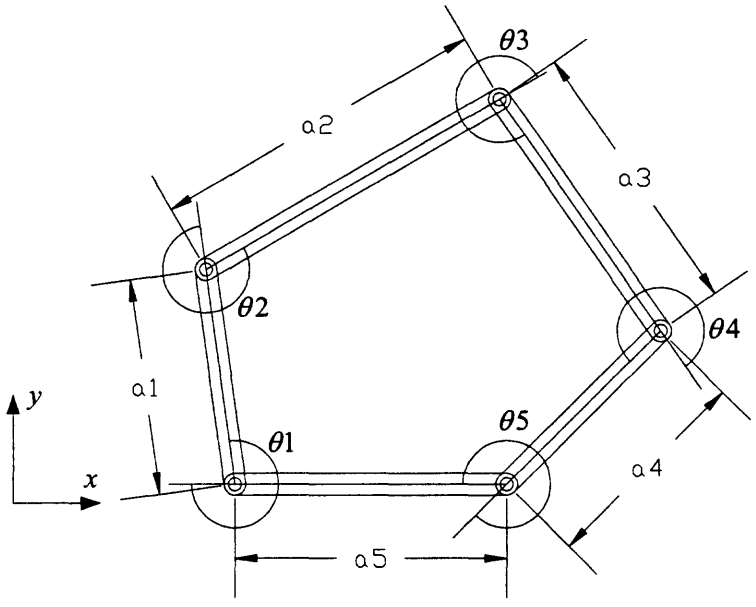

Figure A.6 Planar five bar mechanism with relative joint rotation angles (θ) and linkage lengths (a).

Given

$$ {}^{2}_{3}\hat{M} \cdot {}^{3}_{4}\hat{M} - {}^{1}_{2}\hat{M}^{T} \cdot {}^{5}_{1}\hat{M}^{T} \cdot {}^{4}_{5}\hat{M}^{T} = 0 \tag{A.38} $$

therefore

$$ \begin{bmatrix} z11 & z12 & z13 \\ z21 & z22 & z23 \\ z31 & z32 & z33 \end{bmatrix} = \begin{bmatrix} 0 & 0 & 0 \\ 0 & 0 & 0 \\ 0 & 0 & 0 \end{bmatrix} \tag{A.39} $$

where

$$ {}^{n}_{n+1}\hat{M} = \begin{bmatrix} \cos\theta_n & -\sin\theta_n & ea_n \cdot \sin\theta_n \\ \sin\theta_n & \cos\theta_n & -ea_n \cdot \cos\theta_n \\ 0 & ea_n & 1 \end{bmatrix} \tag{A.40} $$

and

$$z11 = (c\theta_2\ c\theta_3 - s\theta_2\ s\theta_3 + s\theta_4(c\theta_5\ s\theta_1 + c\theta_1\ s\theta_5) - c\theta_4(c\theta_1\ c\theta_5 - s\theta_1\ s\theta_5))e^0 + (-a_4\ a_5\ s\theta_1\ s\theta_4)e^2 \quad \text{(A.41)}$$

$$z12 = (-c\theta_3\ s\theta_2 - c\theta_2\ s\theta_3 - c\theta_4(c\theta_5\ s\theta_1 + c\theta_1\ s\theta_5) + -s\theta_4(c\theta_1\ c\theta_5 - s\theta_1\ s\theta_5))e^0 + (a_4\ a_5\ c\theta_4\ s\theta_1 + a_2\ a_3\ s\theta_2)e^2 \quad \text{(A.42)}$$

$$z13 = (-a_5\ s\theta_1 + a_2\ s\theta_2 + a_3\ c\theta_3\ s\theta_2 + a_3\ c\theta_2\ s\theta_3 - a_4(c\theta_5\ s\theta_1 + c\theta_1\ s\theta_5))e^1 \quad \text{(A.43)}$$

$$z21 = (c\theta_4\ c\theta_5\ s\theta_1 + c\theta_3\ s\theta_2 + c\theta_2\ s\theta_3 + c\theta_1\ c\theta_5\ s\theta_4 + c\theta_1\ c\theta_4\ s\theta_5 - s\theta_1\ s\theta_4\ s\theta_5)e^0 + (-a_1\ a_4\ s\theta_4 - a_4\ a_5\ c\theta_1\ s\theta_4 - a_1\ a_5\ c\theta_5\ s\theta_4 - a_1\ a_5\ c\theta_4\ s\theta_5)e^2 \quad \text{(A.44)}$$

$$z22 = (c\theta_2\ c\theta_3 - c\theta_1\ c\theta_4\ c\theta_5 - s\theta_2\ s\theta_3 + c\theta_5\ s\theta_1\ s\theta_4 + c\theta_4\ s\theta_1\ s\theta_5 + c\theta_1\ s\theta_4\ s\theta_5)e^0 + (-a_2\ a_3\ c\theta_2 + a_1\ a_4\ c\theta_4 + a_4\ a_5\ c\theta_1\ c\theta_4 + a_1\ a_5\ c\theta_4\ c\theta_5 - a_1\ a_5\ s\theta_4\ s\theta_5)e^2 \quad \text{(A.45)}$$

$$z23 = (-a_1 - a_5\ c\theta_1 - a_2\ c\theta_2 - a_3\ c\theta_2\ c\theta_3 - a_4\ c\theta_1\ c\theta_5 + a_3\ s\theta_2\ s\theta_3 + a_4\ s\theta_1\ s\theta_5)e^1 \quad \text{(A.46)}$$

$$z31 = (-a_1\ c\theta_4\ c\theta_5\ s\theta_1 + a_2\ s\theta_3 - a_4\ s\theta_4 - a_5\ c\theta_5\ s\theta_4 - a_1\ c\theta_1\ c\theta_5\ s\theta_4 - a_5\ c\theta_4\ s\theta_5\ -a_1\ c\theta_1\ c\theta_4\ s\theta_5 + a_1\ s\theta_1\ s\theta_4\ s\theta_5)e^1 \quad \text{(A.47)}$$

$$z32 = (a_3 + a_2\ c\theta_3 + a_4\ c\theta_4 + a_5\ c\theta_4\ c\theta_5 + a_1\ c\theta_1\ c\theta_4\ c\theta_5 - a_1\ c\theta_5\ s\theta_1\ s\theta_4 - a_1\ c\theta_4\ s\theta_1\ s\theta_5 - a_5\ s\theta_4\ s\theta_5 - a_1\ c\theta_1\ s\theta_4\ s\theta_5)e^1 \quad \text{(A.48)}$$

$$z33 = (a_1\ a_5\ c\theta_1 - a_2\ a_3\ c\theta_3 + a_4\ a_5\ c\theta_5 + a_1\ a_4\ c\theta_1\ c\theta_5 - a_1\ a_4\ s\theta_1\ s\theta_5)e^2 \quad \text{(A.49)}$$

In Equations A.41 through A.49, the coefficient of e^0 is the real component; the coefficient of e^1 is the dual component. Variables "cθ" and "sθ" represent cos(θ) and sin(θ), respectively.

A.4 Displacement Equations for Spherical Five-Bar Mechanism

Equation A.50 defines the displacement of an arbitrary rigid body point **p** on an R-R dyad of a spherical five-bar mechanism (see Figure A.7).

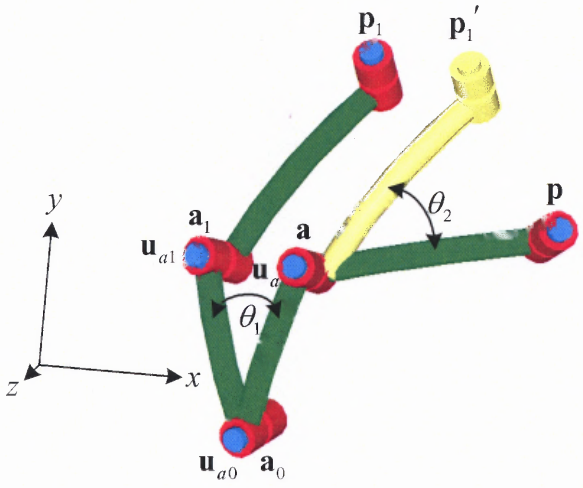

Figure A.7 Displacement of a spherical mechanism R-R dyad.

$$\mathbf{p} = [R_{\theta 2,\, ua}](\mathbf{p}_1' - \mathbf{a}) + \mathbf{a} \tag{A.50}$$

where

$$\mathbf{p}_1' = [R_{\theta 1,\, ua0}](\mathbf{p}_1 - \mathbf{a}_0) + \mathbf{a}_0 \tag{A.51}$$

$$\mathbf{a} = [R_{\theta 1,\, ua0}](\mathbf{a}_1 - \mathbf{a}_0) + \mathbf{a}_0 \tag{A.52}$$

$$\mathbf{u}_a = [R_{\theta 1,\, ua0}]\mathbf{u}_{a1} \tag{A.53}$$

and

$$[R_{\theta,u}] = \begin{bmatrix} u_x^2(1-\cos\theta)+\cos\theta & u_x u_y(1-\cos\theta)-u_z\sin\theta & u_x u_z(1-\cos\theta)+u_y\sin\theta \\ u_x u_y(1-\cos\theta)+u_z\sin\theta & u_y^2(1-\cos\theta)+\cos\theta & u_y u_z(1-\cos\theta)-u_x\sin\theta \\ u_x u_z(1-\cos\theta)-u_y\sin\theta & u_y u_z(1-\cos\theta)+u_x\sin\theta & u_z^2(1-\cos\theta)+\cos\theta \end{bmatrix} \tag{A.54}$$

Equations A.58 through A.66 are used to calculate angles θ_1 through θ_5 (see Figure A.8). These equations were derived using the dual number formulation [50] in Equations A.55 through A.57.

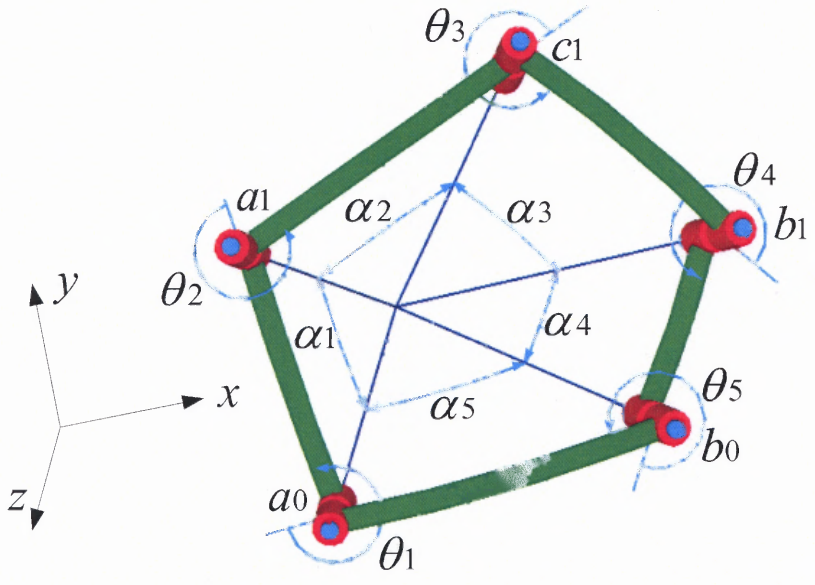

Figure A.8 Spherical five-bar mechanism with relative joint rotation angles (θ) and joint axis angles (α).

Given

$$ {}^{2}_{3}\hat{M} \cdot {}^{3}_{4}\hat{M} - {}^{1}_{2}\hat{M}^{T} \cdot {}^{5}_{1}\hat{M}^{T} \cdot {}^{4}_{5}\hat{M}^{T} = 0 \tag{A.55} $$

therefore

$$ \begin{bmatrix} z11 & z12 & z13 \\ z21 & z22 & z23 \\ z31 & z32 & z33 \end{bmatrix} = \begin{bmatrix} 0 & 0 & 0 \\ 0 & 0 & 0 \\ 0 & 0 & 0 \end{bmatrix} \tag{A.56} $$

where

$$ {}^{n}_{n+1}\hat{M} = \begin{bmatrix} \cos\theta_n & -\cos\alpha_n \sin\theta_n & \sin\alpha_n \sin\theta_n \\ \sin\theta_n & \cos\alpha_n \cos\theta_n & -\sin\alpha_n \cos\theta_n \\ 0 & \sin\alpha_n & \cos\alpha_n \end{bmatrix} \tag{A.57} $$

$$z11 = c\theta_2\ c\theta_3 - c\alpha_2\ s\theta_2\ s\theta_3 - s\alpha_4\ s\alpha_5\ s\theta_1\ s\theta_4 + c\alpha_4\ s\theta_4(c\alpha_5\ c\theta_5\ s\theta_1 + c\theta_1\ s\theta_5) - c\theta_4(c\theta_1\ c\theta_5 - c\alpha_5\ s\theta_1\ s\theta_5) \quad \text{(A.58)}$$

$$z12 = c\theta_4\ s\alpha_4\ s\alpha_5\ s\theta_1 - c\alpha_2\ c\alpha_3\ c\theta_3\ s\theta_2 + s\alpha_2\ s\alpha_3\ s\theta_2 - c\alpha_3\ c\theta_2\ s\theta_3 - c\alpha_4\ c\theta_4(c\alpha_5\ c\theta_5\ s\theta_1 + c\theta_1\ s\theta_5) - s\theta_4(c\theta_1\ c\theta_5 - c\alpha_5\ s\theta_1\ s\theta_5) \quad \text{(A.59)}$$

$$z13 = -c\alpha_4\ s\alpha_5\ s\theta_1 + c\alpha_3\ s\alpha_2\ s\theta_2 + c\alpha_2\ c\theta_3\ s\alpha_3\ s\theta_2 + c\theta_2\ s\alpha_3\ s\theta_3 - s\alpha_4(c\alpha_5\ c\theta_5\ s\theta_1 + c\theta_1\ s\theta_5) \quad \text{(A.60)}$$

$$z21 = c\theta_3\ s\theta_2 + c\alpha_2\ c\theta_2\ s\theta_3 - s\alpha_4(c\alpha_5\ s\alpha_1 + c\alpha_1\ c\theta_1\ s\alpha_5)s\theta_4 - c\theta_4(-c\alpha_1\ c\theta_5\ s\theta_1 - c\alpha_1\ c\alpha_5\ c\theta_1\ s\theta_5 + s\alpha_1\ s\alpha_5\ s\theta_5) + c\alpha_4\ s\theta_4(c\alpha_1\ c\alpha_5\ c\theta_1\ c\theta_5 - c\theta_5\ s\alpha_1\ s\alpha_5 - c\alpha_1\ s\theta_1\ s\theta_5) \quad \text{(A.61)}$$

$$z22 = c\alpha_2\ c\alpha_3\ c\theta_2\ c\theta_3 - c\theta_2\ s\alpha_2\ s\alpha_3 + c\theta_4\ s\alpha_4(c\alpha_5\ s\alpha_1 + c\alpha_1\ c\theta_1\ s\alpha_5) - c\alpha_3\ s\theta_2\ s\theta_3 - s\theta_4(-c\alpha_1\ c\theta_5\ s\theta_1 - c\alpha_1\ c\alpha_5\ c\theta_1\ s\theta_5 + s\alpha_1\ s\alpha_5\ s\theta_5) - c\alpha_4\ c\theta_4(c\alpha_1\ c\alpha_5\ c\theta_1\ c\theta_5 - c\theta_5\ s\alpha_1\ s\alpha_5 - c\alpha_1\ s\theta_1\ s\theta_5) \quad \text{(A.62)}$$

$$z23 = -c\alpha_3\ c\theta_2\ s\alpha_2 - c\alpha_2\ c\theta_2\ c\theta_3\ s\alpha_3 - c\alpha_4(c\alpha_5\ s\alpha_1 + c\alpha_1\ c\theta_1\ s\alpha_5) + s\alpha_3\ s\theta_2\ s\theta_3 - s\alpha_4(c\alpha_1\ c\alpha_5\ c\theta_1\ c\theta_5 - c\theta_5\ s\alpha_1\ s\alpha_5 - c\alpha_1\ s\theta_1\ s\theta_5) \quad \text{(A.63)}$$

$$z31 = s\alpha_2\ s\theta_3 - s\alpha_4(c\alpha_1\ c\alpha_5 - c\theta_1\ s\alpha_1\ s\alpha_5)s\theta_4 - c\theta_4(c\theta_5\ s\alpha_1\ s\theta_1 + c\alpha_5\ c\theta_1\ s\alpha_1\ s\theta_5 + c\alpha_1\ s\alpha_5\ s\theta_5) + c\alpha_4\ s\theta_4(-c\alpha_5\ c\theta_1\ c\theta_5\ s\alpha_1 - c\alpha_1\ c\theta_5\ s\alpha_5 + s\alpha_1\ s\theta_1\ s\theta_5) \quad \text{(A.64)}$$

$$z32 = c\alpha_3\ c\theta_3\ s\alpha_2 + c\alpha_2\ s\alpha_3 + c\theta_4\ s\alpha_4(c\alpha_1\ c\alpha_5 - c\theta_1\ s\alpha_1\ s\alpha_5) - s\theta_4(c\theta_5\ s\alpha_1\ s\theta_1 + c\alpha_5\ c\theta_1\ s\alpha_1\ s\theta_5 + c\alpha_1\ s\alpha_5\ s\theta_5) - c\alpha_4\ c\theta_4(-c\alpha_5\ c\theta_1\ c\theta_5\ s\alpha_1 - c\alpha_1\ c\theta_5\ s\alpha_5 + s\alpha_1\ s\theta_1\ s\theta_5) \quad \text{(A.65)}$$

$$z33 = c\alpha_2\ c\alpha_3 - c\theta_3\ s\alpha_2\ s\alpha_3 - c\alpha_4(c\alpha_1\ c\alpha_5 - c\theta_1\ s\alpha_1\ s\alpha_5) - s\alpha_4(-c\alpha_5\ c\theta_1\ c\theta_5\ s\alpha_1 - c\alpha_1\ c\theta_5\ s\alpha_5 + s\alpha_1\ s\theta_1\ s\theta_5) \quad \text{(A.66)}$$

In Equations A.58 through A.66, variables "cθ" and "sθ" represent cos(θ) and sin(θ) respectively and variables "cα" and "sα" represent cos(α) and sin(α), respectively.

APPENDIX B

MATHEMATICA MODELS

B.1 Adjustable Four-Bar Path Generator

The following MATHEMATICA models include four sections. Section B.1.1 illustrated how to programming the synthesis design equations for planar four-bar path generator by MATHEMATICA language. Section B.1.2 illustrated the Dual-number method and the displacement equations for planar four-bar path generator. Section B.1.3 illustrated plane-to-sphere projection method, dual-number method and displacement equations for spherical four-bar path generator. Section B.1.4 illustrates the sphere-to-plane projection method for spherical four-bar path generator.

B.1.1 Synthesis Design of Planar Four-Bar Path Generator

```
D1j[θ_,p1x_,p1y_,pjx_,pjy_]={{Cos[θ],-Sin[θ],pjx-p1x Cos[θ]+p1y
    Sin[θ]},{Sin[θ],Cos[θ],pjy-p1x Sin[θ]-p1y Cos[θ]},{0,0,1}}
a0={{0},{a0y},{1}}
a1={{a1x},{a1y},{1}}
a1n={{a1nx},{a1ny},{1}}
b0={{1},{b0y},{1}}
b1={{b1x},{b1y},{1}}
b1n={{b1nx},{b1ny},{1}}
p1={{-0.6953},{1.2291},{1}}
p2={{-0.6019},{1.3026},{1}}
p3={{-0.5020},{1.3675},{1}}
p4={{-0.3964},{1.4233},{1}}
p5={{-0.6953},{1.2291},{1}}
p6={{-0.5883},{1.2796},{1}}
p7={{-0.4774},{1.3193},{1}}
θ12=-2.1573*Pi/180;
θ23=-2.0611*Pi/180;
θ34=-1.9722*Pi/180;
θ56=-1.9182*Pi/180;
θ67=-1.8614*Pi/180;
D12=D1j[θ12,p1[[1,1]],p1[[2,1]],p2[[1,1]],p2[[2,1]]]
D13=D1j[θ12+θ23,p1[[1,1]],p1[[2,1]],p3[[1,1]],p3[[2,1]]]
```

```
D14=D1j[θ12+θ23+θ34,p1[[1,1]],p1[[2,1]],p4[[1,1]],p4[[2,1]]]
D56=D1j[θ56,p5[[1,1]],p5[[2,1]],p6[[1,1]],p6[[2,1]]]
D57=D1j[θ56+θ67,p5[[1,1]],p5[[2,1]],p7[[1,1]],p7[[2,1]]]
E1=Transpose[(D12.a1-a0)].(D12.a1-a0)-1.^2
E2=Transpose[(D13.a1-a0)].(D13.a1-a0)-1.^2
E3=Transpose[(D14.a1-a0)].(D14.a1-a0)-1.^2
E4=Transpose[(D56.a1n-a0)].(D56.a1n-a0)-1.^2
E5=Transpose[(D57.a1n-a0)].(D57.a1n-a0)-1.^2
FindRoot[{E1[[1,1]]==0,E2[[1,1]]==0,E3[[1,1]]==0,E4[[1,1]]==0,E5[[1,1]]
    ==0},{a0y,0.1},{a1x,-0.7},{a1y,0.6},
    {a1nx,-0.5},{a1ny,0.7}]
F1=Transpose[(D12.b1-b0)].(D12.b1-b0)-1.5^2
F2=Transpose[(D13.b1-b0)].(D13.b1-b0)-1.5^2
F3=Transpose[(D14.b1-b0)].(D14.b1-b0)-1.5^2
F4=Transpose[(D56.b1n-b0)].(D56.b1n-b0)-1.5^2
F5=Transpose[(D57.b1n-b0)].(D57.b1n-b0)-1.5^2
FindRoot[{F1[[1,1]]==0,F2[[1,1]]==0,F3[[1,1]]==0,F4[[1,1]]==0,F5[[1,1]]
    ==0},{b0y,0.1},{b1x,0.6},{b1y,1.5},{b1nx,1.0},{b1ny,1.4}]
```

B.1.2 Displacement Analysis for Planar Four-Bar Path Generator

```
MyMaxIterations=1000;
ClearAll[cθ1,sθ1,a1,cθ2,sθ2,a2,cθ3,sθ3,a3,cθ4,sθ4,a4];
M[cθ_,sθ_,a_]:={{cθ,-sθ,e a sθ},{sθ,cθ,-e a cθ},{0,e a, 1}}
M2=M[cθ2,sθ2,a2] ;
M3=M[cθ3,sθ3,a3];
M4=M[cθ4,sθ4,a4];
M1=M[cθ1,sθ1,a1];
Z=M2.M3-Transpose[M1].Transpose[M4];
z11=Z[[1,1]];
z12=Z[[1,2]];
z13=Z[[1,3]];
z21=Z[[2,1]];
z22=Z[[2,2]];
z23=Z[[2,3]];
z31=Z[[3,1]];
z32=Z[[3,2]];
z33=Z[[3,3]];
equ11=Coefficient[z11,e,0]==0;
equ12=Coefficient[z12,e,0]==0;
equ13=Coefficient[z13,e,1]==0;
equ21=Coefficient[z21,e,0]==0;
equ22=Coefficient[z22,e,0]==0;
equ23=Coefficient[z23,e,1]==0;
equ31=Coefficient[z31,e,1]==0;
equ32=Coefficient[z32,e,1]==0;
p1p={-0.6953,1.2291};
p2p={-0.6019,1.3026};
p3p={-0.5020,1.3675};
p4p={-0.3964,1.4233};
p5p={-0.6953,1.2291};
p6p={-0.5883,1.2796};
p7p={-0.4774,1.3193};
```

```
a0p={0.0000,-0.0092378};
a1p={-0.76744,0.63171};
a1np={-0.45554,0.88092};
b0p={1.0000,-0.016575};
b1p={0.58693,1.4253};
b1np={1.0472,1.4827};
a1=Sqrt[(a1p-a0p).(a1p-a0p)];
a2=Sqrt[(b1p-a1p).(b1p-a1p)];
a3=Sqrt[(b0p-b1p).(b0p-b1p)];
a4=Sqrt[(a0p-b0p).(a0p-b0p)];
θ1begin=  ArcCos[(b0p-a0p).(a1p-a0p)/Sqrt[(b0p-a0p).(b0p-
    a0p)]/Sqrt[(a1p-a0p).(a1p-a0p)]]+Pi
MR[θ_]:={{Cos[θ],-Sin[θ]},{Sin[θ],Cos[θ]}};
For[k=1;θ1=θ1begin,k≤MyMaxIterations,
    k++;θ1=θ1-20/MyMaxIterations*Pi/180.,
    deltaθ1[k]=θ1-θ1begin;
    cθ1=Cos[θ1];sθ1=Sin[θ1];
    Answer=FindRoot[{equ11,equ12,equ13,equ32,equ31,equ23},{cθ2,-
    0.3},{sθ2,-0.9},{cθ3,-0.2},{sθ3,-0.8},{cθ4,-0.1},{sθ4,-0.9}];
    anscθ2=Answer[[1,2]];anssθ2=Answer[[2,2]];
    θ2=Which[anscθ2≥0 && anssθ2≥0,ArcCos[anscθ2],
    anscθ2<0 && anssθ2>0,ArcCos[anscθ2],
    anscθ2≤0 && anssθ2≤0,2*Pi-ArcCos[anscθ2],
    anscθ2>0 && anssθ2<0,-ArcCos[anscθ2]];
    If[k==1,θ2begin=θ2,];
    deltaθ2[k]=θ2-θ2begin;
    newa1[k]=MR[deltaθ1[k]].{{(a1p-a0p)[[1]]},{(a1p-
    a0p)[[2]]}}+{{a0p[[1]]},{a0p[[2]]}};
    p11[k]=MR[deltaθ1[k]].{{(p1p-a0p)[[1]]},{(p1p-
    a0p)[[2]]}}+{{a0p[[1]]},{a0p[[2]]}};
    newp1[k]=MR[deltaθ2[k]].(p11[k]-newa1[k])+newa1[k];
    square2[k]=(newp1[k][[1]]-p2p[[1]])^2+(newp1[k][[2]]-p2p[[2]])^2;
    square3[k]=(newp1[k][[1]]-p3p[[1]])^2+(newp1[k][[2]]-p3p[[2]])^2;
    square4[k]=(newp1[k][[1]]-p4p[[1]])^2+(newp1[k][[2]]-p4p[[2]])^2;
    ];
For[k=1;minsqrt2=999;minsqrt3=999;minsqrt4=999;myk2;myk3;myk4,k≤MyMaxIt
    erations,k=k+1,
    If[minsqrt2>square2[k][[1]],minsqrt2=square2[k][[1]];myk2=k,];
    If[minsqrt3>square3[k][[1]],minsqrt3=square3[k][[1]];myk3=k,];
    If[minsqrt4>square4[k][[1]],minsqrt4=square4[k][[1]];myk4=k,];
    ];
newp1[myk2]
newp1[myk3]
newp1[myk4]
deltaθ1[myk2]*180/Pi
deltaθ1[myk3]*180/Pi
deltaθ1[myk4]*180/Pi
```

B.1.3 Spherical Four-Bar Path Generator by Plane-to-Sphere Projection

```
RadiusOfSphere=1;
TheMaxIterations=500;
ProjectionLength=7
ClearAll[p1p,p2p,p3p,p4p,p5p,p6p,p7p,p1,p2,p3,p4,p5,p6,p7];
```

```
Plane2Sphere[{x_,y_},r_,d_]:={r*x/Sqrt[d^2+x^2+y^2],r*y/Sqrt[d^2+x^2+y^
    2],r*d/Sqrt[d^2+x^2+y^2]}
p1p={-0.6953,1.2291};p2p={-0.6019,1.3026};
p3p={-0.5020,1.3675};p4p={-0.3964,1.4233};
p5p={-0.6953,1.2291};p6p={-0.5883,1.2796};
p7p={-0.4774,1.3193};
p1=Plane2Sphere[p1p,RadiusOfSphere,ProjectionLength]
p2=Plane2Sphere[p2p,RadiusOfSphere,ProjectionLength]
p3=Plane2Sphere[p3p,RadiusOfSphere,ProjectionLength]
p4=Plane2Sphere[p4p,RadiusOfSphere,ProjectionLength]
p5=Plane2Sphere[p5p,RadiusOfSphere,ProjectionLength]
p6=Plane2Sphere[p6p,RadiusOfSphere,ProjectionLength]
p7=Plane2Sphere[p7p,RadiusOfSphere,ProjectionLength]
ClearAll[a0p,a1p,a1np,b0p,b1p,b1np,a0,a1,a1n,b0,b1,b1n,α1,α2,α3,α4,cα1,
    sα1,cα2,sα2,cα3,sα3,cα4,sα4];
a0p={0.0000,-0.0092378};
a1p={-0.76744,0.63171};
a1np={-0.45554,0.88092};
b0p={1.0000,-0.016575};
b1p={0.58693,1.4253};
b1np={1.0472,1.4827};
a0=Plane2Sphere[a0p,RadiusOfSphere,ProjectionLength];
a1=Plane2Sphere[a1p,RadiusOfSphere,ProjectionLength];
a1n=Plane2Sphere[a1np,RadiusOfSphere,ProjectionLength];
b0=Plane2Sphere[b0p,RadiusOfSphere,ProjectionLength];
b1=Plane2Sphere[b1p,RadiusOfSphere,ProjectionLength];
b1n=Plane2Sphere[b1np,RadiusOfSphere,ProjectionLength];
α1=ArcCos[a0.a1/Sqrt[a0.a0]/Sqrt[a1.a1]];
α2=ArcCos[a1.b1/Sqrt[b1.b1]/Sqrt[a1.a1]];
α3=ArcCos[b1.b0/Sqrt[b1.b1]/Sqrt[b0.b0]];
α4=ArcCos[a0.b0/Sqrt[a0.a0]/Sqrt[b0.b0]];
cα1=Cos[α1];sα1=Sin[α1];cα2=Cos[α2];sα2=Sin[α2];
cα3=Cos[α3];sα3=Sin[α3];cα4=Cos[α4];sα4=Sin[α4];
AngleBTAxes[{ax_,ay_,az_},{bx_,by_,bz_}]:={-(az by-ay bz)/(-ay bx+ax
    by),-(az bx-ax bz)/(ay bx-ax by),1}
alpha1v=AngleBTAxes[a0,a1];
alpha4v=AngleBTAxes[a0,b0];
ϕ10=ArcCos[alpha1v.alpha4v/Sqrt[alpha1v.alpha1v]/Sqrt[alpha4v.alpha4v]];
ϕ100=Pi-ϕ10+Pi;
ClearAll[cθ1,sθ1,cθ2,sθ2,cθ3,sθ3,cθ4,sθ4];
M[cθ_,sθ_,cα_,sα_]:={{cθ,-cα sθ,sα sθ},{sθ,cα cθ,-sα cθ},{0,sα, cα}}
M2=M[cθ2,sθ2,cα2,sα2];
M3=M[cθ3,sθ3,cα3,sα3];
M4=M[cθ4,sθ4,cα4,sα4];
M1=M[cθ1,sθ1,cα1,sα1];
Z=M2.M3-Transpose[M1].Transpose[M4];
z11=Z[[1,1]];
z12=Z[[1,2]];
z13=Z[[1,3]];
z21=Z[[2,1]];
z22=Z[[2,2]];
z23=Z[[2,3]];
z31=Z[[3,1]];
z32=Z[[3,2]];
z33=Z[[3,3]];
cθ2g=-0.3;sθ2g=-0.9;cθ3g=-0.17;sθ3g=-0.9;cθ4g=-0.17;sθ4g=-0.9;
```

```
For[ϕ1=ϕ100;k=1,k≤TheMaxIterations,
    ϕ1=ϕ1-20/TheMaxIterations*Pi/180.;
    k=k+1,
    cθ1=Cos[ϕ1];sθ1=Sin[ϕ1];
    Angles=FindRoot[{z11==0,z12==0,z13==0,z21==0,z22==0,z23==0},{cθ2,cθ
    2g},{sθ2,sθ2g},{cθ3,cθ3g},{sθ3,sθ3g},{cθ4,cθ4g},{sθ4,sθ4g}];
    cθ2g=Angles[[1,2]];sθ2g=Angles[[2,2]];
    cθ3g=Angles[[3,2]];sθ3g=Angles[[4,2]];
    cθ4g=Angles[[5,2]];sθ4g=Angles[[6,2]];
    anscθ2=Angles[[1,2]];anssθ2=Angles[[2,2]];
    θ2=Which[anscθ2≥0 && anssθ2≥0,ArcCos[anscθ2],anscθ2<0 &&
    anssθ2>0,ArcCos[anscθ2],
    anscθ2≤0 && anssθ2≤0,2*Pi-ArcCos[anscθ2],
    anscθ2>0 && anssθ2<0,-ArcCos[anscθ2]];
    If[k==1,θ2begin=θ2,];
    deltaθ2[k]=θ2-θ2begin;
    deltaθ1[k]=ϕ1-ϕ100;
    ]
Ru[α_,u_]:={{u[[1,1]]^2*(1-Cos[α])+Cos[α],u[[1,1]] u[[2,1]] (1-Cos[α])-
    u[[3,1]] Sin[α],u[[1,1]] u[[3,1]] (1-Cos[α])+u[[2,1]]
    Sin[α]},{u[[1,1]] u[[2,1]] (1-Cos[α])+u[[3,1]] Sin[α],u[[2,1]]^2
    (1-Cos[α])+Cos[α],u[[2,1]] u[[3,1]] (1-Cos[α])-u[[1,1]]
    Sin[α]},{u[[1,1]] u[[3,1]] (1-Cos[α])-u[[2,1]] Sin[α],u[[2,1]]
    u[[3,1]] (1-Cos[α])+u[[1,1]] Sin[α],u[[3,1]]^2 (1-Cos[α])+Cos[α]}};
uak={{uax},{uay},{uaz}};
a0axis={{a0[[1]]},{a0[[2]]},{a0[[3]]}};
b0axis={{b0[[1]]},{b0[[2]]},{b0[[3]]}};
For[k=1,k≤TheMaxIterations,k++,
    NewA1[k]=Ru[deltaθ1[k],a0axis].(a1-a0)+a0;
    a1axis={{NewA1[k][[1]]},{NewA1[k][[2]]},{NewA1[k][[3]]}};
    p1temp[k]=Ru[deltaθ1[k],a0axis].(p1-a0)+a0;
    NewP1[k]=Ru[deltaθ2[k],a1axis].(p1temp[k]-NewA1[k])+NewA1[k];
    ]
P11=p4;
For[k=1;minsqrt=9999;myk,k≤TheMaxIterations,k++,
    toleranceErr[k]=Sqrt[(NewP1[k][[1]]-P11[[1]])^2+(NewP1[k][[2]]-
    P11[[2]])^2+(NewP1[k][[3]]-P11[[3]])^2];
    If[minsqrt>toleranceErr[k],minsqrt=toleranceErr[k];myk=k,];
    ]
myanswer2[ProjectionLength]={myk,deltaθ1[myk]*180/Pi,NewP1[myk],Project
    ionLength,minsqrt*ProjectionLength}
```

B.1.4 Planar Four-Bar Path Generator by Sphere-to-Plane Projection

```
RadiusOfSphere=1;
DistanceOfProjection=11
MyMaxiterations=400;
ClearAll[p1p,p2p,p3p,p4p,p5p,p6p,p7p,p1,p2,p3,p4,p5,p6,p7];
ProjectionFun[{x_,y_,z_},d_]:={d/z*x,d/z*y}
p1={-0.06269,0.1108,0.9919};
p2={-0.05426,0.1174,0.9916};
p3={-0.04524,0.1232,0.9913};
p4={-0.03572,0.1282,0.9911};
p5={-0.06269,0.1108,0.9919};
```

```
p6={-0.05305,0.1154,0.9919};
p7={-0.04305,0.1190,0.9920};
p1p=ProjectionFun[p1,DistanceOfProjection]
p2p=ProjectionFun[p2,DistanceOfProjection]
p3p=ProjectionFun[p3,DistanceOfProjection]
p4p=ProjectionFun[p4,DistanceOfProjection]
p5p=ProjectionFun[p5,DistanceOfProjection]
p6p=ProjectionFun[p6,DistanceOfProjection]
p7p=ProjectionFun[p7,DistanceOfProjection]
ClearAll[a0p,a1p,a1np,b0p,b1p,b1np,a0,a1,a1n,b0,b1,b1n];
a0={0.0000,-0.0008398,1.0000};
a1={-0.06948,0.05719,0.9959};
a1n={-0.04124,0.07976,0.9960};
b0={0.09054,-0.001501,0.9959};
b1={0.05284,0.1283,0.9903};
b1n={0.09393,0.1330,0.9867};
a0p=ProjectionFun[a0,DistanceOfProjection]
a1p=ProjectionFun[a1,DistanceOfProjection]
a1np=ProjectionFun[a1n,DistanceOfProjection]
b0p=ProjectionFun[b0,DistanceOfProjection]
b1p=ProjectionFun[b1,DistanceOfProjection]
b1np=ProjectionFun[b1n,DistanceOfProjection]
ClearAll[cθ1,sθ1,a1,cθ2,sθ2,a2,cθ3,sθ3,a3,cθ4,sθ4,a4,M1,M2,M3,M4];
M[cθ_,sθ_,a_]:={{cθ,-sθ,e a sθ},{sθ,cθ,-e a cθ},{0,e a, 1}}
M2=M[cθ2,sθ2,a2] ;
M3=M[cθ3,sθ3,a3];
M4=M[cθ4,sθ4,a4];
M1=M[cθ1,sθ1,a1];
Z=M2.M3-Transpose[M1].Transpose[M4];
z11=Z[[1,1]];
z12=Z[[1,2]];
z13=Z[[1,3]];
z21=Z[[2,1]];
z22=Z[[2,2]];
z23=Z[[2,3]];
z31=Z[[3,1]];
z32=Z[[3,2]];
z33=Z[[3,3]];
equ11=Coefficient[z11,e,0]==0
equ12=Coefficient[z12,e,0]==0
equ13=Coefficient[z13,e,1]==0
equ21=Coefficient[z21,e,0]==0
equ22=Coefficient[z22,e,0]==0
equ23=Coefficient[z23,e,1]==0
equ31=Coefficient[z31,e,1]==0
equ32=Coefficient[z32,e,1]==0
ClearAll[a1,a2,a3,a4];
a1=Sqrt[(a1p-a0p).(a1p-a0p)]
a2=Sqrt[(b1p-a1p).(b1p-a1p)]
a3=Sqrt[(b0p-b1p).(b0p-b1p)]
a4=Sqrt[(a0p-b0p).(a0p-b0p)]
MR[θ_]:={{Cos[θ],-Sin[θ]},{Sin[θ],Cos[θ]}};
ClearAll[θ1begin,θ1];
θ1begin=ArcCos[(b0p-a0p).(a1p-a0p)/Sqrt[(b0p-a0p).(b0p-a0p)]/Sqrt[(a1p-
    a0p).(a1p-a0p)]]+Pi;
For[k=1;θ1=θ1begin,k≤MyMaxiterations,
    k++;θ1=θ1-20/MyMaxiterations*Pi/180.,
```

```
      delta θ1[k]=θ1-θ1begin;
      cθ1=Cos[θ1];
      sθ1=Sin[θ1];
      Answer=FindRoot[{equ11,equ12,equ13,equ32,equ31,equ23},{cθ2,-
      0.3},{sθ2,-0.9},{cθ3,-0.2},{sθ3,-0.8},{cθ4,-0.1},{sθ4,-0.9}];
      anscθ2=Answer[[1,2]];
      anssθ2=Answer[[2,2]];
      θ2=Which[anscθ2≥0 && anssθ2≥0,ArcCos[anscθ2],
      anscθ2<0 && anssθ2>0,ArcCos[anscθ2],
      anscθ2≤0 && anssθ2≤0,2*Pi-ArcCos[anscθ2],
      anscθ2>0 && anssθ2<0,-ArcCos[anscθ2]];
      If[k==1,θ2begin=θ2,];
      delta θ2[k]=θ2-θ2begin;
      newa1[k]=MR[delta θ1[k]].{{(a1p-a0p)[[1]]},{(a1p-
      a0p)[[2]]}}+{{a0p[[1]]},{a0p[[2]]}};
      p11[k]=MR[delta θ1[k]].{{(p1p-a0p)[[1]]},{(p1p-
      a0p)[[2]]}}+{{a0p[[1]]},{a0p[[2]]}};
      newp1[k]=MR[delta θ2[k]].(p11[k]-newa1[k])+newa1[k];
      square2[k]=(newp1[k][[1]]-p2p[[1]])^2+(newp1[k][[2]]-p2p[[2]])^2;
      square3[k]=(newp1[k][[1]]-p3p[[1]])^2+(newp1[k][[2]]-p3p[[2]])^2;
      square4[k]=(newp1[k][[1]]-p4p[[1]])^2+(newp1[k][[2]]-p4p[[2]])^2;
      ]
For[k=1;minsqrt2=999;minsqrt3=999;minsqrt4=999;minsqrt5=999;myk2;myk3;m
      yk4;myk5,
      k≤MyMaxiterations,k=k+1,
      If[minsqrt2>square2[k][[1]],minsqrt2=square2[k][[1]];myk2=k,];
      If[minsqrt3>square3[k][[1]],minsqrt3=square3[k][[1]];myk3=k,];
      If[minsqrt4>square4[k][[1]],minsqrt4=square4[k][[1]];myk4=k,];
      ]
StructuralErr_Position2[DistanceOfProjection]=Sqrt[minsqrt2]/DistanceOf
      Projection
StructuralErr_Position3[DistanceOfProjection]=Sqrt[minsqrt3]/DistanceOf
      Projection
StructuralErr_Position4[DistanceOfProjection]=Sqrt[minsqrt4]/DistanceOf
      Projection
newp1[myk2]
newp1[myk3]
newp1[myk4]
delta θ1[myk2]*180/Pi
delta θ1[myk3]*180/Pi
delta θ1[myk4]*180/Pi
```

B.2 Adjustable Four-Bar Function Generator

The following MATHEMATICA models include three sections. Section B.2.1 illustrated how to programming the synthesis design equations and angle displacement analysis for four-bar function generator by MATHEMATICA language. Section B.2.2 illustrated

plane-to-sphere projection method, dual-number method and displacement equations for spherical four-bar function generator. Section B.2.3 illustrated the sphere-to-plane projection method for spherical four-bar function generator.

B.2.1 Synthesis Design and Displacement Analysis of Planar Four-Bar Function Generator

```
ClearAll[a0,a1,b0,b1,b1n];
D1j[θ_,ϕ_]={{Cos[θ-ϕ],-Sin[θ-ϕ],1-Cos[ϕ]},{Sin[θ-ϕ],Cos[θ-
      ϕ],Sin[ϕ]},{0,0,1}  }
a0={{0},{0},{1}};
a1={{-0.2},{a1y},{1}};
b0={{1},{0},{1}};
b1={{b1x},{b1y},{1}};
b1n={{b1nx},{b1ny},{1}};
θ12=-10.*Pi/180;
θ13=-20.*Pi/180;
θ14=-30.*Pi/180;
θ15=-15.*Pi/180;
θ16=-30.*Pi/180;
ϕ12=-7.50426541*Pi/180;
ϕ13=-14.96321349*Pi/180;
ϕ14=-22.26300237*Pi/180;
ϕ15=-9.73488647*Pi/180;
ϕ16=-18.9814518*Pi/180;
D12=D1j[θ12,ϕ12];
D13=D1j[θ13,ϕ13];
D14=D1j[θ14,ϕ14];
D15=D1j[θ15,ϕ15];
D16=D1j[θ16,ϕ16];
E1=Transpose[(D12.a1-b1)].(D12.a1-b1)-1.^2;
E2=Transpose[(D13.a1-b1)].(D13.a1-b1)-1.^2;
E3=Transpose[(D14.a1-b1)].(D14.a1-b1)-1.^2;
E4=Transpose[(D15.a1-b1n)].(D15.a1-b1n)-1.^2;
E5=Transpose[(D16.a1-b1n)].(D16.a1-b1n)-1.^2;
answer=FindRoot[{E1[[1,1]]==0,E2[[1,1]]==0,E3[[1,1]]==0,E4[[1,1]]==0,E5
      [[1,1]]==0},{a1y,0.7},{b1x,0.6},{b1y,1.3},{b1nx,0.7},{b1ny,1.2}];
a0p={0,0};
a1p={-0.2,answer[[1,2]]};
b0p={1,0};
b1p={answer[[2,2]],answer[[3,2]]};
b1np={answer[[4,2]],answer[[5,2]]};
a1=Sqrt[(a1p-a0p).(a1p-a0p)];
a2=Sqrt[(b1p-a1p).(b1p-a1p)];
a3=Sqrt[(b0p-b1p).(b0p-b1p)];
a4=Sqrt[(a0p-b0p).(a0p-b0p)];
ClearAll[cθ1,sθ1,cθ2,sθ2,cθ3,sθ3,cθ4,sθ4];
M[cθ_,sθ_,a_]:={{cθ,-sθ,e a sθ},{sθ,cθ,-e a cθ},{0,e a, 1}}
M2=M[cθ2,sθ2,a2];
M3=M[cθ3,sθ3,a3];
```

```
M4=M[cθ4,sθ4,a4];
M1=M[cθ1,sθ1,a1];
Z=M2.M3-Transpose[M1].Transpose[M4];
zz11=Z[[1,1]];
zz12=Z[[1,2]];
zz13=Z[[1,3]];
zz21=Z[[2,1]];
zz22=Z[[2,2]];
zz23=Z[[2,3]];
zz31=Z[[3,1]];
zz32=Z[[3,2]];
zz33=Z[[3,3]];
equ11=Coefficient[zz11,e,0]==0;
equ12=Coefficient[zz12,e,0]==0;
equ13=Coefficient[zz13,e,1]==0;
equ21=Coefficient[zz21,e,0]==0;
equ22=Coefficient[zz22,e,0]==0;
equ23=Coefficient[zz23,e,1]==0;
equ31=Coefficient[zz31,e,1]==0;
equ32=Coefficient[zz32,e,1]==0;
θ1begin=ArcCos[(b0p-a0p).(a1p-a0p)/Sqrt[(b0p-a0p).(b0p-a0p)]/Sqrt[(a1p-
      a0p).(a1p-a0p)]]+Pi;
For[k=1;θ1=θ1begin,k≤5,
   k++;θ1=θ1-10*Pi/180,
   deltaθ1[k]=θ1-θ1begin;
   cθ1=Cos[θ1];
   sθ1=Sin[θ1];
   Answer[k]=FindRoot[{equ11,equ12,equ13,equ32,equ31,equ23},
         {cθ2,-0.1},{sθ2,-0.8},{cθ3,-0.5},{sθ3,-0.5},{cθ4,-0.1},
         {sθ4,-0.9}];
   anscθ2=Answer[k][[1,2]];
   anssθ2=Answer[k][[2,2]];
   anscθ4=Answer[k][[5,2]];
   anssθ4=Answer[k][[6,2]];
   θ2=Which[anscθ2≥0 && anssθ2≥0,ArcCos[anscθ2],
      anscθ2<0 && anssθ2>0,ArcCos[anscθ2],
      anscθ2≤0 && anssθ2≤0,2*Pi-ArcCos[anscθ2],
      anscθ2>0 && anssθ2<0,-ArcCos[anscθ2]];
   θ4=Which[anscθ4≥0 && anssθ4≥0,ArcCos[anscθ4],
      anscθ4<0 && anssθ4>0,ArcCos[anscθ4],
      anscθ4≤0 && anssθ4≤0,2*Pi-ArcCos[anscθ4],
      anscθ4>0 && anssθ4<0,-ArcCos[anscθ4]];
   If[k==1,θ2begin=θ2;θ4begin=θ4,];
   deltaθ2[k]=θ2-θ2begin;
   deltaθ4[k]=θ4-θ4begin;
   ]
deltaθ1[1]*180/Pi
deltaθ4[1]*180/Pi
deltaθ1[2]*180/Pi
deltaθ4[2]*180/Pi
deltaθ1[3]*180/Pi
deltaθ4[3]*180/Pi+360
deltaθ1[4]*180/Pi
deltaθ4[4]*180/Pi+360
```

B.2.2 Spherical Four-Bar Function Generator by Plane-to-Sphere Projection

```
RadiusOfSphere=1;
DistanceOfProjection=8
ProjectionFun[{x_,y_},r_,d_]:={r*x/Sqrt[d^2+x^2+y^2],r*y/
      Sqrt[d^2+x^2+y^2],r*d/Sqrt[d^2+x^2+y^2]};
ClearAll[α1,α2,α3,α4,cα1,sα1,cα2,sα2,cα3,sα3,cα4,sα4];
a0p={0.,0.};
a1p={-0.2,0.6838};
b0p={1,0.};
b1p={0.771257,0.921844};
b1np={0.726739,1.05898};
a0=ProjectionFun[a0p,RadiusOfSphere,DistanceOfProjection];
a1=ProjectionFun[a1p,RadiusOfSphere,DistanceOfProjection];
b0=ProjectionFun[b0p,RadiusOfSphere,DistanceOfProjection];
b1=ProjectionFun[b1p,RadiusOfSphere,DistanceOfProjection];
b1n=ProjectionFun[b1np,RadiusOfSphere,DistanceOfProjection];
α1=ArcCos[a0.a1/Sqrt[a0.a0]/Sqrt[a1.a1]];
α2=ArcCos[a1.b1/Sqrt[b1.b1]/Sqrt[a1.a1]];
α3=ArcCos[b1.b0/Sqrt[b1.b1]/Sqrt[b0.b0]];
α4=ArcCos[a0.b0/Sqrt[a0.a0]/Sqrt[b0.b0]];
cα1=Cos[α1];sα1=Sin[α1];cα2=Cos[α2];sα2=Sin[α2];
cα3=Cos[α3];sα3=Sin[α3];cα4=Cos[α4];sα4=Sin[α4];
AngleBTAxes[{ax_,ay_,az_},{bx_,by_,bz_}]:=
      If[ax==0 && ay==0 ,{-by,bx,0},{-(az by-ay bz)/(-ay bx+ax by),-(az
      bx-ax bz)/(ay bx-ax by),1}]
alpha1v=AngleBTAxes[a0,a1];
alpha4v=AngleBTAxes[a0,b0];
ϕ10=ArcCos[alpha1v.alpha4v/Sqrt[alpha1v.alpha1v]/
      Sqrt[alpha4v.alpha4v]]+Pi
ClearAll[cθ1,sθ1,cθ4,sθ4,cθ3,sθ3,cθ2,sθ2];
M[cθ_,sθ_,cα_,sα_]:={{cθ,-cα sθ,sα sθ},{sθ,cα cθ,-sα cθ},{0,sα, cα}}
M2=M[cθ2,sθ2,cα2,sα2];
M3=M[cθ3,sθ3,cα3,sα3];
M4=M[cθ4,sθ4,cα4,sα4];
M1=M[cθ1,sθ1,cα1,sα1];
Z=M2.M3-Transpose[M1].Transpose[M4];
z11=Z[[1,1]]
z12=Z[[1,2]]
z13=Z[[1,3]]
z21=Z[[2,1]]
z22=Z[[2,2]]
z23=Z[[2,3]]
z31=Z[[3,1]]
z32=Z[[3,2]]
z33=Z[[3,3]]
For[ϕ1=ϕ10;k=1,k≤8,ϕ1=ϕ1-5.*Pi/180;k=k+1,
   cθ1=Cos[ϕ1];
   sθ1=Sin[ϕ1];
   Angles=FindRoot[{z11==0,z12==0,z13==0,z21==0,z22==0,
         z23==0},{cθ2,0.1},{sθ2,-0.95},{cθ3,-0.1},{sθ3,-0.9},{cθ4,-
         0.2},{sθ4,-0.9}];
   anscθ4=Angles[[5,2]];
   anssθ4=Angles[[6,2]];
   θ4=Which[anscθ4≥0 && anssθ4≥0,ArcCos[anscθ4],
      anscθ4<0 && anssθ4>0,ArcCos[anscθ4],
```

```
      ansc$\theta$4≤0 && anss$\theta$4≤0,2*Pi-ArcCos[ansc$\theta$4],
      ansc$\theta$4>0 && anss$\theta$4<0,2*Pi-ArcCos[ansc$\theta$4]];
   If[k==1,$\theta$4begin=$\theta$4;Print[Angles],];
   delta$\theta$4[k]=$\theta$4-$\theta$4begin;
   delta$\theta$1[k]=$\phi$1-$\phi$10;
   ]
output12[DistanceOfProjection]=delta$\theta$4[3]*180/Pi
output13[DistanceOfProjection]=delta$\theta$4[5]*180/Pi
output14[DistanceOfProjection]=delta$\theta$4[7]*180/Pi
```

B.2.3 Planar Four-Bar Function Generator by Sphere-to-Plane Projection

```
RadiusOfSphere=1;
DistanceOfProjection=6
ProjectionFun[{x_,y_,z_},d_]:={d/z*x,d/z*y};
ClearAll[a0p,a1p,a1np,b0p,b1p,b1np,a0,a1,a1n,b0,b1,b1n];
a0={0.,0.,1.};
a1={-0.00666479,0.0227869,0.999718};
b0={0.0333148,0.,0.999445};
b1={0.025688,0.0307035,0.999198};
b1n={0.0242025,0.035267,0.999085};
a0p=ProjectionFun[a0,DistanceOfProjection];
a1p=ProjectionFun[a1,DistanceOfProjection];
b0p=ProjectionFun[b0,DistanceOfProjection];
b1p=ProjectionFun[b1,DistanceOfProjection];
b1np=ProjectionFun[b1n,DistanceOfProjection];
ClearAll[c$\theta$1,s$\theta$1,c$\theta$2,s$\theta$2,c$\theta$3,s$\theta$3,c$\theta$4,s$\theta$4,a1,a2,a3,a4];
M[c$\theta$_,s$\theta$_,a_]:={{c$\theta$,-s$\theta$,e a s$\theta$},{s$\theta$,c$\theta$,-e a c$\theta$},{0,e a, 1}}
M2=M[c$\theta$2,s$\theta$2,a2] ;
M3=M[c$\theta$3,s$\theta$3,a3];
M4=M[c$\theta$4,s$\theta$4,a4];
M1=M[c$\theta$1,s$\theta$1,a1];
Z=M2.M3-Transpose[M1].Transpose[M4];
z11=Z[[1,1]];
z12=Z[[1,2]];
z13=Z[[1,3]];
z21=Z[[2,1]];
z22=Z[[2,2]];
z23=Z[[2,3]];
z31=Z[[3,1]];
z32=Z[[3,2]];
z33=Z[[3,3]];
equ11=Coefficient[z11,e,0]==0
equ12=Coefficient[z12,e,0]==0
equ13=Coefficient[z13,e,1]==0
equ21=Coefficient[z21,e,0]==0
equ22=Coefficient[z22,e,0]==0
equ23=Coefficient[z23,e,1]==0
equ31=Coefficient[z31,e,1]==0
equ32=Coefficient[z32,e,1]==0
a1=Sqrt[(a1p-a0p).(a1p-a0p)]
a2=Sqrt[(b1p-a1p).(b1p-a1p)]
a3=Sqrt[(b0p-b1p).(b0p-b1p)]
a4=Sqrt[(a0p-b0p).(a0p-b0p)]
```

```
ClearAll[θ1begin,θ1];
θ1begin=ArcCos[(b0p-a0p).(a1p-a0p)/Sqrt[(b0p-a0p).(b0p-a0p)]/Sqrt[(a1p-
      a0p).(a1p-a0p)]]+Pi;
For[k=1;θ1=θ1begin,k≤8,k++;θ1=θ1-5*Pi/180,
   deltaθ1[k]=θ1-θ1begin;
   cθ1=Cos[θ1];sθ1=Sin[θ1];
   Answer=FindRoot[{equ11,equ12,equ13,equ32,equ31,equ23},
        {cθ2,-0.3},{sθ2,-0.9},{cθ3,-0.2},{sθ3,-0.8},{cθ4,-0.1},{sθ4,-
        0.9}];
   anscθ4=Answer[[5,2]];
   anssθ4=Answer[[6,2]];
   θ4=Which[anscθ4≥0 && anssθ4≥0,ArcCos[anscθ4],
      anscθ4<0 && anssθ4>0,ArcCos[anscθ4],
      anscθ4≤0 && anssθ4≤0,2*Pi-ArcCos[anscθ4],
      anscθ4>0 && anssθ4<0,2*Pi-ArcCos[anscθ4]];
   If[k==1,θ4begin=θ4,];
   deltaθ4[k]=θ4-θ4begin;
   ]
Position1[DistanceOfProjection]=deltaθ4[3]*180/Pi
Position2[DistanceOfProjection]=deltaθ4[5]*180/Pi
Position3[DistanceOfProjection]=deltaθ4[7]*180/Pi
```

B.3 Adjustable Four-Bar Motion Generator

The following MATHEMATICA models include four sections. Section B.3.1 illustrated how to programming the synthesis design equations for planar four-bar motion generator by MATHEMATICA language. Section B.3.2 illustrated the Dual-number method and the displacement equations for planar four-bar motion generator. Section B.3.3 illustrated plane-to-sphere projection method, dual-number method and displacement equations for spherical four-bar motion generator. Section B.3.4 illustrates the sphere-to-plane projection method for spherical four-bar motion generator.

B.3.1 Synthesis Design of Planar Four-Bar Motion Generator

```
Dlj[p_,q_,r_,p1_,q1_,r1_]:={{p1[[1,1]],q1[[1,1]],r1[[1,1]]},
      {p1[[2,1]],q1[[2,1]],r1[[2,1]]},{1,1,1} }.
```

```
      Inverse[{{p[[1,1]],q[[1,1]],r[[1,1]]},
      {p[[2,1]],q[[2,1]],r[[2,1]]},{1,1,1} }];
a0={{0},{a0y},{1}};
a1={{a1x},{a1y},{1}};
a1n={{a1nx},{a1ny},{1}};
b0={{1.5},{b0y},{1}};
b1={{b1x},{b1y},{1}};
b1n={{b1nx},{b1ny},{1}};
p1={{-0.1950},{1.3709},{1}};q1={{0.0401},{2.0111},{1}};
r1={{0.8807},{1.8467},{1}};
p2={{-0.1122},{1.4136},{1}};q2={{0.1369},{2.0484},{1}};
r2={{0.9737},{1.8655},{1}};
p3={{-0.0259},{1.4501},{1}};q3={{0.2366},{2.0796},{1}};
r3={{1.0693},{1.8790},{1}};
p4={{0.0634},{1.4802},{1}};q4={{0.3386},{2.1043},{1}};
r4={{1.1671},{1.8869},{1}};
p5={{-0.1950},{1.3709},{1}};q5={{0.0401},{2.0111},{1}};
r5={{0.8807},{1.8467},{1}};
p6={{-0.1162},{1.3909},{1}};q6={{0.1088},{2.0347},{1}};
r6={{0.9518},{1.8835},{1}};
p7={{-0.0370},{1.4034},{1}};q7={{0.1764},{2.0511},{1}};
r7={{1.0220},{1.9151},{1}};
D12=D1j[p1,q1,r1,p2,q2,r2];
D13=D1j[p1,q1,r1,p3,q3,r3];
D14=D1j[p1,q1,r1,p4,q4,r4];
D56=D1j[p5,q5,r5,p6,q6,r6];
D57=D1j[p5,q5,r5,p7,q7,r7];
E1=Transpose[(D12.a1-a0)].(D12.a1-a0)-1.^2;
E2=Transpose[(D13.a1-a0)].(D13.a1-a0)-1.^2;
E3=Transpose[(D14.a1-a0)].(D14.a1-a0)-1.^2;
E4=Transpose[(D56.a1n-a0)].(D56.a1n-a0)-1.^2;
E5=Transpose[(D57.a1n-a0)].(D57.a1n-a0)-1.^2;
FindRoot[{E1[[1,1]]==0,E2[[1,1]]==0,E3[[1,1]]==0,E4[[1,1]]==0,E5[[1,1]]
      ==0},{a0y,0.01},{a1x,-0.6},{a1y,0.7},
      {a1nx,-0.2},{a1ny,0.9}]
F1=Transpose[(D12.b1-b0)].(D12.b1-b0)-1.5^2;
F2=Transpose[(D13.b1-b0)].(D13.b1-b0)-1.5^2;
F3=Transpose[(D14.b1-b0)].(D14.b1-b0)-1.5^2;
F4=Transpose[(D56.b1n-b0)].(D56.b1n-b0)-1.5^2;
F5=Transpose[(D57.b1n-b0)].(D57.b1n-b0)-1.5^2;
FindRoot[{F1[[1,1]]==0,F2[[1,1]]==0,F3[[1,1]]==0,F4[[1,1]]==0,F5[[1,1]]
      ==0},{b0y,0.01},{b1x,1.3},{b1y,1.5},{b1nx,0.8},{b1ny,1.3}]
```

B.3.2 Displacement Analysis for Planar Four-Bar Motion Generator

```
MyMaxIterations=800;
ClearAll[cθ1,sθ1,a1,cθ2,sθ2,a2,cθ3,sθ3,a3,cθ4,sθ4,a4];
M[cθ_,sθ_,a_]:={{cθ,-sθ,e a sθ},{sθ,cθ,-e a cθ},{0,e a, 1}}
M2=M[cθ2,sθ2,a2] ;
M3=M[cθ3,sθ3,a3];
M4=M[cθ4,sθ4,a4];
M1=M[cθ1,sθ1,a1];
Z=M2.M3-Transpose[M1].Transpose[M4];
z11=Z[[1,1]]
```

```
z12=Z[[1,2]]
z13=Z[[1,3]]
z21=Z[[2,1]]
z22=Z[[2,2]]
z23=Z[[2,3]]
z31=Z[[3,1]]
z32=Z[[3,2]]
z33=Z[[3,3]]
equ11=Coefficient[z11,e,0]==0
equ12=Coefficient[z12,e,0]==0
equ13=Coefficient[z13,e,1]==0
equ21=Coefficient[z21,e,0]==0
equ22=Coefficient[z22,e,0]==0
equ23=Coefficient[z23,e,1]==0
equ31=Coefficient[z31,e,1]==0
equ32=Coefficient[z32,e,1]==0
p1p={-0.1950,1.3709};q1p={0.0401,2.0111};
r1p={0.8807,1.8467};p2p={-0.1122,1.4136};
q2p={0.1369,2.0484};r2p={0.9737,1.8655};
p3p={-0.0259,1.4501};q3p={0.2366,2.0796};
r3p={1.0693,1.8790};p4p={0.0634,1.4802};
q4p={0.3386,2.1043};r4p={1.1671,1.8869};
p5p={-0.1950,1.3709};q5p={0.0401,2.0111};
r5p={0.8807,1.8467};p6p={-0.1162,1.3909};
q6p={0.1088,2.0347};r6p={0.9518,1.8835};
p7p={-0.0370,1.4034};q7p={0.1764,2.0511};
r7p={1.0220,1.9151};a0p={0,-0.0261977};
a1p={-0.6384,0.743255};
a1np={-0.260506,0.939355};
b0p={1.5,-0.0881517};
b1p={1.28305,1.39579};
b1np={0.839614,1.25892};
a1=Sqrt[(a1p-a0p).(a1p-a0p)];
a2=Sqrt[(b1p-a1p).(b1p-a1p)];
a3=Sqrt[(b0p-b1p).(b0p-b1p)];
a4=Sqrt[(a0p-b0p).(a0p-b0p)];
θ1begin=ArcCos[(b0p-a0p).(a1p-a0p)/Sqrt[(b0p-a0p).(b0p-a0p)]/Sqrt[(a1p-
      a0p).(a1p-a0p)]]+Pi
MR[θ_]:={{Cos[θ],-Sin[θ]},{Sin[θ],Cos[θ]}};
cθ2t=-0.3; sθ2t=-0.9; cθ3t=-0.2; sθ3t= -0.8; cθ4t=-0.1;  sθ4t=-0.9;
For[k=1;θ1=θ1begin,k≤MyMaxIterations,
     k++;θ1=θ1-20./MyMaxIterations*Pi/180,
     delta θ1[k]=θ1-θ1begin;
     cθ1=Cos[θ1];
     sθ1=Sin[θ1];
     Answer=FindRoot[{equ11,equ12,equ13,equ32,equ31,equ23},{cθ2,cθ2t},{s
          θ2,sθ2t},{cθ3,cθ3t},{sθ3,sθ3t},{cθ4,cθ4t},{sθ4,sθ4t}];
     cθ2t=Answer[[1,2]];sθ2t=Answer[[2,2]];cθ3t=Answer[[3,2]];
     sθ3t=Answer[[4,2]];
     cθ4t=Answer[[5,2]];sθ4t=Answer[[6,2]];
     ansc θ1=cθ1;anss θ1=sθ1;
     ansc θ2=Answer[[1,2]];anss θ2=Answer[[2,2]];
     ansc θ3=Answer[[3,2]];
     anss θ3=Answer[[4,2]];ansc θ4=Answer[[5,2]];
     anss θ4=Answer[[6,2]];
```

```
      θ2=Which[ansc θ2≥0 && anss θ2≥0,ArcCos[ansc θ2],ansc θ2<0 &&
           anss θ2>0,ArcCos[ansc θ2],ansc θ2≤0 && anss θ2≤0,2*Pi-
           ArcCos[ansc θ2],ansc θ2>0 && anss θ2<0,-ArcCos[ansc θ2]];
      If[k==1,θ2begin=θ2,];
      delta θ2[k]=θ2-θ2begin;
      newa1[k]=MR[delta θ1[k]].{{(a1p-a0p)[[1]]},{(a1p-
           a0p)[[2]]}}+{{a0p[[1]]},{a0p[[2]]}};
      p11[k]=MR[delta θ1[k]].{{(p1p-a0p)[[1]]},{(p1p-
           a0p)[[2]]}}+{{a0p[[1]]},{a0p[[2]]}};
      q11[k]=MR[delta θ1[k]].{{(q1p-a0p)[[1]]},{(q1p-
           a0p)[[2]]}}+{{a0p[[1]]},{a0p[[2]]}};
      r11[k]=MR[delta θ1[k]].{{(r1p-a0p)[[1]]},{(r1p-
           a0p)[[2]]}}+{{a0p[[1]]},{a0p[[2]]}};
      newp1[k]=MR[delta θ2[k]].(p11[k]-newa1[k])+newa1[k];
      newq1[k]=MR[delta θ2[k]].(q11[k]-newa1[k])+newa1[k];
      newr1[k]=MR[delta θ2[k]].(r11[k]-newa1[k])+newa1[k];
      squarep2[k]=(newp1[k][[1]]-p2p[[1]])^2+(newp1[k][[2]]-p2p[[2]])^2;
      squarep3[k]=(newp1[k][[1]]-p3p[[1]])^2+(newp1[k][[2]]-p3p[[2]])^2;
      squarep4[k]=(newp1[k][[1]]-p4p[[1]])^2+(newp1[k][[2]]-p4p[[2]])^2;
      squareq2[k]=(newq1[k][[1]]-q2p[[1]])^2+(newq1[k][[2]]-q2p[[2]])^2;
      squareq3[k]=(newq1[k][[1]]-q3p[[1]])^2+(newq1[k][[2]]-q3p[[2]])^2;
      squareq4[k]=(newq1[k][[1]]-q4p[[1]])^2+(newq1[k][[2]]-q4p[[2]])^2;
      squarer2[k]=(newr1[k][[1]]-r2p[[1]])^2+(newr1[k][[2]]-r2p[[2]])^2;
      squarer3[k]=(newr1[k][[1]]-r3p[[1]])^2+(newr1[k][[2]]-r3p[[2]])^2;
      squarer4[k]=(newr1[k][[1]]-r4p[[1]])^2+(newr1[k][[2]]-r4p[[2]])^2;
      square2[k]=squarep2[k]+squareq2[k]+squarer2[k];
      square3[k]=squarep3[k]+squareq3[k]+squarer3[k];
      square4[k]=squarep4[k]+squareq4[k]+squarer4[k];
      ]
For[k=1;minsqrt2=999;minsqrt3=999;minsqrt4=999;myk2;myk3;myk4,
      k≤MyMaxIterations,k=k+1,
      If[minsqrt2>square2[k][[1]],minsqrt2=square2[k][[1]];myk2=k,];
      If[minsqrt3>square3[k][[1]],minsqrt3=square3[k][[1]];myk3=k,];
      If[minsqrt4>square4[k][[1]],minsqrt4=square4[k][[1]];myk4=k,];
      ]
newp1[myk2]
newp1[myk3]
newp1[myk4]
newq1[myk2]
newq1[myk3]
newq1[myk4]
newr1[myk2]
newr1[myk3]
newr1[myk4]
delta θ1[myk2]*180/Pi
delta θ1[myk3]*180/Pi
delta θ1[myk4]*180/Pi
SErrp2=Sqrt[minsqrt2]/3
SErrp3=Sqrt[minsqrt3]/3
SErrp4=Sqrt[minsqrt4]/3
```

B.3.3 Spherical Four-Bar Motion Generator by Plane-to-Sphere Projection

```
MyMaxIterations=400;
```

```
RadiusOfSphere=1;
DistanceOfProjection=7
ProjectionFun[{x_,y_},r_,d_]:={r*x/Sqrt[d^2+x^2+y^2],r*y/Sqrt[d^2+x^2+y
    ^2],r*d/Sqrt[d^2+x^2+y^2]}
p1p={-0.1950,1.3709};q1p={0.0401,2.0111};
r1p={0.8807,1.8467};p2p={-0.1122,1.4136};
q2p={0.1369,2.0484};r2p={0.9737,1.8655};
p3p={-0.0259,1.4501};q3p={0.2366,2.0796};
r3p={1.0693,1.8790};p4p={0.0634,1.4802};
q4p={0.3386,2.1043};r4p={1.1671,1.8869};
p5p={-0.1950,1.3709};q5p={0.0401,2.0111};
r5p={0.8807,1.8467};p6p={-0.1162,1.3909};
q6p={0.1088,2.0347};r6p={0.9518,1.8835};
p7p={-0.0370,1.4034};q7p={0.1764,2.0511};
r7p={1.0220,1.9151};
p1=ProjectionFun[p1p,RadiusOfSphere,DistanceOfProjection]
p2=ProjectionFun[p2p,RadiusOfSphere,DistanceOfProjection]
p3=ProjectionFun[p3p,RadiusOfSphere,DistanceOfProjection]
p4=ProjectionFun[p4p,RadiusOfSphere,DistanceOfProjection]
p5=ProjectionFun[p5p,RadiusOfSphere,DistanceOfProjection]
p6=ProjectionFun[p6p,RadiusOfSphere,DistanceOfProjection]
p7=ProjectionFun[p7p,RadiusOfSphere,DistanceOfProjection]
q1=ProjectionFun[q1p,RadiusOfSphere,DistanceOfProjection]
q2=ProjectionFun[q2p,RadiusOfSphere,DistanceOfProjection]
q3=ProjectionFun[q3p,RadiusOfSphere,DistanceOfProjection]
q4=ProjectionFun[q4p,RadiusOfSphere,DistanceOfProjection]
q5=ProjectionFun[q5p,RadiusOfSphere,DistanceOfProjection]
q6=ProjectionFun[q6p,RadiusOfSphere,DistanceOfProjection]
q7=ProjectionFun[q7p,RadiusOfSphere,DistanceOfProjection]
r1=ProjectionFun[r1p,RadiusOfSphere,DistanceOfProjection]
r2=ProjectionFun[r2p,RadiusOfSphere,DistanceOfProjection]
r3=ProjectionFun[r3p,RadiusOfSphere,DistanceOfProjection]
r4=ProjectionFun[r4p,RadiusOfSphere,DistanceOfProjection]
r5=ProjectionFun[r5p,RadiusOfSphere,DistanceOfProjection]
r6=ProjectionFun[r6p,RadiusOfSphere,DistanceOfProjection]
r7=ProjectionFun[r7p,RadiusOfSphere,DistanceOfProjection]
a0p={0,-0.0261977};
a1p={-0.6384,0.743255};
a1np={-0.260506,0.939355};
b0p={1.5,-0.0881517};
b1p={1.28305,1.39579};
b1np={0.839614,1.25892};
a0=ProjectionFun[a0p,RadiusOfSphere,DistanceOfProjection]
a1=ProjectionFun[a1p,RadiusOfSphere,DistanceOfProjection]
a1n=ProjectionFun[a1np,RadiusOfSphere,DistanceOfProjection]
b0=ProjectionFun[b0p,RadiusOfSphere,DistanceOfProjection]
b1=ProjectionFun[b1p,RadiusOfSphere,DistanceOfProjection]
b1n=ProjectionFun[b1np,RadiusOfSphere,DistanceOfProjection]
α1=ArcCos[a0.a1/Sqrt[a0.a0]/Sqrt[a1.a1]];
α2=ArcCos[a1.b1/Sqrt[b1.b1]/Sqrt[a1.a1]];
α3=ArcCos[b1.b0/Sqrt[b1.b1]/Sqrt[b0.b0]];
α4=ArcCos[a0.b0/Sqrt[a0.a0]/Sqrt[b0.b0]];
cα1=Cos[α1];sα1=Sin[α1];cα2=Cos[α2];sα2=Sin[α2];
cα3=Cos[α3];sα3=Sin[α3];cα4=Cos[α4];sα4=Sin[α4];
AngleBTAxes[{ax_,ay_,az_},{bx_,by_,bz_}]:=
      {-(az by-ay bz)/(-ay bx+ax by),-(az bx-ax bz)/(ay bx-ax by),1}
alpha1v=AngleBTAxes[a0,a1];
```

```
alpha2v=AngleBTAxes[a1,b1];
alpha3v=AngleBTAxes[b1,b0];
alpha4v=AngleBTAxes[a0,b0];
ϕ10=ArcCos[alpha1v.alpha4v/Sqrt[alpha1v.alpha1v]/Sqrt[alpha4v.alpha4v]];
ϕ40=ArcCos[alpha3v.alpha4v/Sqrt[alpha3v.alpha3v]/Sqrt[alpha4v.alpha4v]];
ϕ20=ArcCos[alpha1v.alpha2v/Sqrt[alpha1v.alpha1v]/Sqrt[alpha2v.alpha2v]];
ϕ30=ArcCos[alpha3v.alpha2v/Sqrt[alpha3v.alpha3v]/Sqrt[alpha2v.alpha2v]];
ϕ100=Pi-ϕ10+Pi;
ϕ100*180/Pi
ClearAll[cθ1,sθ1,cθ2,sθ2,cθ3,sθ3,cθ4,sθ4];
M[cθ_,sθ_,cα_,sα_]:={{cθ,-cα sθ,sα sθ},{sθ,cα cθ,-sα cθ},{0,sα, cα}}
M2=M[cθ2,sθ2,cα2,sα2];
M3=M[cθ3,sθ3,cα3,sα3];
M4=M[cθ4,sθ4,cα4,sα4];
M1=M[cθ1,sθ1,cα1,sα1];
Z=M2.M3-Transpose[M1].Transpose[M4];
zz11=Z[[1,1]];
zz12=Z[[1,2]];
zz13=Z[[1,3]];
zz21=Z[[2,1]];
zz22=Z[[2,2]];
zz23=Z[[2,3]];
zz31=Z[[3,1]];
zz32=Z[[3,2]];
zz33=Z[[3,3]];
tcθ2=-0.3;tsθ2=-0.9;tcθ3=-0.17;tsθ3=-0.9;tcθ4=-0.17;tsθ4=-0.9;
For[ϕ1=ϕ100;k=1,k≤MyMaxIterations,
   ϕ1=ϕ1-20./MyMaxIterations*Pi/180;k=k+1,
   cθ1=Cos[ϕ1];
   sθ1=Sin[ϕ1];
    Angles=FindRoot[{zz11==0,zz12==0,zz13==0,zz21==0,zz22==0,zz23==0},{
        cθ2,tcθ2},{sθ2,tsθ2},{cθ3,tcθ3},{sθ3,tsθ3},{cθ4,tcθ4},{sθ4,tsθ
        4}];
   tcθ2=Angles[[1,2]];tsθ2=Angles[[2,2]];
   tcθ3=Angles[[3,2]];tsθ3=Angles[[4,2]];
   tcθ4=Angles[[5,2]];tsθ4=Angles[[6,2]];
   anscθ2=Angles[[1,2]];
   anssθ2=Angles[[2,2]];
   θ2=
    Which[anscθ2≥0 && anssθ2≥0,ArcCos[anscθ2],
      anscθ2<0 && anssθ2>0,ArcCos[anscθ2],
      anscθ2≤0 && anssθ2≤0,2*Pi-ArcCos[anscθ2],
      anscθ2>0 && anssθ2<0,-ArcCos[anscθ2]];
   If[k==1,θ2begin=θ2,];
   deltaθ2[k]=θ2-θ2begin;
   deltaθ1[k]=ϕ1-ϕ100;
   ]
Ru[α_,u_]:={{u[[1,1]]^2*(1-Cos[α])+Cos[α],
      u[[1,1]] u[[2,1]] (1-Cos[α])-u[[3,1]] Sin[α],
      u[[1,1]] u[[3,1]] (1-Cos[α])+u[[2,1]] Sin[α]},
      {u[[1,1]] u[[2,1]] (1-Cos[α])+u[[3,1]] Sin[α],
      u[[2,1]]^2 (1-Cos[α])+Cos[α],
      u[[2,1]] u[[3,1]] (1-Cos[α])-u[[1,1]] Sin[α]},
      {u[[1,1]] u[[3,1]] (1-Cos[α])-u[[2,1]] Sin[α],
      u[[2,1]] u[[3,1]] (1-Cos[α])+u[[1,1]] Sin[α],
      u[[3,1]]^2 (1-Cos[α])+Cos[α]}};
uak={{uax},{uay},{uaz}};
```

```
a0axis={{a0[[1]]},{a0[[2]]},{a0[[3]]}};
b0axis={{b0[[1]]},{b0[[2]]},{b0[[3]]}};
For[k=1,k≤MyMaxIterations,k++,
   NewA1[k]=Ru[delta$\theta$1[k],a0axis].(a1-a0)+a0;
   a1axis={{NewA1[k][[1]]},{NewA1[k][[2]]},{NewA1[k][[3]]}};
   p1temp[k]=Ru[delta$\theta$1[k],a0axis].(p1-a0)+a0;
   q1temp[k]=Ru[delta$\theta$1[k],a0axis].(q1-a0)+a0;
   r1temp[k]=Ru[delta$\theta$1[k],a0axis].(r1-a0)+a0;
   NewP1[k]=Ru[delta$\theta$2[k],a1axis].(p1temp[k]-NewA1[k])+NewA1[k];
   NewQ1[k]=Ru[delta$\theta$2[k],a1axis].(q1temp[k]-NewA1[k])+NewA1[k];
   NewR1[k]=Ru[delta$\theta$2[k],a1axis].(r1temp[k]-NewA1[k])+NewA1[k];
   ]
P11=p4;Q11=q4;R11=r4;
For[k=1;minsqrt=9999;myk,k≤MyMaxIterations,k++,
   toleranceErr[k]=(Sqrt[(NewP1[k][[1]]-P11[[1]])^2+(NewP1[k][[2]]-
         P11[[2]])^2+ (NewP1[k][[3]]-P11[[3]])^2]+Sqrt[(NewQ1[k][[1]]-
         Q11[[1]])^2+(NewQ1[k][[2]]-Q11[[2]])^2+ (NewQ1[k][[3]]-
         Q11[[3]])^2]+Sqrt[(NewR1[k][[1]]-R11[[1]])^2+(NewR1[k][[2]]-
         R11[[2]])^2+ (NewR1[k][[3]]-R11[[3]])^2])/3.;
   If[minsqrt>toleranceErr[k],minsqrt=toleranceErr[k]; myk=k,];
   ]
myanswer4[DistanceOfProjection]={delta$\theta$1[myk]*180/Pi,
DistanceOfProjection,toleranceErr[myk]*DistanceOfProjection}
P11=p3;Q11=q3;R11=r3;
For[k=1;minsqrt=9999;myk,k≤MyMaxIterations,k++,
   toleranceErr[k]=(Sqrt[(NewP1[k][[1]]-P11[[1]])^2+(NewP1[k][[2]]-
         P11[[2]])^2+ (NewP1[k][[3]]-P11[[3]])^2]+Sqrt[(NewQ1[k][[1]]-
         Q11[[1]])^2+(NewQ1[k][[2]]-Q11[[2]])^2+ (NewQ1[k][[3]]-
         Q11[[3]])^2]+Sqrt[(NewR1[k][[1]]-R11[[1]])^2+(NewR1[k][[2]]-
         R11[[2]])^2+ (NewR1[k][[3]]-R11[[3]])^2])/3.;
   If[minsqrt>toleranceErr[k],minsqrt=toleranceErr[k]; myk=k,];
   ]
myanswer3[DistanceOfProjection]={delta$\theta$1[myk]*180/Pi,
DistanceOfProjection,toleranceErr[myk]*DistanceOfProjection}
P11=p2;Q11=q2;R11=r2;
For[k=1;minsqrt=9999;myk,k≤MyMaxIterations,k++,
   toleranceErr[k]=(Sqrt[(NewP1[k][[1]]-P11[[1]])^2+(NewP1[k][[2]]-
         P11[[2]])^2+ (NewP1[k][[3]]-P11[[3]])^2]+Sqrt[(NewQ1[k][[1]]-
         Q11[[1]])^2+(NewQ1[k][[2]]-Q11[[2]])^2+ (NewQ1[k][[3]]-
         Q11[[3]])^2]+Sqrt[(NewR1[k][[1]]-R11[[1]])^2+(NewR1[k][[2]]-
         R11[[2]])^2+ (NewR1[k][[3]]-R11[[3]])^2])/3.;
    If[minsqrt>toleranceErr[k],minsqrt=toleranceErr[k];myk=k,];
   ]
myanswer2[DistanceOfProjection]={delta$\theta$1[myk]*180/Pi,DistanceOfProjecti
    on,toleranceErr[myk]*DistanceOfProjection}
```

B.3.4 Planar Four-Bar Motion Generator by Sphere-to-Plane Projection

```
RadiusOfSphere=1;
DistanceOfProjection=7
ClearAll[p1p,p2p,p3p,p4p,p5p,p6p,p7p,p1,p2,p3,p4,p5,p6,p7];
UnProjectionFun[{x_,y_,z_},d_]:={d/z*x,d/z*y}
p1={-0.0273,0.1921,0.9810};q1={0.0055,0.2761,0.9611};
r1={0.1208,0.2532,0.9598};
```

```
p2={-0.0157,0.1979,0.9801};q2={0.0188,0.2808,0.9596};
r2={0.1332,0.2552,0.9577};
p3={-0.0036,0.2028,0.9792};q3={0.0324,0.2846,0.9581};
r3={0.1460,0.2565,0.9555};
p4={0.0089,0.2069,0.9783};q4={0.0463,0.2876,0.9566};
r4={0.1589,0.2570,0.9533};
p5={-0.0273,0.1921,0.9810};q5={0.0055,0.2761,0.9611};
r5={0.1208,0.2532,0.9598};
p6={-0.0163,0.1949,0.9807};q6={0.0149,0.2791,0.9602};
r6={0.1302,0.2576,0.9574};
p7={-0.0052,0.1966,0.9805};q7={0.0242,0.2811,0.9594};
r7={0.1394,0.2613,0.9551};
p1p=UnProjectionFun[p1,DistanceOfProjection]
p2p=UnProjectionFun[p2,DistanceOfProjection]
p3p=UnProjectionFun[p3,DistanceOfProjection]
p4p=UnProjectionFun[p4,DistanceOfProjection]
p5p=UnProjectionFun[p5,DistanceOfProjection]
p6p=UnProjectionFun[p6,DistanceOfProjection]
p7p=UnProjectionFun[p7,DistanceOfProjection]
q1p=UnProjectionFun[q1,DistanceOfProjection]
q2p=UnProjectionFun[q2,DistanceOfProjection]
q3p=UnProjectionFun[q3,DistanceOfProjection]
q4p=UnProjectionFun[q4,DistanceOfProjection]
q5p=UnProjectionFun[q5,DistanceOfProjection]
q6p=UnProjectionFun[q6,DistanceOfProjection]
q7p=UnProjectionFun[q7,DistanceOfProjection]
r1p=UnProjectionFun[r1,DistanceOfProjection]
r2p=UnProjectionFun[r2,DistanceOfProjection]
r3p=UnProjectionFun[r3,DistanceOfProjection]
r4p=UnProjectionFun[r4,DistanceOfProjection]
r5p=UnProjectionFun[r5,DistanceOfProjection]
r6p=UnProjectionFun[r6,DistanceOfProjection]
r7p=UnProjectionFun[r7,DistanceOfProjection]
ClearAll[a0p,a1p,a1np,b0p,b1p,b1np,a0,a1,a1n,b0,b1,b1n];
a0={0.0000,-0.0008398,1.0000};
a1={-0.06948,0.05719,0.9959};
a1n={-0.04124,0.07976,0.9960};
b0={0.09054,-0.001501,0.9959};
b1={0.05284,0.1283,0.9903};
b1n={0.09393,0.1330,0.9867};
a0p=UnProjectionFun[a0,DistanceOfProjection]
a1p=UnProjectionFun[a1,DistanceOfProjection]
a1np=UnProjectionFun[a1n,DistanceOfProjection]
b0p=UnProjectionFun[b0,DistanceOfProjection]
b1p=UnProjectionFun[b1,DistanceOfProjection]
b1np=UnProjectionFun[b1n,DistanceOfProjection]
On the Design of slide-crank mechanisms part II: Multi-phase path and
function generation
plane mechanism by Dual Number
ClearAll[cθ1,sθ1,a1,cθ2,sθ2,a2,cθ3,sθ3,a3,cθ4,sθ4,a4,M1,M2,M3,M4];
M[cθ_,sθ_,a_]:={{cθ,-sθ,e a sθ},{sθ,cθ,-e a cθ},{0,e a, 1}}
M2=M[cθ2,sθ2,a2];
M3=M[cθ3,sθ3,a3];
M4=M[cθ4,sθ4,a4];
M1=M[cθ1,sθ1,a1];
Z=M2.M3-Transpose[M1].Transpose[M4];
zz11=Z[[1,1]];
```

```
zz12=Z[[1,2]];
zz13=Z[[1,3]];
zz21=Z[[2,1]];
zz22=Z[[2,2]];
zz23=Z[[2,3]];
zz31=Z[[3,1]];
zz32=Z[[3,2]];
zz33=Z[[3,3]];
equ11=Coefficient[zz11,e,0]==0
equ12=Coefficient[zz12,e,0]==0
equ13=Coefficient[zz13,e,1]==0
equ21=Coefficient[zz21,e,0]==0
equ22=Coefficient[zz22,e,0]==0
equ23=Coefficient[zz23,e,1]==0
equ31=Coefficient[zz31,e,1]==0
equ32=Coefficient[zz32,e,1]==0
p1p={-0.6953,1.2291}
p2p={-0.6019,1.3026}
p3p={-0.5020,1.3675}
p4p={-0.3964,1.4233}
p5p={-0.6953,1.2291}
p6p={-0.5883,1.2796}
p7p={-0.4774,1.3193}
a0p={0.0000,-0.0092};
a1p={-0.7674,0.6317};
a1np={-0.4555,0.8809};
b0p={1.0000,-0.0166};
b1p={0.5869,1.4252};
b1np={1.0472,1.4827};
ClearAll[a1,a2,a3,a4];
a1=Sqrt[(a1p-a0p).(a1p-a0p)]
a2=Sqrt[(b1p-a1p).(b1p-a1p)]
a3=Sqrt[(b0p-b1p).(b0p-b1p)]
a4=Sqrt[(a0p-b0p).(a0p-b0p)]
MR[θ_]:={{Cos[θ],-Sin[θ]},{Sin[θ],Cos[θ]}};
ClearAll[θ1begin,θ1];
θ1begin=ArcCos[(b0p-a0p).(a1p-a0p)/Sqrt[(b0p-a0p).(b0p-a0p)]/Sqrt[(a1p-
      a0p).(a1p-a0p)]]+Pi;
For[k=1;θ1=θ1begin,k≤4000,k++;θ1=θ1-0.02*Pi/180,
   deltaθ1[k]=θ1-θ1begin;
   cθ1=Cos[θ1];
   sθ1=Sin[θ1];
   Answer=FindRoot[{equ11,equ12,equ13,equ32,equ31,equ23},
        {cθ2,-0.3},{sθ2,-0.9},{cθ3,-0.2},{sθ3,-0.8},{cθ4,-0.1},{sθ4,-
        0.9}];
   anscθ2=Answer[[1,2]];
   anssθ2=Answer[[2,2]];
   θ2=Which[anscθ2≥0 && anssθ2≥0,ArcCos[anscθ2],
      anscθ2<0 && anssθ2>0,ArcCos[anscθ2],
      anscθ2≤0 && anssθ2≤0,2*Pi-ArcCos[anscθ2],
      anscθ2>0 && anssθ2<0,-ArcCos[anscθ2]];
   If[k==1,θ2begin=θ2,];
   deltaθ2[k]=θ2-θ2begin;
   newa1[k]=MR[deltaθ1[k]].{{(a1p-a0p)[[1]]},{(a1p-
         a0p)[[2]]}}+{{a0p[[1]]},{a0p[[2]]}};
   p11[k]=MR[deltaθ1[k]].{{(p1p-a0p)[[1]]},{(p1p-
         a0p)[[2]]}}+{{a0p[[1]]},{a0p[[2]]}};
```

```
    newp1[k]=MR[delta02[k]].(p11[k]-newa1[k])+newa1[k];
    square2[k]=(newp1[k][[1]]-p2p[[1]])^2+(newp1[k][[2]]-p2p[[2]])^2;
    square3[k]=(newp1[k][[1]]-p3p[[1]])^2+(newp1[k][[2]]-p3p[[2]])^2;
    square4[k]=(newp1[k][[1]]-p4p[[1]])^2+(newp1[k][[2]]-p4p[[2]])^2;
    ]
For[k=1;minsqrt2=999;minsqrt3=999;minsqrt4=999;
    minsqrt5=999;myk2;myk3;myk4;myk5,
    k≤4000,
    k=k+1,
      If[minsqrt2>square2[k][[1]],minsqrt2=square2[k][[1]];myk2=k,];
      If[minsqrt3>square3[k][[1]],minsqrt3=square3[k][[1]];myk3=k,];
      If[minsqrt4>square4[k][[1]],minsqrt4=square4[k][[1]];myk4=k,];
    ]
StructuralErr2[DistanceOfProjection]=Sqrt[minsqrt2]/DistanceOfProjectio
n;
StructuralErr3[DistanceOfProjection]=Sqrt[minsqrt3]/DistanceOfProjectio
n;
StructuralErr4[DistanceOfProjection]=Sqrt[minsqrt4]/DistanceOfProjectio
n;
newp1[myk2]
newp1[myk3]
newp1[myk4]
delta01[myk2]*180/Pi
delta01[myk3]*180/Pi
delta01[myk4]*180/Pi
Sqrt[square2[myk2]]
Sqrt[square3[myk3]]
Sqrt[square4[myk4]]
StructuralErr2[DistanceOfProjection]
StructuralErr3[DistanceOfProjection]
StructuralErr4[DistanceOfProjection]
```

B.4 Adjustable Five-Bar Path Generator

The following MATHEMATICA models include four sections. Section B.4.1 illustrated how to programming the synthesis design equations for planar five-bar path generator by MATHEMATICA language. Section B.4.2 illustrated the Dual-number method and the displacement equations for planar five-bar path generator. Section B.4.3 illustrated plane-to-sphere projection method, dual-number method and displacement equations for spherical five-bar path generator. Section B.4.4 illustrates the sphere-to-plane projection method for spherical five-bar path generator.

B.4.1 Synthesis Design of Planar Five-Bar Path Generator

```
D1j[θ_,p1x_,p1y_,pjx_,pjy_]={
      {Cos[θ],-Sin[θ],pjx-p1x Cos[θ]+p1y*Sin[θ]},
      {Sin[θ],Cos[θ],pjy-p1x Sin[θ]-p1y Cos[θ]},{0,0,1}};
Tj[ϕ_,b0x_,b0y_]={{Cos[ϕ],-Sin[ϕ],-b0x Cos[ϕ]+b0y
    Sin[ϕ]+b0x},{Sin[ϕ],Cos[ϕ],-b0x Sin[ϕ]-b0y Cos[ϕ]+b0y},{0,0,1}};
p1={{0.1816},{1.8993},{1}};
p2={{0.2756},{1.8648},{1}};
p3={{0.3573},{1.7945},{1}};
p4={{0.4207},{1.6891},{1}};
p5={{0.1816},{1.8993},{1}};
p6={{0.3565},{1.9074},{1}};
p7={{0.5237},{1.8873},{1}};
θ12=4.8260*Pi/180;
θ13=9.8795*Pi/180;
θ14=15.2680*Pi/180;
θ56=-0.04756*Pi/180;
θ57=0.3145*Pi/180;
D12=D1j[θ12,p1[[1,1]],p1[[2,1]],p2[[1,1]],p2[[2,1]]];
D13=D1j[θ13,p1[[1,1]],p1[[2,1]],p3[[1,1]],p3[[2,1]]];
D14=D1j[θ14,p1[[1,1]],p1[[2,1]],p4[[1,1]],p4[[2,1]]];
D56=D1j[θ56,p5[[1,1]],p5[[2,1]],p6[[1,1]],p6[[2,1]]];
D57=D1j[θ57,p5[[1,1]],p5[[2,1]],p7[[1,1]],p7[[2,1]]];
ClearAll[a0x,a0y,a1x,a1y,a1nx,a1ny,b0x,b0y,b1x,b1y,c1x,c1y,c1nx,c1ny];
a0={{0.0},{a0y},{1}};
a1={{a1x},{a1y},{1}};
a1n={{a1nx},{a1ny},{1}};
b0={{1.25},{0},{1}};
c1={{c1x},{c1y},{1}};
c1n={{c1nx},{c1ny},{1}};
R1=1.0;
R2=1.0;
ϕ1=45.0*Pi/180;
b1={{b0[[1,1]]+R2 Cos[ϕ1]},{b0[[2,1]]+R2 Sin[ϕ1]},{1}};
E1=Transpose[(D12.a1-a0)].(D12.a1-a0)-R1^2;
E2=Transpose[(D13.a1-a0)].(D13.a1-a0)-R1^2;
E3=Transpose[(D14.a1-a0)].(D14.a1-a0)-R1^2;
E4=Transpose[(D56.a1n-a0)].(D56.a1n-a0)-R1^2;
E5=Transpose[(D57.a1n-a0)].(D57.a1n-a0)-R1^2;
answ1=FindRoot[{E1[[1,1]]==0,E2[[1,1]]==0,E3[[1,1]]==0,
      E4[[1,1]]==0,E5[[1,1]]==0},{a0y,0.0},{a1x,0.1},{a1y,0.9},
      {a1nx,-0.1},{a1ny,0.9}]
a0y=answ1[[1,2]]
a1x=answ1[[2,2]]
a1y=answ1[[3,2]]
a1nx=answ1[[4,2]]
a1ny=answ1[[5,2]]
θ1=ArcCos[Transpose[(a1-a0)].(b0-a0)/
      Sqrt[Transpose[(a1-a0)].(a1-a0)]/
      Sqrt[Transpose[b0-a0].(b0-a0)]][[1,1]];
```

```
θ2=ArcCos[Transpose[(D12.a1-a0)].(b0-a0)/
      Sqrt[Transpose[(D12.a1-a0)].(D12.a1-a0)]/
      Sqrt[Transpose[b0-a0].(b0-a0)]][[1,1]];
θ3=ArcCos[Transpose[(D13.a1-a0)].(b0-a0)/
      Sqrt[Transpose[(D13.a1-a0)].(D13.a1-a0)]/
      Sqrt[Transpose[b0-a0].(b0-a0)]][[1,1]];
θ4=ArcCos[Transpose[(D14.a1-a0)].(b0-a0)/
      Sqrt[Transpose[(D14.a1-a0)].(D14.a1-a0)]/
      Sqrt[Transpose[b0-a0].(b0-a0)]][[1,1]];
θ5=ArcCos[Transpose[(a1n-a0)].(b0-a0)/
      Sqrt[Transpose[(a1n-a0)].(a1n-a0)]/
      Sqrt[Transpose[b0-a0].(b0-a0)]][[1,1]];
θ6=ArcCos[Transpose[(D56.a1n-a0)].(b0-a0)/
      Sqrt[Transpose[(D56.a1n-a0)].(D56.a1n-a0)]/
      Sqrt[Transpose[b0-a0].(b0-a0)]][[1,1]];
θ7=ArcCos[Transpose[(D57.a1n-a0)].(b0-a0)/
      Sqrt[Transpose[(D57.a1n-a0)].(D57.a1n-a0)]/
      Sqrt[Transpose[b0-a0].(b0-a0)]][[1,1]];
kθϕ=0.5;
T12=Tj[kθϕ (θ2-θ1),b0[[1,1]],b0[[2,1]]];
T13=Tj[kθϕ (θ3-θ1),b0[[1,1]],b0[[2,1]]];
T14=Tj[kθϕ (θ4-θ1),b0[[1,1]],b0[[2,1]]];
T56=Tj[kθϕ (θ6-θ5),b0[[1,1]],b0[[2,1]]];
T57=Tj[kθϕ (θ7-θ5),b0[[1,1]],b0[[2,1]]];
F1=(Transpose[D12.c1-T12.b1].(D12.c1-T12.b1)-R3^2);
F2=(Transpose[D13.c1-T13.b1].(D13.c1-T13.b1)-R3^2);
F3=(Transpose[(D14.c1-T14.b1)].(D14.c1-T14.b1)-R3^2);
F4=(Transpose[(D56.c1n-T56.b1)].(D56.c1n-T56.b1)-R3^2);
F5=(Transpose[(D57.c1n-T57.b1)].(D57.c1n-T57.b1)-R3^2);
ans2=FindRoot[{F1[[1,1]]==0,F2[[1,1]]==0,F3[[1,1]]==0,
      F4[[1,1]]==0,F5[[1,1]]==0},{c1x,0.9},{c1y,1.5},
      {c1nx,1.2},{c1ny,1.8},{R3,1.3}]
c1x=ans2[[1,2]]
c1y=ans2[[2,2]]
c1nx=ans2[[3,2]]
c1ny=ans2[[4,2]]
R3=ans2[[5,2]]
```

B.4.2 Displacement Analysis for Planar Five-Bar Path Generator

```
ClearAll[cθ2,sθ2,a2,cθ3,sθ3,a3,cθ4,sθ4,a4,cθ1,sθ1,a1,cθ5,sθ5,a5,z11,z12,
    z13,z21,z22,z23,z31,z32,z33];
M[cθ_,sθ_,a_]:={{cθ,-sθ,e a sθ},{sθ,cθ,-e a cθ},{0,e a, 1}}
M2=M[cθ2,sθ2,a2];
M3=M[cθ3,sθ3,a3];
M4=M[cθ4,sθ4,a4];
M1=M[cθ1,sθ1,a1];
M5=M[cθ5,sθ5,a5];
Z=M2.M3-Transpose[M1].Transpose[M5].Transpose[M4];
z11=Z[[1,1]];
z12=Z[[1,2]];
z13=Z[[1,3]];
z21=Z[[2,1]];
z22=Z[[2,2]];
```

```
z23=Z[[2,3]];
z31=Z[[3,1]];
z32=Z[[3,2]];
z33=Z[[3,3]];
equ11=Coefficient[z11,e,0]
equ12=Coefficient[z12,e,0]
equ13=Coefficient[z13,e,1]
equ23=Coefficient[z23,e,1]
equ31=Coefficient[z31,e,1]
equ32=Coefficient[z32,e,1]
p1p={0.1816,1.8993};
p2p={0.2756,1.8648};
p3p={0.3573,1.7945};
p4p={0.4207,1.6891};
p5p={0.1816,1.8993};
p6p={0.3565,1.9074};
p7p={0.5237,1.8873};
a0p={0.0000,0.000412039};
a1p={0.121889,0.993036};
a1np={-0.134435,0.991261};
b0p={1.25,0};
b1p={1.95711,0.707107};
c1p={0.891267,1.45417};
c1np={1.21674,1.77753};
a1=Sqrt[(a1p-a0p).(a1p-a0p)]
a2=Sqrt[(a1p-c1p).(a1p-c1p)]
a3=Sqrt[(c1p-b1p).(c1p-b1p)]
a4=Sqrt[(b1p-b0p).(b1p-b0p)]
a5=Sqrt[(b0p-a0p).(b0p-a0p)]
θ1begin=ArcCos[(b0p-a0p).(a1p-a0p)/Sqrt[(b0p-a0p).(b0p-a0p)]/Sqrt[(a1p-
    a0p).(a1p-a0p)]]+Pi;
θ5begin=2 Pi-45.*Pi/180.
MR[θ_]:={{Cos[θ],-Sin[θ]},{Sin[θ],Cos[θ]}}
kθΦ=0.5
θ50=2. Pi-45.*Pi/180
tcθ2=0.6;tsθ2=-0.8;tcθ3=0.4;tsθ3=-0.9;tcθ4=-0.2;tsθ4=-0.9;
For[k=1;θ1=θ1begin,
    k≤15300,
    k++;θ1=θ1-0.002*Pi/180,
    deltaθ1[k]=θ1-θ1begin;
    deltaθ5[k]=kθΦ*deltaθ1[k];
    θ5=θ50-deltaθ5[k];
    cθ1=Cos[θ1];
    sθ1=Sin[θ1];
    cθ5=Cos[θ5];
    sθ5=Sin[θ5];
    Answer=FindRoot[{equ11,equ12,equ13,equ32,equ31,equ23},{cθ2,tcθ2},{s
        θ2,tsθ2},{cθ3,tcθ3},{sθ3,tsθ3},{cθ4,tcθ4},{sθ4,tsθ4}];
    tcθ2=Answer[[1,2]];tsθ2=Answer[[2,2]];
    tcθ3=Answer[[3,2]];tsθ3=Answer[[4,2]];
    tcθ4=Answer[[5,2]];tsθ4=Answer[[6,2]];
    anscθ2=Answer[[1,2]];
    anssθ2=Answer[[2,2]];
    θ2=Which[anscθ2≥0 && anssθ2≥0,ArcCos[anscθ2],
        anscθ2<0 && anssθ2>0,ArcCos[anscθ2],
        anscθ2≤0 && anssθ2≤0,2*Pi-ArcCos[anscθ2],
        anscθ2>0 && anssθ2<0,-ArcCos[anscθ2]];
```

```
    delta$\theta$2[k]=$\theta$2-$\theta$2begin;
    newa1[k]=MR[delta$\theta$1[k]].{{(a1p-a0p)[[1]]},{(a1p-
        a0p)[[2]]}}+{{a0p[[1]]},{a0p[[2]]}};
    p11[k]=MR[delta$\theta$1[k]].{{(p1p-a0p)[[1]]},{(p1p-
        a0p)[[2]]}}+{{a0p[[1]]},{a0p[[2]]}};
    newp1[k]=MR[delta$\theta$2[k]].(p11[k]-newa1[k])+newa1[k];
    square2[k]=(newp1[k][[1]]-p2p[[1]])^2+(newp1[k][[2]]-p2p[[2]])^2;
    square3[k]=(newp1[k][[1]]-p3p[[1]])^2+(newp1[k][[2]]-p3p[[2]])^2;
    square4[k]=(newp1[k][[1]]-p4p[[1]])^2+(newp1[k][[2]]-p4p[[2]])^2;
    ]
For[k=1;minsqrt2=999;minsqrt3=999;minsqrt4=999;myk2;myk3;myk4,k≤15300,k
    =k+1,
    If[minsqrt2>square2[k][[1]],minsqrt2=square2[k][[1]];myk2=k,];
    If[minsqrt3>square3[k][[1]],minsqrt3=square3[k][[1]];myk3=k,];
    If[minsqrt4>square4[k][[1]],minsqrt4=square4[k][[1]];myk4=k,];
    ]
newp1[myk2]
newp1[myk3]
newp1[myk4]
delta$\theta$1[myk2]*180/Pi
delta$\theta$1[myk3]*180/Pi
delta$\theta$1[myk4]*180/Pi
```

B.4.3 Spherical Five -Bar Path Generator by Plane-to-Sphere Projection

```
MyMaxSteps=1000;
RadiusOfSphere=1;
DistanceOfProjection=7
ClearAll[p1p,p2p,p3p,p4p,p5p,p6p,p7p,p1,p2,p3,p4,p5,p6,p7];
ProjectionFun[{x_,y_},r_,d_]:={r*x/Sqrt[d^2+x^2+y^2],r*y/
    Sqrt[d^2+x^2+y^2],r*d/Sqrt[d^2+x^2+y^2]}
p1p={0.1816,1.8993};
p2p={0.2756,1.8648};
p3p={0.3573,1.7945};
p4p={0.4207,1.6891};
p5p={0.1816,1.8993};
p6p={0.3565,1.9074};
p7p={0.5237,1.8873};
p1=ProjectionFun[p1p,RadiusOfSphere,DistanceOfProjection]
p2=ProjectionFun[p2p,RadiusOfSphere,DistanceOfProjection]
p3=ProjectionFun[p3p,RadiusOfSphere,DistanceOfProjection]
p4=ProjectionFun[p4p,RadiusOfSphere,DistanceOfProjection]
p5=ProjectionFun[p5p,RadiusOfSphere,DistanceOfProjection]
p6=ProjectionFun[p6p,RadiusOfSphere,DistanceOfProjection]
p7=ProjectionFun[p7p,RadiusOfSphere,DistanceOfProjection]
ClearAll[a0p,a1p,a1np,b0p,b1p,b1np,a0,a1,a1n,b0,b1,b1n,α1,α2,α3,α4,cα1,
    sα1,cα2,sα2,cα3,sα3,cα4,sα4];
a0p={0.0000,0.000412039};
a1p={0.121889,0.993036};
a1np={-0.134435,0.991261};
b0p={1.25,0};
b1p={1.95711,0.707107};
c1p={0.891267,1.45417};
c1np={1.21674,1.77753};
```

```
a0=ProjectionFun[a0p,RadiusOfSphere,DistanceOfProjection]
a1=ProjectionFun[a1p,RadiusOfSphere,DistanceOfProjection]
a1n=ProjectionFun[a1np,RadiusOfSphere,DistanceOfProjection]
b0=ProjectionFun[b0p,RadiusOfSphere,DistanceOfProjection]
b1=ProjectionFun[b1p,RadiusOfSphere,DistanceOfProjection]
c1=ProjectionFun[c1p,RadiusOfSphere,DistanceOfProjection]
c1n=ProjectionFun[c1np,RadiusOfSphere,DistanceOfProjection]
α1=ArcCos[a0.a1/Sqrt[a0.a0]/Sqrt[a1.a1]];
α2=ArcCos[a1.c1/Sqrt[c1.c1]/Sqrt[a1.a1]];
α3=ArcCos[c1.b1/Sqrt[c1.c1]/Sqrt[b1.b1]];
α4=ArcCos[b1.b0/Sqrt[b1.b1]/Sqrt[b0.b0]];
α5=ArcCos[a0.b0/Sqrt[a0.a0]/Sqrt[b0.b0]];
cα1=Cos[α1];sα1=Sin[α1];cα2=Cos[α2];sα2=Sin[α2];
cα3=Cos[α3];sα3=Sin[α3];cα4=Cos[α4];sα4=Sin[α4];cα5=Cos[α5];sα5=Sin[α5];
AngleBTAxes[{ax_,ay_,az_},{bx_,by_,bz_}]:={-(az by-ay bz)/(-ay bx+ax
    by),
    -(az bx-ax bz)/(ay bx-ax by),1}
alpha1v=AngleBTAxes[a0,a1];
alpha2v=AngleBTAxes[a1,c1];
alpha3v=AngleBTAxes[c1,b1];
alpha4v=AngleBTAxes[b1,b0];
alpha5v=AngleBTAxes[b0,a0];
ϕ10=ArcCos[alpha5v.alpha1v/Sqrt[alpha1v.alpha1v]/Sqrt[alpha5v.alpha5v]]
    +Pi;
ϕ20=ArcCos[alpha1v.alpha2v/Sqrt[alpha1v.alpha1v]/Sqrt[alpha2v.alpha2v]];
ϕ30=ArcCos[alpha3v.alpha2v/Sqrt[alpha3v.alpha3v]/Sqrt[alpha2v.alpha2v]];
ϕ40=ArcCos[alpha3v.alpha4v/Sqrt[alpha3v.alpha3v]/Sqrt[alpha4v.alpha4v]]
    +Pi;
ϕ50=ArcCos[alpha4v.alpha5v/Sqrt[alpha5v.alpha5v]/Sqrt[alpha4v.alpha4v]]
    +Pi;
Dual Nuber method for spherical mechanism.
ClearAll[cθ1,sθ1,cθ2,sθ2,cθ3,sθ3,cθ4,sθ4,cθ5,sθ5];
M[cθ_,sθ_,cα_,sα_]:={{cθ,-cα sθ,sα sθ},{sθ,cα cθ,-sα cθ},{0,sα, cα}}
M2=M[cθ2,sθ2,cα2,sα2];
M3=M[cθ3,sθ3,cα3,sα3];
M4=M[cθ4,sθ4,cα4,sα4];
M1=M[cθ1,sθ1,cα1,sα1];
M5=M[cθ5,sθ5,cα5,sα5];
Z=M2.M3-Transpose[M1].Transpose[M5].Transpose[M4];
z11=Z[[1,1]];
z12=Z[[1,2]];
z13=Z[[1,3]];
z21=Z[[2,1]];
z22=Z[[2,2]];
z23=Z[[2,3]];
z31=Z[[3,1]];
z32=Z[[3,2]];
z33=Z[[3,3]];
Spherical Mechanism by Dual Number Method
tcθ2=0.6;tsθ2=-0.7;tcθ3=0.3;tsθ3=-0.9;tcθ4=-0.2;tsθ4=-0.9;
For[ϕ1=ϕ10;k=1,k≤MyMaxSteps,
   ϕ1=ϕ1-33./MyMaxSteps*Pi/180;k=k+1,
   deltaϕ1[k]=ϕ1-ϕ10;
   deltaϕ5[k]=(ϕ1-ϕ10)*0.5;
   ϕ5=ϕ50-deltaϕ5[k];
   cθ1=Cos[ϕ1];
   sθ1=Sin[ϕ1];
```

```
   cθ5=Cos[ϕ5];
   sθ5=Sin[ϕ5];
    Angles=FindRoot[{z11==0,z12==0,z13==0,z21==0,z22==0,z23==0},{cθ2,tc
        θ2},{sθ2,tsθ2},{cθ3,tcθ3},{sθ3,tsθ3},{cθ4,tcθ4},{sθ4,tsθ4}];
   tcθ2=Angles[[1,2]];tsθ2=Angles[[2,2]];
   tcθ3=Angles[[3,2]];tsθ3=Angles[[4,2]];
   tcθ4=Angles[[5,2]];tsθ4=Angles[[6,2]];
   anscθ2=Angles[[1,2]];
   anssθ2=Angles[[2,2]];
   θ2=Which[anscθ2≥0 && anssθ2≥0,ArcCos[anscθ2],
      anscθ2<0 && anssθ2>0,ArcCos[anscθ2],
      anscθ2≤0 && anssθ2≤0,2*Pi-ArcCos[anscθ2],
      anscθ2>0 && anssθ2<0,2*Pi-ArcCos[anscθ2]];
   If[k==1,θ2begin=θ2,];
   deltaθ2[k]=θ2-θ2begin;
   deltaθ1[k]=ϕ1-ϕ10;
   ]
Ru[α_,u_]:={{u[[1,1]]^2*(1-Cos[α])+Cos[α],u[[1,1]] u[[2,1]]
    (1-Cos[α])-u[[3,1]] Sin[α],u[[1,1]] u[[3,1]] (1-Cos[α])+
    u[[2,1]] Sin[α]},{u[[1,1]] u[[2,1]] (1-Cos[α])+u[[3,1]]
    Sin[α],u[[2,1]]^2 (1-Cos[α])+Cos[α],u[[2,1]] u[[3,1]] (1-Cos[α])-
    u[[1,1]] Sin[α]},{u[[1,1]] u[[3,1]] (1-Cos[α])-u[[2,1]]
    Sin[α],u[[2,1]] u[[3,1]] (1-Cos[α])+
    u[[1,1]] Sin[α],u[[3,1]]^2 (1-Cos[α])+Cos[α]}};
uak={{uax},{uay},{uaz}};
a0axis={{a0[[1]]},{a0[[2]]},{a0[[3]]}};
b0axis={{b0[[1]]},{b0[[2]]},{b0[[3]]}};
For[k=1,k≤MyMaxSteps,k++,
   NewA1[k]=Ru[deltaθ1[k],a0axis].(a1-a0)+a0;
   a1axis={{NewA1[k][[1]]},{NewA1[k][[2]]},{NewA1[k][[3]]}};
   p1temp[k]=Ru[deltaθ1[k],a0axis].(p1-a0)+a0;
   NewP1[k]=Ru[deltaθ2[k],a1axis].(p1temp[k]-NewA1[k])+NewA1[k];
   ]
Pd=p2;
For[k=1;minsqrt=9999;myk,k≤MyMaxSteps,k++,
   toleranceErr[k]=Sqrt[(NewP1[k][[1]]-Pd[[1]])^2+
   (NewP1[k][[2]]-Pd[[2]])^2+(NewP1[k][[3]]-Pd[[3]])^2];
    If[minsqrt>toleranceErr[k],minsqrt=toleranceErr[k];myk=k,];
   ]
myanswer2[DistanceOfProjection]={myk,deltaθ1[myk]*180/Pi,
    DistanceOfProjection,NewP1[myk], minsqrt*DistanceOfProjection}
Pd=p3;
For[k=1;minsqrt=9999;myk,k≤MyMaxSteps,k++,
   toleranceErr[k]=Sqrt[(NewP1[k][[1]]-Pd[[1]])^2+
   (NewP1[k][[2]]-Pd[[2]])^2+(NewP1[k][[3]]-Pd[[3]])^2];
    If[minsqrt>toleranceErr[k],minsqrt=toleranceErr[k]; myk=k,];
   ]
myanswer3[DistanceOfProjection]={myk,deltaθ1[myk]*180/Pi,DistanceOfProj
    ection,NewP1[myk],minsqrt*DistanceOfProjection}
Pd=p4;
For[k=1;minsqrt=9999;myk,k≤MyMaxSteps,k++,
   toleranceErr[k]=Sqrt[(NewP1[k][[1]]-Pd[[1]])^2+
   (NewP1[k][[2]]-Pd[[2]])^2+(NewP1[k][[3]]-Pd[[3]])^2];
    If[minsqrt>toleranceErr[k],minsqrt=toleranceErr[k];myk=k,];
   ]
myanswer4[DistanceOfProjection]={myk,deltaθ1[myk]*180/Pi,DistanceOfProj
    ection,NewP1[myk],minsqrt*DistanceOfProjection}
```

B.4.4 Planar Five -Bar Path Generator by Sphere-to-Plane Projection

```
MyMaxSteps=320;
RadiusOfSphere=1;
DistanceOfProjection=6
ClearAll[p1p,p2p,p3p,p4p,p5p,p6p,p7p,p1,p2,p3,p4,p5,p6,p7];
ProjectionFun[{x_,y_,z_},d_]:={d/z*x,d/z*y}
p1={0.0339334,0.354899,0.934289}
p2={0.0515763,0.348982,0.935709}
p3={0.0671077,0.337041,0.939095}
p4={0.0794622,0.319039,0.944405}
p5={0.0339334,0.354899,0.934289}
p6={0.0664699,0.355638,0.932257}
p7={0.0975245,0.351457,0.931111}
p1p=ProjectionFun[p1,DistanceOfProjection]
p2p=ProjectionFun[p2,DistanceOfProjection]
p3p=ProjectionFun[p3,DistanceOfProjection]
p4p=ProjectionFun[p4,DistanceOfProjection]
p5p=ProjectionFun[p5,DistanceOfProjection]
p6p=ProjectionFun[p6,DistanceOfProjection]
p7p=ProjectionFun[p7,DistanceOfProjection]
ClearAll[a0p,a1p,a1np,b0p,b1p,b1np,a0,a1,a1n,b0,b1,b1n];
a0={0.,0.0000824078,1.};
a1={0.023904,0.194747,0.980562};
a1n={-0.0263645,0.1944,0.980568};
b0={0.242536,0,0.970143};
b1={0.361374,0.130565,0.923234};
c1={0.168708,0.27526,0.946451};
c1n={0.22349,0.326496,0.918397};
a0p=ProjectionFun[a0,DistanceOfProjection]
a1p=ProjectionFun[a1,DistanceOfProjection]
a1np=ProjectionFun[a1n,DistanceOfProjection]
b0p=ProjectionFun[b0,DistanceOfProjection]
b1p=ProjectionFun[b1,DistanceOfProjection]
c1p=ProjectionFun[c1,DistanceOfProjection]
c1np=ProjectionFun[c1n,DistanceOfProjection]
ClearAll[cθ2,sθ2,a2,cθ3,sθ3,a3,cθ4,sθ4,a4,cθ1,sθ1,a1,cθ5,sθ5,a5,zz11,zz
    12,z13,zz21,zz22,zz23,zz31,zz32,zz33];
M[cθ_,sθ_,a_]:={{cθ,-sθ,e a sθ},{sθ,cθ,-e a cθ},{0,e a, 1}}
M2=M[cθ2,sθ2,a2];
M3=M[cθ3,sθ3,a3];
M4=M[cθ4,sθ4,a4];
M1=M[cθ1,sθ1,a1];
M5=M[cθ5,sθ5,a5];
Z=M2.M3-Transpose[M1].Transpose[M5].Transpose[M4];
z11=Z[[1,1]];
z12=Z[[1,2]];
z13=Z[[1,3]];
z21=Z[[2,1]];
z22=Z[[2,2]];
z23=Z[[2,3]];
z31=Z[[3,1]];
z32=Z[[3,2]];
```

```
z33=Z[[3,3]];
equ11=Coefficient[z11,e,0]
equ12=Coefficient[z12,e,0]
equ13=Coefficient[z13,e,1]
equ23=Coefficient[z23,e,1]
equ31=Coefficient[z31,e,1]
equ32=Coefficient[z32,e,1]
ClearAll[a1,a2,a3,a4];
a1=Sqrt[(a1p-a0p).(a1p-a0p)]
a2=Sqrt[(c1p-a1p).(c1p-a1p)]
a3=Sqrt[(b1p-c1p).(b1p-c1p)]
a4=Sqrt[(b0p-b1p).(b0p-b1p)]
a5=Sqrt[(a0p-b0p).(a0p-b0p)]
ClearAll[θ1begin,θ1];
θ1begin=ArcCos[(b0p-a0p).(a1p-a0p)/Sqrt[(b0p-a0p).(b0p-a0p)]/Sqrt[(a1p-
    a0p).(a1p-a0p)]]+Pi;
θ5begin=2 Pi-45.*Pi/180.
MR[θ_]:={{Cos[θ],-Sin[θ]},{Sin[θ],Cos[θ]}};
kθΦ=0.5;
θ50=2. Pi-45.*Pi/180;
tcθ2=0.6;tsθ2=-0.8;tcθ3=0.4;tsθ3=-0.9;tcθ4=-0.2;tsθ4=-0.9;
For[k=1;θ1=θ1begin,k≤MyMaxSteps,
    k++;θ1=θ1-32/MyMaxSteps*Pi/180.,
    delta θ1[k]=θ1-θ1begin;
    delta θ5[k]=kθΦ*delta θ1[k];
    θ5=θ50-delta θ5[k];
    cθ1=Cos[θ1];sθ1=Sin[θ1];
    cθ5=Cos[θ5];sθ5=Sin[θ5];
    Answer=FindRoot[{equ11,equ12,equ13,equ32,equ31,equ23},{cθ2,tcθ2},{s
    θ2,tsθ2},{cθ3,tcθ3},{sθ3,tsθ3},{cθ4,tcθ4},{sθ4,tsθ4}];
    tcθ2=Answer[[1,2]];tsθ2=Answer[[2,2]];
    tcθ3=Answer[[3,2]];tsθ3=Answer[[4,2]];
    tcθ4=Answer[[5,2]];tsθ4=Answer[[6,2]];
    anscθ2=Answer[[1,2]];anssθ2=Answer[[2,2]];
    θ2=Which[anscθ2≥0 && anssθ2≥0,ArcCos[anscθ2],
    anscθ2<0 && anssθ2>0,ArcCos[anscθ2],
    anscθ2≤0 && anssθ2≤0,2*Pi-ArcCos[anscθ2],
    anscθ2>0 && anssθ2<0,-ArcCos[anscθ2]];
    If[k==1,θ2begin=θ2;Print[Answer],];
    delta θ2[k]=θ2-θ2begin;
    newa1[k]=MR[delta θ1[k]].{{(a1p-a0p)[[1]]},{(a1p-
    a0p)[[2]]}}+{{a0p[[1]]},{a0p[[2]]}};
    p11[k]=MR[delta θ1[k]].{{(p1p-a0p)[[1]]},{(p1p-
    a0p)[[2]]}}+{{a0p[[1]]},{a0p[[2]]}};
    newp1[k]=MR[delta θ2[k]].(p11[k]-newa1[k])+newa1[k];
    square2[k]=(newp1[k][[1]]-p2p[[1]])^2+(newp1[k][[2]]-p2p[[2]])^2;
    square3[k]=(newp1[k][[1]]-p3p[[1]])^2+(newp1[k][[2]]-p3p[[2]])^2;
    square4[k]=(newp1[k][[1]]-p4p[[1]])^2+(newp1[k][[2]]-p4p[[2]])^2;
    ]
For[k=1;minsqrt2=999;minsqrt3=999;minsqrt4=999;myk2;myk3;myk4,k≤MyMaxSt
    eps,k=k+1,
    If[minsqrt2>square2[k][[1]],minsqrt2=square2[k][[1]];myk2=k,];
    If[minsqrt3>square3[k][[1]],minsqrt3=square3[k][[1]];myk3=k,];
    If[minsqrt4>square4[k][[1]],minsqrt4=square4[k][[1]];myk4=k,];
    ]
StructuralErr2[DistanceOfProjection]=Sqrt[minsqrt2]/
    DistanceOfProjection
```

```
StructuralErr3[DistanceOfProjection]=Sqrt[minsqrt3]/
    DistanceOfProjection
StructuralErr4[DistanceOfProjection]=Sqrt[minsqrt4]/
    DistanceOfProjection
newp1[myk2]
newp1[myk3]
newp1[myk4]
delta01[myk2]*180/Pi
delta01[myk3]*180/Pi
delta01[myk4]*180/Pi
```

B.5 Adjustable Five-Bar Motion Generator

The following MATHEMATICA models include four sections. Section B.5.1 illustrated how to programming the synthesis design equations for planar five-bar motion generator by MATHEMATICA language. Section B.5.2 illustrated the dual-number method and the displacement equations for planar five-bar motion generator. Section B.5.3 illustrated plane-to-sphere projection method, dual-number method and displacement equations for spherical five-bar motion generator. Section B.5.4 illustrates the sphere-to-plane projection method for spherical five-bar motion generator.

B.5.1 Synthesis Design of Planar Five-Bar Motion Generator

```
D1j[p_,q_,r_,p1_,q1_,r1_]:={{p1[[1,1]],q1[[1,1]],r1[[1,1]]},{p1[[2,1]],
      q1[[2,1]],r1[[2,1]]},{1,1,1} } . Inverse[
      {{p[[1,1]],q[[1,1]],r[[1,1]]},{p[[2,1]],q[[2,1]],r[[2,1]]},{1,1,1
      } }];
Tj[ϕ_,b0x_,b0y_]={{Cos[ϕ],-Sin[ϕ],-b0x Cos[ϕ]+b0y
      Sin[ϕ]+b0x},{Sin[ϕ],Cos[ϕ],-b0x Sin[ϕ]-b0y Cos[ϕ]+b0y},{0,0,1}};
p1={{-0.1348},{1.4949},{1}};q1={{0.1853},{1.9430},{1}};
r1={{0.7769},{1.9430},{1}};
p2={{-0.0057},{1.4353},{1}};q2={{0.2756},{1.9087},{1}};
r2={{0.8652},{1.9585},{1}};
p3={{0.1149},{1.3419},{1}};q3={{0.3534},{1.8382},{1}};
r3={{0.9363},{1.9397},{1}};
p4={{0.2219},{1.2157},{1}};q4={{0.4128},{1.7322},{1}};
r4={{0.9835},{1.8880},{1}};
p5={{-0.1348},{1.4949},{1}};q5={{0.1853},{1.9430},{1}};
r5={{0.7769},{1.9430},{1}};
p6={{0.0397},{1.5033},{1}};q6={{0.3602},{1.9511},{1}};
r6={{0.9518},{1.9506},{1}};
p7={{0.2095},{1.4813},{1}};q7={{0.5271},{1.9311},{1}};
r7={{1.1187},{1.9343},{1}};
D12=D1j[p1,q1,r1,p2,q2,r2]
D13=D1j[p1,q1,r1,p3,q3,r3]
D14=D1j[p1,q1,r1,p4,q4,r4]
D56=D1j[p5,q5,r5,p6,q6,r6]
D57=D1j[p5,q5,r5,p7,q7,r7]
ClearAll[a0x,a0y,a1x,a1y,a1nx,a1ny,b0x,b0y,b1x,b1y,c1x,c1y,c1nx,c1ny]
a0={{0.0},{a0y},{1}};
a1={{a1x},{a1y},{1}};
a1n={{a1nx},{a1ny},{1}};
```

```
b0={{1.25},{0},{1}};
c1={{c1x},{c1y},{1}};
c1n={{c1nx},{c1ny},{1}};
R1=1.0;
R2=1.0;
ϕ1=45.0*Pi/180;
b1={{b0[[1,1]]+R2 Cos[ϕ1]},{b0[[2,1]]+R2 Sin[ϕ1]},{1}}
E1=Transpose[(D12.a1-a0)].(D12.a1-a0)-R1^2
E2=Transpose[(D13.a1-a0)].(D13.a1-a0)-R1^2
E3=Transpose[(D14.a1-a0)].(D14.a1-a0)-R1^2
E4=Transpose[(D56.a1n-a0)].(D56.a1n-a0)-R1^2
E5=Transpose[(D57.a1n-a0)].(D57.a1n-a0)-R1^2
answ1=FindRoot[{E1[[1,1]]==0,E2[[1,1]]==0,E3[[1,1]]==0,
      E4[[1,1]]==0,E5[[1,1]]==0},{a0y,0.01},{a1x,0.1},{a1y,
      0.9},{a1nx,-0.1},{a1ny,0.9}]
a0y=answ1[[1,2]]
a1x=answ1[[2,2]]
a1y=answ1[[3,2]]
a1nx=answ1[[4,2]]
a1ny=answ1[[5,2]]
θ1=ArcCos[Transpose[(a1-a0)].(b0-a0)/Sqrt[Transpose[(a1-a0)].(a1-
      a0)]/Sqrt[Transpose[b0-a0].(b0-a0)]][[1,1]];
θ2=ArcCos[Transpose[(D12.a1-a0)].(b0-a0)/Sqrt[Transpose[(D12.a1-
      a0)].(D12.a1-a0)]/Sqrt[Transpose[b0-a0].(b0-a0)]][[1,1]];
θ3=ArcCos[Transpose[(D13.a1-a0)].(b0-a0)/Sqrt[Transpose[(D13.a1-
      a0)].(D13.a1-a0)]/Sqrt[Transpose[b0-a0].(b0-a0)]][[1,1]];
θ4=ArcCos[Transpose[(D14.a1-a0)].(b0-a0)/Sqrt[Transpose[(D14.a1-
      a0)].(D14.a1-a0)]/Sqrt[Transpose[b0-a0].(b0-a0)]][[1,1]];
θ5=ArcCos[Transpose[(a1n-a0)].(b0-a0)/Sqrt[Transpose[(a1n-a0)].(a1n-
      a0)]/Sqrt[Transpose[b0-a0].(b0-a0)]][[1,1]];
θ6=ArcCos[Transpose[(D56.a1n-a0)].(b0-a0)/Sqrt[Transpose[(D56.a1n-
      a0)].(D56.a1n-a0)]/Sqrt[Transpose[b0-a0].(b0-a0)]][[1,1]];
θ7=ArcCos[Transpose[(D57.a1n-a0)].(b0-a0)/Sqrt[Transpose[(D57.a1n-
      a0)].(D57.a1n-a0)]/Sqrt[Transpose[b0-a0].(b0-a0)]][[1,1]];
kθϕ=0.5;
T12=Tj[kθϕ(θ2-θ1),b0[[1,1]],b0[[2,1]]]
T13=Tj[kθϕ(θ3-θ1),b0[[1,1]],b0[[2,1]]]
T14=Tj[kθϕ(θ4-θ1),b0[[1,1]],b0[[2,1]]]
T56=Tj[kθϕ(θ6-θ5),b0[[1,1]],b0[[2,1]]]
T57=Tj[kθϕ(θ7-θ5),b0[[1,1]],b0[[2,1]]]
F1=Transpose[D12.c1-T12.b1].(D12.c1-T12.b1)-R3^2
F2=Transpose[D13.c1-T13.b1].(D13.c1-T13.b1)-R3^2
F3=(Transpose[(D14.c1-T14.b1)].(D14.c1-T14.b1)-R3^2)
F4=(Transpose[(D56.c1n-T56.b1)].(D56.c1n-T56.b1)-R3^2)
F5=(Transpose[(D57.c1n-T57.b1)].(D57.c1n-T57.b1)-R3^2)
FindRoot[{F1[[1,1]]==0,F2[[1,1]]==0,F3[[1,1]]==0,
    F4[[1,1]]==0,F5[[1,1]]==0},{c1x,0.9},{c1y,1.5},{c1nx,
    1.2},{c1ny,1.8},{R3,1.3}]
```

B.5.2 Displacement Analysis for Planar Five-Bar Motion Generator

```
p1p={-0.1348,1.4949};
p2p={-0.0057,1.4353};
p3p={0.1149,1.3419};
```

```
p4p={0.2219,1.2157};
p5p={-0.1348,1.4949};
p6p={0.0397,1.5033};
p7p={0.2095,1.4813};
q1p={0.1853,1.9430};
q2p={0.2756,1.9087};
q3p={0.3534,1.8382};
q4p={0.4128,1.7322};
q5p={0.1853,1.9430};
q6p={0.3602,1.9511};
q7p={0.5271,1.9311};
r1p={0.7769,1.9430};
r2p={0.8652,1.9585};
r3p={0.9363,1.9397};
r4p={0.9835,1.8880};
r5p={0.7769,1.9430};
r6p={0.9518,1.9506};
r7p={1.1187,1.9343};
a0p={0,-0.00229193};
a1p={0.121248,0.990334};
a1np={-0.134977,0.988511};
b0p={1.25,0};
b1p={1.9571,0.7071};
c1p={0.889398,1.45516};
c1np={1.21532,1.7792};
M[cθ_,sθ_,a_]:={{cθ,-sθ,e a sθ},{sθ,cθ,-e a cθ},{0,e a, 1}}
M2=M[cθ2,sθ2,a2] ;
M3=M[cθ3,sθ3,a3];
M4=M[cθ4,sθ4,a4];
M1=M[cθ1,sθ1,a1];
M5=M[cθ5,sθ5,a5];
Z=M2.M3-Transpose[M1].Transpose[M5].Transpose[M4];
z11=Z[[1,1]];
z12=Z[[1,2]];
z13=Z[[1,3]];
z21=Z[[2,1]];
z22=Z[[2,2]];
z23=Z[[2,3]];
z31=Z[[3,1]];
z32=Z[[3,2]];
z33=Z[[3,3]];
equ11=Coefficient[z11,e,0]
equ12=Coefficient[z12,e,0]
equ13=Coefficient[z13,e,1]
equ23=Coefficient[z23,e,1]
equ31=Coefficient[z31,e,1]
equ32=Coefficient[z32,e,1]

a1=Sqrt[(a1p-a0p).(a1p-a0p)]
a2=Sqrt[(a1p-c1p).(a1p-c1p)]
a3=1.30373
a4=1
a5=Sqrt[(b0p-a0p).(b0p-a0p)]
θ1begin=ArcCos[(b0p-a0p).(a1p-a0p)/Sqrt[(b0p-a0p).(b0p-a0p)]/Sqrt[(a1p-
      a0p).(a1p-a0p)]]+Pi
θ5begin=2 Pi-45.*Pi/180.
MR[θ_]:={{Cos[θ],-Sin[θ]},{Sin[θ],Cos[θ]}}
```

```
kθΦ=0.5
θ50=2.*Pi-45.*Pi/180
tcθ2=0.6;tsθ2=-0.8;tcθ3=0.4;tsθ3=-0.9;tcθ4=-0.2;tsθ4=-0.9;
For[k=1;θ1=θ1begin,k≤6200,
      k++;θ1=θ1-0.005*Pi/180,
      deltaθ1[k]=θ1-θ1begin;
      deltaθ5[k]=kθΦ * deltaθ1[k];
      θ5=θ50-deltaθ5[k];
      cθ1=Cos[θ1];
      sθ1=Sin[θ1];
      cθ5=Cos[θ5];
      sθ5=Sin[θ5];
      Answer=FindRoot[{equ11,equ12,equ13,equ32,equ31,equ23},{cθ2,tcθ2},
      {sθ2,tsθ2},{cθ3,tcθ3},{sθ3,tsθ3},{cθ4,tcθ4},{sθ4,tsθ4}];
      tcθ2=Answer[[1,2]];tsθ2=Answer[[2,2]];
      tcθ3=Answer[[3,2]];tsθ3=Answer[[4,2]];
      tcθ4=Answer[[5,2]];tsθ4=Answer[[6,2]];
      anscθ2=Answer[[1,2]];
      anssθ2=Answer[[2,2]];
      θ2=Which[anscθ2≥0 && anssθ2≥0,ArcCos[anscθ2],
         anscθ2<0 && anssθ2>0,ArcCos[anscθ2],
         anscθ2≤0 && anssθ2≤0,2*Pi-ArcCos[anscθ2],
         anscθ2>0 && anssθ2<0,-ArcCos[anscθ2]];
      deltaθ2[k]=θ2-θ2begin;
      newa1[k]=MR[deltaθ1[k]].{{(a1p-a0p)[[1]]},{(a1p-a0p)[[2]]}}+
         {{a0p[[1]]}, {a0p[[2]]}};
      p11[k]=MR[deltaθ1[k]].{{(p1p-a0p)[[1]]},{(p1p-
      a0p)[[2]]}}+{{a0p[[1]]},
         {a0p[[2]]}};
      q11[k]=MR[deltaθ1[k]].{{(q1p-a0p)[[1]]},{(q1p-
      a0p)[[2]]}}+{{a0p[[1]]},
         {a0p[[2]]}};r11[k]=MR[deltaθ1[k]].{{(r1p-a0p)[[1]]},
         {(r1p-a0p)[[2]]}}+{{a0p[[1]]},{a0p[[2]]}};
      newp1[k]=MR[deltaθ2[k]].(p11[k]-newa1[k])+newa1[k];
      newq1[k]=MR[deltaθ2[k]].(q11[k]-newa1[k])+newa1[k];
      newr1[k]=MR[deltaθ2[k]].(r11[k]-newa1[k])+newa1[k];
      square2[k]=(newp1[k][[1]]-p2p[[1]])^2+(newp1[k][[2]]-p2p[[2]])^2;
      square3[k]=(newp1[k][[1]]-p3p[[1]])^2+(newp1[k][[2]]-p3p[[2]])^2;
      square4[k]=(newp1[k][[1]]-p4p[[1]])^2+(newp1[k][[2]]-p4p[[2]])^2;
      squareq2[k]=(newq1[k][[1]]-q2p[[1]])^2+(newq1[k][[2]]-q2p[[2]])^2;
      squareq3[k]=(newq1[k][[1]]-q3p[[1]])^2+(newq1[k][[2]]-q3p[[2]])^2;
      squareq4[k]=(newq1[k][[1]]-q4p[[1]])^2+(newq1[k][[2]]-q4p[[2]])^2;
      squarer2[k]=(newr1[k][[1]]-r2p[[1]])^2+(newr1[k][[2]]-r2p[[2]])^2;
      squarer3[k]=(newr1[k][[1]]-r3p[[1]])^2+(newr1[k][[2]]-r3p[[2]])^2;
      squarer4[k]=(newr1[k][[1]]-r4p[[1]])^2+(newr1[k][[2]]-r4p[[2]])^2;
      tot2[k]=square2[k]+squareq2[k]+squarer2[k];
      tot3[k]=square3[k]+squareq3[k]+squarer3[k];
      tot4[k]=square4[k]+squareq4[k]+squarer4[k];
      ]

For[k=1;minsqrt2=999;minsqrt3=999;minsqrt4=999;
      minsqrtq2=999;minsqrtq3=999;
      minsqrtq4=999;minsqrtr2=999;minsqrtr3=999;
      minsqrtr4=999;myk2;myk3;myk4;mykq2;mykq3;mykq4;mykr2;mykr3;mykr4,
      k≤6200,
      k=k+1,
      If[minsqrt2>tot2[k][[1]],minsqrt2=tot2[k][[1]];myk2=k,];
```

```
      If[minsqrt3>tot3[k][[1]],minsqrt3=tot3[k][[1]];myk3=k,];
      If[minsqrt4>tot4[k][[1]],minsqrt4=tot4[k][[1]];myk4=k,];
      ]
newp1[myk2]
newp1[myk3]
newp1[myk4]
newq1[myk2]
newq1[myk3]
newq1[myk4]
newr1[myk2]
newr1[myk3]
newr1[myk4]
delta$\theta$1[myk2]*180/Pi
delta$\theta$1[myk3]*180/Pi
delta$\theta$1[myk4]*180/Pi
```

B.5.3 Spherical Five -Bar Motion Generator by Plane-to-Sphere Projection

```
TheMaxIteration=200;
RadiusOfSphere=1;
DistanceOfProjection=6
p1p={-0.1348,1.4949};p2p={-0.0057,1.4353};
p3p={0.1149,1.3419};p4p={0.2219,1.2157};
p5p={-0.1348,1.4949};p6p={0.0397,1.5033};
p7p={0.2095,1.4813};
q1p={0.1853,1.9430};q2p={0.2756,1.9087};
q3p={0.3534,1.8382};q4p={0.4128,1.7322};
q5p={0.1853,1.9430};q6p={0.3602,1.9511};
q7p={0.5271,1.9311};
r1p={0.7769,1.9430};r2p={0.8652,1.9585};
r3p={0.9363,1.9397};r4p={0.9835,1.8880};
r5p={0.7769,1.9430};r6p={0.9518,1.9506};
r7p={1.1187,1.9343};
a0p={0,-0.00229193};a1p={0.121248,0.990334};
a1np={-0.134977,0.988511}; b0p={1.25,0};b1p={1.9571,0.7071};
c1p={0.889398,1.45516};c1np={1.21532,1.7792};
ClearAll[p1p,p2p,p3p,p4p,p5p,p6p,p7p,p1,p2,p3,p4,p5,p6,p7];
ProjectionFun[{x_,y_},r_,d_]:={r*x/Sqrt[d^2+x^2+y^2],r*y/Sqrt[d^2+x^2+y
   ^2],r*d/ Sqrt[d^2+x^2+y^2]}
p1=ProjectionFun[p1p,RadiusOfSphere,DistanceOfProjection];
p2=ProjectionFun[p2p,RadiusOfSphere,DistanceOfProjection];
p3=ProjectionFun[p3p,RadiusOfSphere,DistanceOfProjection];
p4=ProjectionFun[p4p,RadiusOfSphere,DistanceOfProjection];
p5=ProjectionFun[p5p,RadiusOfSphere,DistanceOfProjection];
p6=ProjectionFun[p6p,RadiusOfSphere,DistanceOfProjection];
p7=ProjectionFun[p7p,RadiusOfSphere,DistanceOfProjection];
q1=ProjectionFun[q1p,RadiusOfSphere,DistanceOfProjection];
q2=ProjectionFun[q2p,RadiusOfSphere,DistanceOfProjection];
q3=ProjectionFun[q3p,RadiusOfSphere,DistanceOfProjection];
q4=ProjectionFun[q4p,RadiusOfSphere,DistanceOfProjection];
q5=ProjectionFun[q5p,RadiusOfSphere,DistanceOfProjection];
q6=ProjectionFun[q6p,RadiusOfSphere,DistanceOfProjection];
q7=ProjectionFun[q7p,RadiusOfSphere,DistanceOfProjection];
r1=ProjectionFun[r1p,RadiusOfSphere,DistanceOfProjection];
```

```
r2=ProjectionFun[r2p,RadiusOfSphere,DistanceOfProjection];
r3=ProjectionFun[r3p,RadiusOfSphere,DistanceOfProjection];
r4=ProjectionFun[r4p,RadiusOfSphere,DistanceOfProjection];
r5=ProjectionFun[r5p,RadiusOfSphere,DistanceOfProjection];
r6=ProjectionFun[r6p,RadiusOfSphere,DistanceOfProjection];
r7=ProjectionFun[r7p,RadiusOfSphere,DistanceOfProjection];
a0=ProjectionFun[a0p,RadiusOfSphere,DistanceOfProjection];
a1=ProjectionFun[a1p,RadiusOfSphere,DistanceOfProjection];
a1n=ProjectionFun[a1np,RadiusOfSphere,DistanceOfProjection];
b0=ProjectionFun[b0p,RadiusOfSphere,DistanceOfProjection];
b1=ProjectionFun[b1p,RadiusOfSphere,DistanceOfProjection];
c1=ProjectionFun[c1p,RadiusOfSphere,DistanceOfProjection];
c1n=ProjectionFun[c1np,RadiusOfSphere,DistanceOfProjection];
α1=ArcCos[a0.a1/Sqrt[a0.a0]/Sqrt[a1.a1]];
α2=ArcCos[a1.c1/Sqrt[c1.c1]/Sqrt[a1.a1]];
α3=ArcCos[c1.b1/Sqrt[c1.c1]/Sqrt[b1.b1]];
α4=ArcCos[b1.b0/Sqrt[b1.b1]/Sqrt[b0.b0]];
α5=ArcCos[a0.b0/Sqrt[a0.a0]/Sqrt[b0.b0]];
cα1=Cos[α1];sα1=Sin[α1];cα2= Cos[α2];sα2=Sin[α2];
cα3=Cos[α3];sα3=Sin[α3];cα4=
Cos[α4];sα4=Sin[α4];cα5=Cos[α5];sα5=Sin[α5];
AngleBetweenAxies[{ax_,ay_,az_},{bx_,by_,bz_}]:={-(az by-ay bz)/(-ay
   bx+ax by),-(az bx-ax bz)/(ay bx-ax by),1}
alpha1v=AngleBetweenAxies[a0,a1];
alpha2v=AngleBetweenAxies[a1,c1];
alpha3v=AngleBetweenAxies[c1,b1];
alpha4v=AngleBetweenAxies[b1,b0];
alpha5v=AngleBetweenAxies[b0,a0];
ϕ10=ArcCos[alpha5v.alpha1v/Sqrt[alpha1v.alpha1v]/Sqrt[alpha5v.alpha5v]]+
Pi;
ϕ50=2Pi-
ArcCos[alpha4v.alpha5v/Sqrt[alpha5v.alpha5v]/Sqrt[alpha4v.alpha4v]];
ClearAll[cθ1,sθ1,cθ2,sθ2,cθ3,sθ3,cθ4,sθ4,cθ5,sθ5];
M[cθ_,sθ_,cα_,sα_]:={{cθ,-cα sθ,sα sθ},{sθ,cα cθ,-sα cθ},{0,sα, cα}}
M2=M[cθ2,sθ2,cα2,sα2] ;
M3=M[cθ3,sθ3,cα3,sα3];
M4=M[cθ4,sθ4,cα4,sα4];
M1=M[cθ1,sθ1,cα1,sα1];
M5=M[cθ5,sθ5,cα5,sα5];
Z=M2.M3-Transpose[M1].Transpose[M5].Transpose[M4];
z11=Z[[1,1]];
z12=Z[[1,2]];
z13=Z[[1,3]];
z21=Z[[2,1]];
z22=Z[[2,2]];
z23=Z[[2,3]];
z31=Z[[3,1]];
z32=Z[[3,2]];
z33=Z[[3,3]];
tcθ2=0.6;tsθ2=-0.7;tcθ3=0.3;tsθ3=-0.9;tcθ4=-0.2;tsθ4=-0.9;
For[ϕ1=ϕ10;k=1,k≤TheMaxIteration,
   ϕ1=ϕ1-32./TheMaxIteration*Pi/180;k=k+1,
   deltaϕ1[k]= ϕ1-ϕ10;
   deltaϕ5[k]=(ϕ1-ϕ10)*0.5;
   ϕ5=ϕ50-deltaϕ5[k];
```

```
   cθ1=Cos[ϕ1];
   sθ1=Sin[ϕ1];
   cθ5=Cos[ϕ5];
   sθ5=Sin[ϕ5];
   Angles=FindRoot[{z11=0,z12=0,z13=0,z21=0,z22=0,z23=0},{cθ2,tcθ2},{sθ
      2,tsθ2},{cθ3,tcθ3}, {sθ3,tsθ3},{cθ4,tcθ4},{sθ4,tsθ4}];
   tcθ2=Angles[[1,2]];tsθ2=Angles[[2,2]];
   tcθ3=Angles[[3,2]];tsθ3=Angles[[4,2]];
   tcθ4=Angles[[5,2]];tsθ4=Angles[[6,2]];
   θ2=Which[tcθ2≥0 && tsθ2≥0,ArcCos[tcθ2],tcθ2<0 &&
      tsθ2>0,ArcCos[tcθ2],tcθ2≤0 && tsθ2≤0,2*Pi-ArcCos[tcθ2],tcθ2>0 &&
      tsθ2<0,2*Pi-ArcCos[tcθ2]];
   If[k=1,θ2begin=θ2,];
   deltaθ2[k]=θ2-θ2begin;
   deltaθ1[k]=ϕ1-ϕ10;
   ]
Ru[α_,u_]:={  {u[[1,1]]^2*(1-Cos[α])+Cos[α], u[[1,1]] u[[2,1]] (1-
   Cos[α])-u[[3,1]] Sin[α],u[[1,1]] u[[3,1]] (1-Cos[α])+u[[2,1]] Sin[α]
   },
   {u[[1,1]] u[[2,1]] (1-Cos[α])+u[[3,1]] Sin[α], u[[2,1]]^2 (1-
   Cos[α])+Cos[α], u[[2,1]] u[[3,1]] (1-Cos[α])- u[[1,1]] Sin[α] },
   {u[[1,1]] u[[3,1]] (1-Cos[α])-u[[2,1]] Sin[α], u[[2,1]] u[[3,1]] (1-
   Cos[α])+u[[1,1]] Sin[α],u[[3,1]]^2 (1-Cos[α])+Cos[α]}  };
uak={{uax},{uay},{uaz}};
a0axis={{a0[[1]]},{a0[[2]]},{a0[[3]]}};
b0axis={{b0[[1]]},{b0[[2]]},{b0[[3]]}};
For[k=1,k≤TheMaxIteration,k++,
   NewA1[k]=Ru[deltaθ1[k],a0axis].(a1-a0)+a0;
   a1axis={{NewA1[k][[1]]},{NewA1[k][[2]]},{NewA1[k][[3]]}};
   p1temp[k]=Ru[deltaθ1[k],a0axis].(p1-a0)+a0;
   NewP1[k]=Ru[deltaθ2[k],a1axis].(p1temp[k]-NewA1[k])+NewA1[k];
   q1temp[k]=Ru[deltaθ1[k],a0axis].(q1-a0)+a0;
   NewQ1[k]=Ru[deltaθ2[k],a1axis].(q1temp[k]-NewA1[k])+NewA1[k];
   r1temp[k]=Ru[deltaθ1[k],a0axis].(r1-a0)+a0;
   NewR1[k]=Ru[deltaθ2[k],a1axis].(r1temp[k]-NewA1[k])+NewA1[k];
   ]
Pd=p4;Qd=q4;Rd=r4;
For[k=1;minsqrt=9999;myk,k≤TheMaxIteration,k++,
   toleranceErr[k]=(Sqrt[(NewP1[k][[1]]-Pd[[1]])^2+(NewP1[k][[2]]-
      Pd[[2]])^2+ (NewP1[k][[3]]-Pd[[3]])^2]+Sqrt[(NewQ1[k][[1]]-
      Qd[[1]])^2+(NewQ1[k][[2]]-Qd[[2]])^2+(NewQ1[k][[3]]-
      Qd[[3]])^2]+Sqrt[(NewR1[k][[1]]-Rd[[1]])^2+(NewR1[k][[2]]-
      Rd[[2]])^2+(NewR1[k][[3]]-Rd[[3]])^2])/3;
   If[minsqrt>toleranceErr[k],minsqrt=toleranceErr[k];myk=k,];
   ]
myanswer4[DistanceOfProjection]={deltaθ1[myk]*180/Pi,DistanceOfProjecti
   on, minsqrt*DistanceOfProjection}
Pd=p3;Qd=q3;Rd=r3;
For[k=1;minsqrt=9999;myk,k≤TheMaxIteration,k++,
   toleranceErr[k]=(Sqrt[(NewP1[k][[1]]-Pd[[1]])^2+(NewP1[k][[2]]-
      Pd[[2]])^2+ (NewP1[k][[3]]-Pd[[3]])^2]+Sqrt[(NewQ1[k][[1]]-
      Qd[[1]])^2+(NewQ1[k][[2]]-Qd[[2]])^2+(NewQ1[k][[3]]-
      Qd[[3]])^2]+Sqrt[(NewR1[k][[1]]-Rd[[1]])^2+(NewR1[k][[2]]-
      Rd[[2]])^2+(NewR1[k][[3]]-Rd[[3]])^2])/3;
   If[minsqrt>toleranceErr[k],minsqrt=toleranceErr[k];myk=k,];
   ]
```

```
myanswer3[DistanceOfProjection]={delta$\theta$1[myk]*180/Pi,DistanceOfProjecti
   on, minsqrt*DistanceOfProjection}
Pd=p2;Qd=q2;Rd=r2;
For[k=1;minsqrt=9999;myk,k≤TheMaxIteration,k++,
   toleranceErr[k]=(Sqrt[(NewP1[k][[1]]-Pd[[1]])^2+(NewP1[k][[2]]-
      Pd[[2]])^2+ (NewP1[k][[3]]-Pd[[3]])^2]+Sqrt[(NewQ1[k][[1]]-
      Qd[[1]])^2+(NewQ1[k][[2]]-Qd[[2]])^2+(NewQ1[k][[3]]-
      Qd[[3]])^2]+Sqrt[(NewR1[k][[1]]-Rd[[1]])^2+(NewR1[k][[2]]-
      Rd[[2]])^2+(NewR1[k][[3]]-Rd[[3]])^2])/3;
   If[minsqrt>toleranceErr[k],minsqrt=toleranceErr[k];myk=k,];
   ]
myanswer2[DistanceOfProjection]={delta$\theta$1[myk]*180/Pi,DistanceOfProjecti
   on, minsqrt*DistanceOfProjection}
```

B.5.4 Planar Five -Bar Motion Generator by Sphere-to-Plane Projection

```
MyMaxSteps=320;
RadiusOfSphere=1;
DistanceOfProjection=5
ClearAll[p1p,p2p,p3p,p4p,p5p,p6p,p7p,p1,p2,p3,p4,p5,p6,p7];
ProjectionFun[{x_,y_,z_},d_]:={d/z*x,d/z*y}
p1={-0.021795,0.241702,0.970106}
p2={-0.000923932,0.232652,0.97256}
p3={0.0186851,0.21822,0.975721}
p4={0.036223,0.198451,0.979441}
p5={-0.021795,0.241702,0.970106}
p6={0.00641815,0.243033,0.969997}
p7={0.0338794,0.239549,0.970293}
q1={0.0293685,0.307949,0.950949}
q2={0.04373,0.302857,0.952032}
q3={0.0562272,0.292464,0.954622}
q4={0.0659565,0.276768,0.95867}
q5={0.0293685,0.307949,0.950949}
q6={0.0569979,0.308741,0.949437}
q7={0.0833346,0.305307,0.948601}
r1={0.122261,0.305771,0.944223}
r2={0.135812,0.307429,0.941829}
r3={0.146873,0.304272,0.941194}
r4={0.154481,0.296554,0.942439}
r5={0.122261,0.305771,0.944223}
r6={0.149173,0.305713,0.940365}
r7={0.174726,0.302113,0.937123}
p1p=ProjectionFun[p1,DistanceOfProjection]
p2p=ProjectionFun[p2,DistanceOfProjection]
p3p=ProjectionFun[p3,DistanceOfProjection]
p4p=ProjectionFun[p4,DistanceOfProjection]
p5p=ProjectionFun[p5,DistanceOfProjection]
p6p=ProjectionFun[p6,DistanceOfProjection]
p7p=ProjectionFun[p7,DistanceOfProjection]
q1p=ProjectionFun[q1,DistanceOfProjection]
q2p=ProjectionFun[q2,DistanceOfProjection]
q3p=ProjectionFun[q3,DistanceOfProjection]
q4p=ProjectionFun[q4,DistanceOfProjection]
q5p=ProjectionFun[q5,DistanceOfProjection]
```

```
q6p=ProjectionFun[q6,DistanceOfProjection]
q7p=ProjectionFun[q7,DistanceOfProjection]
r1p=ProjectionFun[r1,DistanceOfProjection]
r2p=ProjectionFun[r2,DistanceOfProjection]
r3p=ProjectionFun[r3,DistanceOfProjection]
r4p=ProjectionFun[r4,DistanceOfProjection]
r5p=ProjectionFun[r5,DistanceOfProjection]
r6p=ProjectionFun[r6,DistanceOfProjection]
r7p=ProjectionFun[r7,DistanceOfProjection]
ClearAll[a0p,a1p,a1np,b0p,b1p,b1np,a0,a1,a1n,b0,b1,b1n];
a0={0,-0.000381988,1.};a1={0.0199343,0.16282,0.986454};
a1n={-0.0221915,0.16252,0.986456};b0={0.203954,0,0.97898};
b1={0.308175,0.111344,0.944791};
c1={0.142585,0.233286,0.961898};
c1n={0.190634,0.279084,0.941154};
a0p=ProjectionFun[a0,DistanceOfProjection]
a1p=ProjectionFun[a1,DistanceOfProjection]
a1np=ProjectionFun[a1n,DistanceOfProjection]
b0p=ProjectionFun[b0,DistanceOfProjection]
b1p=ProjectionFun[b1,DistanceOfProjection]
c1p=ProjectionFun[c1,DistanceOfProjection]
c1np=ProjectionFun[c1n,DistanceOfProjection]
ClearAll[cθ2,sθ2,a2,cθ3,sθ3,a3,cθ4,sθ4,a4,cθ1,sθ1,a1,cθ5,sθ5,a5,zz11,zz
    12,z13,zz21,zz22,zz23,zz31,zz32,zz33];
M[cθ_,sθ_,a_]:={{cθ,-sθ,e a sθ},{sθ,cθ,-e a cθ},{0,e a, 1}}
M2=M[cθ2,sθ2,a2];
M3=M[cθ3,sθ3,a3];
M4=M[cθ4,sθ4,a4];
M1=M[cθ1,sθ1,a1];
M5=M[cθ5,sθ5,a5];
Z=M2.M3-Transpose[M1].Transpose[M5].Transpose[M4];
zz11=Z[[1,1]];
zz12=Z[[1,2]];
zz13=Z[[1,3]];
zz21=Z[[2,1]];
zz22=Z[[2,2]];
zz23=Z[[2,3]];
zz31=Z[[3,1]];
zz32=Z[[3,2]];
zz33=Z[[3,3]];
equ11=Coefficient[zz11,e,0]
equ12=Coefficient[zz12,e,0]
equ13=Coefficient[zz13,e,1]
equ23=Coefficient[zz23,e,1]
equ31=Coefficient[zz31,e,1]
equ32=Coefficient[zz32,e,1]
ClearAll[a1,a2,a3,a4];
a1=Sqrt[(a1p-a0p).(a1p-a0p)]
a2=Sqrt[(c1p-a1p).(c1p-a1p)]
a3=Sqrt[(b1p-c1p).(b1p-c1p)]
a4=Sqrt[(b0p-b1p).(b0p-b1p)]
a5=Sqrt[(a0p-b0p).(a0p-b0p)]
ClearAll[θ1begin,θ1];
θ1begin=ArcCos[(b0p-a0p).(a1p-a0p)/Sqrt[(b0p-a0p).(b0p-a0p)]/Sqrt[(a1p-
    a0p).(a1p-a0p)]]+Pi;
θ5begin=2 Pi-45.*Pi/180.
MR[θ_]:={{Cos[θ],-Sin[θ]},{Sin[θ],Cos[θ]}};
```

```
kθϕ=0.5;
θ50=2. Pi-45.*Pi/180;
tcθ2=0.6;tsθ2=-0.8;tcθ3=0.4;tsθ3=-0.9;tcθ4=-0.2;tsθ4=-0.9;
For[k=1;θ1=θ1begin,k≤MyMaxSteps,k++;θ1=θ1-32./MyMaxSteps*Pi/180.,
    deltaθ1[k]=θ1-θ1begin;
    deltaθ5[k]=kθϕ*deltaθ1[k];
    θ5=θ50-deltaθ5[k];
    cθ1=Cos[θ1];sθ1=Sin[θ1];cθ5=Cos[θ5];sθ5=Sin[θ5];
    Answer=FindRoot[{equ11,equ12,equ13,equ32,equ31,equ23},{cθ2,tcθ2},{s
        θ2,tsθ2},{cθ3,tcθ3},{sθ3,tsθ3},{cθ4,tcθ4},{sθ4,tsθ4}];
    tcθ2=Answer[[1,2]];tsθ2=Answer[[2,2]];
    tcθ3=Answer[[3,2]];tsθ3=Answer[[4,2]];
    tcθ4=Answer[[5,2]];tsθ4=Answer[[6,2]];
    anscθ2=Answer[[1,2]];anssθ2=Answer[[2,2]];
    θ2=Which[anscθ2≥0 && anssθ2≥0,ArcCos[anscθ2],anscθ2<0 &&
        anssθ2>0,ArcCos[anscθ2],anscθ2≤0 && anssθ2≤0,2*Pi-
        ArcCos[anscθ2],anscθ2>0 && anssθ2<0,-ArcCos[anscθ2]];
    If[k==1,θ2begin=θ2;Print[Answer],];
    delta θ2[k]=θ2-θ2begin;
    newa1[k]=MR[deltaθ1[k]].{{(a1p-a0p)[[1]]},{(a1p-
        a0p)[[2]]}}+{{a0p[[1]]},{a0p[[2]]}};
    p11[k]=MR[deltaθ1[k]].{{(p1p-a0p)[[1]]},{(p1p-
        a0p)[[2]]}}+{{a0p[[1]]},{a0p[[2]]}};
    q11[k]=MR[deltaθ1[k]].{{(q1p-a0p)[[1]]},{(q1p-
        a0p)[[2]]}}+{{a0p[[1]]},{a0p[[2]]}};
    r11[k]=MR[deltaθ1[k]].{{(r1p-a0p)[[1]]},{(r1p-
        a0p)[[2]]}}+{{a0p[[1]]},{a0p[[2]]}};
    newp1[k]=MR[deltaθ2[k]].(p11[k]-newa1[k])+newa1[k];
    newq1[k]=MR[deltaθ2[k]].(q11[k]-newa1[k])+newa1[k];
    newr1[k]=MR[deltaθ2[k]].(r11[k]-newa1[k])+newa1[k];
    square2[k]=(newp1[k][[1]]-p2p[[1]])^2+(newp1[k][[2]]-
        p2p[[2]])^2+(newq1[k][[1]]-q2p[[1]])^2+(newq1[k][[2]]-
        q2p[[2]])^2+(newr1[k][[1]]-r2p[[1]])^2+(newr1[k][[2]]-
        r2p[[2]])^2;
    square3[k]=(newp1[k][[1]]-p3p[[1]])^2+(newp1[k][[2]]-
        p3p[[2]])^2+(newq1[k][[1]]-q3p[[1]])^2+(newq1[k][[2]]-
        q3p[[2]])^2+(newr1[k][[1]]-r3p[[1]])^2+(newr1[k][[2]]-
        r3p[[2]])^2;
    square4[k]=(newp1[k][[1]]-p4p[[1]])^2+(newp1[k][[2]]-
        p4p[[2]])^2+(newq1[k][[1]]-q4p[[1]])^2+(newq1[k][[2]]-
        q4p[[2]])^2+(newr1[k][[1]]-r4p[[1]])^2+(newr1[k][[2]]-
        r4p[[2]])^2;
    ]
For[k=1;minsqrt2=999;minsqrt3=999;minsqrt4=999;myk2;myk3;myk4,
    k≤MyMaxSteps,k=k+1,
    If[minsqrt2>square2[k][[1]],minsqrt2=square2[k][[1]];myk2=k,];
    If[minsqrt3>square3[k][[1]],minsqrt3=square3[k][[1]];myk3=k,];
    If[minsqrt4>square4[k][[1]],minsqrt4=square4[k][[1]];myk4=k,];
    ]
StructuralErr[DistanceOfProjection]=Sqrt[minsqrt4]/DistanceOfProjection;
deltaθ1[myk2]*180/Pi
deltaθ1[myk3]*180/Pi
deltaθ1[myk4]*180/Pi
StructuralErr[DistanceOfProjection]
```

REFERENCES

[1] http://wwwrobot.gmc.ulaval.ca/recherche/theme01_a.html, March 1, 2004.

[2] http://dionne.me.coe.fit.edu/~rassl/research.html#fan, March 1, 2004.

[3] Tong, S. and Chiang, C.H., "Syntheses of Planar and Spherical Four-Bar Path Generators by the Pole Method," *Mechanism and Machine Theory,* Vol. 27, No. 2, pp. 143-155 (1992).

[4] Chang, C.F., Lu, D.M., and Hwang, W.M., "Synthesis of Spherical Four-Bar Path Generator Satisfying the Prescribed Tangents at Two Cusps," *Journal of Mechanical Engineering Science,* Vol. 211, No. 3, pp. 211-216 (1997).

[5] Angeles, J. and Liu, Z., "Constrained Least-Square Method for the Optimization of Spherical Four-Bar Path Generators," *Journal of Mechanical Design, Transactions of the ASME,* Vol. 114, No. 3, pp. 394-405 (1992).

[6] Lin, C., "Complete Solution of the Five-Position Synthesis for Spherical Four-Bar Mechanisms," *Journal of Marine Science and Technology,* Vol. 6, No. 1, pp. 17-27 (1998).

[7] Funabshi, H., Iwatsuki, N. and Yoshiaki, Y., "A Synthesis of Crank Length Adjusting Mechanisms," *Bulletin of JSME,* Vol. 29, No. 252, pp. 1946-1951 (1986).

[8] Tao, D.C. and Krishnamoorthy, S., "Linkage Mechanism Adjustable for Variable Coupler Curves with Cusps," *Mechanism and Machine Theory,* Vol. 13, No. 6, pp. 577-583 (1977).

[9] Kay, F. J. and Haws, R.E., "Adjustable Mechanisms for Exact Path Generation," *Journal of Engineering for Industry, Transactions of the ASME,* Vol. 97, No, 2, pp. 702-707 (1975).

[10] Zhou, H. and Cheung, E.H.M., "Analysis and Optimal Synthesis of Adjustable Linkages for Path Generation," *Mechatronics,* Vol. 12, No. 7, pp. 949-961 (2002).

[11] Ullah, I. and Kota, S., "Optimal Synthesis of Mechanisms for Path Generation Using Fourier Descriptors and Global Search Methods," *Journal of Mechanical Design, Transactions of the ASME,* Vol. 119, No. 4, pp. 504-510 (1997).

[12] Sandor, G.N., Kaufman. R.E., Erdman, A.G., Foster, T.J., Sadler, J.P., Smith, C.Z., and Kershaw, T.N., "Kinematic Synthesis of Geared Linkages," *Journal of Mechanisms,* Vol. 5, No. 1, pp. 59-87 (1970).

[13] Balli, S.S. and Chand, S., " Five-Bar Motion and Path Generators with Variable Topology for Motion Between Extreme Positions," *Mechanism and Machine Theory,* Vol. 37, No. 11, pp. 1435-1445 (2002).

[14] Starns, G. and Flugrad, D.R., " Five-Bar Path Generation Synthesis By Continuation Methods," *Journal of Mechanical Design, Transactions of the ASME,* Vol. 115, No. 4, pp. 988-994 (1993).

[15] Connor, A.M., Douglas, S.S., and Gilmartin, M.J., "Synthesis of Hybrid Five-Bar Path Generating Mechanisms Using Genetic Algorithms," *IEE Conference Publication,* No. 414, pp. 313-318 (1995).

[16] Freudenstein, F. and Roth, B., "Synthesis of Path-Generating Mechanisms by Numerical Methods," *Journal of Engineering for Industry,* pp. 298-306 (1963).

[17] McGovern, J. F. and Sandor, G.N., "Kinematic Synthesis of Adjustable Mechanisms (Part 1: Function Generation)," *Journal of Engineering for Industry, Transactions of the ASME,* Vol. 95, No. 2, pp. 417-422 (1973).

[18] Chang, C.F., "Synthesis of Adjustable Four-Bar Mechanisms Generating Circular Arcs with Specified Tangential Velocities," *Mechanism and Machine Theory,* Vol. 36, No. 3, pp. 387-395 (2001).

[19] Beaudrot, C.B., "Synthesis of Four-Bar Linkages Adjustable for Several Approximate Straight-Line Motions of a Coupler Point," *Journal of Engineering for Industry, Transactions of the ASME,* pp. 172-178 (1969).

[20] Shimojima, H., Ogawa, K., Fujiwara, A., and Sato, O., "Kinematic Synthesis of Adjustable Mechanisms," *Bulletin of JSME,* Vol. 26, No. 214, pp. 627-632 (1983).

[21] Tao, D.C. and Yan, H.S., "Technology Transfer in the Design of Adjustable Linkages," *Journal of Mechanical Design, Transactions of the ASME,* pp. 495-498 (1979).

[22] Liu, Z. and Angeles, J., "Least-Square Optimization of Planar and Spherical Four-Bar Function Generator Under Mobility Constraints," *Journal of Mechanical Design, Transactions of the ASME,* Vol. 114, No. 4, pp. 569-573 (1992).

[23] Lin, C. and Chiang C.H., "Synthesis of Planar and Spherical Geared Five-Bar Function Generators by the Pole Method", *Mechanism and Machine Theory,* Vol. 27, No. 2 pp. 131-141 (1992).

[24] Sodhi, R.S. and Wilhelm, A.J., "Design of a Four-Revolute Spherical Function Generator with Transmission Effectiveness by Curve Matching," *Mechanism and Machine Theory,* Vol. 20, No. 6. pp. 577-585 (1985).

[25] Chen, J. and Chiang, C.H., "Fourth-Order Synthesis of Spherical Four-Bar Function Generators," *Mechanism and Machine Theory,* Vol. 18, No. 6, pp. 451-456 (1983).

[26] Raot, A.C., "Synthesis of Geared Planar Four-Bar Linkages and Cams to Generate Functions of Two Variables," *Mechanism and Machine Theory,* Vol. 15, pp. 137-143 (1979).

[27] Watanabe, K., "Approximate Synthesis of Plane Four-Bar Mechanism for Function Generation," *Bulletin of the JSME,* Vol. 17, No. 109, pp. 951-958 (1974).

[28] Chuang, S. H. and Chiang, C. H., "Fifth-Order Synthesis of Plane Four-Bar Function Generators Optimized by Varying Scale Factors," *Mechanism and Machine Theory,* Vol. 22, No, 1, pp. 55-63 (1987).

[29] Chiang, C.H., Pennestri, E. and Chung, W., "On a Technique for Higher-Order Synthesis of Four-Bar Function Generators," *Mechanism and Machine Theory,* Vol. 24, No. 3, pp. 195-205 (1989).

[30] Beale, D. and Simionescu, P.A., "Optimum Synthesis of the Four-Bar Function Generator in its Symmetric Embodiment: The Ackermann Steering Linkage," *Mechanism and Machine Theory,* Vol. 37, No. 12, pp. 1487-1504 (2002).

[31] Todorov, T. S., "Synthesis of Four-Bar Mechanisms by Freudenstein-Chebyshev," *Mechanism and Machine Theory,* Vol. 37, No. 12, pp. 1505-1512 (2002).

[32] Yin, Z.W. and Wu, J. K., "Optimal Synthesis of Linkages Considering Structural Error and Clearances," *American Society of Mechanical Engineers, Design Engineering Division,* Vol. 25, pp. 295-299 (1990).

[33] McGovern, J.F. and Sandor, G.N., "Kinematic Synthesis of Adjustable Mechanisms: Path Generation," *Journal of Engineering for Industry, Transactions of the ASME,* Vol. 95, No. 2, pp. 423-429 (1973).

[34] Naik, D.P. and Amarnath, C., "Synthesis of Adjustable Four-Bar Function Generators Through Five-Bar Loop Closure Equations," *Mechanism and Machine Theory,* Vol. 24. No. 6. pp. 523-526 (1989).

[35] Basu, P.S. and Farhang, K., "Kinematic Analysis and Design of Two-Input, Five-Bar Mechanisms Driven by Relatively Small Cranks," *American Society of Mechanical Engineers, Design Engineering Division (Publication) DE, v 47, Flexible Mechanisms, Dynamics, and Analysis,* pp. 377-386 (1992).

[36] Furlong, T.J., Vance, J.M., and Larochelle, P.M.," Spherical Mechanism Synthesis in Virtual Reality," *Journal of Mechanical Design, Transactions of the ASME,* Vol. 121, No. 4, pp. 515-520 (1999).

[37] Sodhi, R.S. and Shoup, T.E., "Axodes for the Four-Revolute Spherical Mechanism," *Mechanism and Machine Theory,* Vol. 17, No. 3, pp. 173-178 (1982).

[38] Sodhi, R.S. and Shoup, T.E., "ISA Synthesis for the Four-Revolute Spherical Mechanism," *International Symposium on Design and Synthesis, Tokyo, Japan* (1984).

[39] Gilmartin, M.J. and Duffy, J., "Type and Mobility Analysis of the Spherical Four-Link Mechanism," *International Mechanical Engineering Conference on Mechanisms,* pp. 90-97 (1972).

[40] McCarthy, M.J. and Bodduluri, R.M., "Avoiding Singular Configurations in Finite Position Synthesis of Spherical 4R Mechanisms," *Mechanism and Machine Theory,* Vol. 35, pp. 451-462 (2000).

[41] McCarthy, M.J. and Bodduluri, R.M., "Finite Position Synthesis Using the Image Curve of a Spherical Four-Bar Motion," *Journal of Mechanical Design, Transactions of the ASME,* Vol. 114, No. 1, pp. 55-60 (1992).

[42] Ruth, D.A. and McCarthy, M.J., "The Design of Spherical 4R Linkages for Four Specified Orientations," *Mechanism and Machine Theory,* Vol. 34, pp. 677-692 (1999).

[43] Wang, S. and Sodhi, R.S., "Kinematic Synthesis of Adjustable Moving Pivot Four-Bar Mechanisms for Multi-Phase Motion Generation," *Mechanism and Machine Theory,* Vol. 31, No. 4, pp. 459-474 (1996).

[44] Ahmad, A. and Waldron, K.J., "Synthesis of Adjustable Planar Four-Bar Mechanisms," *Mechanism and Machine Theory,* Vol. 14, No. 6, pp. 405-411 (1979).

[45] Dhingra, A.K. and Mani, N.K., "Finite and Multiply-Separated Kinematic Synthesis of Link and Geared Mechanisms," *Trends and Developments in Mechanics, Machines and Robotics,* Vol. 1, pp. 317-326 (1988).

[46] Wilhelm, A.J., "Kinematic Synthesis of Adjustable Linkages for Motion Generation," *Ph.D. Dissertation,* Wichita State University (1989).

[47] Chuenchom, T. and Kota, S., "Synthesis of Programmable Mechanisms Using Adjustable Dyads," *Journal of Mechanical Design, Transactions of the ASME,* Vol. 29, No. 5, pp. 232-237 (1997).

[48] Suh, C.H. and Radcliffe, C.W., "Kinematics and Mechanism Design," John Wiley and Sons, New York, 1978.

[49] Sandor, G.N. and Erdman, A.G., "Advanced Mechanism Design Analysis and Synthesis," Prentice-Hall, Englewood Cliffs, 1984.

[50] Fischer, I.S., "Dual-Number Methods in Kinematics, Statics And Dynamics," CRC Press, 1999.

[51] Oberg, E., Jones, F.D., Horton, H.L. and Ryfeel, H.H., "Machinery's Handbook 26th Edition," Industrial Press, New York, 2000.